Stimulus responses and targeted plasticity of the macaque motor cortex using intracortical microstimulation

Richy J. Yun

A dissertation

submitted in partial fulfillment of the

requirements for the degree of

Doctor of Philosophy

University of Washington

2022

Reading Committee:

Eberhard E. Fetz, Chair

Steve I. Perlmutter

Amy L. Orsborn

Program Authorized to Offer Degree:

Bioengineering

University of Washington

Abstract

Stimulus response and targeted plasticity of the macaque motor cortex using intracortical microstimulation

Richy J. Yun

Chair of the Supervisory Committee:

Eberhard E. Fetz

Department of Physiology and Biophysics

Electrical stimulation is a commonly used tool for probing neural circuits in both research and clinical settings. Stimulation delivered directly to the cerebral cortex, intracortical microstimulation (ICMS), has often been used to induce targeted plasticity between a pre- and postsynaptic site. However, the results often require a long conditioning period, are highly variable, and depend on the cortical site pairs. The following dissertation describes experiments performed to better understand both the behavioral and neural effects of ICMS and utilizes that knowledge for a more effective spike-timing dependent plasticity (STDP) protocol. First, ICMS is delivered at different phases of unimanual movement to assess its effects beyond the stimulated hemisphere and dependence of the changes observed on the movement state. Next, gamma-triggered stimulation as a proxy for-population triggered stimulation is explored for

inducing STDP. Then single neuron responses to ICMS and the dependencies of the responses to underlying spontaneous activity as well as how they change over time are characterized. The single neuron responses are subsequently used as a measure of connectivity in a paired stimulation paradigm to induce STDP. Finally, different behavioral states during sleep and waking are determined, and the underlying neural dynamics are compared to lay the groundwork for assessing plasticity throughout different brain states. The combined results strongly suggest the significance of specific timing in delivering ICMS, indicate the role of inhibitory responses, and provide insights for future applications of ICMS.

Table of Contents

List of Figures and Tables

Acknowledgements

My childhood dream was to become a scientist. It took me 4 years into graduate school to notice I had realized that dream. As surreal as it was, I could only think of my gratitude towards everyone that has supported and encouraged me throughout my journey.

I would like to first thank Dr. Eberhard Fetz. I could not have asked for a better mentor for providing me with guidance but also allowing me to truly explore the field. His excitement and rumination over any new finding, no matter how simple, always kept me engaged and searching for the next discovery. It only takes a couple conversations with Eb to realize he is a genuine scientist, always curious and never satisfied, filled to the brim with questions and hypotheses. I have the utmost respect and admiration for his approach to science and hope to apply it in all my future endeavors.

Thank you to everyone in the Fetz and Perlmutter labs. Though not officially my advisor, Dr. Steve Perlmutter functioned as one for all intents and purposes throughout my graduate career. His sensible advice in all things scientific and logistical guided me toward much more efficient paths. Dr. Jonathan Mishler was a great friend as well as a supportive colleague. We kept each other going through failed experiments, unforeseen roadblocks, and personal circumstances. I was very fortunate to have someone so understanding and reliable along for the ride, and I'm grateful for his friendship throughout our PhDs. Dr. Irene Rembado was a selfless mentor, colleague, and friend. I will always fondly remember the dinners she hosted, conversations we had about neuroscience or otherwise, and everything she taught me in the lab. She also taught me how to truly be a mentor, and I credit a large part of my success to her mentorship.

Dr. Andrew Bogaard introduced me to the lab, and I thank him for his work on Chapter 1 and convincing me to join the lab. Dr. Samira Moorjani provided helpful discussion on Chapters 3 and 4, and I'm grateful for her and her family's warm hospitality. Dr. Stavros Zanos gave me advice when I was first rotating in the lab to make sure I am always learning something new, which I follow to this day. Larry Shupe was constantly willing to help no matter how small the issue, and he has greatly elevated my understanding of coding and troubleshooting hardware. Rob Robinson provided surgical expertise and a healthy degree of caution that let me avoid catastrophic failures. Dr. Bethany Kondiles gave great advice on what to expect during the latter stages of my PhD and was always ready to commiserate with any problems I had. Dr. Brian Mogen convinced me to avoid the spinal cord in monkeys, which in hindsight likely saved me from months of suffering.

I would also like to thank Rebekah Schaefer, Lucia Shumaker, and Rebecca Burch for helping with animal training, margin cleaning, surgery preparations, and managing the lab. It is truly astonishing how much of an impact a capable lab manager can have. Thank you to Miles Keating and Martin Rios, two undergraduate students that helped collect data for Chapters 3 and 5, and who helped hone my mentoring skills.

Beyond the Fetz and Perlmutter labs, I would also like to acknowledge Dr. Rajesh Rao. Though not my advisor, he was present in most of my meetings and gave great feedback and provided thoughtful discussion for each project. He also recommended I join the Center for Neurotechnology Student Leadership Council. The CNT community taught me about leadership, how to create an interactive academic group, and provided funding for several years of my graduate career.

I also thank the Washington National Primate Center and the animal technicians and veterinarians for help with animal care and surgery. I would like to especially thank Dr. Keith Vogel who, through many delays to his retirement and numerous trips between Bainbridge Island and the UW campus at odd hours, taught me how to properly care for animals with implants and techniques for efficient surgical procedures. Although mentally and physically demanding at times, I would not trade the experiences I have had in the primate center for anything.

Thank you to my committee members: Dr. Amy Orsborn for her sharp questions always keeping me on my toes, Dr. Azadeh Yazdan-Shahmorad for her advice on surviving graduate school and assistance beyond my PhD, and Dr. Matt Reynolds for readily stepping in at the last minute.

And of course, thank you to the 7 monkeys that made the work in this dissertation possible – Igor, Kato, Ubi, Spanky, Jafar, Kronk, and Lorde. It is not common practice to write out names of the animal subjects, but I would like to properly commemorate them here for taking part in the experiments.

I would also like to acknowledge mentors and colleagues from earlier in my science career. Thank you to the Moritz lab where I did my first rotation, and Dr. David Bjanes in particular for his mentorship and showing me how to be resourceful in a research setting. Thank you to everyone in the Nicolelis lab. Dr. Eric Thomson's trust in my capabilities emboldened my decision to pursue science. Dr. Konstantin Hartmann taught me how to be efficient in the lab by thinking outside the box and has been a wonderful friend throughout the years. Ivan Zea showed me that hard work does indeed pay off, and to not be afraid of new opportunities.

Outside of academia, I want to give a warm thanks to all the friends that spent time with me, whether playing video games, playing board games, camping, hiking, or traveling. The

friendships I have been fortunate enough to forge throughout the years have kept me sane and grounded, especially throughout the pandemic. Special thanks to Kyle Griffith and Xavier de Gunten for their belief in my success regardless of my never-ending worries.

Finally, I have been fortunate to have an incredible family behind me. Thank you to my parents for trusting my decision to pursue graduate school in a field they did not understand. The sacrifices they have made are beyond anything anyone could expect, and I would not be who I am without their love and support. Thank you to my sister, Jina Yun, for always being confident in my abilities and trying her hardest to convince me to believe in myself.

Last but definitely not least, I would like to thank my wonderful partner Bryanna Lloyd for her patience and undying support that gave me the will and courage to pursue my dreams.

Introduction

Electrical stimulation was first found to excite the brain in 1870 by Fritsch and Hitzig (Fritsch & Hitzig, 1870). Since the discovery, electrical stimulation has been used to probe various brain structures, providing insight into neurobiology and neuroanatomy. More recently, stimulation with both surface and depth electrodes are being used in medical applications for neuroprostheses and to treat various neurological conditions including epilepsy, Parkinson's disease, and essential tremor (Borchers et al., 2012; Hartmann et al., 2016; Lebedev & Nicolelis, 2017; McPherson et al., 2015; Perlmutter & Mink, 2006).

A particular application of electrical stimulation is to induce targeted plasticity, typically with intracortical microstimulation (ICMS). A robust and effective method can lead to improving connections and bridging gaps caused by injury or neurodegenerative diseases. As a result, stimulus induced plasticity via spike-timing dependent plasticity (STDP) has been extensively demonstrated both *in vitro* and *in vivo* (Bi & Poo, 1998; Jackson et al., 2006; Markram et al., 1998, 2011). However, previous paradigms require a lot of stimulation leading to long conditioning periods, report inconsistent changes in synaptic strength, and the results depend heavily on the specific sites that were tested (Rebesco & Miller, 2011a; Seeman et al., 2017; Zanos et al., 2018). Thus, there is a need to better harness the utility of electrical stimulation for STDP.

One approach is to improve our understanding of how ICMS activates cortical circuits. Stimulation is assumed to be purely excitatory in the context of stimulus-induced plasticity, but studies have shown that single neurons also have a strong inhibitory response to ICMS that is likely driven by local feedforward and feedback inhibitory networks (Butovas et al., 2006; Dadarlat et al., 2019; Logothetis et al., 2010; Michelson et al., 2019). Although our

understanding of how cortical circuitry is activated by stimulation is growing, we still do not understand the dependencies of the stimulus responses on ongoing neural dynamics or the relationship between the excitatory and inhibitory responses.

Another approach to use electrical stimulation more effectively is to determine the effects of specific timing of stimulation. Most plasticity studies deliver ICMS across various behavioral states or even overnight; however, evidence shows that stimulation delivered during different brain states, such as different phases of movement or different stages of sleep, produce varying effects (Pascual-Leone et al., 1992; Rembado et al., 2017; Richardson & Fetz, 2017; Wolters et al., 2003). There is a need to better understand how the underlying brain state affects responses to ICMS and subsequent changes in neural circuitry. STDP experiments also typically use static inter-stimulus intervals (ISI) or broad steps of several milliseconds (Rebesco & Miller, 2011a; Seeman et al., 2017). Higher temporal specificity in stimulus timing will shed light on stimulus-induced STDP and lead to more effective stimulation paradigms.

Finally, various other plasticity mechanisms must be considered. Short-term plasticity is present during tonic stimulation, the induced changes depending on the stimulus frequency and the cell and synapse type (Blackman et al., 2013; Losonczy et al., 2002; Zucker & Regehr, 2002). Homeostatic plasticity is a compensatory mechanism that limits the positive feedback loop of Hebbian plasticity with synaptic scaling (Miller et al., 2000; Turrigiano, 2008, 2012). Plasticity also often does not follow classic STDP, and sometimes follows anti-Hebbian rules or is unidirectional (Feldman, 2012; Markram et al., 2011; Miller et al., 2000).

This dissertation aims to better understand the neural response to intracortical microstimulation and stimulus-induced plasticity by applying electrical stimulation to the motor cortex of intact,

behaving macaques. In the following studies I present research in which I explore the effects of stimulation and changes in dynamics of single neurons and local field potentials:

Chapter 1 demonstrates the dependence of behavioral and neurological changes on the specific timing of stimulation relative to unimanual movement. Stimulation delivered before movement sped up the trigger limb, whereas stimulation delivered after contralateral limb movement slowed down the contralateral limb but sped up the ipsilateral limb. These results show changes in interhemispheric inhibition resulting in various changes in behavior, which was additionally reflected in modulation of interhemispheric alpha coherence. Changes in the motor cortex may result in much more global changes that must be considered when employing stimulation techniques.

Chapter 2 explores the pitfalls of applying gamma-triggered stimulation as a method for triggering from population-based activity to induce STDP. Two factors prevented the implementation of an effective stimulation paradigm. 1) The delays introduced from band pass filters lasted at least a whole cycle of gamma and was unavoidable without specialized hardware. 2) Stimulation of a postsynaptic site resulted in a large gamma component in the presynaptic site, likely due to both stimulus artifact and stimulus response, leading to a positive feedback loop. These two factors must be resolved to carry out proper cycle-triggered stimulation.

Chapter 3 characterizes the excitatory and inhibitory responses of single neurons to ICMS. The excitatory response had two dependencies that were previously unexplored – 1) The timing of stimulation since the most recent spike and 2) the spontaneous firing rate of the spike. Both responses often changed over time due to repetitive stimulation, likely due to short-term plasticity, with more changes occurring due to higher frequency stimulation. These relationships and changes over time must be taken into account when employing ICMS paradigms.

Chapter 4 illustrates paired stimulation with higher temporal specificity in ISIs. Using the probability of evoking a spike in the postsynaptic site when delivering ICMS to the presynaptic site as a measure of synaptic connectivity strength showed depression even with positive ISIs. Comparing the changes in synaptic strength to the single unit response revealed that stimulation occurring during the inhibitory response results in depression, suggesting that the paired stimulation may be strengthening the connections to the local inhibitory circuitry. Thus, inhibition may play a larger role in ICMS paradigms than initially thought, resulting in STDP being more complex *in vivo*.

Chapter 5 shows classification of different behavioral brain states during sleep and waking as a prerequisite for delivering ICMS overnight. States were accurately classified as confirmed by concurrent electrooculography recordings as well as kinematic metrics recorded with the Microsoft Kinect. Assessing changes in spiking patterns, spike-field synchrony, and cross-frequency phase-amplitude coupling showed that delta oscillations may be playing a role in the reactivation of cortical circuitry during sleep for skill and memory consolidation.

The work in this dissertation has resulted in the following manuscripts:

Chapter 1.

Richy Yun, Andrew R. Bogaard, Andrew G. Richardson, Stavros Zanos, Steve I. Perlmutter, Eberhard E. Fetz (2021). Cortical stimulation paired with volitional unimanual movement affects interhemispheric communication. *Frontiers in Neuroscience* 15:782188.

Chapter 3.

Richy Yun, Jonathan H. Mishler, Steve I. Perlmutter, Rajesh P.N. Rao, Eberhard E. Fetz (2022). Responses of cortical neurons to intracortical microstimulation in awake primates. *bioRxiv*. doi: https://doi.org/10.1101/2022.03.30.486457

Chapter 4.

Richy Yun, Jonathan H. Mishler, Rajesh P.N. Rao, Steve I. Perlmutter, Eberhard E. Fetz (2022). Paired stimulation for spike-timing dependent plasticity quantified with single neuron responses in primate motor cortex. *bioRxiv*. doi: https://doi.org/10.1101/2022.05.04.490684

Chapter 5.

Richy Yun, Jonathan H. Mishler, Irene Rembado, Rajesh P.N. Rao, Steve I. Perlmutter, Eberhard E. Fetz (2022). Local field potentials and single unit dynamics in motor cortex of unconstrained macaques during different behavioral states. *bioRxiv*. doi: https://doi.org/10.1101/2022.04.28.489967

General Methods

Animals and implants

The following studies were conducted with 7 male pigtail macaques (*Macaca nemestrina*): Monkeys Ig, Ka, U, Kr, In, S, and J.

Monkey Ig received 8 custom epidural electrodes bilaterally. Epidural electrodes were constructed with 0.01-inch platinum wire insulated with heat-shrink tubing, with a ~0.5 mm exposed tip.

Monkeys Ka and U were implanted with custom-made electrodes combining epidural and depth electrodes called “dual electrodes” (detailed in Seeman et al., 2017) over left and right sensorimotor cortex (Ka: 2 electrodes bilaterally, U: 7 electrodes bilaterally). In brief, dual electrodes were constructed using two 0.005-inch bare platinum-iridium (PtIr) wire rods. For each dual electrode, two rods soldered to lead wires were secured in a small piece of polytetrafluoroethylene (PTFE) tubing with silicon glue. The other end of the lead wires was soldered to connectors. The tips of the rods were placed ~0.5 and 2–2.5 mm from the edge of the PTFE tube such that the shorter rod would reach layer I of the cortex, and the longer rod layer V.

Monkeys Kr, S, and J were implanted with 96-channel Utah microelectrode arrays (Blackrock Microsystems; 10x10, 400 µm inter-electrode distance, 1.5 mm depth, Iridium oxide) in the hand region of primary motor cortex (M1). They additionally received a “halo” implant made with 3/8” aluminum into an egg-shaped oval 17 cm long and 15.3 cm wide for holding the Neurochip3 (Shupe et al., 2021) during overnight recordings (Figure 0.1).

Monkey J was also implanted with electrooculography (EOG) electrodes to track eye movements (Figure 0.2). EOG electrodes consisted of a titanium washer ((#4, 0.25” OD, 0.032” thick) with a

0.016” hole drilled into it and a 34-gauge silver-plated copper microwire with silicone shielding (Cooner Wire, AS155-34) threaded through the hole and soldered to the washer.

Surgical procedures

Surgeries were performed under isoflurane anesthesia and aseptic conditions. After each surgery, animals received postoperative courses of analgesics and antibiotics. Animals did not show signs of discomfort or pain related to any implanted devices after recovery, and all exposed implants were regularly disinfected biweekly with chlorohexidine and treated with antibiotics to prevent infection. All procedures conformed to the National Institutes of Health *Guide for the Care and Use of Laboratory Animals* and were approved by the University of Washington Institutional Animal Care and Use Committee.

Epidural electrodes and dual electrodes

An incision was made along the midline of the scalp, and muscle and connective tissue were resected to expose the skull. Titanium skull screws were placed in the skull around the edge of the exposure for electrical grounds and mechanical stability. Small holes for the electrodes were drilled over the sensorimotor cortex with a 1 mm bit using stereotactic coordinates. One electrode was placed with forceps into each hole until resistance was felt between the rod and the dura. Dual electrodes (Supplementary Figure 1.1) were additionally pushed through the dura and into the cortex until a second resistance was felt between the shorter rod and the dura. After all electrodes for one hemisphere were implanted, a thin coat of dental acrylic (methyl methacrylate) was used to seal the holes and hold the electrodes in place. A titanium casing was then placed over the implant and secured to the skull screws with acrylic.

Utah electrode array

Implantation of the Utah array was guided by stereotaxic coordinates. A 1.5 cm wide square craniotomy was performed over the hand region of the primary motor cortex to expose the dura. Three sides of the exposed dura were cut to expose the cortex; a Utah array was implanted, and the dura was sutured over the array. Two reference wires were inserted below the dura and two were inserted between the dura and the skull. The bone flap from the craniotomy was returned, held in place by a titanium strap screwed onto the skull with 2.5 mm x 6 mm titanium skull screws. A second smaller titanium strap was fastened to the skull to secure the wire bundle. The connector pedestal for the array was attached to the skull with eight titanium skull screws and the incision closed around the pedestal base. Additional skull screws were placed around the base of the connector pedestal and a thin coat of dental acrylic (methyl methacrylate) was applied to the skull between the screws and the connector base for additional stability.

Halo implant

Four titanium straps were affixed to the skull by titanium bone screws. Two were implanted bilaterally over the occipital ridge, and two were placed temporally bilaterally. After the plates integrated with the skull for 6 weeks, an aluminum ring (halo) was mounted on four pins seated in each plate (Figure 0.1). A titanium can with a plexiglass top to house the Neurochip3 was attached to the halo during all Neurochip3 recording sessions.

EOG electrodes

An incision was made to the dorsal and lateral margins of both orbits to expose the skull. A small hole was drilled in each incision, a titanium skull screw (2 mm x 6 mm) was used to hold down the EOG electrodes (Figure 0.2), and the wires of the electrodes were tunneled beneath the tissue along the skull. Another incision was made along the top of the skull to secure a pedestal with 8

skull screws and allow access to the electrode wires. The inside of the pedestal was filled with surgical silicone adhesive (Kwik-Sil, World Precision Instruments) to prevent infection. Connectors were fastened to the wires postoperatively.

Recording and stimulation

All recording and stimulation was performed using one of the following systems: g.USBamp (g.tec medical engineering GmbH, 2.4 or 9.6 kHz), Neural Interface Processor (Ripple Neuro, 30 kHz), or the Neurochip3 (Fetz Group, 20 kHz) (Shupe & Fetz, 2021). The number of channels and sampling rate of recording and stimulation paradigm for each study is outlined in the individual methods.

Spike sorting

Spikes in Chapters 3, 4, and 5 were sorted offline using two-window discrimination with custom MATLAB (Mathworks) code. The cortical recording was bandpass filtered between 1000 and 2000 Hz with a first-order Butterworth filter. Then a negative threshold and two windows, one each to capture the trough and the peak of the spike waveform, were manually chosen. All traces crossing the threshold and through the two windows was denoted as a spike.

Coherence measurements

Magnitude-squared coherence was used in Chapters 1, 2, and 5 to calculate synchrony within the same frequencies of local field potentials:

$$C_{xy} = \frac{\left|P_{xy}(f)\right|^2}{P_{xx}(f)P_{yy}(f)} \qquad \text{Equation 0.1}$$

where C_{xy} is the coherence between x and y, $P_{xy}(f)$ is the cross-spectral density between x and y, and $P_{xx}(f)$ and $P_{yy}(f)$ are the spectral densities of x and y respectively. Coherence was calculated between all combinations of channel pairs at every 0.1 Hz intervals.

Funding sources

The work presented in this dissertation was supported by the National Institutes of Health (NS012542, RR00166, and NS118781) and the National Science Foundation (EEC-1028725).

Figures

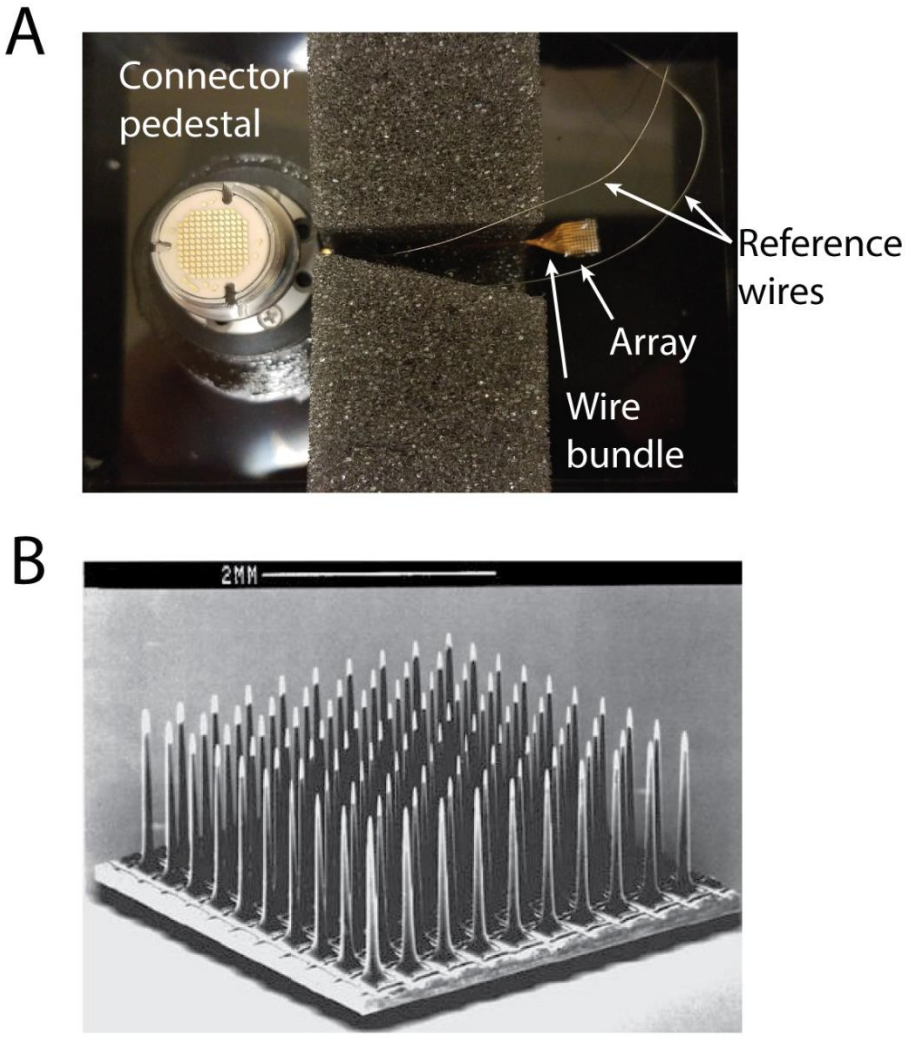

Figure 0.1 Utah array and connector pedestal

A. Picture of the Utah array module with the connector pedestal and reference wires. The pedestal was secured to the skull with skull screws and the reference wires inserted under or on top of the dura. **B.** Image of the Utah array electrodes, from S. J. Kim et al., 2006. Each electrode is 1.5 mm long with 400 μm interelectrode distance.

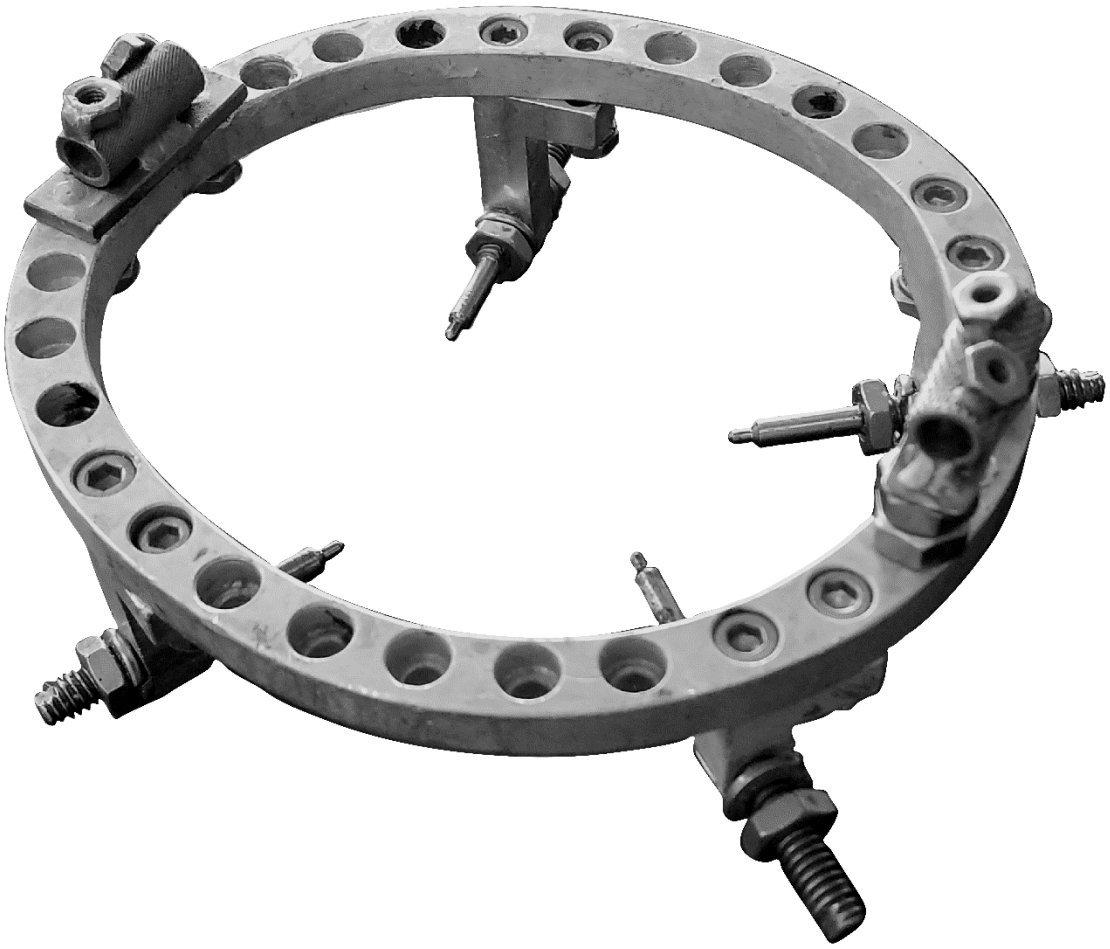

Figure 0.2 Halo implant

Example of the halo implant with the pins and supports for affixing the halo to the skull. Plexiglass rods were inserted into the two cylindrical brackets for head-fixing animals during task performance. A titanium can to house the Neurochip3 was affixed to the halo with nuts and bolts on one of the holes along the perimeter.

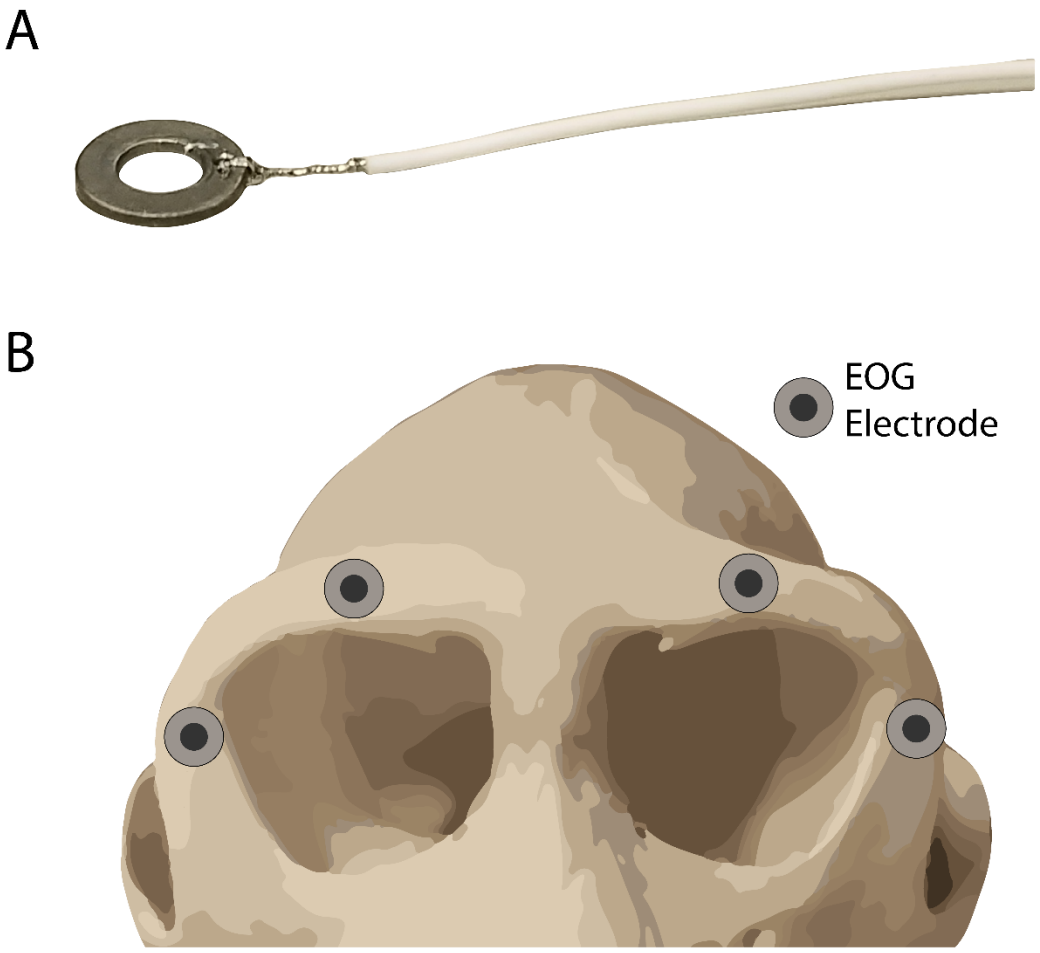

Figure 0.3 EOG implant

A) Electrode design. Each electrode consisted of a titanium washer with microwire threaded through a hole and soldered onto the washer. It was then fastened to the skull with a titanium skull screw. **B)** Electrode placement. An electrode was placed on each dorsal and lateral margins of both orbits. Recordings were performed differentially between a dorsal and a lateral electrode, not necessarily from same orbit as eye movements during REM sleep are binocular.

Chapter 1. Cortical stimulation paired with volitional unimanual movement affects interhemispheric communication

Abstract

Cortical stimulation (CS) of the motor cortex can cause excitability changes in both hemispheres, showing potential to be a technique for clinical rehabilitation of motor function. However, previous studies that have investigated the effects of delivering CS during movement typically focus on a single hemisphere. On the other hand, studies exploring interhemispheric interactions typically deliver CS at rest. We sought to bridge these two approaches by documenting the consequences of delivering CS to a single motor cortex during different phases of contralateral and ipsilateral limb movement, and simultaneously assessing changes in interactions within and between the hemispheres via local field potential (LFP) recordings. Three macaques were trained in a unimanual reaction time (RT) task and implanted with epidural or intracortical electrodes over bilateral motor cortices. During a given session CS was delivered to one hemisphere with respect to movements of either the contralateral or ipsilateral limb. Stimulation delivered before contralateral limb movement onset shortened the contralateral limb RT. In contrast, stimulation delivered after the end of contralateral movement increased contralateral RT but decreased ipsilateral RT. Stimulation delivered before ipsilateral limb movement decreased ipsilateral RT. All other stimulus conditions as well as random stimulation and periodic stimulation did not have consistently significant effects on either limb. Simultaneous LFP recordings from one animal revealed correlations between changes in interhemispheric alpha band coherence and changes in RT, suggesting that alpha activity may be indicative of interhemispheric communication. These results show that changes caused by CS to the functional coupling within and between precentral cortices is contingent on the timing of CS relative to movement.

Introduction

Cortical stimulation (CS) delivered during different phases of movement has been shown to affect motor function (Bütefisch et al., 2004; Edwardson et al., 2015; Pascual-Leone et al., 1992; Thabit et al., 2010). However, these studies often have limited timing of stimulation and examine one limb and the contralateral hemisphere in isolation. Although limb movements are predominantly driven by the contralateral motor cortex, entirely unilateral movements elicit correlated activity in the ipsilateral hemisphere (Cardoso et al., 2001; Donchin et al., 1998; Tanji et al., 1988). Evidence shows that the motor cortex recruits transcallosal networks that primarily evoke interhemispheric inhibition (IHI) in homologous regions of the contralateral motor cortex (Cincotta & Ziemann, 2008; Ferbert et al., 1992; Hübers et al., 2008).

IHI has been directly demonstrated with transcranial magnetic stimulation (TMS) using a paired-pulse paradigm. A test stimulus following a conditioning stimulus of the contralateral hemisphere with a 6-15 ms delay results in depressed motor evoked potentials (MEPs) (Daskalakis et al., 2002; Di Lazzaro et al., 1999; Ferbert et al., 1992). The interstimulus interval (ISI) between the conditioning and test stimulus affects the strength of IHI; ISIs of 3-5 ms can even produce facilitation of the MEPs (Ferbert et al., 1992; Hanajima et al., 2001). Similar to the paired-pulse paradigms, stimulation of the ipsilateral M1 during voluntary movements attenuates the electromyographic (EMG) activity of the moving limb, termed the ipsilateral silent period (iSP) (Cincotta & Ziemann, 2008; Ferbert et al., 1992; Giovannelli et al., 2009). IHI is additionally modulated by various attributes of the motor output, such as the finesse of movements and contraction strength (Kuo et al., 2017; Morishita et al., 2012; Perez & Cohen, 2008). Further findings document complex interactions of IHI with various intracortical inhibitory circuits in the motor cortex (Chen et al., 2003; Daskalakis et al., 2002).

These studies indicate the potential impact of IHI on cortical activity throughout unilateral movements (Figure 1.1). However, the associated temporal dynamics are not well understood because paired-pulse paradigms are typically performed at rest and iSP experiments typically deliver stimulation during tonic contraction. The effects of stimuli delivered before, during, and after a brief unilateral movement remain to be compared to determine how stimulation and interhemispheric interactions affect preparation and execution of movements. Additionally, the changes caused by stimulation are usually considered on a trial-by-trial basis without regard for possible prolonged effects. Another open question is how long the effects of a single stimulus last.

In addition, despite extensive research on the behavioral effects of IHI in M1, there have been surprisingly few relevant neural recordings. Different frequency bands of local field potentials (LFPs) exhibit unique modulation throughout movement planning, execution, and termination, and are thought to reflect underlying excitatory and inhibitory circuitry (Baker et al., 1999; Engel et al., 2001; Murthy & Fetz, 1996a). In particular interest are the alpha band (8-12 Hz) (Hummel et al., 2002; Jensen & Mazaheri, 2010) and the beta band (15-30 Hz) (Engel & Fries, 2010; Heinrichs-Graham et al., 2017; Murthy & Fetz, 1996a) which have both been shown to be consistently modulated during visuomotor tasks and associated with top-down processing. Correlated changes in LFP bands and behavior induced by CS would shed light on the dynamics of IHI.

This study probed the temporal dynamics of unimanual movement and the relevance of interhemispheric interactions by delivering CS at different phases of a cued voluntary movement. Monkeys performed a unimanual reaction time (RT) task as we delivered electrical CS to one hemisphere during either contralateral or ipsilateral hand movements; stimuli were timed to

arrive during movement preparation, during movement execution, or after movement completion. We tracked the RT of both limbs throughout the experiment and found that RT of the trigger limb (tRT) decreases if the stimulation is delivered before movement, and tRT decreases but the RT of the non-trigger limb (ntRT) increases if the stimulation is delivered after the movement of the contralateral limb. Additionally, we simultaneously recorded LFPs from the motor cortices of both hemispheres and performed coherence analysis to elucidate the neural correlates of interhemispheric communication. Changes in interhemispheric LFP coherence suggest that alpha oscillations may be a signature of interhemispheric communication.

Materials and Methods

Subjects and implants

Experiments were conducted with 3 male pigtail macaques (*Macaca nemestrina*; Monkeys I, Ka and U). Monkey Ka will be referred to as Monkey K within this chapter. Monkey I received 8 custom epidural electrodes bilaterally (Supplementary Figure 1.1A). Monkeys K and U were implanted with custom-made electrodes combining epidural and depth electrodes called "dual electrodes" (Supplementary Figure 1.1B, detailed in Seeman et al., 2017) over left and right sensorimotor cortex (U: 7 electrodes bilaterally, K: 2 electrodes bilaterally; Supplementary Figure 1.1A). Refer to General Methods for full details on implants and surgical procedures.

Behavior

During each session, the monkeys were seated in a primate chair facing a monitor (Figure 1.2A) and 3-axis accelerometers were affixed to the dorsum of each hand. The vertical position of two cursors on the screen were controlled by the z-axis of each accelerometer (rectified and smoothed with a 50 ms boxcar filter). Each trial began with a 0.5 second delay, followed by target boxes at the bottom of the screen to cue the animal to hold at rest. After holding for 2-3 seconds, one of the target boxes moved up (the "GO" signal) to cue a quick, unilateral wrist extension to drive the associated cursor into the box within 0.85 seconds. When the cursor was held in the target for 0-200 ms while the other cursor stayed in the start box, an apple smoothie reward was delivered with an audio tone. Trials were randomly selected to be left or right limb and the task was performed throughout the experiment.

Cortical stimulation

Each stimulus consisted of a 10-pulse train delivered at 333 Hz. Pulses were negative leading with a 200 µs phase width. 200 µs phase width pulses have been shown to reliably activate

cortical circuitry and have also been used to induce plasticity in the primate cortex (Jackson et al., 2006; Logothetis et al., 2010). CS was bipolar, delivered between two adjacent electrodes for epidural electrodes (Monkey I) or between the surface and intracortical contacts of dual electrodes (Monkeys K and U). Current amplitude was determined daily as the lowest intensity to elicit movement in the contralateral limb as determined by the investigator using the accelerometer trace. The stimulated hemisphere was chosen randomly each session, and CS was triggered by either the contralateral limb (Contralateral CS experiments) or the ipsilateral limb (Ipsilateral CS experiments). The timing of CS for each session was determined randomly before each experiment and kept consistent throughout the session.

For Monkeys I and K, CS was delivered to 100% of the trigger trials during stimulation (e.g., 100% of contralateral trials in Contralateral CS experiments). However, the suprathreshold stimulation completely obscured LFPs in the stimulated hemisphere. To obtain artifact-free LFP recordings during stimulation, CS was delivered to only a random 50% of the trials for Monkey U (e.g., 50% of contralateral trials in Contralateral CS experiments). The data from Monkey U was used for all LFP analysis of the conditioning period (Cond epoch, see *Experimental design*).

Control experiments consisted of no stimulation, periodic stimulation, or randomly timed stimulation. There was no difference between baseline left and right limb RT, so all behavioral data was combined as RT of the limb with respect to the stimulated hemisphere. Thus, RTs during Contralateral CS, Ipsilateral CS, and randomly timed experiments are presented as the trigger limb RT (tRT) and non-trigger limb RT (ntRT). Data for Contralateral CS and control experiments are from all three monkeys and Ipsilateral CS experiments are from Monkeys K and U.

Experimental design

The timeline of an individual experimental session is depicted in Figure 1.2B. In each session the initial 500 trials were collected to characterize RT in the absence of CS (Pre epoch). We discarded the first 25 trials to avoid warm-up effects as the monkey settled into the task. After the Pre epoch, CS was initiated and continued for about 1000 trials (Cond epoch). At the end of conditioning, another 500 trials were collected (Post epoch) to determine the longevity of any induced changes. Each session lasted for 1.5-2.5 hours. One session was performed per day to prevent any effects from propagating between sessions. All changes in RT are shown as the difference between the RTs during the Cond or Post epoch and the median RT during the Pre epoch (ΔRT).

Movement onset was determined by threshold crossing of the smoothed rectified acceleration trace (see *Recordings and analysis*). The sessions were labeled according to the response phase during which stimuli were delivered relative to movement onset – preparatory phase, CS_{prep}: -300-0 ms; during movement, CS_{move}: 0-300 ms; after movement, CS_{relax}: 300-600 ms (Figure 1.2C, Supplementary Figure 1.2). We ensured a delay of 2-3 seconds between trials such that CS_{relax} could not be construed as CS_{prep} of the next trial.

Recordings and analysis

Behavioral data, including cursor position, target presentation time, and raw accelerometer signal, were recorded at a sampling rate of 1 kHz (National Instruments Multifunction I/O Device). During the task, cursor position was driven by accelerometer signals generated by each wrist (Figure 1.3A). RT was measured offline using the raw accelerometer signal processed in three steps: 1) band-pass filtered between 10 and 150 Hz, 2) rectified, and 3) low pass filtered at 5 Hz. We calculated a movement threshold as 1/6 the peak of the median response over the last

600ms from trial completion as this ensured we did not detect the stimulus induced movement as movement onset (Supplementary Figure 1.3). RT was defined as the time between the target presentation (GO signal) and the threshold crossing of the processed accelerometer response (Figure 1.3A).

For each animal, LFPs were recorded single-ended between each individual electrode and a distant reference from the same hemisphere. Sampling rates were 9.6 kHz for Monkeys U and K, and 2.4 kHz for Monkey I (g.USBamp, g.tec medical engineering GmbH). LFP frequency bands were extracted using a third-order bandpass Butterworth filter (alpha: 8-12 Hz, beta: 15-30 Hz, low gamma: 30-50 Hz). Instantaneous amplitude for each filtered signal was calculated offline as the absolute value of the Hilbert transform. Spectral density and cross-spectral densities were calculated using the multitaper method (Chronux software package (Mitra et al., 2018; Mitra & Bokil, 2008)) with an overlapping moving window of 500 ms width and 25 ms steps. LFP traces in figures are the average across all electrodes in the designated hemisphere.

Magnitude-squared coherence was calculated by Equation 0.1. In all coherence analyses, x and y were signals from electrodes in different hemispheres. Coherence traces in figures are the average of all pairwise combinations of electrodes between the two hemispheres.

To assess whether there was a direction of connectivity in the LFP bands we calculated Granger causality (Granger, 1969). Granger causality uses an autoregressive model to determine whether a signal can predict another signal, which would imply a direction of information transfer between the two signals. We used the Multivariate Granger Causality (MVGC) toolbox (Barnett & Seth, 2014) to perform Granger causality analyses on all pairs of channels. LFPs from each channel were preprocessed with a comb notch filter at 60 Hz to ensure predictability did not arise from noise.

All offline analyses were conducted using custom MATLAB scripts.

Statistical Analysis

Each animal's performance fluctuated over time, possibly due to changes in motivation or fatigue. As a result, all statistical tests for RT and LFPs compared the changes in distributions from the no stimulation control experiments (e.g. a difference between the Pre epoch and the Cond epoch in a Contralateral CS experiment was considered significant if it was statistically distinct from the difference between the Pre epoch and the Cond epoch in control sessions). The Wilcoxon rank-sum test was used for all hypothesis testing due to the nonparametric nature of the data.

All box plots show the median and interquartile range. The notch represents:

$$m \pm \frac{1.57\, IQR}{\sqrt{n}} \qquad \text{Equation 1.1}$$

where m is the median, IQR is the interquartile range, and n is the number of samples. The full range (whiskers) and outliers have been omitted for clarity.

Results

Data

We recorded a total of 152 sessions from three monkeys (I: 67; K: 31; U: 54). The number of experimental conditions per animal is shown in Table 1.1. Figure 1.3 shows that our movement-detection algorithm successfully detected RTs in single trials. Variability in the trial-by-trial response is evident in the accelerometer snippets aligned with the GO signal (Figure 1.3B, left), and the onset of the earliest responses is evident at around 100-200 ms. Aligning the accelerometer traces with RT (Figure 1.3B, right) demonstrates that the monkeys' movements were consistent.

Contralateral CS

We conducted Contralateral CS experiments in all three monkeys to assess how stimulation of the movement-generating hemisphere affects RTs. Figure 1.4A depicts an example of behavior and stimulation relationship during the task when CS was triggered with right hand movements. We found that stimulation before movement (CS_{prep}, -300-0 ms from RT) significantly decreased the trigger limb RT (tRT) in all monkeys but did not significantly affect the non-trigger limb RT (ntRT) (Figure 1.4B). Surprisingly, stimulation delivered after the movements had concluded (CS_{relax}, 300-600 ms from RT) had pronounced effects in subsequent movements associated with both limbs; CS_{relax} significantly slowed tRT but sped up ntRT (Figure 1.4B). Stimulation during movement execution (CS_{move}, 0-300 ms from RT) did not produce a significant or consistent change in either limb's RT. Changes were denoted to be significantly different from control experiments if they were significant for all three monkeys.

Ipsilateral CS

To further investigate the role of the non-movement generating hemisphere during unilateral movement, we also tested whether CS delivered to the ipsilateral hemisphere could generate changes in RT. These experiments were conducted in Monkeys K and U. Figure 1.5A depicts an example behavior and stimulation relationship during the task when CS was triggered with left hand movements. Similar to Contralateral CS, we found that CS_{prep} significantly shortened tRT and CS_{move} did not produce a significant or consistent change in RTs of either limb (Figure 1.5B). CS_{relax} also did not produce any significant effects. Changes were denoted to be significantly different from control experiments if they were significant for both monkeys.

Persistence of changes in RT

Previous studies suggested that CS paired with movements or EMG signals can induce lasting directed plasticity (Bütefisch et al., 2004; Lucas & Fetz, 2013; Thabit et al., 2010). Thus, we tracked the changes in RT over time to determine whether the CS we delivered causes long-term changes. Figure 1.6A shows changes in RT for contra- and ipsilateral trials during the Post epoch for CS_{relax} experiments compared to the Pre epoch. We found that increases in tRT did not persist during the Post epoch but the decrease in ntRT remained consistent in Monkeys I and K. Monkey U did not have a change in the Post epoch, but the effects during the Cond epoch were smaller compared to the other two monkeys. All other stimulus conditions did not have a significant or consistent effect during the Post epoch.

In addition, we analyzed RT of trials without stimulation following a trial with stimulation to document the immediate duration of effects produced by CS. For Monkeys I and K there were no such trials for tRT during Contralateral CS_{prep} and tRT during Ipsilateral CS_{prep} since these trials were always stimulated. The stimulation for CS_{relax}, however, arrives after the completion of

behavior thus providing us with trials not directly affected by the stimulus. Figure 1.6B shows that the increase in tRT and decrease in ntRT induced by Contralateral CS_{relax} were just as evident in trials that occurred up to 4 trials after the most recent stimulation in Monkey I, and at least 1 trial after stimulation for Monkeys K and U.

Control Experiments

To control for changes in natural behavior over time we first tracked the animal's performance without delivering any CS. RT in both limbs slowed over time, becoming significantly slower during the "Post" epoch compared to the "Pre epoch." However, there was no difference between the limbs, which suggests a general behavioral change rather than a specific limb or hemisphere change (Figure 1.7A). To test whether stimulation itself caused any changes, we performed experiments with open-loop periodic stimulation at 0.1 to 0.2 Hz. Figure 1.7B shows that periodic stimulation delivered to one hemisphere during the Cond epoch resulted in large variability, but did not produce consistent changes in either RTs. Periodic stimulation also failed to produce any differential changes between the RTs.

We also performed control experiments to test whether it was necessary that CS was consistently timed to movements over time. Figure 1.7C shows results from Contralateral and Ipsilateral CS experiments in which stimulation for each trial was randomly delivered between -100 and 800 ms relative to the GO signal. These controls showed similar changes compared to the no stimulation condition (increasing RT during later epochs) for both Contralateral and Ipsilateral CS with greater variability.

Changes in cortical LFPs with movement

To examine bilateral cortical activation during unilateral movements and changes with stimulation, we recorded local field potentials (LFPs) of both hemispheres from each animal

throughout the experiment. Movement-related LFP data is from all three animals and LFP data during the Cond epoch is from Monkey U. Any trials with CS were discarded due to the stimulus artifact obscuring LFPs; as the changes in RT persisted several trials beyond the stimulated trial, the trials between stimulation reflects the effects of CS.

LFPs in primary motor cortex (M1) are consistently modulated with respect to movement in a frequency dependent manner (Figure 1.8). The raw LFP of each hemisphere around the estimated RT is complex and multiphasic, as shown in Figure 1.9. We separated the LFPs into different frequency bands (alpha 8-12 Hz, beta 15-30 Hz, and gamma 30-50 Hz) to document the modulation of each band (Figure 1.9). As commonly reported in intracortical recordings, we observed an increase in alpha and gamma amplitude during movement and a decrease in beta amplitude (Buzsaki & Wang, 2012; Canolty et al., 2012). These LFP band dynamics also reflect MEG recordings in human sensorimotor cortex during cued movements; especially notable are the desynchronization of the beta band during movement onset and its subsequent rebound after movement termination (Bardouille & Bailey, 2019; Cheyne, 2013). Ipsilateral movements generated similar features but with lower amplitude compared to contralateral movements.

We also calculated the change in magnitude-squared coherence of all bilateral pair-wise combinations of sites between the two hemispheres (Figure 1.9). Alpha coherence peaks at the onset of movement, similar to alpha amplitude. Beta coherence drops during movement, likely due to desynchronization, although the change begins during movement preparation rather than movement onset. Gamma band coherence was inconsistent across trials and experiments, as gamma likely reflects much more local activity (Buzsáki et al., 2012; Buzsáki & Wang, 2012; Fries et al., 2007), and was therefore omitted from coherence analyses.

To document possible changes in LFPs unrelated to CS over the course of a session, we first tracked how these measures change throughout no stimulation control experiments to document confounding factors such as motivation, fatigue, or attention (Figure 1.10A). The average amplitude of each frequency band was significantly higher during the Pre epoch, perhaps because the animal performed more exaggerated movements before learning to efficiently move the minimal amount for the task, as well as a possible drop in motivation over time (Figure 1.10B). Alpha and beta coherence were also higher in the Pre epoch, also possibly related to the larger movements. To account for these changes, all following LFP analyses are performed with respect to the baseline changes observed in control experiments.

CS modulates interhemispheric alpha coherence

We tracked changes in amplitudes and coherence of alpha and beta band LFP to determine neural correlates of interhemispheric communication. The instantaneous amplitudes of alpha and beta band LFP during contralateral or ipsilateral trials in CS experiments are shown in Supplementary Figure 1.4 and Supplementary Figure 1.5. A large change observed in LFP bands was the decrease in post-movement beta rebound (PMBR), thought to indicate motor termination (Heinrichs-Graham et al., 2017; Pfurtscheller et al., 1996). However, the changes were consistent across stimulus conditions and PMBR has been shown to decrease with lower force, lower rate of force development, and slower termination of movement (Fry et al., 2016; Heinrichs-Graham et al., 2017). Therefore, the changes in PMBR were likely due to the animal's movements becoming smaller over time as they became more accurate and fatigued as shown in Figure 1.10B. Other than the PMBR, there were no clear or consistent differences in LFP band amplitudes during any CS condition compared to control experiments. Ipsilateral CS experiments also showed no significant differences in instantaneous amplitudes of alpha and beta band LFP.

Beta coherence between hemispheres also did not show any consistent changes, but alpha coherence had clear differences from the control (Supplementary Figure 1.6 and Supplementary Figure 1.7). Alpha coherence during trigger trials of Contralateral CS_{prep} was noticeably diminished during the Cond epoch as well as during non-trigger trials of CS_{relax} (Figure 1.11). To quantify their differences, we integrated alpha coherence in a window of -200 ms to 200 ms from RT to capture the peak amplitude. The decreases in alpha coherence during trigger trials of CS_{prep} and non-trigger trials of CS_{relax} were statistically significant, possibly related to the decrease in RT during those conditions (Figure 1.12A). Ipsilateral CS experiments also had a significant decrease in alpha coherence that was associated with a decrease in tRT during CS_{prep} (Figure 1.12b).

There were statistically significant changes in alpha coherence during CS_{move} – a decrease during non-trigger trials of Contralateral CS experiments and a decrease during non-trigger trials of Ipsilateral CS experiments – that were not reflected in their respective RT. However, these changes had a relatively high p-value, and thus could be due to single-animal variability. Comparisons between the change in alpha coherence and change in RT for all experimental conditions and trial types with a significant change in alpha coherence did not reveal a significant correlation (Supplementary Figure 1.8).

As IHI is directed from one hemisphere to another, we additionally explored pairwise Granger causality using the MVGC toolbox (Barnett & Seth, 2014). For baseline analysis we used the same window as the alpha coherence peak (-200 to 200 ms from RT) in trials within the Pre epoch during all conditioning experiments for all channel pairs (Supplementary Figure 1.9). Only 3 out of 32 channels had predictability towards more than one channel on the other hemisphere, and significantly so ($p<0.05$) in less than 10 out of 42 experiments. In contrast, at least 27 out of

32 channels had significant predictability ($p<0.05$) within the same hemisphere for at least 10 experiments. We did not pursue Granger causality any further due to the lack of consistent directionality between hemispheres.

Discussion

Our main finding was that suprathreshold CS delivered to one motor cortex can affect the RT of both limbs, depending on the timing of CS relative to voluntary unilateral movement. We observed that CS can cause distinct changes in RT: 1) Contralateral CS_{prep} decreased tRT, 2) Ipsilateral CS_{prep} also decreased tRT, and 3) Contralateral CS_{relax} increased tRT but 4) decreased ntRT. Figure 1.13 shows proposed mechanistic changes induced by each stimulus condition. These changes persisted for at least 4 trials (~10 seconds) after the most recent stimulus. The most durable change was the decrease in ntRT following Contralateral CS_{relax}, which remained significant during the ~20-minute Post epoch, highlighting the significance of the ipsilateral hemisphere to unilateral movement. The lack of consistent changes in periodic or random stimulation control experiments suggests that changes in RT reflect the effect of consistently timing stimulation to movement throughout the Cond epoch.

We simultaneously recorded cortical LFPs to examine neural dynamics related to movement and how they may be modulated by CS. In control experiments without CS, trial-averaged LFP band amplitude and interhemispheric coherence decreased over time, consistent with the natural increase in RT, perhaps due to increased efficiency in movements or a decrease in motivation. In both contralateral and ipsilateral CS experiments there was a significant change in alpha coherence between the hemispheres that was strongly correlated with decreases in RT, suggesting that alpha may be indicative of IHI.

Stimulation delivered before contralateral movement decreased contralateral limb RT

The suprathreshold stimulation used in our study induces a physical twitch in the animal's contralateral hand. This movement can be processed as a tactile stimulus, and, since response to tactile stimuli is faster than response to visual stimuli, it may thus have led to a faster RT (Chan

& Ng, 2012; Godlove et al., 2014). However, this is unlikely as studies have shown response to electrical microstimulation of the cortex to be significantly slower than response to tactile stimulation in both humans and non-human primates (Caldwell et al., 2019; Godlove et al., 2014).

Suprathreshold stimulus induced movement can also activate cortico-spinal reafferent sensorimotor loops that could lead to changes in RT. Thabit et al. similarly showed a reduction in contralateral limb RT when suprathreshold TMS was delivered to the motor cortex, but also showed that the F-wave in the corresponding muscle generated by stimulation delivered to the peripheral nerve did not change (Thabit et al., 2010). Thus, our results are also likely due to changes in cortical excitability rather than changes in the spinal level.

The changes in cortical excitability could be induced by Hebbian-like potentiation. Activation of the motor cortex immediately before activation of the corresponding periphery has been shown to induce long-term potentiation (LTP) in paired-association stimulation (PAS) studies (Suppa et al., 2017; Wolters et al., 2003). Thabit et al. also showed that the motor-evoked potential (MEP) increased with the reduction in RT (Thabit et al., 2010). However, such a broad increase in excitability of the cortex would suggest a simultaneous change in IHI, and thus the ipsilateral limb RT, which was not observed. We propose that the stimulation interrupted the inhibitory network responsible for mediating IHI from the contralateral hemisphere (Figure 1.13, 1). IHI is highest immediately before movement onset (Beaulé et al., 2012; Duque et al., 2007), and electrical CS has been shown to interrupt cortico-cortical signaling (Griffin et al., 2011; Logothetis et al., 2010). As a result, CS could lead to the disinhibition of the cortex and subsequent faster RT. Additional experiments with subthreshold stimulation could potentially confirm these mechanisms.

Stimulation delivered before ipsilateral movement decreased ipsilateral limb RT

Similar to stimulation delivered before contralateral movement, the reduction in RT cannot be attributed to the animal responding to the induced twitch. In addition, reafferent sensorimotor loops do not play a role as the changes were observed in the ipsilateral limb. As the major pathway between the motor cortex and the ipsilateral limb is the transcallosal inhibitory pathway, the stimulation most likely interrupted the ongoing IHI from the stimulated hemisphere to the contralateral hemisphere, thus disinhibiting the contralateral cortex and speeding up the ipsilateral limb RT (Figure 1.13, 2).

Stimulation delivered after contralateral movement increased contralateral limb RT but decreased ipsilateral limb RT

Paired associative stimulation (PAS) studies have shown that stimulation of the periphery before stimulation of the cortex can induce long-term depression (LTD), thought to be mediated via Hebbian-like mechanisms (Suppa et al., 2017; Wolters et al., 2003). Thabit et al. delivered suprathreshold TMS to the motor cortex after unilateral voluntary movement of the contralateral limb which decreased subsequent MEP amplitudes, also likely through Hebbian-like LTD (Thabit et al., 2010). Our result showing that Contralateral CS_{relax} increased contralateral RT corroborates these studies – stimulation of the movement-generating hemisphere following voluntary movement increased the RT, likely due to decreased excitability of the stimulated cortex (Figure 1.13, 3). In addition, during Contralateral CS_{relax} we observed a simultaneous decrease in ipsilateral RT, possibly due to the decreased excitability leading to disinhibition of IHI (Figure 1.13, 4). Ipsilateral CS_{relax} did not change either RTs, further highlighting the significance of timing CS to specific limb movements.

Alpha band LFP and IHI

Alpha activity has been shown to be inversely related to attention during visuomotor tasks (Jensen & Mazaheri, 2010; Klimesch et al., 2007; Rilk et al., 2011) and is commonly thought of as a resting rhythm. Alpha coherence has similarly been demonstrated to be a measure of reduced cortical activation. When measured during applications of repetitive TMS (rTMS), low-frequency rTMS was shown to induce inhibition and high-frequency stimulation to induce excitation, with corresponding increases and decreases in intra- and interhemispheric alpha coherence (Strens et al., 2002; Thut & Pascual-Leone, 2010). Furthermore, one study applied rTMS in an IHI experiment using a paired-pulse paradigm (Gilio et al., 2003). They demonstrated a decrease in IHI from the stimulated to the non-stimulated hemisphere during delivery of low-frequency rTMS, likely due to disinhibition, though they did not report on relevant LFP measures.

During volitional movement, stimulus-induced IHI of the movement-generating hemisphere has been shown to be highest just before movement but released at movement onset (Beaulé et al., 2012; Duque et al., 2007). The temporal dynamics of interhemispheric alpha coherence in our experiments match these findings; coherence began to rise around the Go signal, reached a peak at movement onset, and decayed during movement execution (Figure 1.9). Changes in RT that were possibly from modulations of IHI (tRT during Contralateral CS_{prep}, tRT during Ipsilateral CS_{prep}, and ntRT during Contralateral CS_{relax}) were associated with corresponding decreases in their alpha coherence magnitude. The increase in tRT during Contralateral CS_{relax} that is likely due to LTD did not have a significant corresponding change in alpha coherence.

Variations in coherence can often be epiphenomena of changes in overt oscillations (Buzsáki & Schomburg, 2015; Srinath & Ray, 2014), we saw no significant changes in alpha amplitude.

Besides changes in amplitude, correlation in amplitude can also greatly affect coherence values (Srinath & Ray, 2014), but we saw very low correlation coefficients (around 0.05) of alpha amplitudes between the hemispheres during movement. Thus, alpha coherence is likely a reflection of changes in synchrony, illustrating interhemispheric alpha coherence as a potential measure of IHI. However, our LFP results during the Cond epoch are drawn from a single animal and further studies are warranted to confirm these findings.

In addition, we explored Granger causality using the MVGC toolbox (Barnett & Seth, 2014). Although we expected signals reflecting IHI to show significant directionality, Granger causality did not reveal any consistent relationships between hemispheres. This may be due to the fact that the time course of IHI is highly volatile, as evidenced by the different changes caused by different ISIs during paired stimulation experiments (Ferbert et al., 1992; Hanajima et al., 2001). Variations within the 400 ms window we tested may have caused difficulties in assessing significant directionality. Another possible explanation is that the frequency range reflecting IHI may be very limited as the only consistent changes in coherence we observed was in the alpha band.

Clinical relevance

Studies of stroke patients have found increased inhibition in the lesioned hemisphere, most likely due to compensatory processes that increase activity in the contralesional hemisphere leading to stronger IHI (Lewis & Perreault, 2007; Liepert et al., 2000; Murase et al., 2004). The mechanisms underlying this "IHI imbalance" has been found to predominantly reside in cortical circuitry rather than subcortical structures or pathways (Murase et al., 2004). IHI has also been shown to be especially modulated by movement in stroke patients (Boddington & Reynolds, 2017).

As a result, efforts towards motor recovery have been focused on reducing IHI using rTMS and transcranial direct current stimulation (tDCS) often used in conjunction with rehabilitation (Boddington & Reynolds, 2017). However, the optimal stimulation paradigms for greatest reduction of IHI and most effective recovery is still undetermined. Our experiments suggest that stimulation of the unaffected hemisphere delivered after voluntary movement of the contralesional limb may depress the cortex, thus disinhibiting the lesioned hemisphere for a potentially more effective motor rehabilitation paradigm.

Conclusions

In conclusion, electrical cortical stimulation delivered to one motor cortex during a unimanual task affected behavior dependent on the timing of stimulation relative to movement. Specifically, stimulation delivered before the contralateral or ipsilateral limb movement sped up the corresponding limb in subsequent trials, likely due to the disruption of ongoing IHI. Stimulation delivered after the contralateral limb movement slowed down the contralateral limb due to STDP-like LTD but sped up the ipsilateral limb as the reduced excitability of the stimulated hemisphere led to the disinhibition of IHI. LFP analyses revealed decreases in interhemispheric alpha coherence during faster reaction times due to decreased IHI, highlighting alpha as a possible measure of interhemispheric communication.

Figures and Tables

Table 1.1 Number of experiments by type

Number of experiment types per animal. Note Monkey I only had 3 Ipsilateral CS experiments and is hence omitted from Ipsilateral CS analyses.

Monkey	Ipsilateral CS	Contralateral CS	No stim	Non-time-locked stim
I	3	41	10	13 (periodic)
K	14	14	3	0
U	20 (50% CS)	22 (50% CS)	4	6 (random)

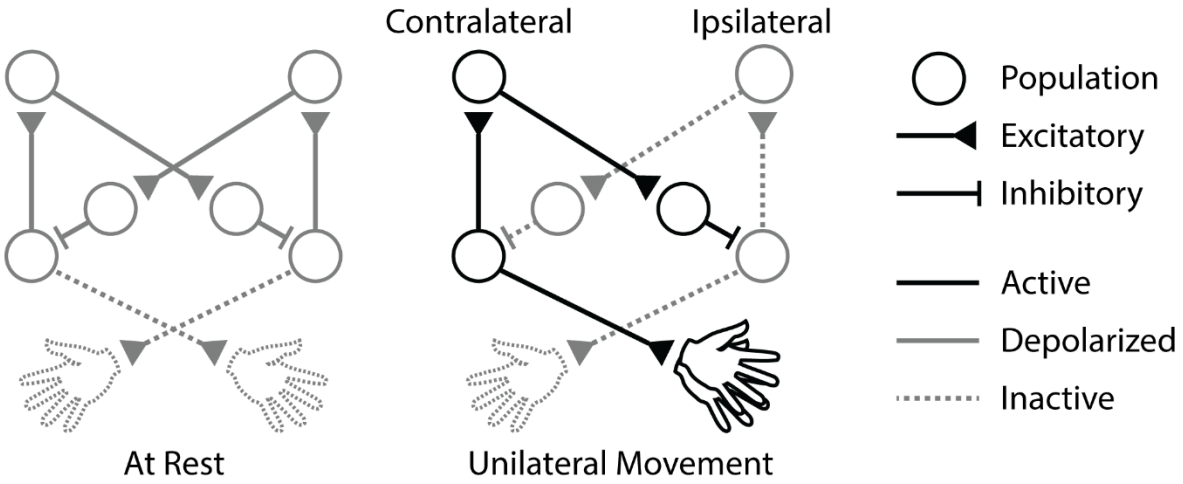

Figure 1.1 Cortical circuitry during unilateral movement

When the animal is at rest, baseline interhemispheric inhibition (IHI) between the motor cortices is depolarized. Unilateral movement activates the contralateral cortex, triggering IHI to the ipsilateral cortex and disinhibiting itself.

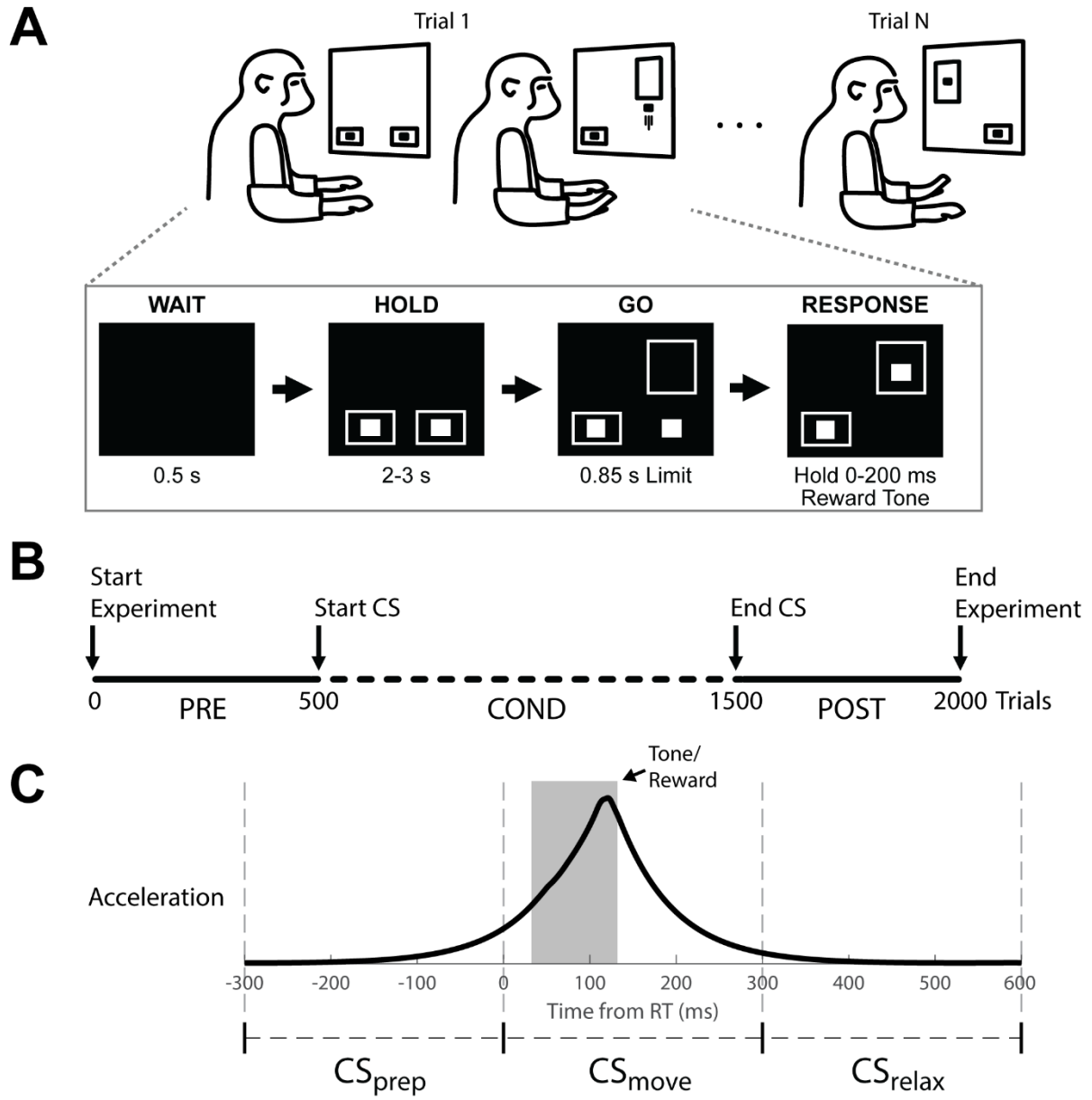

Figure 1.2 Behavioral task, experimental timeline, and stimulus timing

(A) Top: Monkeys were cued to move a cursor into a target box by rapid wrist extension. Trials were randomly selected to be left or right. Bottom: example right hand trial. **(B)** Experimental timeline showing trials before (Pre), during (Cond) and after (Post) cortical stimulation (CS). The task was performed continuously throughout the experiment. **(C)** Stimulus timings are shown with respect to the average accelerometer trace across trials. The stimulus timing was split into three groups relative to movement onset (RT at 0): CS_{prep}, CS_{move}, and CS_{relax}.

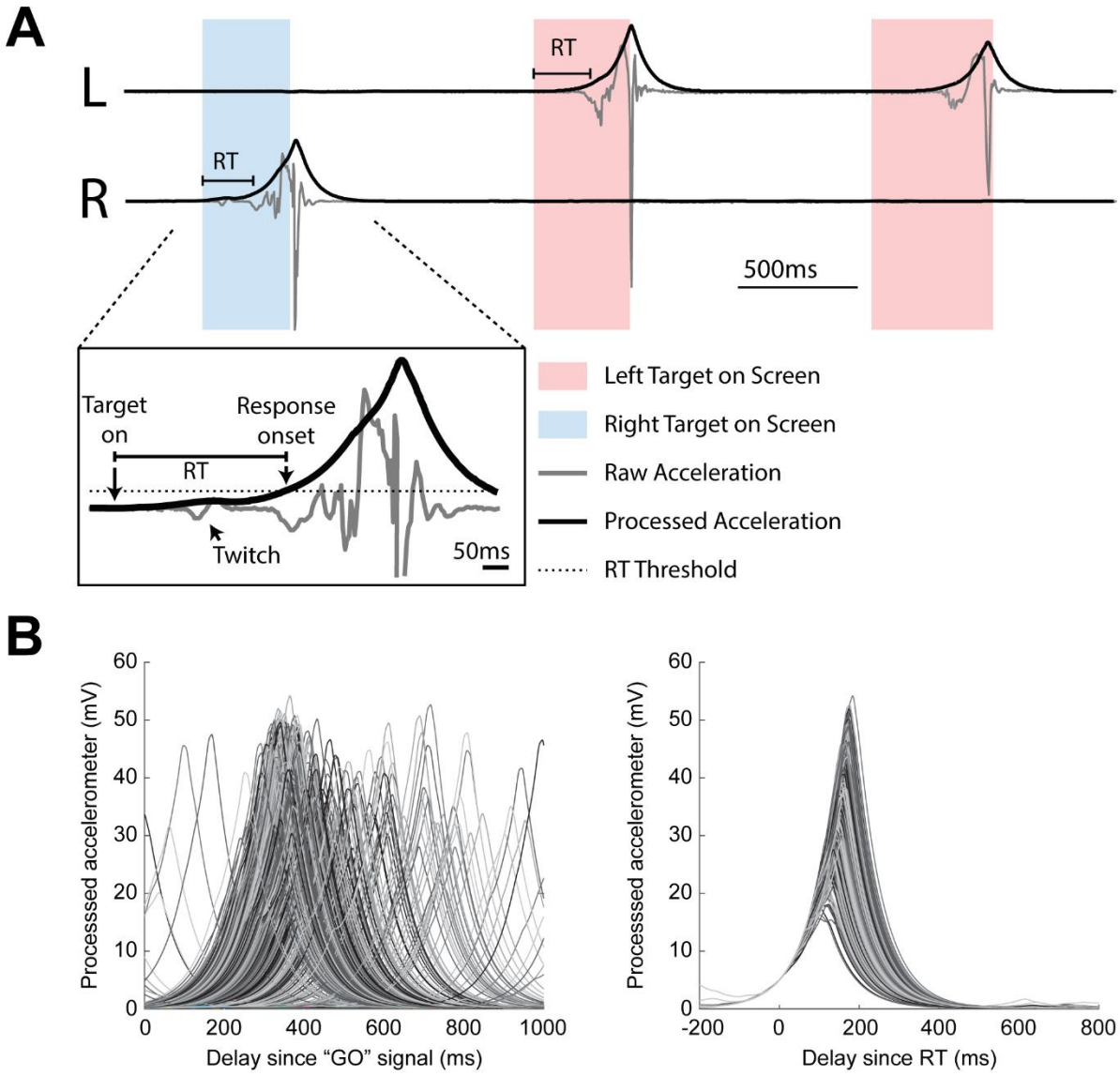

Figure 1.3 Estimating reaction time

(A) Three example trials. Boxes indicate when the monkey was cued to move left (red box) or right (blue box). Responses were required to be unilateral. Inset: identification of reaction time (RT). Raw accelerometer signal (gray) is transformed into a processed signal (black) for RT estimation using a threshold (dotted line). Note the stimulus induced twitch lies below the threshold. **(B)** Aligned processed accelerometer traces. Left: aligned by GO signal. Right: aligned by calculated RT.

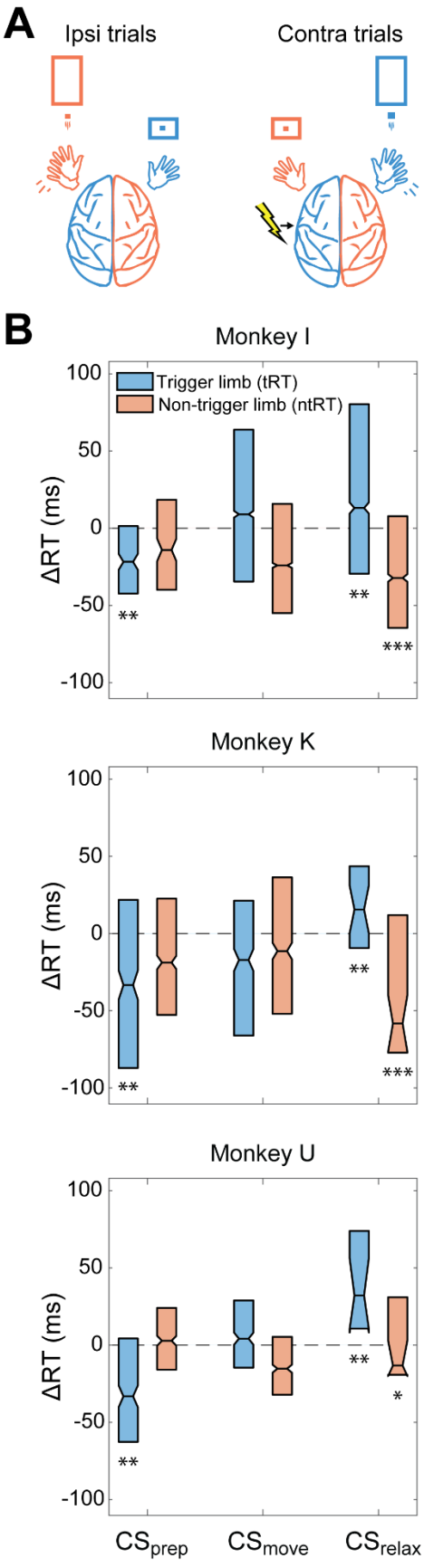

Figure 1.4 Contralateral CS

(A) Example illustration of Contralateral CS and task relationship for left hemispheric stimulation. **(B)** Difference between RTs for trials during the Cond epoch and the median RT of the Pre epoch for each monkey (ΔRT). CS_{prep} significantly decreased tRT in all monkeys. CS_{relax} experiments produced bilateral effects, significantly slowing down tRT and speeding up ntRT. Significance is calculated in comparison with the no stimulation control experiments and only denoted if consistent across all animals (∗: $p<0.01$; ∗∗ : $p<0.001$; ∗ ∗ : $p<0.0001$).

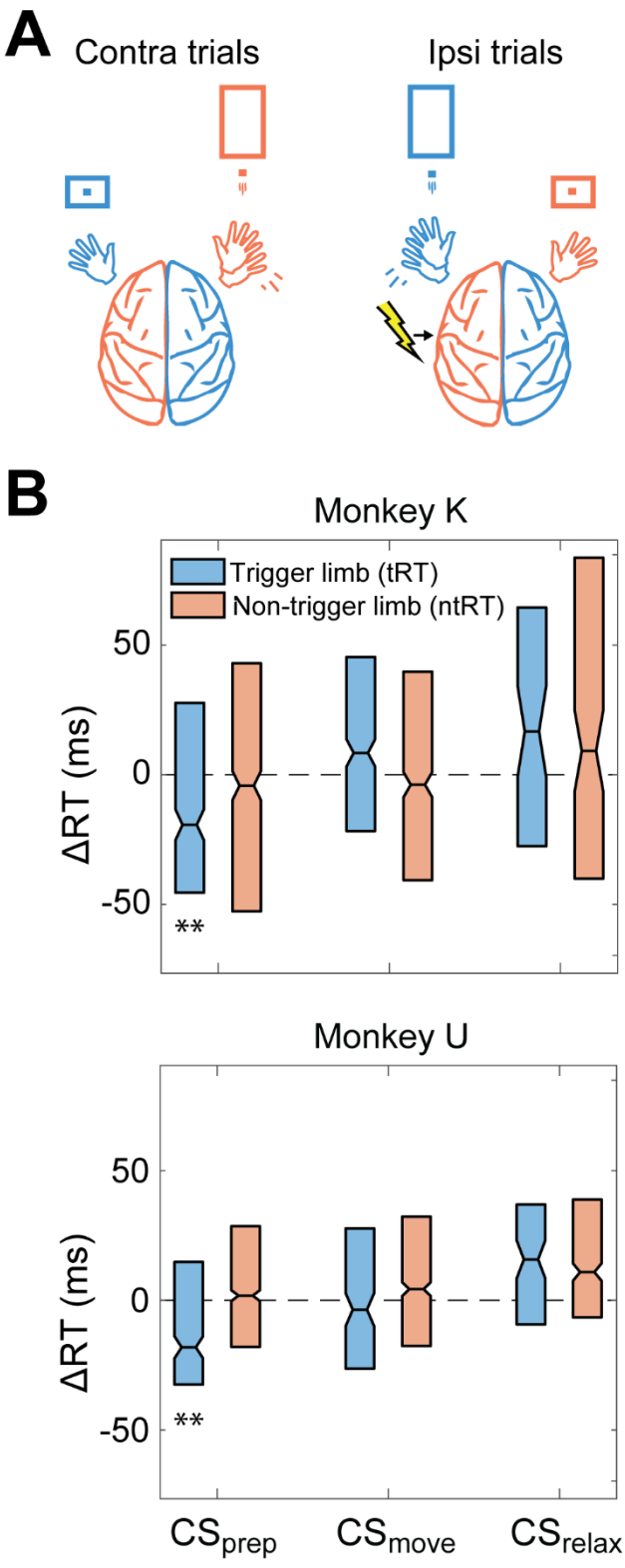

Figure 1.5 Ipsilateral CS

(A) Example illustration of Ipsilateral CS and task relationship for left hemispheric stimulation. **(B)** Difference between RTs for trials during the Cond epoch and the median RT of the Pre epoch for each monkey. CS_{prep} decreased tRT in both monkeys. Significance is calculated in comparison with the no stimulation control experiments and only denoted if consistent across both animals ($*$ $*$: $p<0.001$).

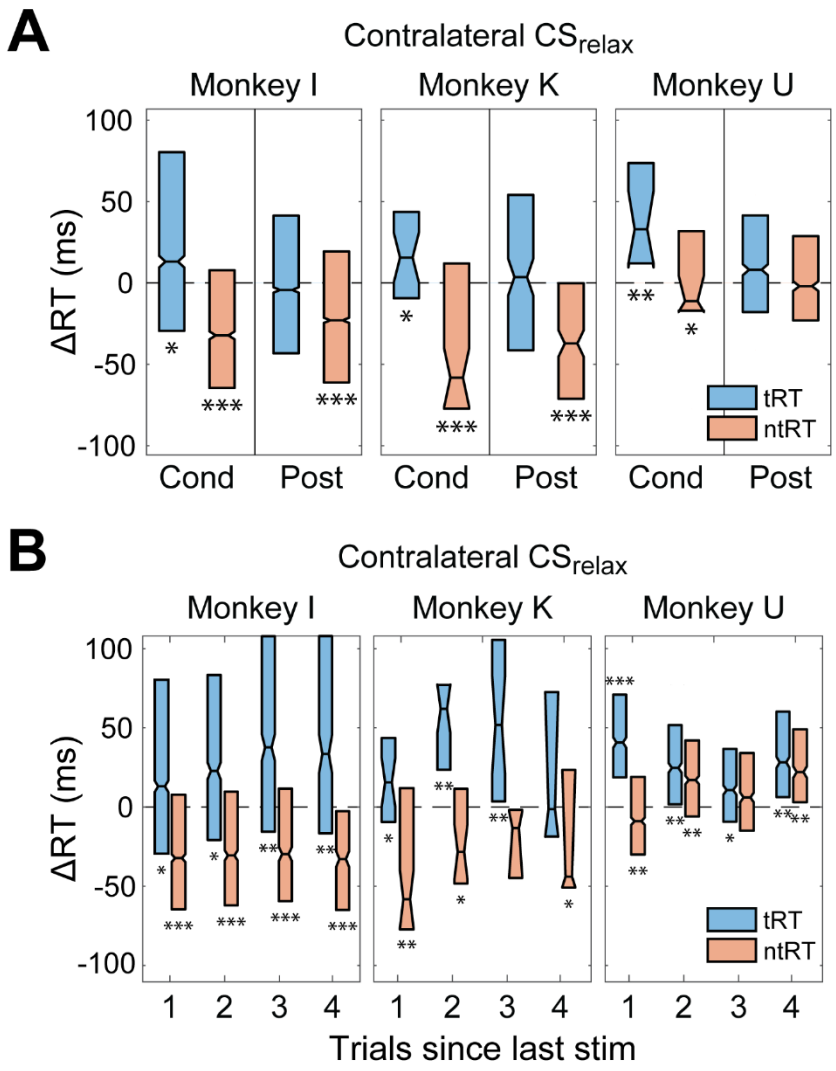

Figure 1.6 Persistence of changes in RT

(A) RT changes of trials ipsilateral to the stimulated hemisphere stayed faster during Post epoch of CS_{relax} experiments in Monkeys I and K. Increases in CRT did not persist (∗ : p<0.01; ∗∗ : p<0.001; ∗∗∗ : p<0.001). **(B)** Effects of CS were persistent in trials arriving long after CS was delivered during experiments with consistently timed CS. (∗ : p<0.01; ∗∗ : p<0.001; ∗∗∗ : p<0.001).

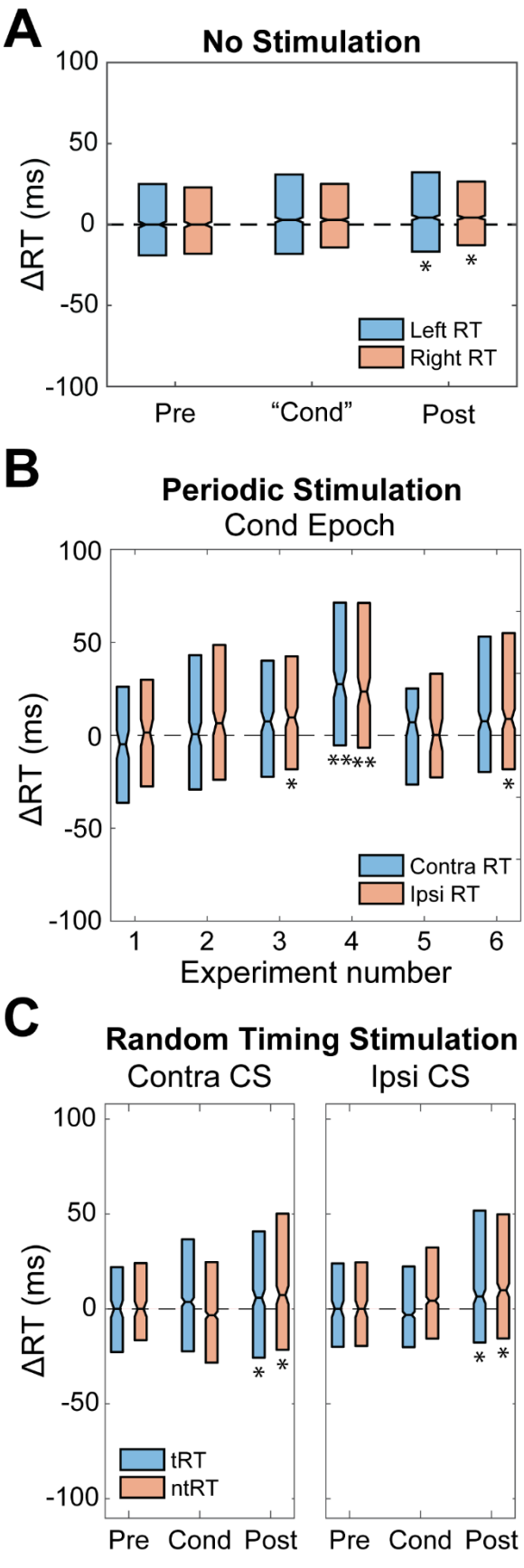

Figure 1.7 Control Experiments

(A) RT relative to the Pre epoch when delivering no stimulation during the "Cond" epoch. The "Cond" epoch was determined using the number of trials. RT slows over time for both limbs and becomes significant by the Post epoch. There was no significant difference between the two limbs. Significance is compared to zero (∗: $p<0.01$). **(B)** Periodic stimulation delivered to one hemisphere did not have consistent changes or produce differential effects in RT associated with either hand. Plots show six different experiments with Monkey I and corresponding change in RT. Contra and Ipsi RT are with respect to the stimulated hemisphere. Significance is compared to zero (∗: $p<0.01$; ∗∗ : $p<0.001$). **(C)** Random stimulus timing delivered to both the movement generating (Contra CS) and non-movement generating (Ipsi CS) hemisphere. There is greater variability in RT compared to the no stimulation condition, but median changes were similar. Significance is compared to zero (∗: $p<0.01$).

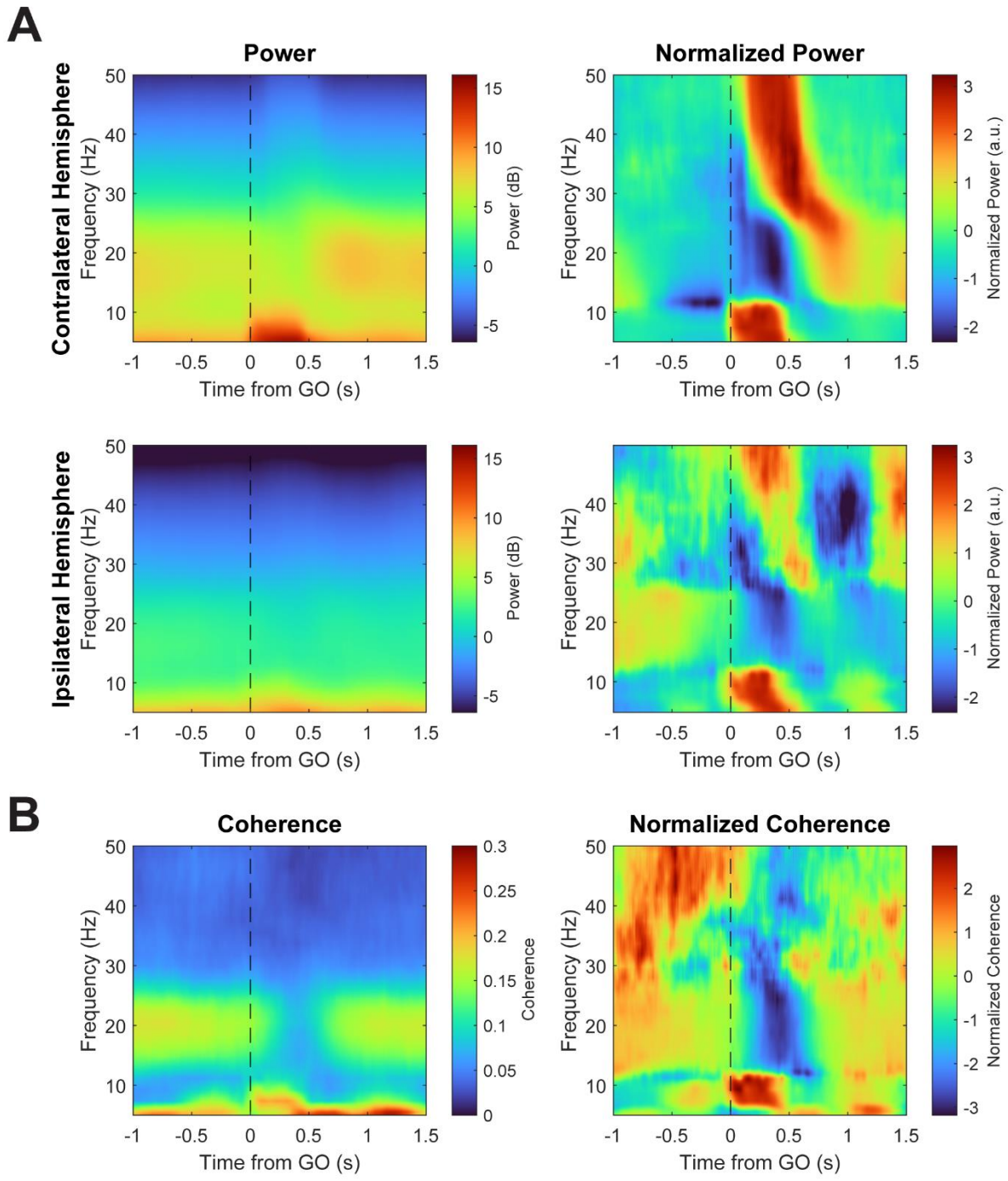

Figure 1.8 Spectral power and coherence during a trial

(A) Spectral power during behavior with respect to the GO signal of the contralateral (top) and ipsilateral hemispheres (bottom) during a Pre epoch, averaged across all three monkeys. The right panels show the spectra normalized across time for each frequency (z-score) to highlight frequency-specific changes over time. **(B)** Coherence between the two hemispheres with respect to the GO signal. The right panel shows coherence normalized across time for each frequency.

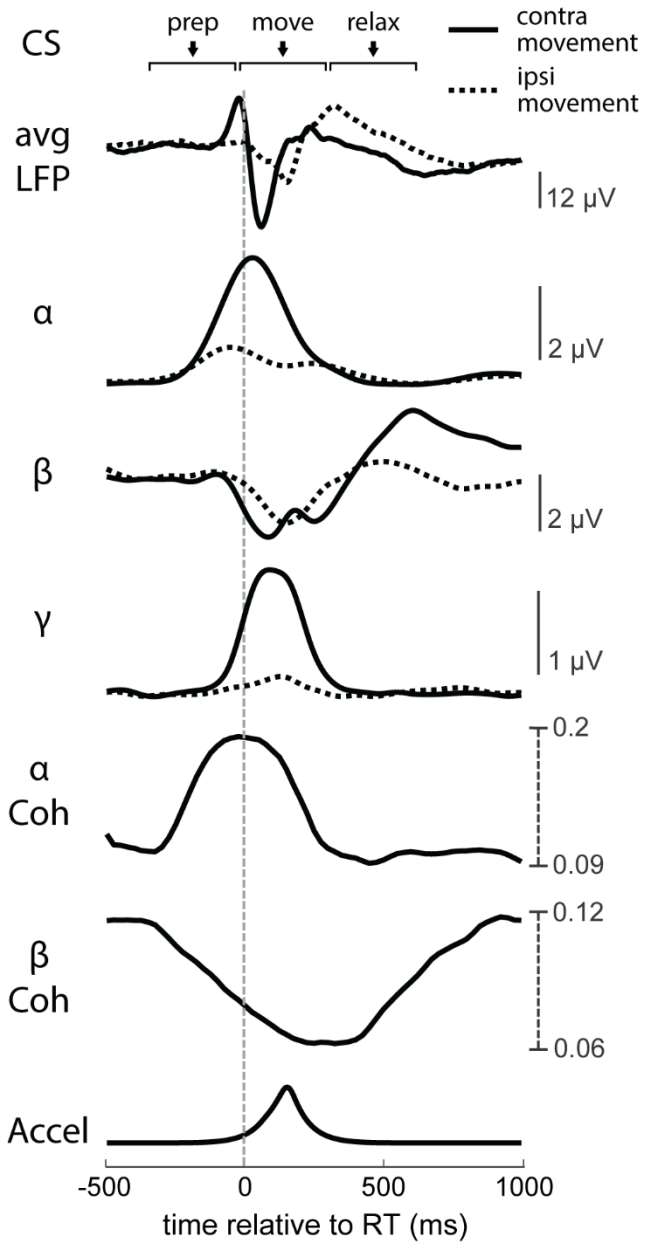

Figure 1.9 Neural dynamics of movement

RT-averaged raw LFP, instantaneous alpha (α), beta (β), and low gamma (γ) intrahemispheric amplitudes, interhemispheric α and β coherence (Coh), and processed accelerometer signal (Accel). Solid lines depict the contralateral hemisphere's trial-triggered averages, and dashed lines depict the ipsilateral hemisphere's trial-triggered averages.

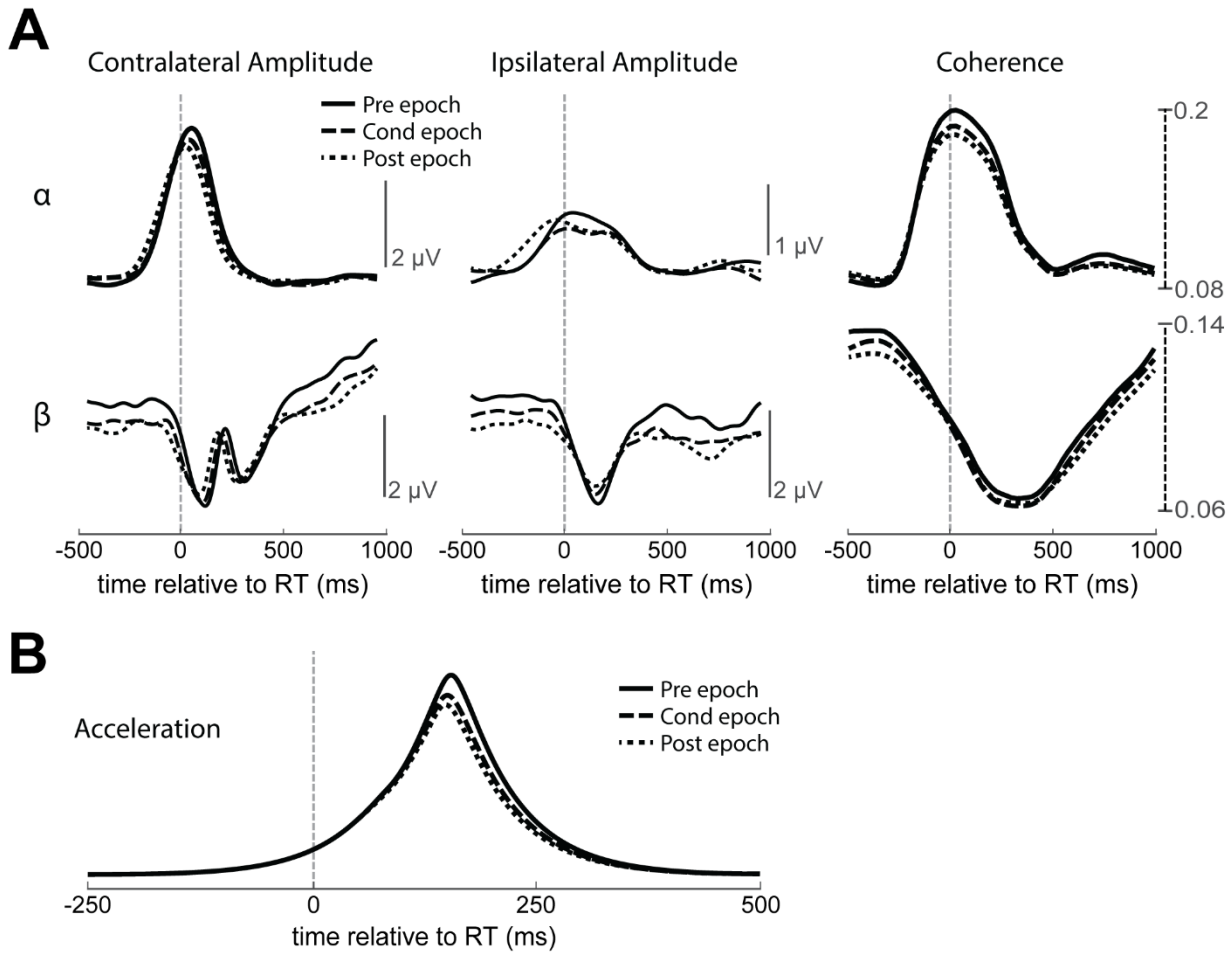

Figure 1.10 Change in amplitude and coherence over time with no stimulation

(A) RT-aligned alpha (α, top) and beta (β, bottom) intrahemispheric amplitude and interhemispheric coherence for all three epochs of no stimulation control experiments. Contralateral and ipsilateral refers to the hemisphere relative to movement. **(B)** Accelerometer traces showing larger movements during the Pre epoch compared to the Cond or Post epochs during no stimulation control experiments.

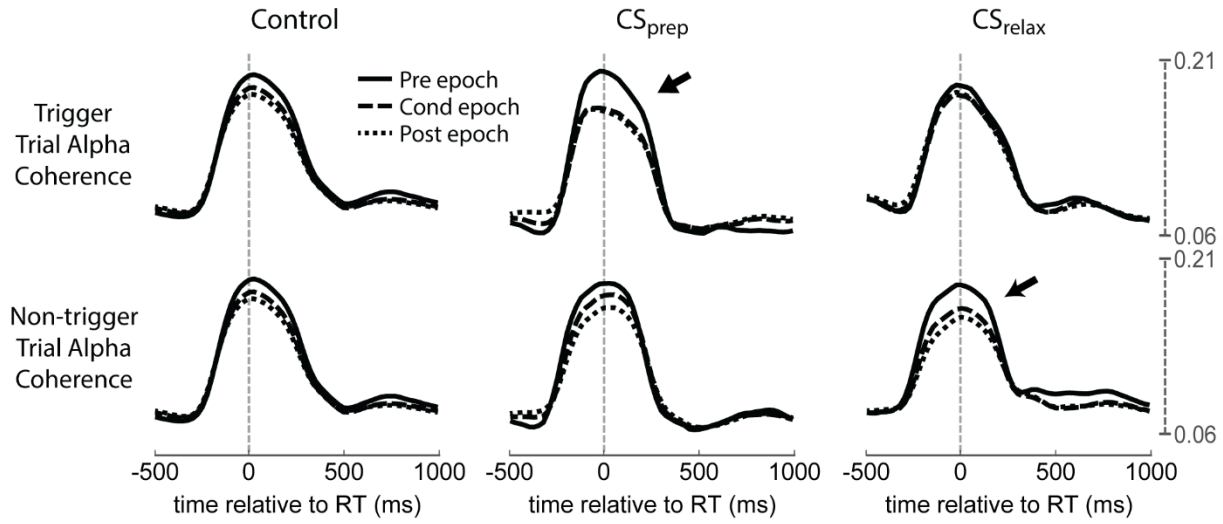

Figure 1.11 Coherence in Contralateral CS experiments

Coherence during each experimental epoch for CS_{prep} and CS_{relax}. Contralateral and ipsilateral refers to limb movement relative to the stimulated hemisphere. Notice the large decrease in contralateral alpha coherence during CS_{prep} and ipsilateral alpha during CS_{relax} (arrows); both RTs decreased during stimulation (Figure 3). CS_{move} did not produce any significant changes. See Supplementary Figure 5 for both alpha and beta coherence for all Contralateral CS conditions.

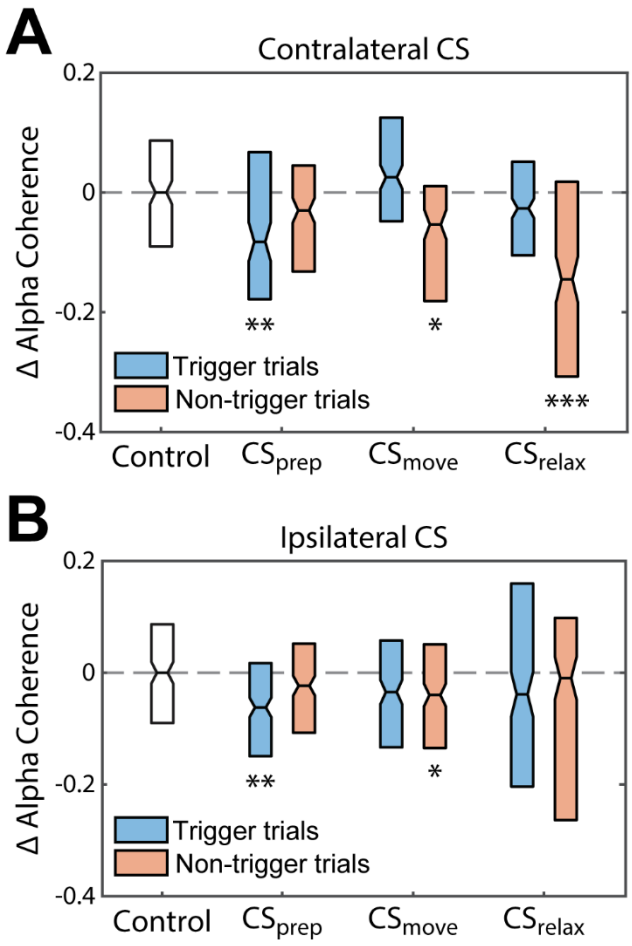

Figure 1.12 Alpha coherence reflects changes in RT

Normalized changes in the integrated interhemispheric alpha coherence peak from the Pre epoch to the Cond epoch (difference between the coherence in the Pre and Cond epochs divided by the coherence in the Pre epoch). The changes in alpha coherence reflect the changes in Monkey U's RT induced by each CS timing for **(A)** Contralateral CS and **(B)** Ipsilateral CS. Statistical testing compares the changes to the control experiment. ($*$: $p<0.01$, $**$ **:** $p<0.001$, $***$ **:** $p<0.0001$).

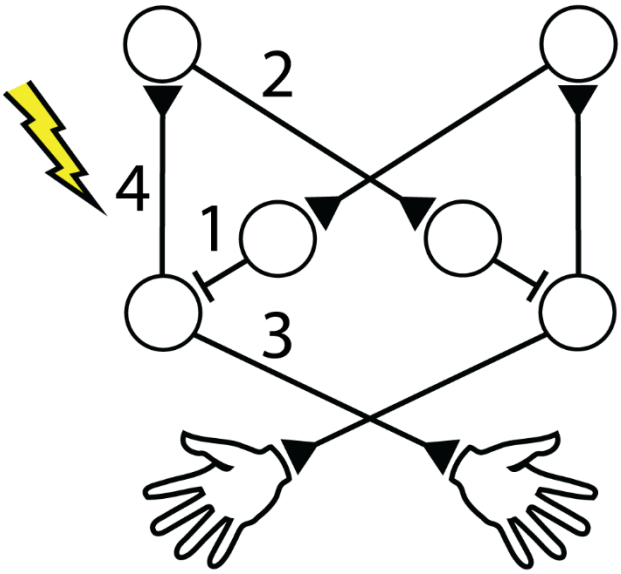

Figure 1.13 Cortical circuitry affected by stimulation

Intra- and interhemispheric circuitry involved in unilateral movement. Numbers identify proposed affected connections with left hemispheric stimulation for 1) decrease in tRT during Contralateral CS_{prep}, 2) decrease in tRT during Ipsilateral CS_{prep}, 3) increase in tRT after Contralateral CS_{relax}, and 4) decrease in ntRT after Contralateral CS_{relax}.

Chapter 2. Challenges of gamma-triggered stimulation for stimulus induced cortical plasticity

Abstract

Hebbian plasticity has been induced *in vivo* using spike-triggered stimulation or paired-stimulation paradigms through spike-timing dependent plasticity (STDP) mechanisms. However, they often require high current amplitudes or are dependent on specific tested sites; thus, a more robust method is required for effective translatable targeted plasticity. A previous study successfully produced bidirectional changes by delivering stimulation locked to specific phases of beta oscillations in the motor cortex (Zanos et al., 2018). We expanded upon the study by delivering stimulation phase-locked to gamma band local field potentials. Gamma LFP is reflective of local population activity, often generated through oscillating activity between excitatory and inhibitory circuitry, and single units have been shown to be phase-locked to the trough of gamma. As such, gamma band LFP may act as a proxy for population activity. Implementing gamma-triggered stimulation in vivo revealed several hurdles that must be overcome to properly assess the effects of stimulation. First, the stimulation itself produced a large gamma component leading to positive feedback loops. Second, the filters used for real-time signal processing introduced delays larger than an entire gamma cycle. Third, cortico-cortical evoked potentials (CCEPs), often used as a measure of connectivity between two cortical sites, changed due to both open-loop stimulation and no stimulation at all.

Introduction

Consistent oscillatory signals are often observed in LFPs, frequently classified into various frequency bands, which have been shown to be relevant to excitatory and/or inhibitory activity as well as behavior, cognition, and other higher order functions (Buzsáki & Draguhn, 2004; Cannon et al., 2014; Engel & Fries, 2010). Individual spikes are highly synchronized with these oscillations in various frequency bands, suggesting that the oscillatory content may be able to provide much more detailed information on the ongoing cortical activity than initially apparent (Buzsáki et al., 2012; Lachaux et al., 1999; Murthy & Fetz, 1996b; Zanos et al., 2012).

Unlike other frequency bands, gamma oscillations are commonly divided into low (30-50 Hz), mid (50-80 Hz), and high (80-120 Hz) ranges. Low gamma has been the most commonly studied range and has been shown to be relevant to both cognition and behavior (Donner et al., 2009; Herrmann et al., 2010; Muthukumaraswamy, 2010). It is thought to be generated by either periodic activity between interneurons – interneuron gamma (ING) (Buzsáki & Wang, 2012; Traub et al., 1996; Wang & Buzsáki, 1996; Whittington et al., 1995) – or between pyramidal cells and interneurons – pyramidal-interneuron gamma (PING) (Brunel & Wang, 2003; Ermentrout & Kopell, 1998; Geisler et al., 2005). Low gamma has even been operantly conditioned with a brain-computer interface; spike activity and synchrony were shown to change with the modulations of the oscillations (Engelhard et al., 2013).

Mid gamma is often included in studies involving low gamma and is also highly relevant in the ING and PING networks due to slight axon conduction or synaptic delays dictating large changes in generated oscillation frequencies (Buzsáki & Wang, 2012; Leung, 1982). High gamma is typically studied in relevance to spiking activity due to its high frequency content (Muller et al., 2018; Ray et al., 2008; Yazdan-Shahmorad et al., 2013), or in the hippocampus for its

synchronization with theta oscillations and relevance to memory (M. R. Cohen & Kohn, 2011; Colgin, 2016; Yamamoto et al., 2014).

As there is strong precedent for gamma activity indicating neural activity, we can potentially use it as a trigger for activity-dependent stimulation. Although classic spike-timing dependent plasticity (STDP) posits the strengthening and weakening of individual synapses (Bi & Poo, 1998; Markram et al., 1998) and successful studies have been reported in vivo (Jackson et al., 2006; Rebesco et al., 2010), they often required delivering stimulation for up to 72 hours. Using population activity as the trigger signal may allow us to strengthen the connections between entire columns of the cortex rather than focusing on a single neuron that may be overwhelmed by background activity and more easily lost over time. In addition, previous work has shown that stimulation triggered to beta oscillations (15-25 Hz) result in bidirectional plasticity dependent on the phase of oscillation (Zanos et al., 2018), and an integrate-and-fire spiking neural network model strongly predicts the ability for gamma-triggered stimulation to create STDP (Shupe & Fetz, 2021).

The aim of this study was to induce bidirectional plasticity by delivering stimulation triggered to gamma band LFP. However, during the process we realized there were several challenges confounding potential results, including a gamma component that follows stimulation leading to a positive feedback loop of stimulation, filter delays resulting in improper timing of stimulation, and changes to baseline CCEP magnitudes within control experiments.

Materials and Methods

Subjects and implants

This study was conducted with Monkey Kr with the Utah array (referred to as Monkey K in this chapter) and Monkey I with dual electrodes using the Ripple Neuro. Refer to General Methods for full details on implants and surgical procedures.

Experiment timeline

The monkeys were seated in a primate chair with both arms restrained and performing a center-out isometric wrist torque task. A trigger channel (Nrec) was chosen such that stimulating it resulted in reliable CCEPs in the stimulated channel (Nstim) (Figure 4.1B). Each experiment consisted of 3 epochs: 1. 2-10 minutes of pre-test stimulation (2-5 Hz, single pulse stimulation of Nrec), 2. 10-60 minutes of conditioning, and 3. post-test stimulation (2-5 Hz, single pulse stimulation of Nrec). 5 minutes of recording without any stimulation was also collected both before and after the experiment.

Cortical stimulation

The signal from Nrec was filtered to mid gamma (50-80 Hz) using a third order Butterworth filter. Mid gamma was chosen over low or high gamma due based on a previous modeling study's prediction on the efficacy of mid gamma triggered stimulation (Shupe & Fetz, 2021). A negative threshold was determined each day as 2 times the standard deviation of a 1-minute baseline recording of the gamma filtered LFP. Each time the LFP crossed the threshold (positive or negative slope, depending on the day) stimulation was delivered to Nstim without a delay. Each stimulus consisted of either single-pulse stimulation or a pulse train of 3 pulses at 333 Hz with an amplitude that ranged from 10 to 40 uA. There was a timeout ranging from 50 to 100 ms after each stimulus to prevent a positive feedback loop from occurring, since stimulating Nstim

often generated a response in Nrec in the gamma range. Conditioning duration was between 10 and 40 minutes per session, with roughly 10 triggered stimuli occurring per second, resulting in between 6000 and 24000 gamma-triggered stimuli.

Calculation of cortico-cortical evoked potentials

Cortico-cortical evoked potentials (CCEPs) were calculated using both peak-to-peak (pk-pk) and root-mean squared (RMS) measures. Pk-pk was calculated by finding the difference between the maximum and minimum values in the stimulus-triggered average response from 0 to 50 ms and RMS was calculated on the stimulus-triggered average in a window of 1.5 to 50 ms.

Results

33 total experiments were conducted with Monkey K using 17 unique channels and 28 unique channel pairs. 14 were positive slope experiments and 19 were negative slope experiments. 25 total experiments were conducted with Monkey I use 18 unique channels and 10 unique channel pairs. 15 were positive slope experiments and 10 were negative slope experiments. We initially delivered single-pulse stimulation at each threshold crossing, but noticed that the stimulation fell into a positive feedback loop because the stimulus response contained a gamma component. As a result, we altered the protocol to have a timeout after a certain number of stimuli occurred in quick succession.

Spikes are synchronized with gamma band LFP

Before performing the experiments, we first confirmed the synchronization of spikes with gamma band LFP to further substantiate our hypothesis of using gamma as a proxy for population spiking activity. Figure 2.2A shows an example of a spike-triggered average of raw and gamma band LFP, filtered offline with a zero-phase filter to ensure there is no time delay between the raw signal and gamma band LFP. The spike is clearly seen in the raw LFP, demonstrating proper spike sorting. The averaged gamma band has a trough at the time of spiking but does not sustain oscillatory activity, with the activity quickly diminishing after a couple cycles.

We additionally tested how stimulation would be triggered by assessing threshold crossings on prestimulus recordings of online filtered gamma band LFP. The threshold was designated to be the average minus two times the standard deviation of gamma band LFP. Figure 2.2B shows the threshold-triggered average of gamma, which again shows little oscillatory activity beyond the detected trough. The triggered average of raw LFP also shows a clear periodic gamma

component, though it occurs much earlier compared to the filtered LFP due to the delay introduced by online filtering.

As the oscillatory activity seen in threshold-triggered averaging could be due to the "blurring" of individual cycles captured by the threshold, we additionally assessed the intervals between the thresholds, an analog to the interstimulus interval (ISI) when not delivering any stimulation. The distribution showed a high peak at 15 to 20 ms (Figure 2.2C). In accordance with the possible periodic activity seen in the threshold-triggered averages, this suggests there may be continuous oscillatory activity triggering stimulation. As filtering the signal introduces a delay, overt oscillatory activity is necessary to adjust the phase on which stimulation was delivered offline (Zanos et al., 2018).

To better assess whether the stimulation is triggered from overt oscillatory activity or by sudden large increases in gamma, we calculated how often the stimuli occur consecutively within the gamma period. If a trigger occured within 1/50 seconds of the previous trigger, we considered it a "consecutive stimulation" possibly reflecting oscillatory activity. Figure 2.2D shows the histogram of the number of consecutive stimuli that would occur within a 10-minute period. There are rarely more than 3 stimuli that occur consecutively, suggesting that though there may be periodic activity it is often very short, consisting of fewer than 3 consecutive cycles.

Stimulation results in a strong gamma component

To determine the characteristics of the signal triggering stimulation, we plotted the stimulus-triggered averages of raw and online filtered gamma band LFPs for each conditioning category, shown in Figure 2.3. The stimulus-triggered averages were calculated by only considering stimuli that occurred more than 100 ms after the previous stimulus to limit the contamination by the stimulus responses.

The gamma component is clearly visible in the averaged raw LFPs in both the positive and negative slope experiments, whereas there is no clear gamma in control experiments with open loop stimulation (Figure 2.3A). All experiment conditions present a notch around 100 ms, which may be an artifact of the 100 ms limit on the considered stimuli. The stimulus responses are large in amplitude and last up to 100 ms following stimulus onset.

The stimulus-triggered averages of the online filtered gamma band LFP shows the large gamma peak immediately preceding the stimulus onset (Figure 2.3B). However, an even larger gamma component is present immediately following stimulation lasting for up to 100 ms. This gamma component is probably driven by the stimulus artifact, as a ringing impulse response produced by the band-pass filter. Although the exponential decay of the amplitude is typical of the ringing artifacts, the duration suggests that the gamma component following stimulation may be in part due to the filtered stimulus response seen in the raw LFP.

Stimulation results in positive feedback

Although the previous analysis suggested the lack of consecutive stimuli when assessed over data with no stimulus, we noticed large chains of stimuli within our initial experiments. As the stimulus-triggered averages suggested a large gamma component following stimulation, plotting the raw and gamma band LFP with respect to delivered stimuli, as shown in Figure 2.4A, showed the presence of a positive feedback loop. As a result, each stimulus led to a subsequent stimulus, only terminating when the stimulus response happened to be weak. Even a timeout of 50 ms following each stimulus was not sufficient to prevent this feedback loop, which required at least a 100 ms timeout (Figure 2.4B).

Experiments thus were performed with a 100 ms timeout following stimuli. However, to ensure we were capturing most of the increased gamma, we allowed for up to 3 consecutive stimuli before the timeout was applied.

Filter design

Although the previous section showed synchrony of spikes with gamma band LFP, real-time filtering of signals can result in a potentially significant time delay, as shown in Figure 2.2B and Figure 2.3. As a result, we analyzed the properties of our filter used to extract gamma band LFP.

We chose infinite impulse response (IIR) filters over finite impulse response (FIR) filters as IIR filters can produce the same fidelity of frequency band isolation with a lower order, resulting in faster computation and low memory consumption. Within IIR filters we chose the Butterworth filter. The Butterworth filter has a flat passband, limiting distortions in the gamma band. Although it does not have as steep a roll-off as its counterparts, a shallower roll-off results in less group delay during real-time filtering.

The Ripple system allows for the use of a custom filter using second order sections. To apply our filter, we converted the transfer function of a 3^{rd} order bandpass Butterworth filter into second order sections using a built-in MATLAB function (tf2sos). Figure 2.5 shows the frequency response of the implemented filter, as well as the group delay, or the time delay between the filtered and raw signals. Though the frequency response clearly captures mid-gamma, the group delay is relatively large, with a maximum of up to 35 milliseconds. The group delay is also not flat in the passband, with peaks at the cut-off frequencies, suggesting possible “smearing” of the frequency components.

We assessed possible solutions in one of two ways: 1. using a different system that allows for more flexible filter design, and 2. using a lower filter order.

The Tucker-Davis Technologies RZ2 Bioamp Processor allows us to define multiple filter stages. A low pass filter followed by a high pass filter may be beneficial for minimizing group delay compared to a single bandpass filter. Using 6^{th} order low and high pass filters to match the 3^{rd} order bandpass filter, Figure 2.5 shows that the frequency response is very similar, but the group delay does indeed decrease with lower peaks at the cut-off frequencies. We repeated the procedure but with a 2^{nd} order bandpass and 4^{th} order low and high pass filters (Figure 2.5B). The group delays decreased by more than 10 ms on average whereas the frequency response was not heavily affected, suggesting a lower order is more appropriate for real-time triggering from filtered signals.

Finally, we tested the frequency response and the group delay of a Bessel filter – an analog filter specifically designed to have minimal and flat group delay – to compare with the previous two implementations. The frequency response of the Bessel filter is less desirable as the passband is not flat and instead peaks at the center frequency; however, the group delay is negligible and flat throughout the passband (Figure 2.5). Although we could not test an experimental setup with the Bessel filter as it requires specialized hardware, the tradeoff between the frequency response and group delay may be desirable for future real-time triggering from a filtered LFP band.

Processing delays

The Ripple Neuro system allows for interfacing with MATLAB through Xippmex. Although this allows for flexible programming for various conditioning paradigms, it adds an additional delay after detection due to software processing. Our system loads the LFP data, determines whether it has crossed the threshold, and delivers stimulation if the timeout has not been engaged.

The distribution of the processing delays for each stimulus across all experiments is shown in Figure 2.6. Although the median delay was 5 ms, there were rare occasions in which the delay was as long as 50 ms. Although the magnitude of the delay is significantly smaller than the delay introduced by the filter, there was high variability with a standard deviation of 5.8 ms. As a result, the processing delays would prevent the stimulation from being delivered consistently at appropriate parts of the gamma band LFP.

Control experiments

We performed control experiments in Monkey I with random stimulation to determine if the CCEPs change before and after conditioning simply due to stimulation itself. We additionally assessed changes in responses of non-stimulated channels within these control experiments. Although the changes in CCEPs as measured with both peak-to-peak (pk-pk) and root-mean squared (RMS) were not statistically significant from zero, there were surprisingly large changes in baseline CCEPs due to stimulation, showing up to 50% change in magnitude (Figure 2.7). The standard deviation of changes in CCEP magnitude for pk-pk and RMS were 13.6% and 9.6% respectively, showing a wide distribution of changes even under control conditions.

Discussion

This chapter outlines the challenges and pitfalls of performing gamma-triggered stimulation for stimulus induced plasticity that can be extended to any LFP band triggered stimulation paradigm. There were three main limiting factors: positive feedback loops of stimulation, filter delays, and the changes to baseline CCEP magnitude.

Feedback loop

Our experiment showed that the stimulation results in a large component in the evoked response in the raw LFP following stimulus onset and a prolonged gamma component in the filtered LFP, both lasting for up to 100 ms. The gamma component may be due largely to ringing from the stimulus artifact, but its duration suggests that the evoked potential may contribute at least in part.

Although in our experiments we allowed for several subsequent stimuli before imposing a timeout in case there were multiple gamma cycles that are spontaneously occurring, this feedback loop brings into question what signals we were triggering from. If the gamma component does indeed reflect the gamma component of the stimulus response, it may represent the population spiking response. As our initial goal was to trigger from gamma band LFP as a proxy for population activity, perhaps allowing the feedback loop to continue may not be detrimental to the experimental design.

However, stimulus responses may be significantly different from spontaneous population activity. Intracortical stimulation activates a random cluster of fibers resulting in the activation of horizontal projections to both excitatory and inhibitory networks (Butovas & Schwarz, 2003; Logothetis et al., 2010; Yun et al., 2022). Such artificial activation of the cortical circuitry via

stimulation of simultaneous inputs may be different from spontaneous activity driving behavior, potentially leading to different changes due to stimulation.

Additional experiments are necessary to determine whether the gamma component following stimulation is a physiological response and if there are differences when triggering from them compared to spontaneous increases in gamma band LFP.

Filter design

Although we chose the best possible filter for real-time signal processing, it still had its limitations. The 3rd order bandpass Butterworth filter resulted in more than 30 ms of group delay, which is more than a full cycle of mid gamma, and more than two full cycles of higher frequencies. Using two separate filters, a low and a high pass filter, with lower order results in much better delays, but still had a maximum of about 20 ms, which is still more than a full cycle of mid gamma.

A Bessel filter would be ideal in limiting group delay while having a less flat passband as a tradeoff. However, Bessel filters are analog and require hardware implementations, and the conversion to a digital domain with transformations destroys the low, constant group delay (Proakis & Manolakis, 2006). Thus, specialized hardware specifically designed to filter LFP signals with lowest group delay would be ideal for real-time triggering from LFP bands.

Finally, though we focused on IIR filters due to their faster computation speed, an FIR filter implementation may have shorter group delay to offset the longer computation. However, additional investigation is required to better understand the feasibility of proper LFP band triggered stimulation.

Changes in CCEP magnitude

Finally, our control experiments in which stimulation was delivered open loop, as well as CCEPs in channels that did not receive any stimulation, changed after conditioning. The distribution of changes in CCEP magnitude was roughly normally distributed around 0 when calculated with either peak-to-peak or root-mean squared but had a high standard deviation. In addition, there were rare occasions with large changes of up to 50%.

These results bring into question the degree to which CCEPs – the averaged LFP response recorded at the postsynaptic site to stimulation delivered to the presynaptic site – accurately reflect synaptic connectivity. The presence of CCEPs does ensure the presence of synaptic connections, but their magnitude may be subject to significant sources of variance. A better understanding of CCEPs and its various peaks and troughs, or the use of a different, more stable measure of connectivity may be required to better understand the effects of stimulation.

Conclusions

In conclusion, there are various factors that limited our approach to gamma-triggered stimulation. Though our hypothesis that triggering from gamma band LFP will be a proxy to triggering from population activity, thus potentially leading to stronger and more robust STDP, still stands, there are various hurdles that must be overcome to properly implement gamma-triggered stimulation *in vivo*.

Figures

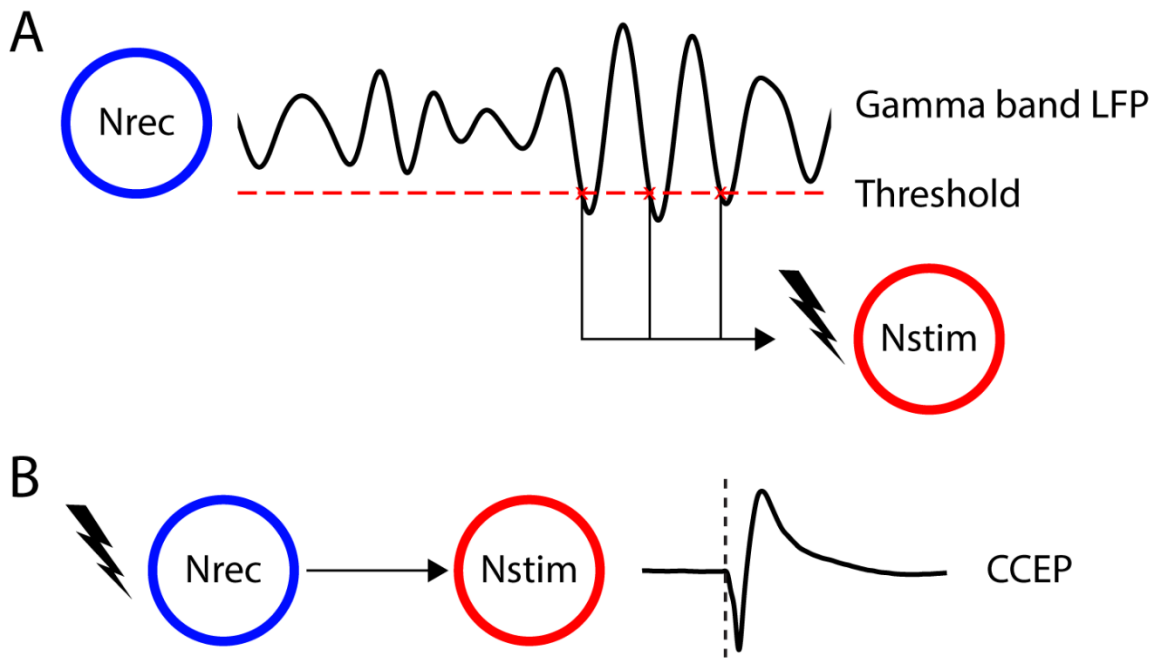

Figure 2.1 Experimental design

A. If the gamma band signal from Nrec crossed the threshold, stimulation was delivered to Nstim. Whether the stimulation was delivered at the negative slope (shown in figure), or positive slope was randomly determined each day. Control experiments were conducted in which stimulation was delivered open loop. **B.** CCEPs from Nrec to Nstim were measured before and after conditioning as a measure of connectivity. The dashed line shows the time of stimulation. Channels other than Nstim often generated CCEPs as well, which were used as control recordings.

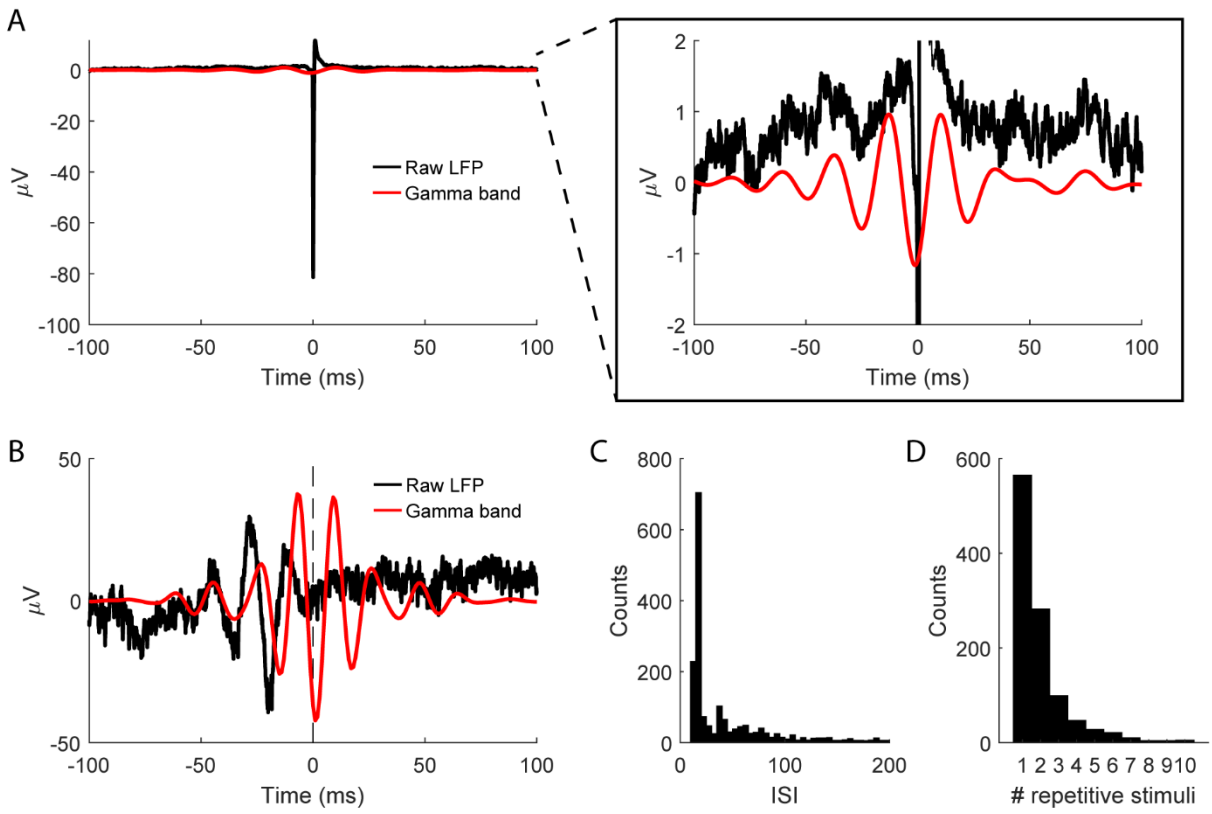

Figure 2.2 Gamma reflects spiking activity

A. Spike-triggered averages of raw LFP (black) and gamma band LFP (red). Raw LFP clearly shows the detected spike (left). A close-up of the triggered averages (right, inset) shows that spikes occurred at the trough of gamma band LFP, but there are at most 2 additional cycles. **B.** Threshold triggered raw LFP (black) and gamma band LFP (red). **C.** Distribution of intervals between thresholds, or interstimulus intervals (ISIs), when not delivering any stimulation. The peak is at 15 to 20 ms. **D.** Number of consecutive stimuli occurring within 1/30 seconds (largest period of gamma). This further confirms that stimulation is not typically driven by oscillatory activity as they usually consist of fewer than three consecutive stimuli.

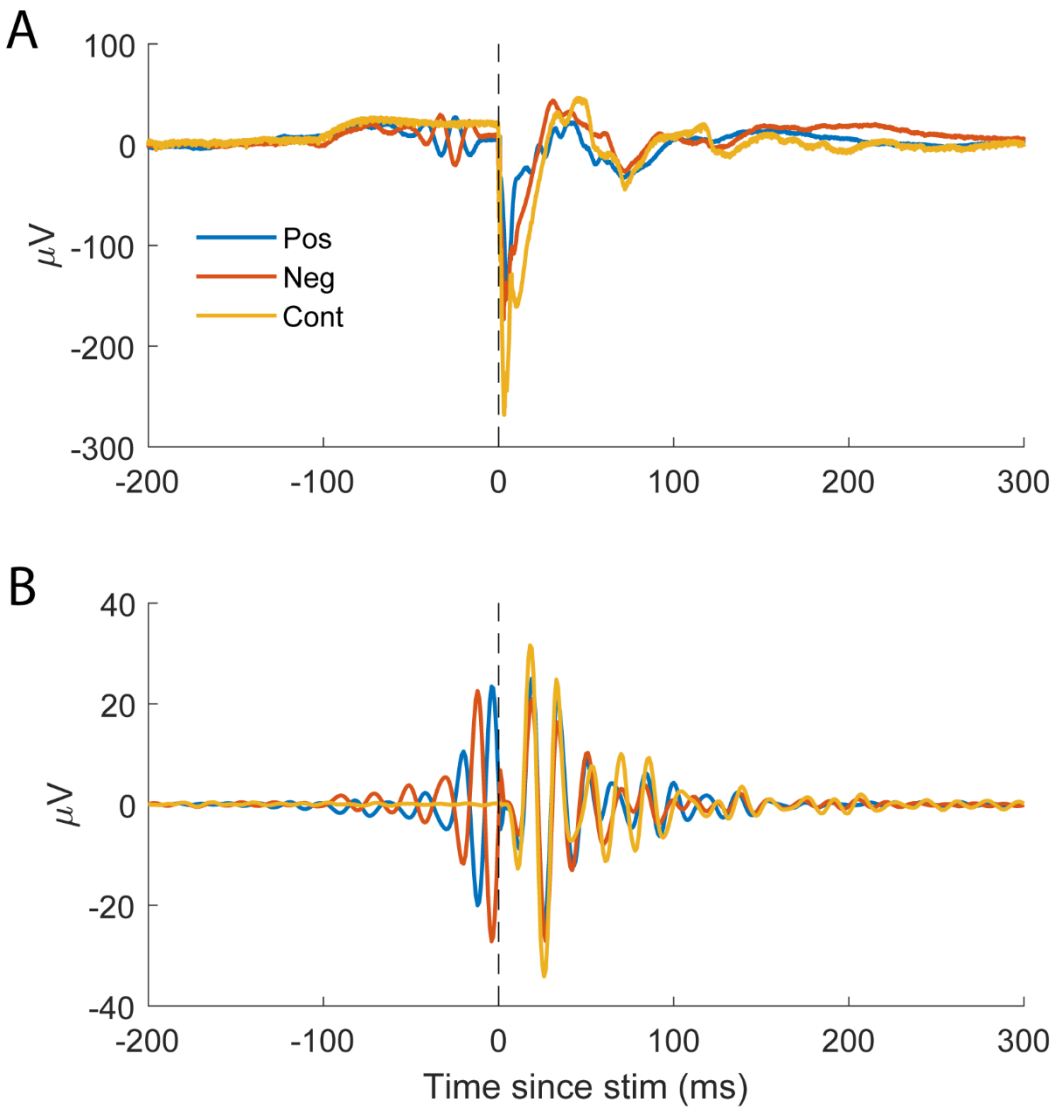

Figure 2.3 Stimulus-triggered averages show responses in gamma band LFP

Stimulus-triggered averages of **A.** raw broadband LFP and **B.** gamma band LFP across positive slope, negative slope, and open-loop control experiments (Pos, Neg, and Cont respectively). The gamma components triggering stimulation are present in the raw LFP average. The stimulus response is large and lasts for up to 100 ms in the raw LFP. There is a large gamma component immediately following stimulation that also lasts for up to 100 ms.

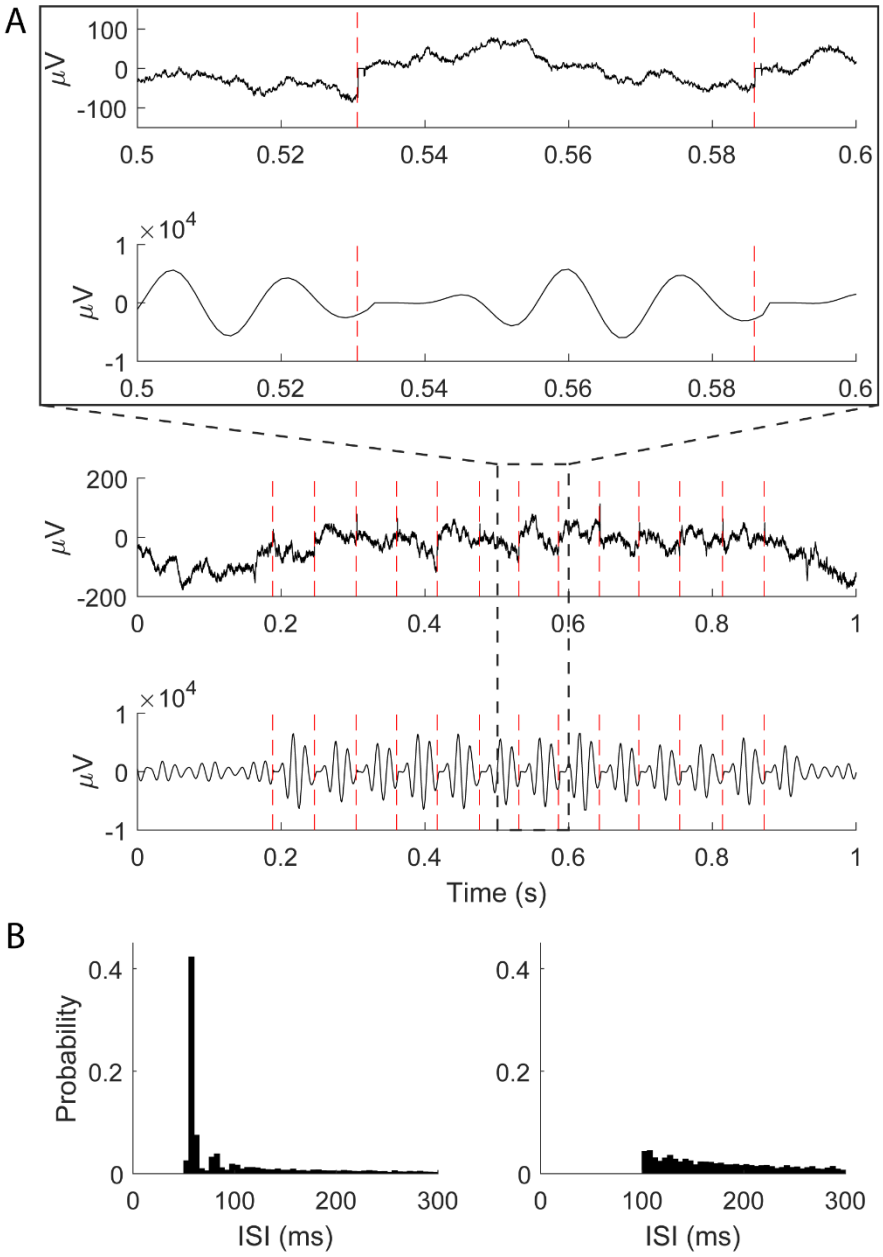

Figure 2.4 Stimulation generates responses in gamma frequency range

A. Example of stimulation from a single-pulse experiment with a timeout of 50 milliseconds following each stimulus with respect to raw LFP (top) and gamma band LFP (bottom). Vertical dashed red lines show stimulation timing. Even with the timeout, the generated response had a high gamma component resulting in a feedback loop. B. Probability distribution of ISIs when using a 50 ms (left) or 100 ms (right) timeout after each stimulus. 50 ms is not enough to prevent the feedback loop as stimuli occur almost immediately following the timeout. The 100 ms timeout does effectively prevent the feedback loop.

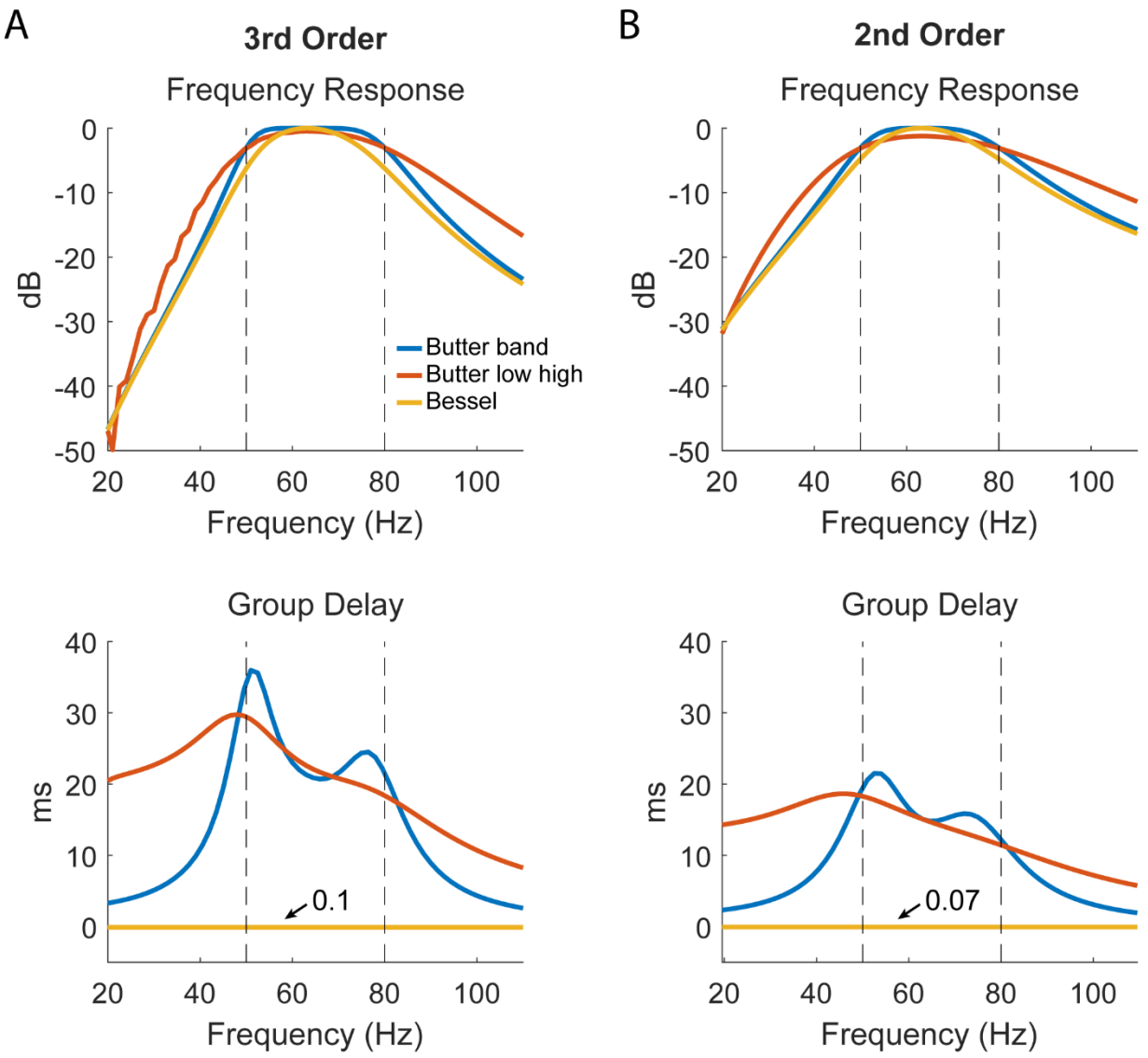

Figure 2.5 Filter properties

Frequency response (top) and group delay (bottom) of a bandpass Butterworth filter, low-pass then high-pass Butterworth filters, and a bandpass Bessel filter. **A.** 3rd order implementation as used in the experiments. A 3rd order bandpass filter translates to 6th order low-pass and high-pass filters. Note the high group delay of the bandpass Butterworth filter with comparable frequency responses in the pass band. **B.** Properties of 2nd order implementation. Note the significantly decreased group delay.

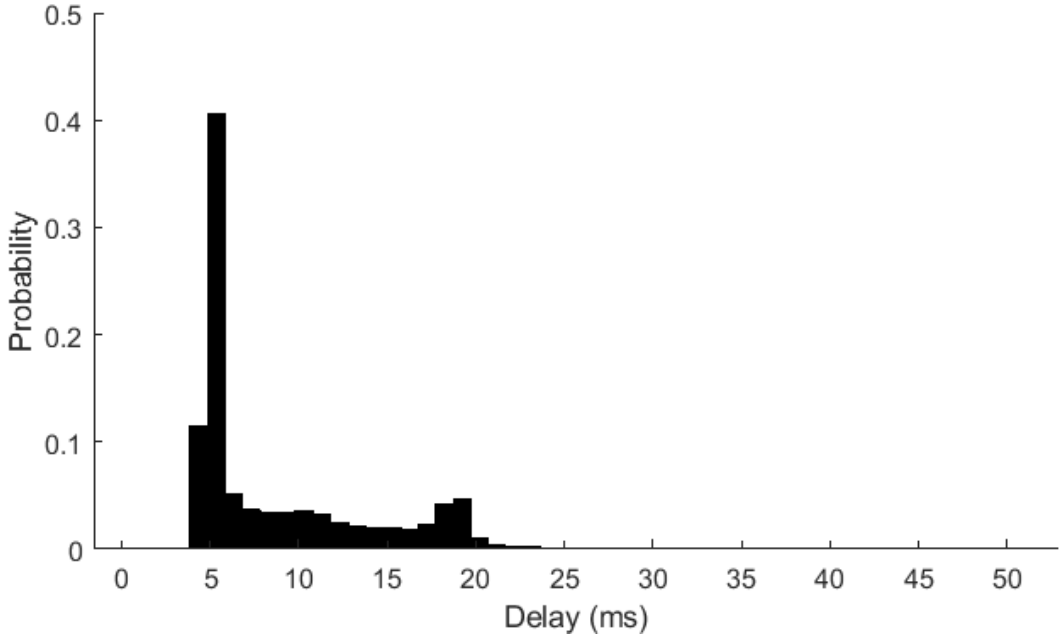

Figure 2.6 MATLAB delays

Distribution of delays caused by MATLAB processing of over 200000 individually triggered stimuli across all experiments. Most delays were less than 25 ms (over 98% of the time) but on rare occasions the delays were as high as 50 ms. Median: 5 ms; mean: 8.7 ms; standard deviation: 5.8 ms.

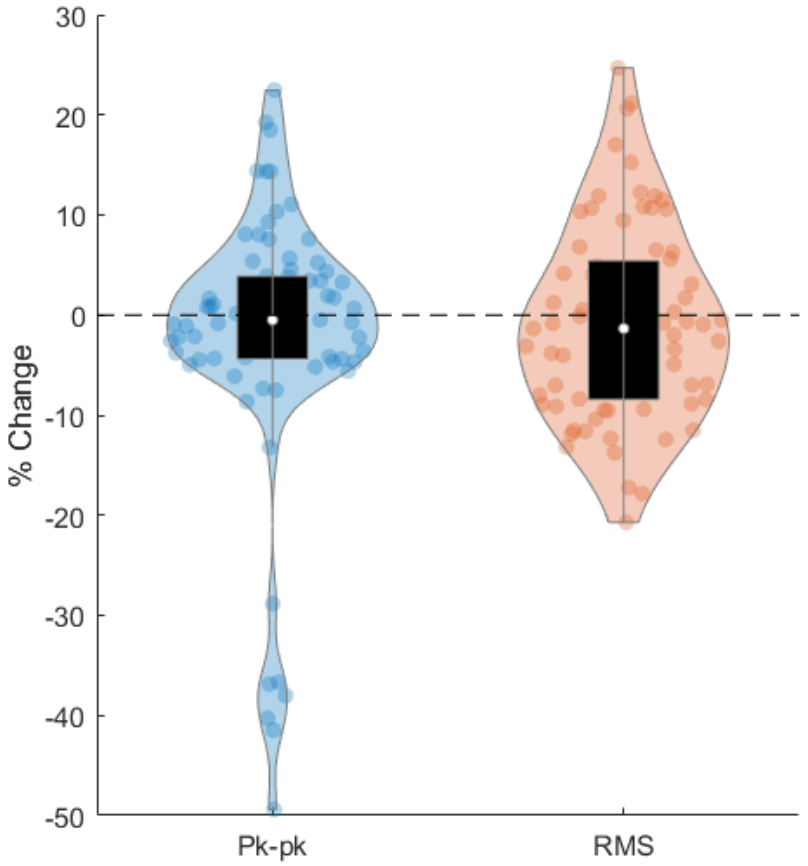

Figure 2.7 Control experiments

Changes in CCEP magnitude in control experiments. Control measurements were obtained from Monkey I, both by replaying the stimulus pattern from a previous experiment and assessing non-stimulated channels. Control results were not statistically significant from 0 using peak-to-peak (left) or root-mean squared (right) (Wilcoxon signed rank test, p=0.68 and 0.26 respectively), but often had large fluctuations of up to a 50% change.

Chapter 3. Responses of cortical neurons to intracortical microstimulation in awake primates

Abstract

Intracortical microstimulation (ICMS) is commonly used in many experimental and clinical paradigms; however, its effects on the activation of neurons are still not completely understood. To document the responses of cortical neurons in awake non-human primates to stimulation, we recorded single-unit activity while delivering single-pulse stimulation via Utah arrays implanted in primary motor cortex of three macaque monkeys. Stimuli between 5-50 μA delivered to single channels reliably evoked spikes in neurons recorded throughout the array with delays of up to 12 milliseconds. ICMS pulses also induced a period of inhibition lasting up to 150 ms that typically followed the initial excitatory response. Higher current amplitudes led to a greater probability of evoking a spike and extended the duration of inhibition. The likelihood of evoking a spike in a neuron was dependent on the spontaneous firing rate as well as the delay between its most recent spike time and stimulus onset. Tonic repetitive stimulation between 2 and 20 Hz often modulated both the probability of evoking spikes and the duration of inhibition; high-frequency stimulation was more likely to change both responses. On a trial-by-trial basis, whether a stimulus evoked a spike did not affect the subsequent inhibitory response; however, their changes over time were often positively or negatively correlated. Our results document the complex dynamics of cortical neural responses to electrical stimulation that need to be considered when utilizing ICMS for scientific and clinical applications.

Introduction

Intracortical microstimulation (ICMS) is widely used for interfacing with the brain in both basic and clinical research, from inducing plasticity to employing sensory neuroprostheses in various animal models (Flesher et al., 2016; Hartmann et al., 2016; Jackson & Fetz, 2011; Lebedev & Nicolelis, 2017). The applicability of ICMS arises from the fact that it has the highest spatial and temporal specificity of all clinically applicable cortical stimulation techniques (Sejnowski et al., 2014). However, the circuit mechanisms that drive the responses of neurons following ICMS, and the ways in which other factors such as timing and stimulation frequency affect the stimulus responses are not fully understood.

ICMS was originally thought to activate neural elements around the electrode tip. Regions closer to the tip would have higher activation in a sphere with an isotropic gradient, and the volume would grow with increasing current amplitude (Ranck, 1975; Stoney et al., 1968; Tehovnik et al., 2006). However, evidence shows that ICMS typically excites axons near the electrode tip that transsynaptically excite neurons up to several millimeters away (Gustafsson & Jankowska, 1976; Hao et al., 2016; Histed et al., 2009; Lesser et al., 2008; Logothetis et al., 2010; McIntyre & Grill, 2000). Additionally, the effects of ICMS are not limited to excitation, and includes a long-lasting inhibitory response that is commonly attributed to GABAergic synapses (Berman et al., 1991; Butovas & Schwarz, 2003; Hao et al., 2016).

Single neuron responses to ICMS are dynamic and can be modulated with repeated stimulation. The changes, in part, also depend on stimulus frequency. In particular, the excitation of neurons generally decreases over time and becomes more localized with higher frequencies (Dadarlat et al., 2019; Michelson et al., 2019). However, the reported frequency ranges and timescales are variable, and the driving processes remain unclear. The changes over time are often attributed to

short-term synaptic plasticity or intrinsic plasticity of neurons which both depend on the frequency and pattern of stimulation (Abbott & Regehr, 2004; Citri & Malenka, 2008; Zucker & Regehr, 2002).

Altogether, these studies demonstrate that the effects of ICMS are not restricted to regions proximal to the electrode tip, and that responses consist of interplay between excitation and inhibition (Borchers et al., 2012; Griffin et al., 2011; Logothetis et al., 2010). Despite our increasing understanding of how ICMS activates cortical circuits, several significant questions remain. How does the background neuronal activity, including firing rate and previous spike time impact the stimulus response? How do the responses change over time as a function of both the frequency of stimulation and proximity to stimulation site? Is the inhibitory response coupled to the excitatory response, or are they independently activated?

We addressed the questions above by delivering ICMS and examining responses of single neurons in primary motor cortex (M1) of three macaque monkeys with chronically implanted Utah arrays. Single-pulse ICMS was delivered to one channel for up to 20 minutes while the spikes of single neurons were simultaneously recorded from all other electrode channels. We tracked the probability of evoking spikes as well as the duration of the evoked inhibition and varied both the sites and frequency of the stimulation between sessions. Our results expand upon previous findings by characterizing the dependencies of the neuronal responses to background neuronal activity, distance, and stimulation frequency, and exploring the interactions between the excitatory and inhibitory responses.

Methods and Materials

Experimental Design

Implants and surgery

Experiments were conducted with 3 male pigtail macaques (*Macaca nemestrina*; Monkeys S, Kr and J). Monkey Kr will be referred to as Monkey K within this chapter. All three animals were implanted with 96-channel Utah microelectrode arrays in the hand region of M1. They also received halos to facilitate overnight recording of neuronal activity. Refer to "General Methods" for full details on implants and surgical procedures.

Electrophysiology

Stimulation and recording of single unit activity were conducted with one of three systems: 1) Neurochip3 (custom bidirectional brain-computer interface developed in our laboratory (Shupe et al., 2021), 32 channels, 20 kHz sampling rate), 2) Neural Interface Processor (Ripple Neuro, 96 channels, 30 kHz sampling rate), or 3) RZ2 BioAmp Processor, PZ5 NeuroDigitizer Amplifier, and IZ2 Electrical Stimulator (Tucker-Davis Technologies, 96 channels, 25 kHz sampling rate).

Experimental Setup

The monkeys were trained to calmly sit in a primate chair while periodically receiving an apple smoothie reward without performing a task (Figure 1). Each session included a prestimulus epoch lasting between 5 and 10 minutes and a stimulus epoch lasting between 5 and 20 minutes. During the stimulus epoch we delivered tonic or Poisson distributed single pulse stimulation (cathodal, biphasic, 200μs phase width) to a single channel at rates between 1-20 Hz. For testing the effects of current amplitude, a range of 2-50 μA was used. Current amplitude was fixed at 15

μA for all other experiments and analyses. The stimulation frequency was fixed during the stimulus epoch for each session.

Data analysis

Evoked spike acquisition

Spikes were sorted using two time-amplitude windows, initially online and subsequently confirmed offline. Stimulus artifacts lasted around 1.1-1.6 ms. Spikes were frequently detected immediately following the artifact (Figure 3.2A). The timing of evoked spikes was found by calculating the peristimulus time histogram (PSTH, 0.5 ms bin widths) of spikes in the window from -20 to 20 ms from the time of stimulation (Figure 3.2B). To isolate the evoked spikes from the spontaneous activity, we defined upper and lower thresholds in the PSTH as the histogram mean plus or minus 2 times the standard deviation from -20 to -2 ms. We then found the largest peak in the PSTH from 1 to 15 ms after stimulation that was larger than the upper threshold and tracked adjacent bins in both directions until we reached the lower threshold on both sides. All spikes occurring within this window were denoted as stimulus-evoked spikes (Figure 3.2C). If no peak was greater than the threshold the spike was not considered to have been evoked by stimulation. The probability of evoked spikes was calculated as the number of evoked spikes divided by the number of total stimuli. For any analysis over time, the evoked spike probability was calculated for stimuli within overlapping 30 second bins with 1 second steps.

We tracked a total of 148 distinct neurons across all experiments. Because of changes in signal fidelity due to electrode drift, we were not able to record all neurons across all sessions. Experiments characterizing the base stimulus responses used unique pairs of stimulated site and recorded spike (n=420). Experiments assessing changes over time used unique trios of stimulated site, stimulation frequency, and recorded spike (n=585).

Inhibitory response acquisition

The inhibitory response was measured using the PSTH in previous studies (Butovas & Schwarz, 2003; Hao et al., 2016). While evoked spike timing can easily be determined with the PSTH due to their high probability and narrow time window, the inhibitory response depends on a broad window with sparse activity, particularly for units with low firing rate. As a result, a large number of stimuli is required to reliably detect inhibition in the PSTH. Therefore, rather than using the PSTH, we measured the duration of inhibition by removing all evoked spikes and calculating the time between the onset of stimulation and the next spontaneous spike (Figure 3.2D). Inhibition was deemed to be stronger when the delay from stimulation onset to the next spontaneous spike was longer, giving us a measure directly comparable to the PSTH but with much higher temporal resolution. We discarded any stimuli for which the subsequent stimuli occurred before the next spontaneous spike. For any analysis over time, we used the median inhibition duration of stimuli within overlapping 30 second bins with 1 second steps.

Evoked spike probability dependencies

To calculate the spontaneous firing rate for each unit over time, we disregarded the times from each stimulus onset to the next spontaneous spike. This effectively removed the stimulus response from the firing rate calculation, providing us with an independent measure of spontaneous activity.

The autocorrelation histograms for the 17 units in which we characterized the evoked spike probability as a function of the time delay between their previous spike times and stimulation onsets were calculated from their respective prestimulus epochs. The histograms were binned between 0 to 50 ms in non-overlapping 1 ms bins.

The dependencies of evoked spike probabilities on the timing of stimulation were calculated by first measuring the delays between each stimulus and the preceding spike. We separated this into two groups corresponding to whether the preceding spike was spontaneous or evoked. Stimuli that did not have a spike following the previous stimulus were discarded from the analysis. To account for the transmission delay from the stimulated site to the evoked spike, we added the average evoked spike latency for each unit to the delays. We then calculated the probability of evoking a spike for stimuli with delays from 0 to 50 ms with 1 ms time bins, then applied a moving average with a 5 ms window. Since the average spike latencies were added to each delay, time bins that were less than the average evoked spike latency were not included in correlation calculations.

Changes over time

Pairwise correlations and their statistical significance between firing rate, evoked spike probability, and inhibition duration over time were calculated using the Pearson correlation coefficient r:

$$r = \frac{\sum(x_i - \bar{x})(y_i - \bar{y})}{\sqrt{\sum(x_i - \bar{x})^2 \sum(y_i - \bar{y})^2}} \qquad \text{Equation 3.1}$$

where $\bar{x}$ is the mean of the x-variable, and $\bar{y}$ is the mean of the y-variable. Firing rate was calculated by removing all times between each stimulus onset to the first spontaneous spike (the inhibitory period) to remove any confounding affects between firing rate and the inhibitory response.

Linear and exponential fits were performed on binned evoked spike probabilities and inhibition durations to determine changes over time due to repetitive stimulation:

Linear	$y = a * t + b$	Equation 3.2
Exponential	$y = a + b * (1 - c)^t$	Equation 3.3

where y is either the evoked spike probability or inhibition duration, t is time and a, b, and c are the fitted variables. Changes were denoted to occur if the analysis of variance (ANOVA) F-statistic resulted in $p<0.05$. The sign of the linear fit slope (a in Equation 2) or the sign of the exponent base (b in Equation 3) of the exponential fit determined whether the changes were classified as increasing or decreasing. Neuron-stimulation site pairs with less than 3% average probability of evoking spikes were disregarded for analyses over time due to their inconsistency. The changes over time in spikes and inhibition were designated to be correlated if their correlation had a p-value less than 0.05.

Statistical analysis

Two-sided Wilcoxon signed-rank test (*signrank*, MATLAB) was used to compare between groups due to the nonparametric nature of the data. Two-sided Wilcoxon rank-sum (*ranksum*, MATLAB) tests were used for paired data. Fisher's exact test (*fishertest*, MATLAB) or two-way analysis of variance (ANOVA) (*anova2*, MATLAB) was used to compare categorical data. The Pearson correlation was used for all correlation tests. The Kolmogorov-Smirnov test was used to compare distributions. P-values for significance and tests used are reported in individual analyses.

Results

Evoked spikes and inhibitory response

We found that ICMS elicited a brief excitatory response followed by a longer inhibition. Electrodes on the Utah array typically showed evoked spikes occurring 1.5 to 10 ms after single-pulse stimulation. The inhibition typically followed the excitatory response and was observed as the suppression of firing in the PSTH for 5 - 100 ms, although in some instances it lasted up to 200 ms. We also observed that stimulus-evoked inhibition could occur in the absence of the excitatory response.

To ensure that stimulation arriving during inhibition was not affecting the stimulus response, we delivered trains of two or three pulses with each subsequent pulse timed to occur during the inhibitory response of the previous stimulus. Single, double, and triple pulse stimuli were delivered to a single channel, randomly interleaved at 2 Hz. Our results across 5 different sessions show that stimuli delivered during the inhibitory response were able to reliably evoke spikes comparable to when stimuli was delivered at other times, as previously reported (Butovas & Schwarz, 2003) (Figure 3.3, left). Furthermore, each stimulus pulse "reset" the inhibitory response such that the duration of inhibition was the same following each pulse train (Figure 3.3, right).

Effects of distance from stimulation site and stimulus amplitude

Evoked spikes occurred with greater probability and less variable latencies for units close to the stimulus electrode than for more distant units. The probability of evoking a spike in electrodes <1 mm from the stimulus site was significantly greater than for further sites ($p=1.3e-14$). In addition, closer sites on average had evoked spikes that occurred at shorter, and less variable latencies ($p=8.5e-29$), suggesting the presence of mono- and polysynaptic activation (Figure

3.4A). The duration of inhibition had a similar trend: recording sites <1 mm from the stimulus site tended to show stronger inhibition compared to further sites (p=0.003) (Figure 3.4B). The probability of evoking spikes and the duration of inhibition increased sigmoidally with the stimulus amplitude for all responsive units (Figure 3.5). The sigmoid curves were always steep: a change of 10 to 20 μA in stimulus intensity generated the difference between 5% and 95% of the maximum value for both evoked spike probability and inhibition duration.

Covarying evoked spikes

If stimulus evoked spikes are activated by cortical circuitry, there must be covarying responses between different spikes. Thus, we determined whether pairs of units were likely to have the same responses for individual stimuli. Figure 3.6A shows the Pearson correlation coefficient between pairs of units plotted against distance from one another. There are clearly pairs with significant correlations, though the correlations are usually weak with the vast majority of correlations having a correlation coefficient less than 0.2. Pairs of units closer together have a significantly higher chance to be correlated, as they are likely modulated by similar circuitry (Figure 3.6A, right).

The presence of covarying pairs even at large distances (>3 mm) led us to analyze whether there was a population wide response driven by an underlying cortical state. For each session, we first collected the total number of evoked spikes generated by each stimulus. Next, we randomly shuffled which stimulus evoked a spike for every evoked spike. We then recalculated the total number of evoked spikes produced by each stimulus. If there is a consistent population response due to an underlying cortical state, the number of evoked spikes generated by each stimulus without shuffling should be significantly higher than the number of evoked spikes after shuffling.

However, we found that the two distributions are not significantly different to one another in any session (Figure 3.6B).

Spontaneous activity affects stimulus responses

In addition to stimulation current and separation of the recording and stimulation sites, we found two other dependencies that affect the response. One is the spontaneous firing rate of the recorded units. Both the evoked spike probability and inhibition duration had statistically significant correlations with spontaneous firing rate over time (Figure 3.7). Table 1 documents the number of units with uncorrelated, positively correlated, or negatively correlated evoked spike probability and inhibition duration with spontaneous firing rate. A slight majority of units tested (300/585, 51%) had evoked spike probabilities that were positively correlated with firing rate and inhibition duration that were negatively correlated with firing rate. We additionally performed a 2-way ANOVA to determine whether the two relationships were dependent on one another but found no significant relationship ($p=0.11$). Units with positively correlated evoked spike probabilities and spontaneous firing rate were typically farther from the stimulated site than units with a negatively correlated relationship (Figure 3.7B left, C left). In contrast, units with positively correlated inhibition duration and spontaneous firing rate were typically closer to the stimulated site (Figure 3.7B right, C right).

The second dependency was the timing of stimuli relative to the most recent spike. We analyzed 17 units (2 from monkey S, 3 from monkey K, and 12 from monkey J). In 14 of the 17 units (2 from monkey S, 3 from monkey K, and 9 from monkey J), the probability of evoking a spike varied as a function of the time between the onset of stimulation and the most recent spontaneous spike. For these 14 units the probability was significantly positively correlated with the unit's autocorrelogram in the absence of stimulation (Figure 3.8, left and middle). The probability

distributions were the same even if the most recent spike was evoked by stimulation rather than being spontaneous. The inhibitory response did not depend on the timing of pre-stimulus spikes.

In 3 of the 17 tested units the probability of evoking a spike did not depend on the timing between the previous spike and stimulus onset. In all 3 of these units the probability of evoking a spike was consistently high (Figure 3.8, right), which suggests that the stimulation amplitude was large enough to evoke spikes regardless of other properties.

Repetitive stimulation changes stimulus response over time

Repetitive microsimulation has been shown to modulate the responses of units to ICMS (Dadarlat et al., 2019; Michelson et al., 2019; Zucker & Regehr, 2002). We documented the effects of repetitive ICMS over the stimulus period ranging from 5 to 20 minutes on the evoked spike probability and the duration of inhibition by delivering stimuli at 2, 5, 10, or 20 Hz. The probability of evoking a spike often increased or decreased over time, following a linear or exponential trend over the course of the session (Figure 3.9A).

The evoked spike probability was significantly more likely to change with higher frequencies of stimulation (Figure 3.9B left, C left). Of the changes, high frequencies (20 Hz) were likely to cause decreases in evoke spike probability compared to lower frequencies. Changes in inhibition duration over time were also more likely to occur at higher frequencies, and high frequencies were more likely to cause increases in inhibition duration. (Figure 3.9B right, C right)

The changes also depended on the distance from the recording site to the stimulated site (Figure 3.10A). The probability of evoking spikes and inhibition duration were significantly more likely to change the closer the units were to the stimulated site (Figure 3.10B, left). The specific change

in evoked spike probability did not have a dependence on distance, but inhibition duration was more likely to decrease in sites further from the stimulated site (Figure 3.10B, right).

Finally, in 72/585 (12%) of units, we also observed changes over time in the latency of the evoked spikes (Figure 3.11A). Latency changes typically occurred in units that were recorded on electrodes closer to the stimulation site, more commonly occurred with high frequency stimulation, and was more likely to increase over time (Figure 3.11B). Of the units with changes in their evoked spike latency, 249/447 (56%) units had increasing latencies and 198/447 (44%) had decreasing latencies. Distance from the stimulated site also played a role, with units closer to stimulation more likely to have changes in their evoked spike latency over time (Figure 3.11C).

Relationship between evoked spikes and inhibition

Since evoked spikes and inhibition often both exhibited changes over time, we sought to determine whether they were directly related on a trial-by-trial basis. Individual stimuli in each experiment were divided into two categories: those that evoked spikes and those that did not. For the unit in Figure 3.12A the PSTHs of the two classifications of stimuli are very similar except for the evoked spike peak. We found no statistical pairwise difference between the inhibition induced by stimuli that evoked spikes compared to the stimuli that did not evoke spikes (585 units, Figure 3.12B).

Although whether a stimulus evokes a spike does not affect the inhibitory response, the mechanisms underlying the changes over time could nevertheless be related. We analyzed the correlation between the probability of evoking a spike and duration of inhibition over time to determine whether they were positively or negatively correlated. Correlations with $p<0.05$ were considered significant, and all other instances were denoted to be uncorrelated. Of the 585 units tested, 30% (173 units) had positively correlated changes in the probability of evoking spikes

and the duration of inhibition, 47% (273 units) had negatively correlated changes, and 23% (135 units) were uncorrelated. Units with positively correlated evoked spike probabilities and inhibition duration tended to be closer to the stimulated site (Figure 3.12C and D).

Spike type does not correlate with stimulus response properties

To determine whether the cell type of the recorded units influenced their responses to ICMS, we used the spike width, calculated as the time between the minimum value of the waveform to the maximum value, to classify each neuron as fast-spiking (FS) or regular-spiking (RS) (Connors & Gutnick, 1990; McCormick et al., 1985).

Figure 3.13A shows an example of the two different spike waveforms, and Figure 3.13B shows the distribution of their spike widths. We separated the units into two groups based on their defined spike width shown at the dotted line in Figure 3.13B. Around 10% of all units fell to the left of the line and were denoted to be FS; the rest were denoted to be RS. We found that the putative cell type did not correlate with the distribution of distances from the stimulated site, whether a spike could be evoked, the probability of evoking a spike, the duration of inhibition, or how any measure changed over time (Figure 3.13C-G). Thus, all results reported herein are independent of the type of neuron recorded.

Discussion

Comparisons to previous studies

ICMS has been shown to predominantly activate neurons transsynaptically (Butovas & Schwarz, 2003; Hussin et al., 2015; Klink et al., 2017). We observed in our study that spike latencies fluctuated more than would occur with antidromic activation, and stimuli that were delivered within 1 millisecond after a spike were still able to evoke spikes. Since antidromic activation would result in collision and an absence of a spike at such short latencies, this suggests that the recorded units were predominantly activated orthodromically. Also consistent with previous experiments, we saw evoked spikes in units recorded up to 4.5 mm away from the stimulation site, which suggests that ICMS activates a distributed population rather than only a concentrated sphere of neurons around the electrode tip (Butovas & Schwarz, 2003; Hao et al., 2016; Histed et al., 2009).

Although the excitatory response was directly measurable in our experiments, the subsequent inhibitory response manifested as a lack of spikes. Butovas et al. concluded that a similar inhibitory response to ICMS was likely caused by $GABA_B$ receptors, which they confirmed with a follow-up study with pharmacological blocks (Butovas et al., 2006; Butovas & Schwarz, 2003). GABAergic inhibition would also explain the similarity in the sigmoidal curves of evoked spikes and inhibition with stimulus amplitude in our experiments – if more excitatory neurons are excited by the higher intensity stimulation, more inhibitory neurons will be activated via feedforward and feedback circuits, thereby increasing the amount of inhibition (Figure 3.14). A lack of relationship between inhibition and distance to stimulation site as well as the presence of inhibition in units without evoked spikes is likely due to the high connectivity of interneurons compared to principal cells (Isaacson & Scanziani, 2011; Matsumura et al., 1996; Rudy et al.,

2013; Tremblay et al., 2016). Interestingly, Hao et al. found that inhibition decreased as a function of distance, which we did not find (Hao et al., 2016). Potential reasons for this discrepancy could be the differences in how we measured inhibition and the stimulus amplitude.

However, we found that inhibition typically lasted between 5-100 ms and rarely over 100 ms, which is significantly shorter than the average time constants of $GABA_B$ inhibitory postsynaptic potentials of 150-200 ms (Bettler et al., 2004; Connors et al., 1988). Therefore, $GABA_A$ mediated inhibition is a more likely candidate to explain our results; previous studies have shown that $GABA_A$ is involved in recurrent polysynaptic inhibition, which we are likely activating via ICMS (Silberberg & Markram, 2007; Zhu et al., 2011). The different animal models and recorded cortical region in these studies may account for these discrepancies.

ICMS activates long horizontal fibers to both feedforward inhibitory networks and the recorded excitatory neurons (Figure 3.14). These afferent fibers have stronger excitatory connections to the inhibitory interneurons than the principal cells, particularly in layer 2/3, which may explain why we sometimes observe an inhibitory response without any excitatory response (Adesnik & Scanziani, 2010; Cruikshank et al., 2007; Helmstaedter et al., 2008). This, coupled with the fact that inhibitory neurons often target somatic or perisomatic compartments (Isaacson & Scanziani, 2011; Rudy et al., 2013; Tremblay et al., 2016), suggests that the observed inhibition may be initially activated via feedforward circuitry, and is subsequently followed by the excitatory response. The excited principal cells may then activate feedback circuitry that contributes to the inhibitory response (Figure 3.14).

Stimulus response depends on network activity and intrinsic membrane properties

Previous research has shown that stimulus responses depend on network activity both *in vitro* (Kumar et al., 2016; Weihberger et al., 2013) and *in vivo* (Kara et al., 2002). Our findings were

consistent with these results; the probability of evoking a spike was often positively correlated with spontaneous firing rate, whereas the duration of inhibition was often negatively correlated with firing rate.

English et al. demonstrated that the transmission probability for postsynaptic spikes of inhibitory neurons in the hippocampus *in vivo* is a function of the timing between the previous postsynaptic spike and presynaptic spike (English et al., 2017). Moreover, that study found that this dependency was independent of whether the previous postsynaptic spike was spontaneous or evoked, which suggested that intrinsic properties of the postsynaptic membrane were responsible for the dependence. Our results extend these outcomes by demonstrating that the timing of the previous spike affects not only the transmission probability for spontaneous presynaptic spikes, but also the stimulus-evoked spikes in cortical neurons. Furthermore, we found that the probability distributions for evoking a spike as a function of the timing between the previous spike time and stimulation onset and the spike train autocorrelation were often significantly positively correlated, which further reinforces the notion that this dependency reflects the intrinsic properties of the recorded units.

Altogether, our results reveal that the stimulus response has at least two dependencies other than stimulus amplitude and distance from stimulus site: the intrinsic membrane properties of the recorded neurons and the activity of the network. However, a sufficiently large stimulus current may saturate the responses and overcome these dependencies.

Repetitive stimulation modulates stimulus responses

Michelson et al. showed that the number of neurons activated by electrical stimulation diminished over time with higher frequencies measured with calcium imaging in a 407 μm x 407 μm window, which was attributed to a diminishing region of activation (Michelson et al., 2019).

Their study showed that changes began at regions distal from the stimulated site when delivering stimuli with frequencies greater than 10 Hz. These results are consistent with our study across the larger spatial field (4x4 mm) of the Utah array, as evoked spikes were more likely to be diminished with higher frequency of stimulation at distances closer to the stimulated site. A large difference we observed was the timecourse of the changes; Michelson et al. reported the changes occurred within seconds and plateaued whereas we observed changes occurring for up to 20 minutes. Additionally, we also observed that in some units the probability of evoking a spike increased over time even at longer distances and higher frequencies, which cannot be fully explained by a diminishing region of activation.

Although we did not explicitly measure the duration of changes induced by repetitive stimulation, we observed that they typically lasted less than 2 minutes. Due to the short-lived nature of the induced changes, various mechanisms of short-term synaptic plasticity such as vesicle depletion and facilitation by calcium influx (Citri & Malenka, 2008; Zucker & Regehr, 2002) may best explain our results. Evidence suggests that different forms of short-term plasticity exist for synaptic connections between different cell-types (Blackman et al., 2013; Losonczy et al., 2002). Beyond these differences, previous *in vitro* work by Markram showed that synaptic connections between pyramidal neurons of the same morphological class and interneurons had similar facilitating and depressing characteristics, but with different time courses (Markram et al., 1998).

Together, these results may explain why the frequency-dependent changes that we measured were different for each unit. Although we did not discern any differences between regular and fast spiking neurons for any measure, there are limitations in such cell type classifications with extracellular recordings. Furthermore, we also observed changes in the latency of evoked spikes

due to repetitive stimulation, which has previously been shown to occur in the presence of short-term plasticity (Boudkkazi et al., 2007). The latencies typically changed more often with higher frequency stimulation in spikes closer to the stimulated site, similar to the evoked spike probability and inhibitory response changes. Future studies with specific differentiation between cell and synapse types may shed more light on whether cell-type specific differences account for the variability across spikes.

Excitation and inhibition are independently activated but modulated together within an interconnected network

The balance between excitation and inhibition within the cortex is a much-studied topic and is highly relevant to neural computation. Though the examined network size, location, and synaptic connections vary greatly, the strong consensus is that excitation and inhibition are generally comodulated (Chen, 2004; Haider, 2006; Isaacson & Scanziani, 2011; Rubin et al., 2017; Turrigiano, 2012; Xue et al., 2014). Whether a stimulus evoked a spike on a trial-by-trial basis did not affect the subsequent inhibitory response, but we found that the probability of evoking a spike and the duration of inhibition were frequently positively or negatively correlated over time. Units close to the stimulated site typically had positively correlated evoked spike probability and inhibition duration, both of which were negatively correlated with firing rate. Units far from the stimulation channel, however, had positively correlated evoked spike probabilities and firing rates, which were both negatively correlated with inhibition duration.

The effect of distance can be explained by the fact that sites closer to stimulation are more likely to be activated by ICMS (Butovas & Schwarz, 2003; Hao et al., 2016). Due to the feedforward and feedback inhibitory circuitry, if the total excitation increased or decreased due to short-term plasticity, the inhibition should change in a positively correlated manner. Sites far from

stimulation, however, are not activated as comprehensively and are thus less likely to be susceptible to short-term plasticity. Similarly, the negative correlations in evoked spike probability and inhibition at these far sites are likely due to network dynamics, whereas the positive correlations in closer sites are likely due changes in short-term plasticity caused by direct activation via ICMS.

Tables and Figures

Table 3.1 Evoked spike probability and inhibition duration correlations with spontaneous firing rate.

The numbers show number of units that fall within that category. Note the high number of units that have a positive correlation between evoked spike probability and spontaneous firing rate and a negative correlation with inhibition duration and spontaneous firing rate (red).

		Inhibition duration and spontaneous firing rate			
		Uncorrelated	Positive Correlation	Negative Correlation	**Total**
Evoked spike probability and spontaneous firing rate	Uncorrelated	10	18	37	**65**
	Positive Correlation	86	77	300	**463**
	Negative Correlation	12	13	32	**57**
	Total	**108**	**108**	**369**	**585**

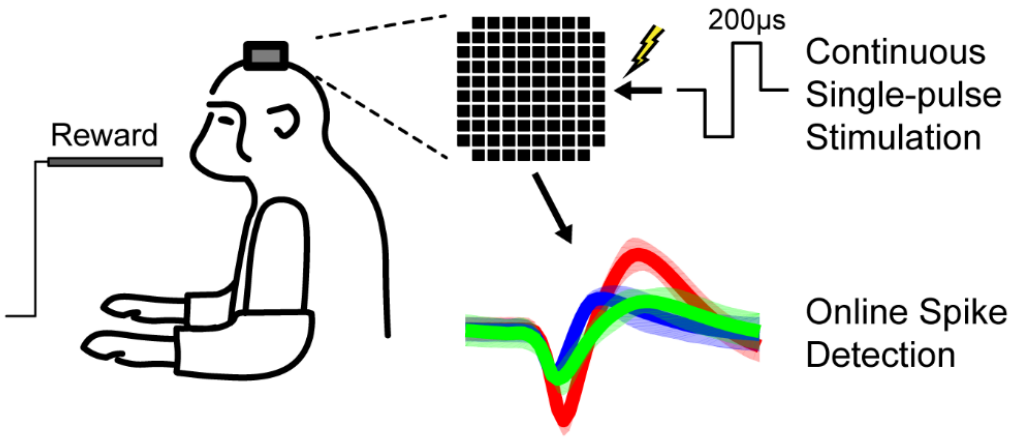

Figure 3.1 Experimental design

Macaques calmly sat in a chair receiving apple smoothie reward through the experiment. Cathodic, 200us phase width, single-pulse ICMS was delivered to one channel of the Utah array in primary motor cortex while unit responses were recorded across the array. Each session consisted of a prestimulus and stimulus epoch.

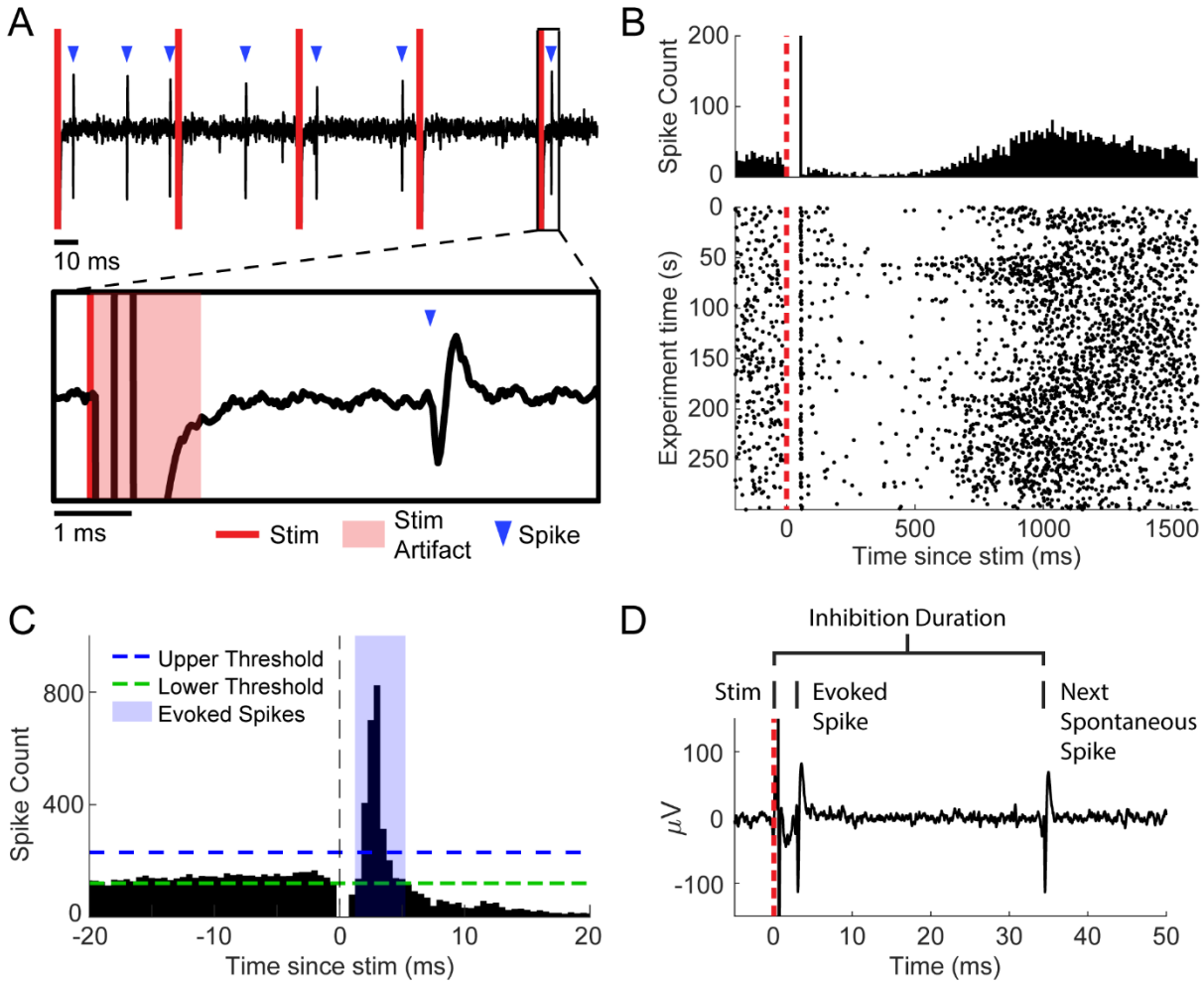

Figure 3.2 Detection of evoked spikes and inhibition

A. Example of filtered data trace. The inset shows a stimulus followed by an evoked spike after 3.5 ms. **B.** Example PSTH (top) and corresponding raster plot (bottom). **C.** Defining evoked spikes. A PSTH with 0.5 ms bins was generated. Peaks after the time of stimulation greater than the upper threshold (mean+2 standard deviations of -20 to -2ms in the PSTH) down to the lower threshold (mean-2 standard deviations) were called evoked spikes. **D.** Defining inhibition. Rather than using the PSTH, the inhibition duration was calculated for each stimulus by taking the time from stimulus onset to the next spontaneous spike.

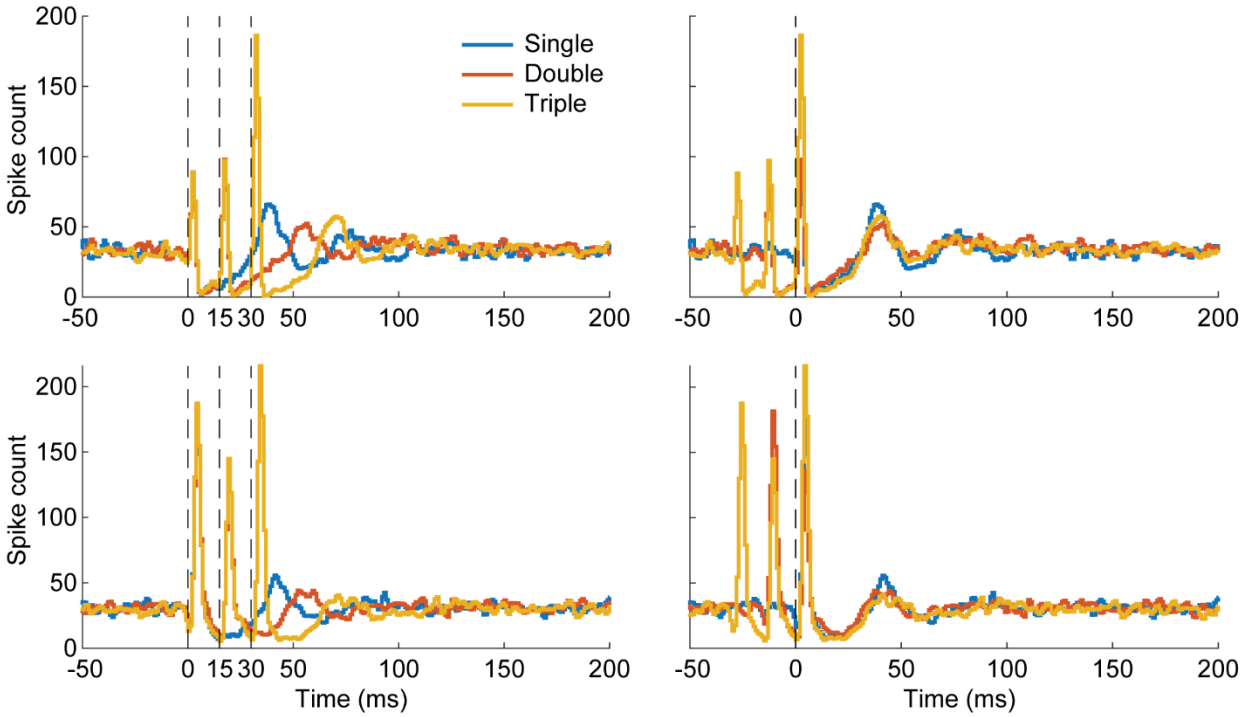

Figure 3.3 Stimulation during inhibition

Two PSTH examples with 1 ms bins of double- and triple-pulse stimulation in which subsequent pulses arrive during the inhibitory response of the previous pulse (left). Spikes were readily evoked even when stimulating during the inhibitory response. Aligning the PSTHs to the final stimulus pulse (right) shows that the inhibition restarts at each stimulus pulse. Each condition consisted of 1500 stimuli.

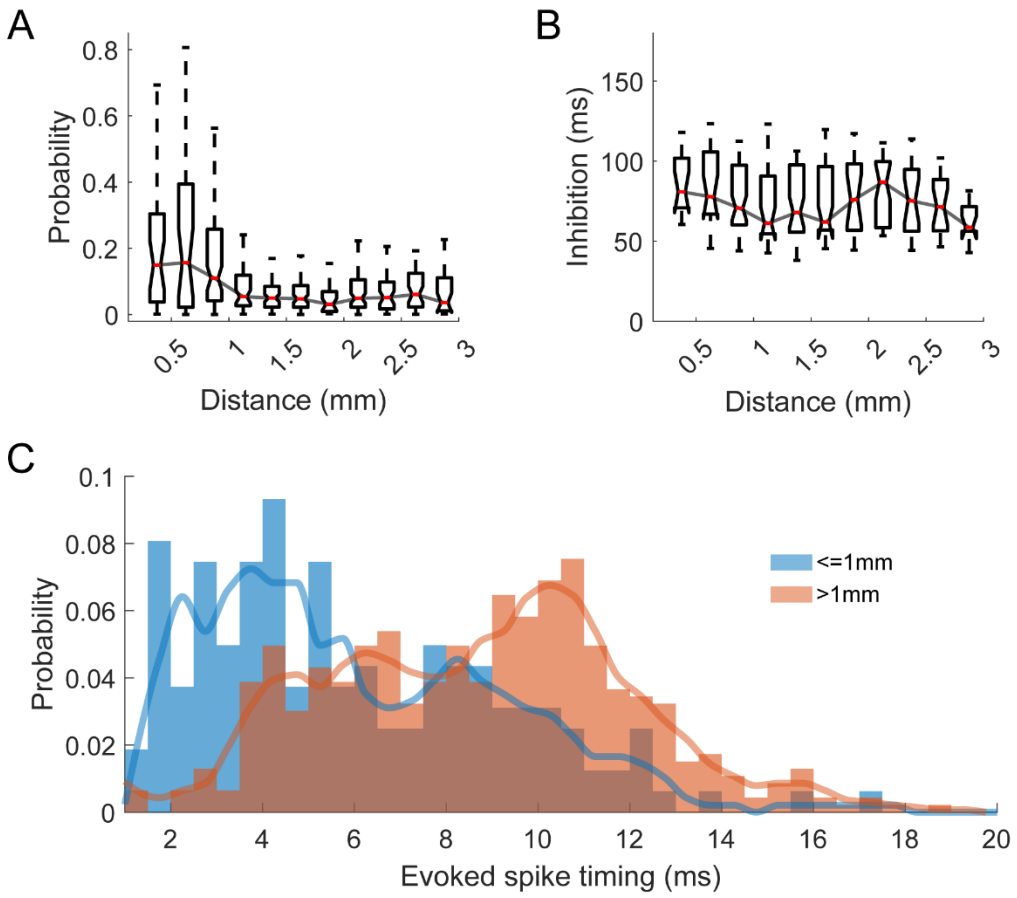

Figure 3.4 Effect of distance from stimulus site on evoked spike probability

A. Evoked spike probability with respect to distance from the stimulated site. **B.** inhibition duration with respect to distance from the stimulated site. **C.** Histogram of evoked spike timings split into sites close (<1mm, n=121) to the stimulated site and all other sites (n=299). The line shows the cubic interpolated moving average over 3 bins.

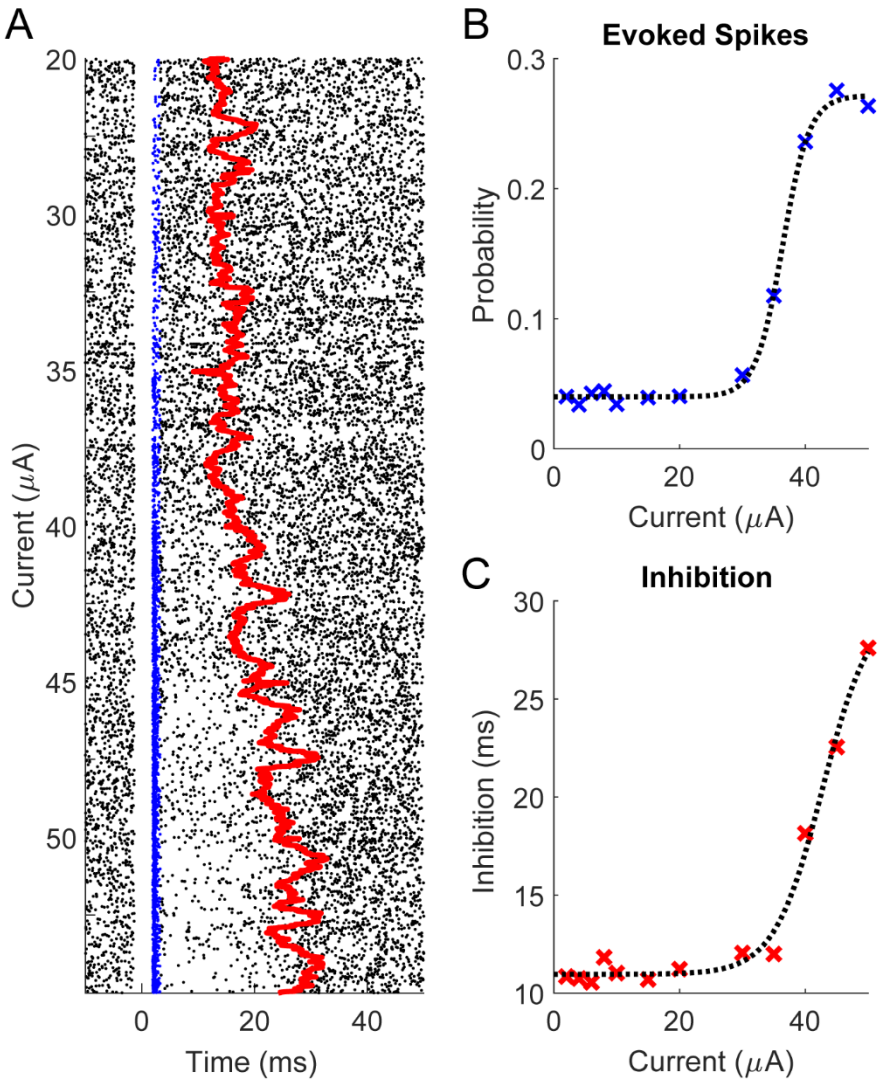

Figure 3.5 Effect of stimulus amplitude on evoked spike probability and inhibition duration

A. An example raster plot of a spike over different stimulus current amplitudes delivered for five minutes each at 2 Hz. Blue dots represent evoked spikes and the red line shows the median of the inhibition duration binned every 30 seconds with 1 second steps. **B.** An example evoked spike probability as a function of amplitude and **c)** inhibition duration as a function of stimulus amplitude. The dashed lines are fitted sigmoidal curves using least-squares regression.

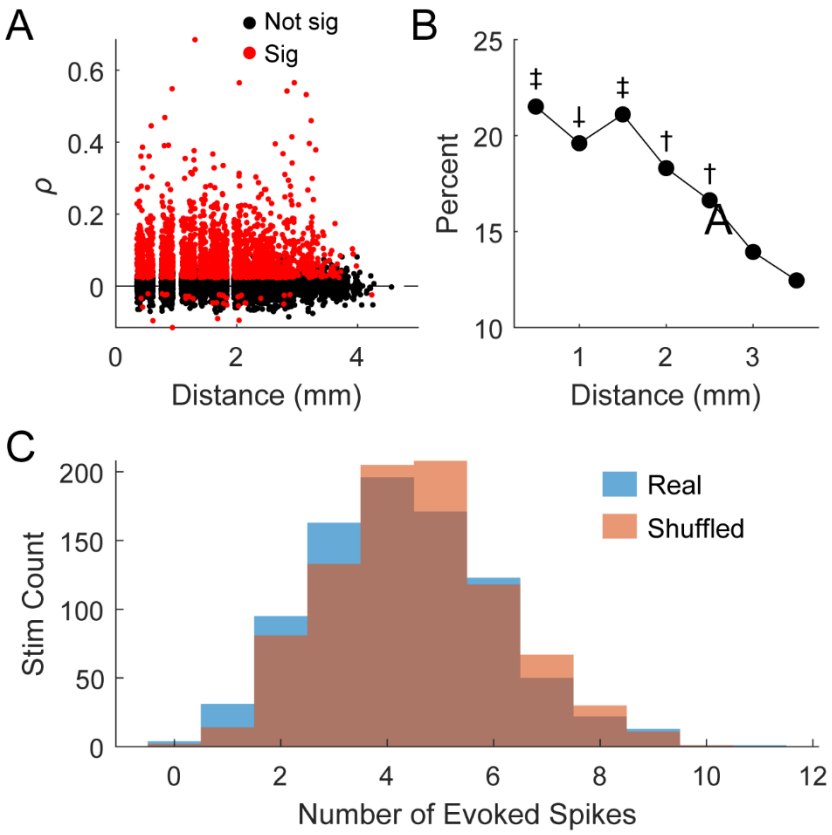

Figure 3.6 Covarying evoked spikes

A. Pearson correlation coefficient between pairs of units on whether individual stimuli evoked a spike or not plotted against the distance between the units (n=585). **B.** Pairs of units closer to each other had a higher chance of having a significant correlation (†: significantly different from the last two points; ‡: significantly different from the last 4 points; ⊥: significantly different from the last 3 points; $p<0.05$, ANOVA). C**.** An example of distributions of stimuli that evoked a specific number of evoked spikes using the true data (Real) and when the evoked spikes were shuffled (Shuffled). The two distributions were not statistically significant from one another ($p=0.11$, Kolmogorov-Smirnov test).

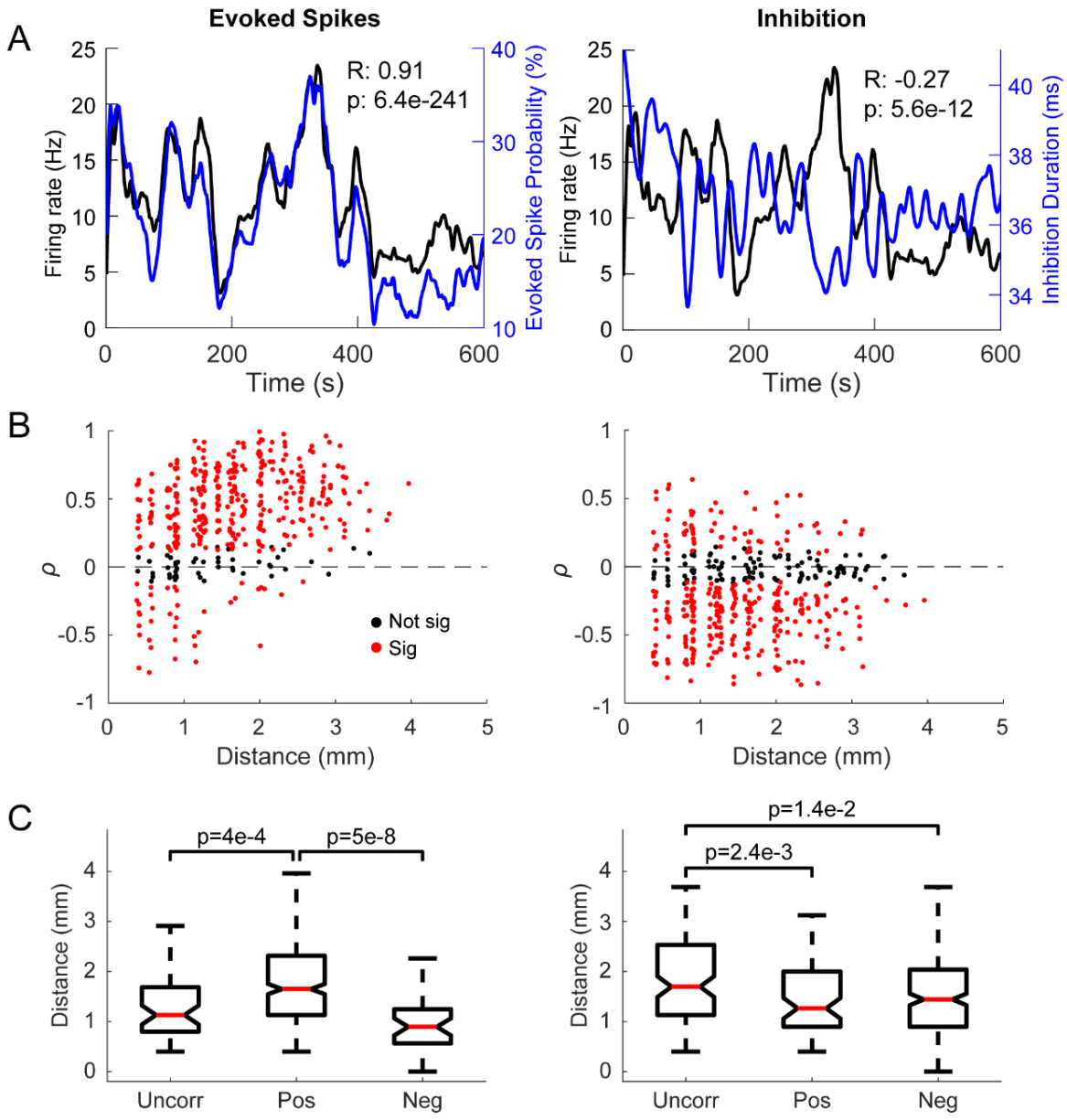

Figure 3.7 Probability of evoking a spike and inhibition duration are related to spontaneous firing rate

A. An example of a neuron with positively correlated firing rate (black) and evoked spike probability (blue) over 10 minutes. The rate and probabilities are averaged over 30 second bins with 1 second steps. **B.** Scatter plot of the Pearson correlation coefficient (ρ) between the spontaneous firing rate and the probability of evoking spikes (left) or the inhibition duration (right) against the distance of the recorded spike from the stimulated site (n=420). **C.** The same unit had a negatively correlated firing rate (black) and inhibition duration (blue). The inhibition duration is also averaged over 30 second bins with 1 second steps. **C.** Distance from the stimulated site for units with uncorrelated, positively correlated, and negatively correlated evoked spike probabilities (left) or inhibition duration (right) with firing rate. Labeled p-values are from the Wilcoxon rank-sum test.

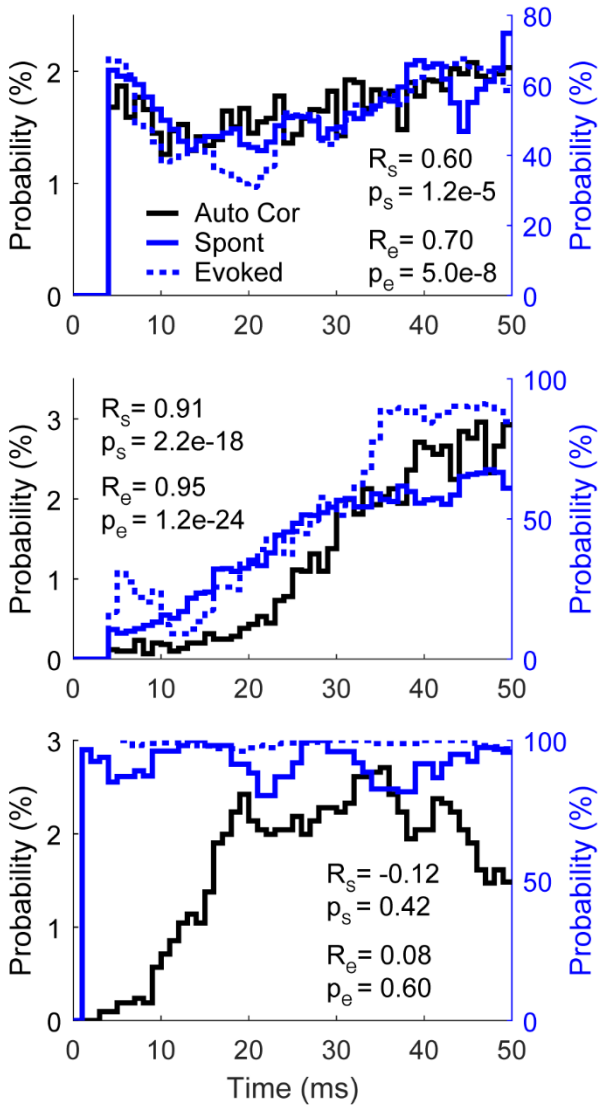

Figure 3.8 Probability of evoking a spike is dependent on the timing of stimulus

Three examples of spike autocorrelations (Auto Cor), and probability of a stimulus evoking a spike relative to timing from the most recent spontaneous (Spont) and evoked (Evoked) spike. Top and middle show two different autocorrelation waveforms with correlated evoked spike probability. They are not aligned in the bottom example; this typically occurs when the probability of evoking a spike is high. All traces show a moving average using 5 ms bins with a 1 ms step size. R_s is the correlation coefficient between Auto Cor and Spont, R_e the correlation coefficient between Auto Cor and Evoked, and p_s and p_e are the corresponding p-values of correlation.

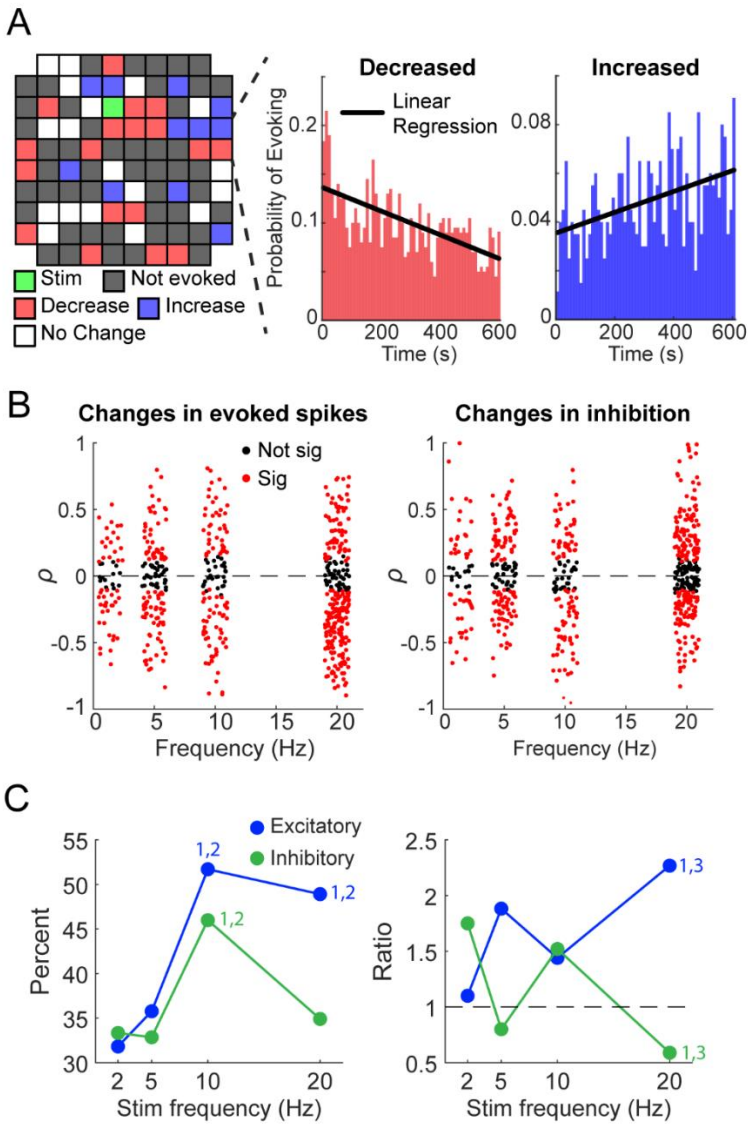

Figure 3.9 Repetitive stimulation changes evoked spike probability and inhibition duration

A. Left: Changes in evoked spikes across the array during a session with 10 Hz repetitive stimulation. A random unit was chosen for each electrode to demonstrate the lack of spatial organization of changes in responses. Right: Examples of changes in the probability of evoking spikes increasing or decreasing over time. **B.** Pearson correlation coefficients of evoked spike probability and inhibition duration plotted against stimulation frequency (n=585). Note that experiments delivered tonic stimulation at 2, 5, 10, or 20 Hz; a jitter was added to the frequencies of each point to better visualize the data. **C.** The percentage of spikes that had significant ($p<0.05$) changes over time for each stimulation frequency for both evoked spike probability and inhibition (left) as well as the ratio of decreases to increases (right). The dashed line of the right plot shows a threshold – if the value is higher (>1) the changes induced are more likely to be decreasing whereas if the value is lower (<1) the changes are more likely to be increasing. Numbers above points denote significance (1: significant from 2 Hz, 2: significant from 5 Hz, 3: significant from 10 Hz; $p<0.05$, ANOVA).

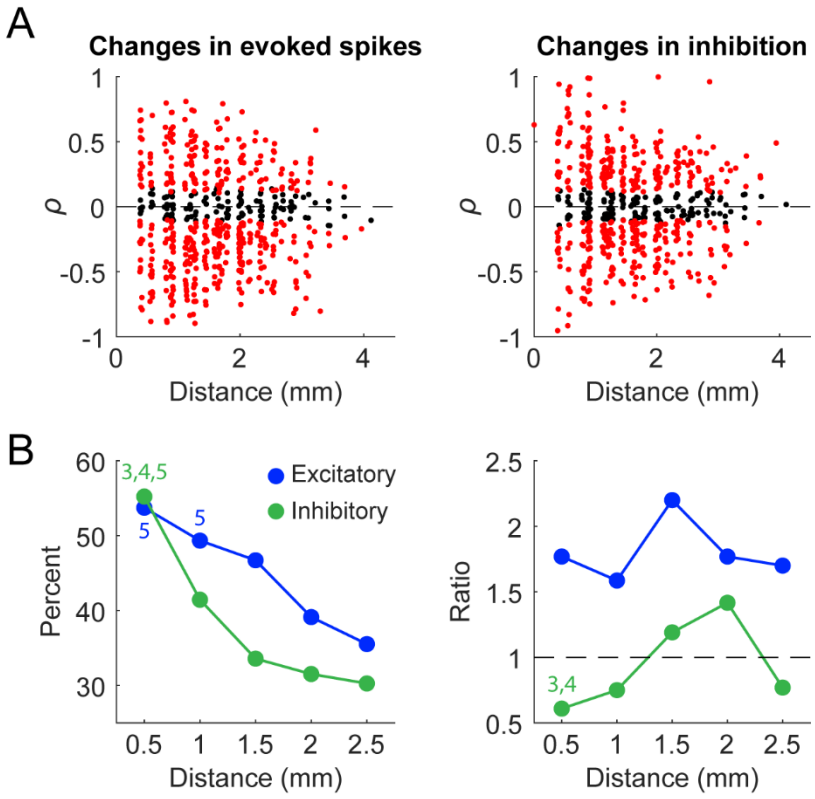

Figure 3.10 Changes in evoked spike probability and inhibition duration with repetitive stimulation with respect to distance

A. Pearson correlation coefficients of evoked spike probability and inhibition duration plotted against distance of the recorded spike from the stimulated site (n=585). Note that experiments delivered tonic stimulation at 2, 5, 10, or 20 Hz; a jitter was added to the frequencies of each point to better visualize the data. **B.** The percentage of spikes that had significant ($p<0.05$) changes over time for each bin of distance (±0.25 mm around each point) for both evoked spike probability and inhibition (left) as well as the ratio of decreases to increases (right). We did not include data points from channels greater than 2.75 mm from the stimulated site to this figure due to the lack of samples. Numbers above points denote significance (3: significant from 1.5 mm, 4: significant from 2 mm, 5: significant from 2.5 mm; $p<0.05$, ANOVA).

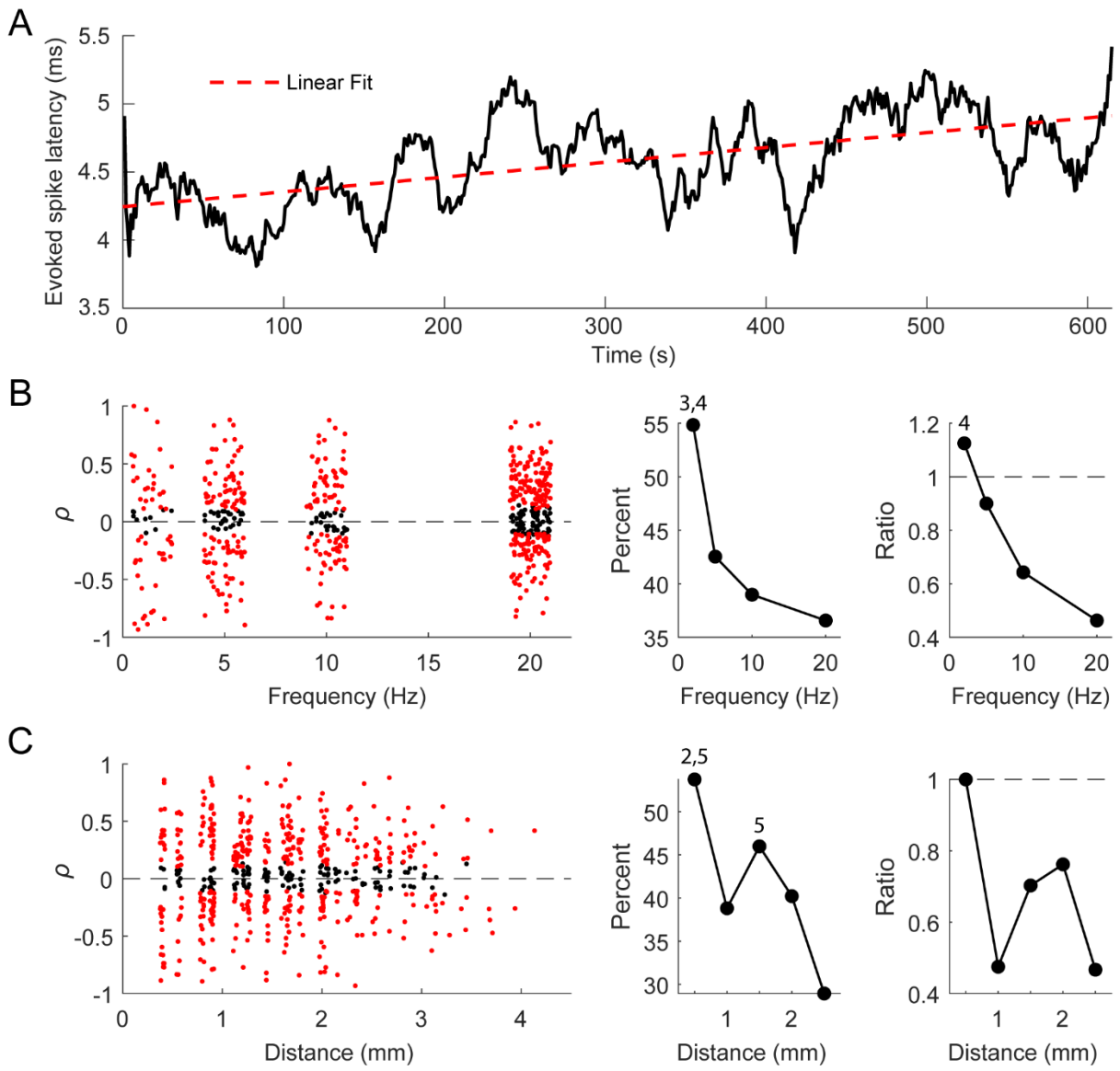

Figure 3.11 Changes in evoked spike latency with repetitive stimulation

A. An example of evoked spike latency changing over time. **B.** Scatter plot of Pearson correlation of the evoked spike latency over time with respect to stimulation frequency (left) (n=585). Percentage of evoked spike latencies with a significant change over time (middle), and the ratio of decreases to increases (right). Numbers above points denote significance (3: significant from 10 Hz, 4: significant from 20 Hz; $p<0.05$, ANOVA). **C.** Scatter plot of Pearson correlation of the evoked spike latency over time with respect to distance from the stimulated site (left). Percentage of evoked spike latencies with a significant change over time (middle), and the ratio of decreases to increases (right). Numbers above points denote significance (2: significant from 1 mm, 5: significant from 2.5 mm; $p<0.05$, ANOVA).

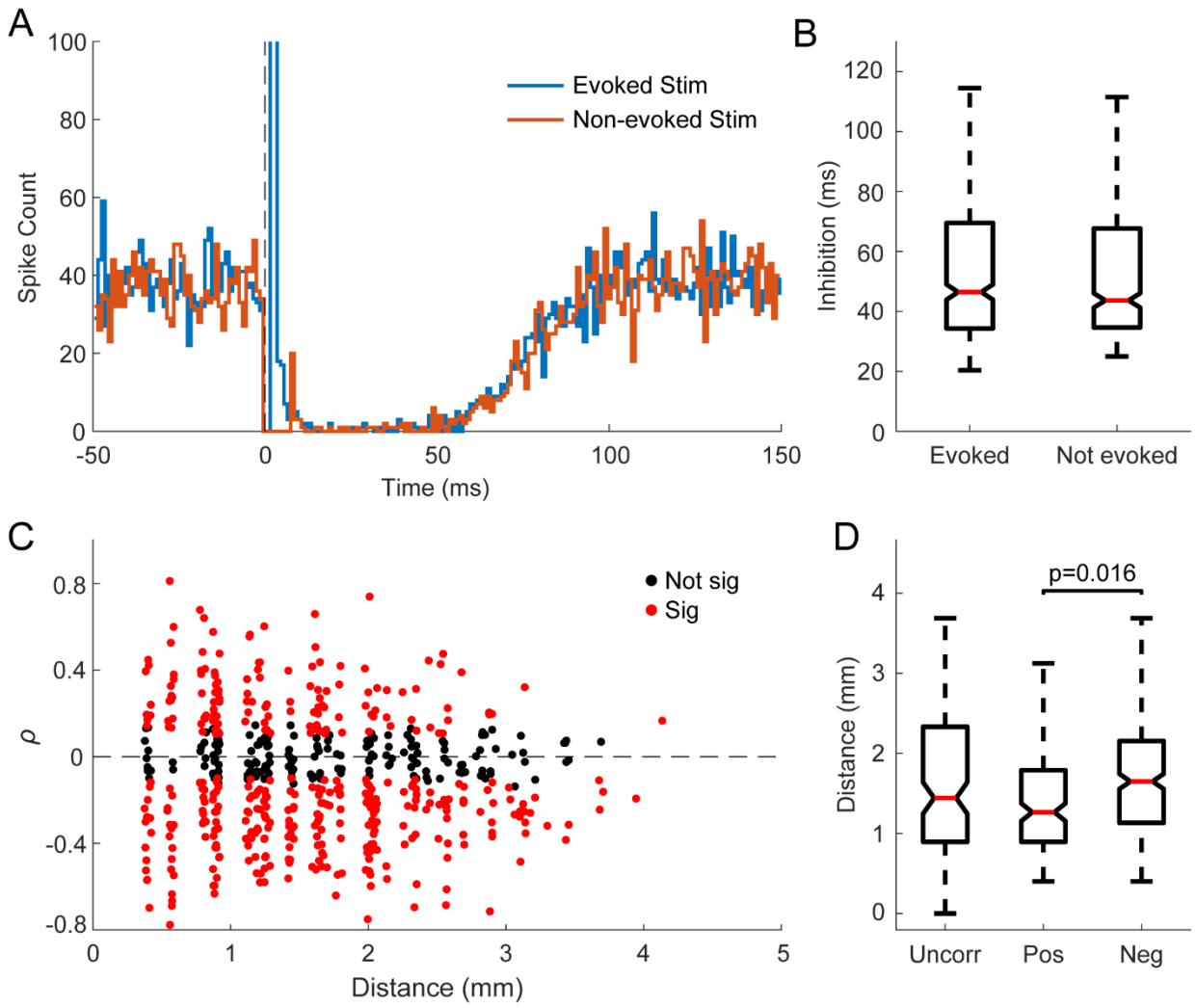

Figure 3.12 Relationship between evoked spikes and inhibition

A. Example PSTH with 1 ms bins following stimuli that evoked spikes and those that did not demonstrating similar inhibitory response. Each condition consisted of 1500 stimuli. Smoothed (2 ms wide gaussian moving window) PSTH of the two different stimulation classifications. Note the inhibition is extremely similar for both. **B.** A comparison of the inhibition strength in the two different classifications for 470 units. There was no statistically significant pairwise difference between the two groups. **C.** Scatter plot of the Pearson correlation coefficient between evoked spike probability and inhibition duration against distance of the recorded spike from the stimulated site. **D.** Comparisons of distance from the stimulus site of units with uncorrelated, positively correlated, and negatively correlated evoked spike probability and inhibition duration. The labeled p-value is from the Wilcoxon rank-sum test.

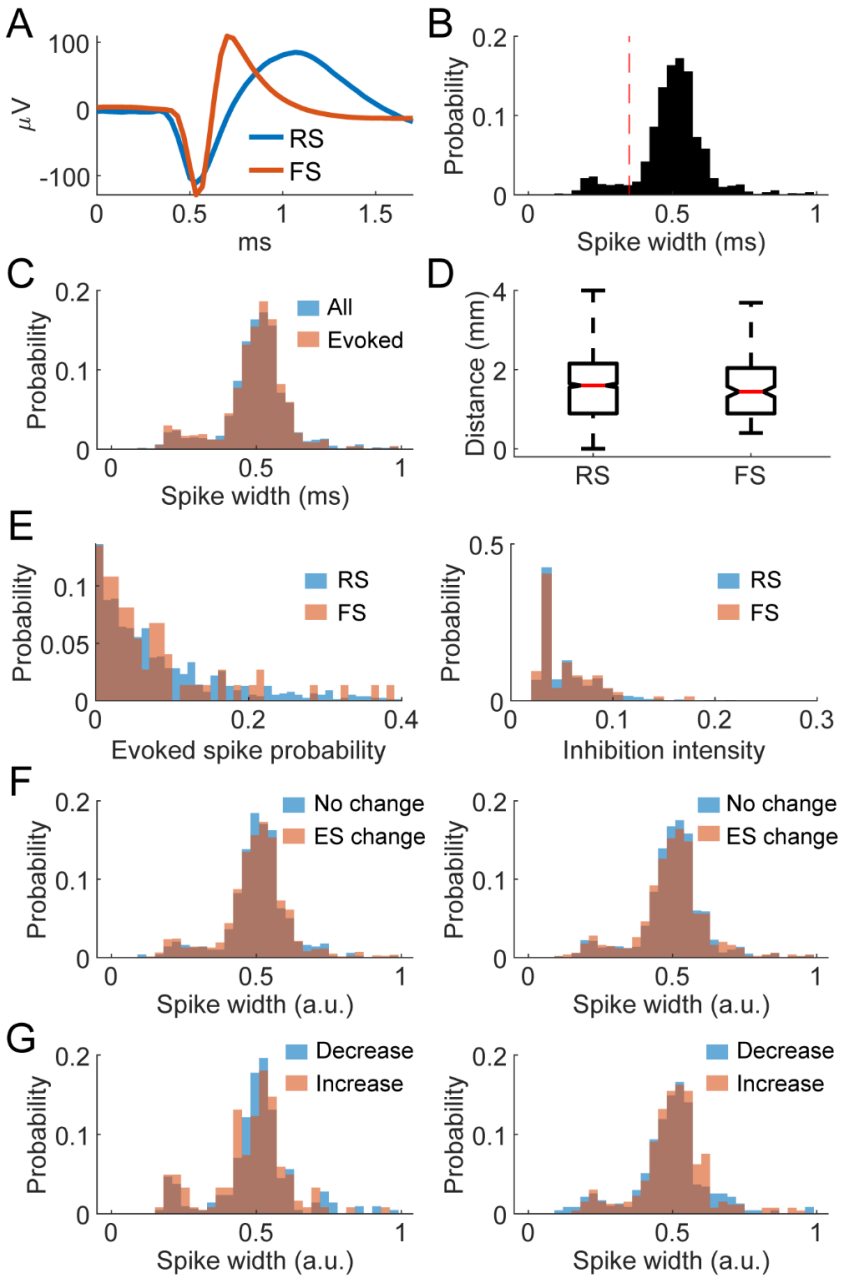

Figure 3.13 Comparisons between regular spiking and fast spiking neurons

A. Example of regular spiking (RS) and fast spiking (FS) neuron waveforms. **B.** Distribution of the widths of spike waveforms (trough to peak time). Vertical dotted line indicates the classification boundary (0.35 ms) – fast spiking neurons fall to the left and regular spiking to the right. **C.** Spike width distribution of all recorded spikes and spikes that were evoked by stimuli. **D.** Distance from the stimulated site of evoked spikes grouped by spike width. **E.** Evoked spike probability distribution (left) and inhibition duration distribution (right) of RS and FS neurons. **F.** Spike width distributions of evoked spike probability change vs no change over time (left) and inhibition duration change vs no change over time (right). **G.** Spike width distributions of evoked spike probability decrease vs increase over time (left) and inhibition duration decrease vs increase over time (right).

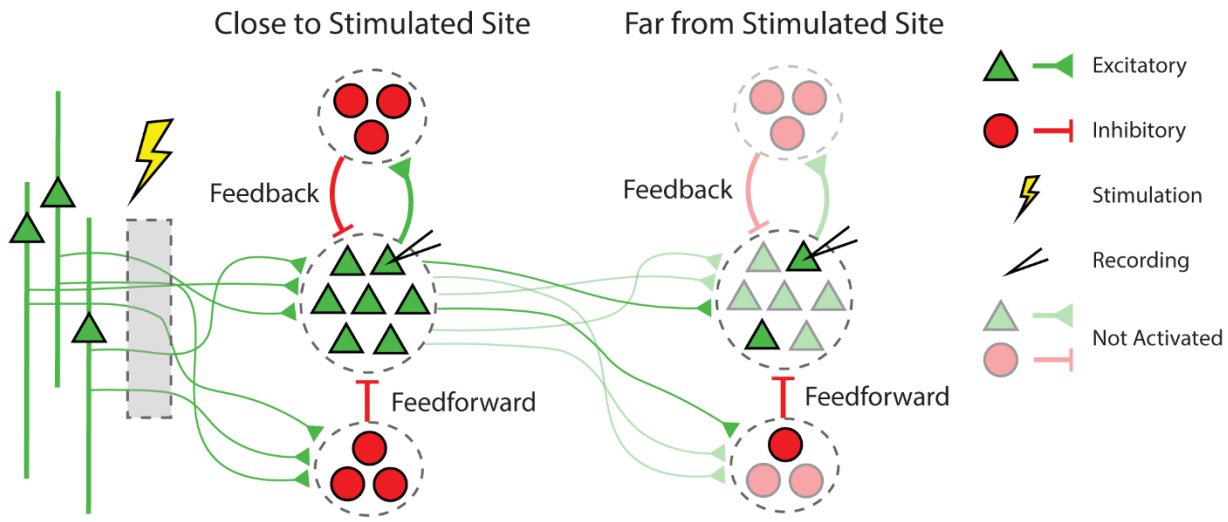

Figure 3.14 Stimulation response circuitry

Schematic of ICMS activated circuitry that generates excitatory and inhibitory responses through feedforward and feedback mechanisms. Stimulation activates axons projecting to the recording site. Sites closer to the stimulated site have more complete activation compared to sites further from the stimulated site. Possible direct connections from the stimulated site to the far site would also be sparsely activated.

Chapter 4. Paired stimulation for spike-timing dependent plasticity quantified with single neuron responses in primate motor cortex

Abstract

Spike-timing dependent plasticity (STDP) has been extensively studied *in vitro* and *in vivo*. Previous studies have demonstrated stimulus induced targeted STDP, but they usually required long conditioning periods and the induced changes were not consistent between different channel pairs. We hypothesized there were two reasons contributing to the difficulties in inducing STDP: 1. the measure of connectivity is poorly understood, and 2. the timing of stimulation is static or has low temporal specificity. To test our hypotheses, we applied paired stimulation to the primary motor cortex of awake primates. Single unit responses to stimulation were used as measures of connectivity, and we applied inter-stimulus intervals (ISIs) from ±0.1 to ±50 ms with sub-millisecond intervals. The excitatory single unit response resulted in very consistent changes after conditioning that was dependent on the ISI. Negative ISIs resulted in depression similar to classic STDP, but positive ISI also often resulted in depression. Normalizing the ISIs to the timing of the excitatory response revealed that potentiation only occurred if the second stimulus arrived before the response. Stimuli occurring around the time of the response often resulted in depression as strong as negative ISIs. We additionally tracked the changes in cortico-cortical evoked potentials (CCEPs), a commonly used measure of connectivity in plasticity experiments. CCEP changes showed a similar but more variable dependence on ISI. These results show that the classic STDP curve may be more difficult to replicate *in vivo* due to interactions between excitatory and inhibitory circuitry, and that CCEPs may not be the ideal measure of changes in strength of connectivity.

Introduction

Since the proposal of Hebbian plasticity (Hebb, 1949), neuroplasticity has been studied extensively. Seminal *in vitro* studies expanded upon Hebb's theory by showing that the specific timing of the pre- and postsynaptic cell activation is crucial for the changes in the synapse, called spike-timing dependent plasticity (STDP); if the postsynaptic cell is activated after the presynaptic cell the synapse is strengthened, and if the postsynaptic cell is activated before the presynaptic cell the synapse is weakened (Bi & Poo, 1998; Markram et al., 1997). Subsequent *in vivo* studies delivered activity-dependent stimulation, in which the postsynaptic site is stimulated immediately following spontaneous activity in the presynaptic site, to increase synaptic strength between cortical or cortico-spinal sites in both rodents and non-human primates (Jackson et al., 2006; McPherson et al., 2015; Nishimura et al., 2013; Rebesco et al., 2010).

Another method of investigating STDP is with paired stimulation, in which both the pre- and postsynaptic sites are directly activated via individual stimuli with a delay called the inter-stimulus interval (ISI). An advantage of paired stimulation is that it can be used to activate the postsynaptic site before the presynaptic site and artificially weaken synapses, a paradigm that is not possible with activity-dependent stimulation. Paired stimulation can also be delivered open loop, and does not require any recording, providing potentially simpler clinical applications. Inducing STDP with paired electrical stimulation has also been demonstrated *in vivo* in both rodents and non-human primates; however, the induced changes were often inconsistent across tested channels (Rebesco & Miller, 2011b; Seeman et al., 2017; Werk et al., 2006). Previous studies also used a limited number of ISIs and required up to 72 hours of continuous stimulation consisting of at least tens of thousands of paired stimuli to produce measurable, lasting changes.

We hypothesized that two factors may be limiting our understanding of applying paired stimulation *in vivo*. First, electrical stimulation in the context of paradigms for inducing plasticity is typically considered to be excitatory, but several studies have shown that stimulus response consists of a short-term excitatory response immediately followed by a long-term inhibitory response that is often strong enough to completely silence the cell for up to hundreds of milliseconds (Butovas & Schwarz, 2003; Logothetis et al., 2010; Yun et al., 2022). Electrical stimulation activates a bundle of fibers that project to the recorded site that excites the recorded neuron but also activates the surrounding inhibitory circuitry resulting in GABAergic inhibition (Butovas et al., 2006). As the dynamics of single unit responses change at sub-millisecond intervals, a more comprehensive set of ISIs with higher specificity may be necessary to fully explore paired stimulation *in vivo*.

Second, plasticity studies *in vivo* typically use macroscopic metrics as a measure of connectivity between two cortical sites, such as motor evoked potentials, directional tuning, coherence, or cortico-cortical evoked potentials (CCEPs) (Jackson et al., 2006; Seeman et al., 2017; Yazdan-Shahmorad et al., 2018). CCEPs are generated by delivering a stimulus to the presynaptic site and calculating the stimulus triggered averages of the local field potential response at the postsynaptic site. Studies usually quantify the response into a single value using the peak-to-peak amplitude or the root-mean square, with a larger value signifying a stronger connection. However, CCEPs are complex and multiphasic, and the underlying sources of various phases and amplitudes of the response are still unclear (Boyer et al., 2018; Keller et al., 2014; Prime et al., 2020). Thus, a more direct measure of connectivity may clarify the changes induced by paired stimulation and their underlying mechanisms.

This study aims to better understand the application of paired electrical stimulation *in vivo* for the induction of STDP. We tested ISIs within a range of ±0.1 to ±50 ms at sub-millisecond intervals between pairs of channels up to 1.2 mm apart with the Utah array in primate motor cortex. We used the probability of a single-pulse stimulus in the presynaptic site evoking a spike in the postsynaptic site as a measure of connectivity strength. CCEPs were measured concurrently to compare the results between different connectivity metrics. In addition, we investigated changes in strength of the inhibitory response and evaluated all changes over a period of 10 minutes after conditioning to elucidate the underlying mechanisms.

Materials and Methods

Experimental design

Implants and surgical procedures

Two pigtail macaque monkeys (*Macaca nemestrina*), J and L, were unilaterally implanted with the Utah array (Blackrock Microsystems, Salt Lake City, UT) in the hand region of primary motor cortex (M1). Refer to "General Methods" for full details on implants and surgical procedures.

Experiment timeline

The two stimulated sites – "Pre" and "Post" sites – were determined by choosing a pair of channels in which stimulating the Pre site reliably evoked spikes in the Post site during a 1-minute preliminary recording. Each experiment consisted of 3 epochs: 1) pre-test – 10 minutes of test stimulation delivered to the Pre site, 2) conditioning – 10 minutes of paired stimulation, and 3) post-test – 10 minutes of test stimulation delivered to the Pre site (Figure 4.1). In addition, 5 minutes of baseline recording with no stimulation was collected both immediately before and after each experiment. As the stimulation could have long-lasting effects, conditioning between each channel pair was limited to once per day. Animals were trained to calmly sit in a primate chair throughout the duration of each experiment.

Cortical stimulation

All stimuli delivered were single-ended, single pulse with 200 μs phase width. Test stimuli were delivered at 5 Hz, Poisson distributed and paired stimulation during Conditioning were delivered at 10 Hz, Poisson distributed. These frequencies have been shown not to heavily affect the stimulus responses over time (Yun et al., 2022). The interstimulus interval (ISI) between the paired stimuli was randomly determined each day. All stimuli used an amplitude of 15 μA as

previous studies showed it to be sufficient to reliably activate the stimulated site and generate responses in sites up to 4 mm away (Butovas & Schwarz, 2003; Hao et al., 2016; Yun et al., 2022). The stimulus intensity was kept the same across all sessions rather than adjusted to the stimulus response to limit current spread. We chose channel pairs in which stimulating one site evoked spikes in the other within 5 ms to ensure the presence of monosynaptic projections. The distance between channel pairs was between 400 and 1200 μm (up to 3 channels apart).

Data analysis

Recording and spike sorting

We used the Neural Interface Processor (Ripple Neuro, Salt Lake City, UT) for both recording and stimulation. All 96 channels of the Utah array were recorded at 30 kHz throughout every experiment. Stimulus artifacts typically lasted 1-1.5 ms, and each stimulus pulse triggered a fast settle of 0.8 ms to minimize the stimulus artifact without affecting the stimulus evoked spike. The signals were bandpass filtered between 1 and 2 kHz for spike sorting to further minimize the artifact.

Spikes were sorted offline using custom MATLAB code through two-window discrimination; a window of -0.5 to 1.5 ms each time the signal crossed a negative threshold were collected, then two time-amplitude windows were manually selected to detect the peak and trough of the spike waveform. The investigator sorting the spikes were blind to the stimulus condition to ensure objective evaluation.

Stimulus evoked spikes and inhibitory response duration

Detailed methods of detecting stimulus evoked spikes and calculating the inhibitory response duration can be found in Yun et al. 2022. In brief, stimulus evoked spikes were found by

calculating the peristimulus time histogram (PSTH) of each spike. To isolate the evoked spikes from the spontaneous activity, we defined upper and lower thresholds in the PSTH as the histogram mean plus or minus 2 times the standard deviation from -20 to -2 ms. We then found the largest peak in the PSTH from 1 to 15 ms after stimulation that was larger than the upper threshold and tracked adjacent bins in both directions until we reached the lower threshold on both sides. All spikes occurring within this window were denoted as stimulus-evoked spikes. If no peak was greater than the threshold the spike was not considered to have been evoked by stimulation. The average latency of evoked spikes was calculated as the median delay of evoked spikes from stimulation onset.

We measured the duration of inhibition by removing all evoked spikes and calculating the time between the onset of stimulation and the next spontaneous spike. Inhibition was deemed to be stronger when the delay from stimulation onset to the next spontaneous spike was longer. We discarded any stimuli for which the subsequent stimuli occurred before the next spontaneous spike.

Cortico-cortical evoked potential calculation

One method of calculating the magnitude of CCEPs is the peak-to-peak amplitude (Seeman et al., 2017; Zanos et al., 2018). However, as CCEPs can vary in timing and waveform the root mean square (RMS) for the area under the curve is sometimes used as a more consistent substitute measure of CCEP magnitude (Dionisio et al., 2019; Enatsu et al., 2013). However, as the changes were much more variable when using RMS or the area under the curve (Supplementary Figure 4.1), comparisons with single unit responses and the changes of measures over time used the peak-to-peak amplitude.

To obtain the peak-to-peak amplitude, stimulus-triggered averages of raw LFPs were calculated from 10 ms before to 50 ms after stimulus onset. The amplitude was then calculated by subtracting the largest trough from the largest peak in a window of 1.5 to 50 ms after stimulation. To obtain the RMS magnitude we calculated the RMS over stimulus triggered averages of raw LFPs from 1.5 to 50 ms after stimulus onset:

$$RMS = \sqrt{\frac{1}{N}\sum_{n=1}^{N}|x_n|^2} \qquad \text{Equation 4.1}$$

where x is the signal and N is the number of samples. The area under the curve was calculated as the sum of the rectified average response in a window of 1.5 to 50 ms after stimulation.

Stimulus artifacts were removed from all CCEP illustrations presented here by blanking out 0 to 1.5 ms from stimulation. If the calculated magnitude was less than 4 standard deviations of the signal from -10 ms to 0 ms of stimulus onset it was assumed there was no CCEP at the recorded site. CCEPs were not present in all channel pairs as they require raw local field potentials (LFPs) which are more susceptible to stimulus artifact compared to detection of single units.

Statistical analyses

Changes in stimulus response were calculated as the percent difference between the responses during the Pre- and Post-test epochs. Fisher's exact test was used to compare the probability of evoking a spike before and after conditioning. Wilcoxon rank-sum test was used to compare changes in inhibition duration due to the nonparametric nature of the distributions. Student's t-test was used to compare changes in CCEPs. Statistical tests used and p-values for significance are reported in individual analyses.

Results

We delivered paired stimulation between pairs of sites in the motor cortex of two monkeys: 86 conditioning experiments and 35 control experiments: 37 conditioning experiments and 11 control experiments with 26 unique channel pairs in Monkey J, and 49 conditioning experiments and 24 control experiments with 14 unique channel pairs in Monkey L. We attempted to test the same channel pair with as many different experimental conditions as possible, but single units were often not stable for extended periods of time.

Stimulus responses

Single-pulse intracortical electrical stimulation reliably evoked spikes followed by a long inhibitory response (Figure 4.2A). We calculated the probability of evoked spikes by finding the peak of the excitatory response and the duration of inhibition by finding the delay of the spike following each stimulus that is not an evoked spike (*Stimulus evoked spikes and inhibitory response duration* in *Methods and Materials*). Channel pairs were chosen such that the evoked spike arrived within 5 ms to ensure the presence of monosynaptic projections, and the inhibitory response lasted between 10 and 100 ms (Figure 4.2B). As the stimulus intensity was kept consistently low across all sessions to limit current spread, there was a wide distribution of initial evoked probabilities (Figure 4.2B).

We also simultaneously measured cortico-cortical evoked potentials (CCEPs) (Figure 4.2C). The responses typically had a narrow trough with the minimum value between 3 and 5 ms followed by a wider peak with the maximum value between 5 and 20 ms, similar to those seen in previous intracortical studies (Seeman et al., 2017; Zanos et al., 2018). The entire response typically lasted about 50 ms after stimulation. To ensure that evoked spikes did not contribute to the CCEPs, we calculated the CCEPs triggered from stimuli that evoked spikes or stimuli that did not evoke

spikes (Figure 4.2C, left). There was no significant difference between the two CCEPs across all experiments, showing that they are independent measures (Figure 4.2C, right).

Stimulus-evoked spikes reflect STDP-like changes

Paired stimulation caused significant changes in the probability of evoking spikes before and after conditioning depending on the ISI (Figure 4.3A). Paired stimulation in which the Pre site was stimulated following the Post site (negative ISIs) resulted in a consistent decrease in the evoked spike probability. This depressive state typically occurred within a 20 ms time window and exponentially decayed with larger ISIs, similar to what is seen in classic spike-timing dependent plasticity (STDP) (Bi & Poo, 1998; Markram et al., 1998).

When the Pre site was stimulated before the Post site (positive ISI) with a very short ISI, there was typically potentiation, again similar to classic STDP effects. However, with ISIs > 1 ms there was high variability in the induced changes. All potentiation occurred with ISIs less than 3 ms, and ISIs of 3-20 ms typically resulted in depression almost as strong as negative ISIs, contradicting classic STDP. ISIs greater than +20 ms had little to no change.

To better understand the timing of the effects of paired stimulation, we additionally analyzed the changes by normalizing the ISI to the average latency of evoked spikes following test stimuli (Figure 4.3B). Positive ISI results became more consistent: ISIs less than the evoked spike latency resulted in a greater change of an increase in evoked spike probability but reversing as it got closer to the evoked spike latency. ISIs less than 0.5 of the evoked spike timing consistently led to potentiation, whereas ISIs immediately before and after the evoked spike delay led to depression. Plotting results for the same channel pairs tested at different ISIs show that the trend holds true; the different ISIs seem to drive the changes rather than the variability between

channel pairs (Figure 4.3C). All data showing changes in responses are plotted against normalized ISI from this point forward.

We additionally analyzed whether there were consistent changes in baseline firing rate of the spikes before and after conditioning, as changes in excitability have been shown to affect both the probability of evoking a spike and the inhibitory response (Yun et al., 2022). However, there were no consistent changes in firing rate before and after conditioning, allowing us to directly compare the measures between the pre- and post-test epochs (Figure 4.4).

Finally, we also assessed whether the initial probabilities affected the highly variable changes observed at positive normalized ISIs between zero and 1 (second pulse delivered within the evoked spike latency). A strong initial response may be more difficult to increase due to saturation of activation, whereas a low initial response may be easier to increase. The initial probability of evoking a spike had a weak but significant negative correlation with the changes induced by conditioning, which may explain the high variability seen in that region of ISIs (Figure 4.5A).

Inhibitory responses

We tracked the changes in the inhibitory response duration of single units following stimulation to elucidate whether the stimulation evoked changes in the inhibitory circuitry. The term "inhibitory" as used here refers to the silencing of the neuron following the stimulus-evoked excitatory response that is likely driven by local inhibitory circuitry. Figure 4.6 shows the percent change in the median inhibitory response after conditioning relative to normalized ISI. The changes were not as large or consistent as the changes in the probability of evoked spikes, and the high variability makes interpretation of the effects of ISI difficult. However, the magnitude of the changes loosely followed classic STDP, with smaller ISIs typically resulting in

larger deviations, suggesting that conditioning was affecting the inhibitory response, and subsequently the local inhibitory circuitry.

CCEPs

We also tracked CCEPs before and after conditioning to compare the two measures of connectivity. Not every channel pair produced CCEPs as CCEPs are calculated with averaged LFP traces which are more variable, especially with the proximity of channel pairs used in our experiments. The changes reflected in CCEPs were not as consistent as with evoked spikes relative to the ISIs of the paired stimulation (Figure 4.7). The negative stimulation condition and the positive stimulation condition that arrived before evoked spikes had similar trends as with evoked spikes but the positive stimulation that arrived after evoked spikes had much higher variation. A large number of changes across the entire ISI spectrum deviated from the classic STDP curve.

We additionally plotted the changes in CCEPs as measured with root-mean squared or the area under the curve, as CCEPs are often complex and multiphasic (Supplementary Figure 4.1). However, the changes in these two measures were extremely variable especially in experiments with small ISIs. In addition, peak-to-peak is the most commonly used metric of CCEPs when used for connectivity analysis. As a result, all following analyses are performed with CCEPs as measured with peak-to-peak.

Comparisons between measures

We tested whether there was a direct relationship between the changes in evoked spike probability and inhibition for all ISIs but found no significant correlation (Figure 4.8). However, changes caused by different ISIs may be due to different mechanisms. As a result, we defined four distinct groups – 1) negative ISI greater than -20 ms, 2) positive ISI less than 10 ms with

potentiation, 3) positive ISI less than 20 ms with depression, 4) all other ISIs (Figure 4.9A). We observed no significant correlation between the three measures in each of the four groups (Supplementary Figure 4.2).

Nevertheless, the measures may have a nonlinear relationship; the same magnitude of change in inhibition duration in one channel pair may manifest differently in another channel pair. Therefore, we simplified the comparisons by grouping the changes in each region rather than looking for a direct correlation. Figure 4.9C shows that the inhibition duration typically increased when evoked spike probability decreased, but only with positive ISIs. CCEPs, on the other hand, were likely to increase with positive ISIs, but not in sessions with decreased evoked spike probability (Figure 4.9C). These results suggest that the changes induced by conditioning are reflected in each measure and that the underlying mechanisms may be affecting one another.

Persistence during the pre- and post-test epochs

We additionally determined whether the measures have baseline fluctuations over time during the pre-test epoch, and whether the changes we induced are consistent across the duration of the 10-minute post-test epoch. Figure 4.10 shows the aggregate z-scored changes in each measure over time, with significance from the first 10 seconds of the epoch denoted in red above. Evoked spike probabilities and inhibition duration were incredibly stable throughout the pre-test epoch, whereas the CCEP magnitude diminished slightly over time on average, though individual traces showed there are instances in which the magnitude increases over time. During the post-test epoch, the evoked spike probability had a slight but significant decrease over time and the inhibition duration had a slight but significant increase over time. The CCEP magnitude average seemed to be decreasing, but there was no statistical significance due to its variability.

However, as before, the changes that we observed during the post-test epoch may be specific to a range of ISIs. Using the four regions of ISIs previously defined, we further separated the changes in the measures over time (Figure 4.11). In sessions with negative ISIs (Figure 4.11, column 1) the inhibition duration change had a slight increase over time. This trend was reflected in the evoked spike probability as well but was not statistically significant. CCEP magnitude decreased over time on average but was highly variable and was not significant. In sessions with positive ISIs with increases in evoked spike probability (Figure 4.11, column 2) there was no consistent significant change over time in any measure. In sessions with positive ISIs with decreases in evoked spike probability (Figure 4.11, column 3) the evoked spike probably was initially low for the first 60 seconds that gradually increased to steady state over the course of the 10-minute epoch. This consistent trend was not reflected in any other measure. Finally, large positive ISIs (Figure 4.11, column 4) showed a decrease in CCEP magnitude over time.

To assess whether the changes in the measures we initially observed were simply due to the averaging of short-term effects, we plotted the previous scatter plots using the first minute of the post-test period and again with the last minute of the post-test period (Figure 4.12). Changes in evoked spike probability were similar to the composite results when using the first minute, but the depression in positive ISIs was exaggerated. The depression was still present when only considering the last minute but was slightly diminished. The increase in probability of evoked spikes at positive ISIs showed a similar trend, being stronger during the first minute compared to the last minute. Interestingly, large positive ISIs resulted depression during the first minute that switched into being generally potentiation during the last minute.

Changes in inhibition duration were more variable during the first minute. The only noticeable consistent change was the decrease during negative ISIs, which were mostly be contained within

smaller ISIs. Changes in CCEPs generally had high magnitudes during the first minute that decreased by the last minute. This may be related to the overall decrease we see in CCEP magnitude over time even during the pre-test epoch before any conditioning.

Control experiments

We performed experiments with six different control conditions: 1) Long delay – ISI of greater than ±100 ms, 2) Random stimulation – conditioning stimuli delivered randomly rather than time locked between the Pre and Post sites, 3) Subthreshold stimulation – 5 μA during conditioning shown to not evoked spikes, 4) No conditioning – no stimulation during conditioning, 5) Pre stimulation only – stimuli delivered only to the Pre site during conditioning, and 6) Post stimulation only – stimuli delivered only to the Post site during conditioning (Figure 4.13).

Changes in evoked spike probability and inhibition duration were all below 20% under any control condition. Evoked spike probability did not have a consistent change under any control condition, but inhibition duration typically decreased during Long delay experiments. CCEPs showed much larger changes of up to over 40%, and typically increased during Long delay experiments.

We also analyzed whether there were changes in any measure during the post-test epoch for each control condition (Supplementary Figure 4.3). Although there was no statistically significant change over time in any condition, CCEP magnitudes typically decreased over time during Long delay and Random stimulation experiments.

Discussion

Summary of findings

Paired electrical stimulation in the primate motor cortex induced changes in connectivity between two sites. The probability of evoking spikes in the postsynaptic site when stimulating the presynaptic site deviated from classic STDP; positive ISIs less than 20 ms often resulted in depression. We observed that potentiation only occurred when the stimulus delivered to the Post site arrived before the evoked spike latency. The duration of the inhibitory response following the stimulus evoked spikes also did not reflect classic STDP, but typically increased when evoked spike probability decreased during positive ISIs. CCEPs also did not reflect classic STDP, resulting in some depression in positive ISI experiments, and typically increased when the evoked spike probability increased as well as with large positive ISIs. Direct comparisons between all three measures did not show any significant correlations.

Analyses of the measures over time showed that both evoked spike probability and inhibition duration were consistent during the pre-test epoch, but CCEPs decreased over time. Further analysis of the post-test epoch showed that evoked spike probabilities increased over time in positive ISIs that induced depression, inhibition duration increased over time in negative ISIs, and CCEPs decreased over time in large positive ISIs. Most control conditions showed that there were no large consistent changes in all measures, but inhibition duration decreased and CCEP magnitude increased during experiments with a long delay between the paired stimuli.

Paired stimulation in vivo and single unit responses

Although delivering electrical stimulation to a cortical site activates excitatory fibers projecting to a neighboring site, it also activates fibers projecting to interneurons in the local circuitry that subsequently inhibit the recorded principal cells (Butovas et al., 2006; Logothetis et al., 2010;

Yun et al., 2022). Thus, improper delay of stimulation delivered to the Post site may enhance the inhibitory activity rather than the firing of the spike (Figure 4.14).

Our findings support this hypothesis as facilitation is only present when the stimulation of the Post site occurs before the evoked spike latency. In addition, the inhibition duration typically lengthens in positive ISI experiments that resulted in fewer stimulus evoked spikes, which further suggests the inhibitory circuitry becomes stronger or more active. The variability in the changes is both likely due to the initial evoked spike probability as well as the fact that inhibitory activity may be occurring as soon as the excitatory response due to their high connectivity and large number of horizontal projections in layer 2/3 (Adesnik & Scanziani, 2010; Isaacson & Scanziani, 2011).

The lack of symmetry in the distribution of changes in evoked spike probabilities is likely due to the specificity of the measure – we are measuring single unit responses in the Post-site and stimulating the Pre-site – resulting in non-specific changes when using negative ISIs. Following STDP, negative ISIs would result in excitatory projections from the Pre-site to the Post-site being weakened and projections from the Post-site to the Pre-site being strengthened. However, there is variability in the magnitude of changes in specific synapses and no guarantee of uniform changes on the synapses to and from the recorded stimulus evoked spike, which may explain the variability present in the strength of depression in negative ISI conditions.

Our findings do not contradict STDP as the changes are likely STDP mediated. The magnitude and direction of change was heavily dependent on the ISI and lasted for at least 10 minutes. Instead, the results suggest that stimulus induced plasticity in vivo is much more complex than previously thought, and the interactions within and between local circuitry must be taken into account.

Additionally, analysis of evoked spike probability and inhibition duration over time showed that the measures fluctuated over the 10-minute post-test epoch, especially in experiments that saw a decrease in the probability with evoked spikes with positive ISIs. As the curves seem to return to equilibrium, one theory could be homeostatic plasticity, but synaptic scaling typically occurs over the timescale of hours or days (Turrigiano, 2008, 2012). Another explanation could be that there are lingering effects of neurotransmitters receptors which can take time to return to baseline. However, the time constants of post-synaptic current of both glutamate and GABA receptors are within 100's of milliseconds, whereas the changes over time we observed lasted for 10's of seconds (Bettler et al., 2004; Thomson & Destexhe, 1999). The timescale does match short-term plasticity (Zucker & Regehr, 2002); however, short-term plasticity is typically induced by open loop stimulation, and as such we should observe the same changes over time regardless of the ISI as well as in control experiments. Thus, we may be observing some other form of regulating plasticity.

Comparison with CCEPs

CCEPs had similar changes as evoked spike probability, but with much higher variability. Although CCEPs are directly indicative of neural responses, they are a measure of population activity which may detract from the changes induced by the conditioning (Keller et al., 2014; Prime et al., 2020; Vincent et al., 2017). This is confirmed in our study in which CCEPs are independent of the stimulus evoked spikes, as they are a result of greater spatial integration. We additionally observed more variable changes in CCEPs due to conditioning relative to the ISI, similar to a previous experiment studying paired stimulations with CCEPs in which a limited number of channel pairs could be induced with STDP (Seeman et al., 2017).

Intracortical CCEPs, especially when used as a measure of connectivity, are most commonly measured using the peak-to-peak amplitude under the assumption that it reflects synchronized firing of spikes – more spikes firing as a result of stimulation result in a larger amplitude CCEP (Seeman et al., 2017; Zanos et al., 2018). However, this interpretation of CCEPs suggests that proper timing of stimulation to arrive at or before the trough should reliably induce potentiation, which was not observed in our study. Instead, CCEPs may be reflective of excitatory responses in conjunction with inhibitory responses and possibly involve complex spatiotemporal summation (Keller et al., 2014; Vincent et al., 2017). Different measures suggested from previous literature, such as root-mean squared and area under the curve, did not provide more consistent results (Prime et al., 2020).

Additionally, we observed that CCEPs typically decrease over time during the pre-test epoch before any conditioning has been applied, also observed in previous studies when using low frequency (<20 Hz) stimulation (Goldring et al., 1961; Vincent et al., 2016, 2017). This may explain the findings in a previous study using CCEPs to assess the effects of paired stimulation which showed a global increase in CCEPs following conditioning (Seeman et al., 2017). The decrease in CCEP amplitude has been attributed to distortions from a saturated amplifier, which is not applicable in our study as the shape of the CCEP does not change over time, or to a desynchronization of cortical networks (Vincent et al., 2016). However, during the post-test epoch we also observed large increases over time, and control experiments also did not provide consistent CCEPs. Additional studies are necessary to fully understand why CCEPs change drastically over time.

Although CCEPs may be a useful metric for assessing the presence of connectivity, they may not be a simple metric for measuring the strength of and changes in connectivity. There is a need to

better understand the neural mechanisms of invoking CCEPs, and the implications behind the latencies and amplitudes of troughs and peaks, especially with how variable CCEPs are between different stimulus intensities and depth of recording.

Implications to in vivo plasticity paradigms

Plasticity paradigms *in vivo* often require high amplitudes or continuous conditioning for long periods of time for changes in connectivity (Jackson et al., 2006; Rebesco & Miller, 2011b; Seeman et al., 2017; Yazdan-Shahmorad et al., 2018). However, our experiment showed consistent changes with just 10 minutes of low amplitude paired stimulation. This is likely attributed to two reasons: the measure we were using is very specific and allowed us to assess smaller changes, and the delay of our stimulation was very exact relative to the stimulus response. Assessing the connectivity with finer details and tailoring stimulation paradigms to the responses may allow for more effective stimulation paradigms that can be reasonable in a clinical setting.

However, even within the cortex there could be discrepancies in stimulus responses and induced plasticity in different cortical regions or even cortical layers. Our study was in the motor cortex, which is notorious for its high interconnectivity, and in layer 2/3 which has more inhibitory horizontal projections. Studies exploring changes in connectivity in different layers, especially layer 5 with its large pyramidal cells, or different cortical regions, like the visual system and its unidirectional information flow, can confirm whether our findings are generalizable.

Conclusions

We applied paired stimulation to the motor cortex of awake primates using a finer temporal gradient of ISIs than tested before. 10 minutes of conditioning generated consistent changes in the responses of single units dependent on the ISI. Contrary to classic STDP, very short, positive

ISIs resulted in depression, likely due to potentiation in the local inhibitory circuitry, suggesting that the dynamics of plasticity in vivo may have a much finer timescale than previously thought due to the interconnected nature of excitatory and inhibitory circuitry. CCEPs showed similar but much more variable results compared to single unit responses, indicating that they may not be the ideal measure for changes in connectivity strength. Better understanding underlying dynamics of stimulus responses and connectivity metrics could lead to more effective plasticity paradigms.

Figures

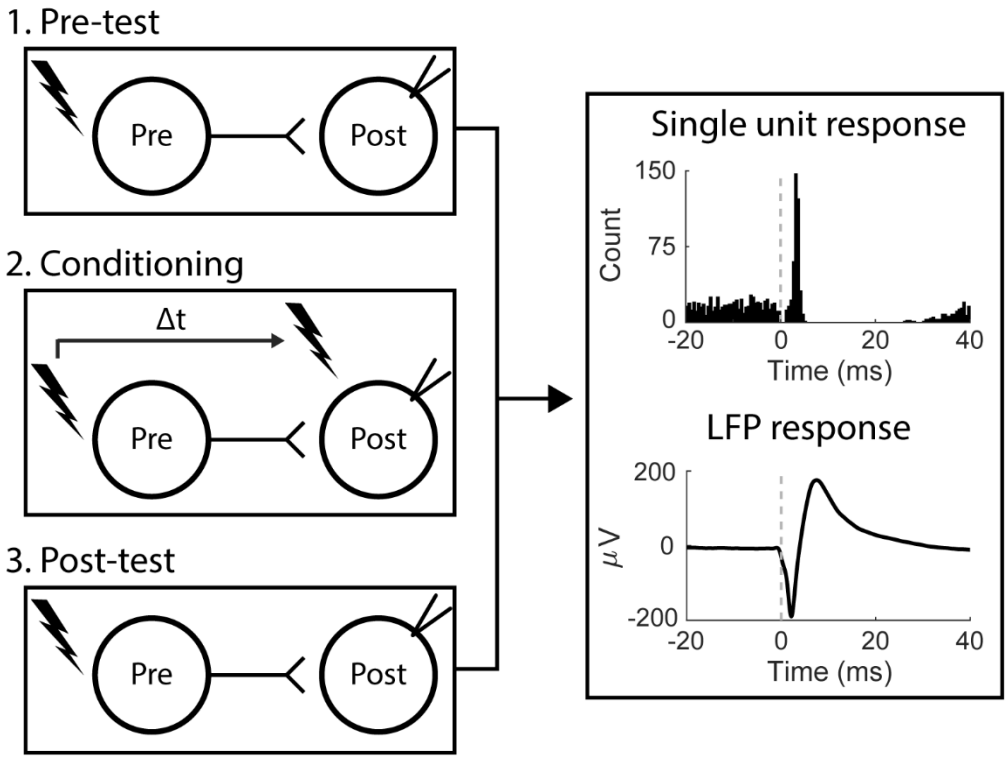

Figure 4.1 Experimental design

Each experiment consisted of three epochs – pre-test, conditioning, and post-test. During the test epochs stimuli were delivered to the presynaptic site and responses captured at the postsynaptic site. Conditioning consisted of paired stimulation between the pre- and postsynaptic sites at a chosen delay, Δt.

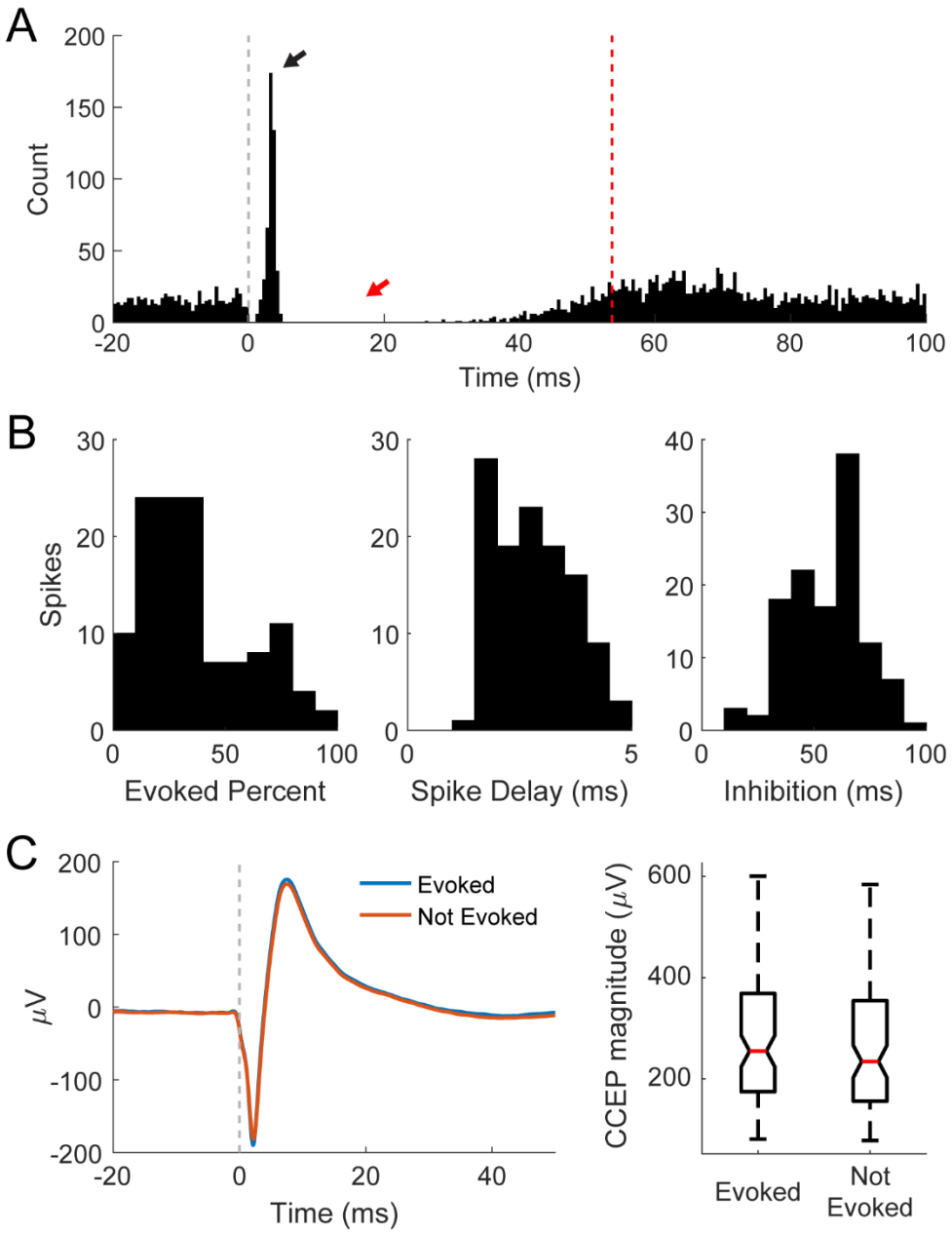

Figure 4.2 Stimulus responses

A) Example PSTH of a spike showing the stimulus evoked spikes (black arrow) occurring quickly after stimulus onset (dashed line) and the strong inhibitory response lasting 10s of milliseconds following the evoked spikes (red arrow). The dashed red line shows the average inhibition duration. **B)** Distributions of preconditioning evoked spike percent, mean spike latency, and inhibition duration. **C)** Example CCEP trace. Example CCEPs showing similarity between CCEPs of stimuli that evoked spikes and those that didn't (left). The same holds for all spikes throughout the experiment (right) showing the independence of the two measures.

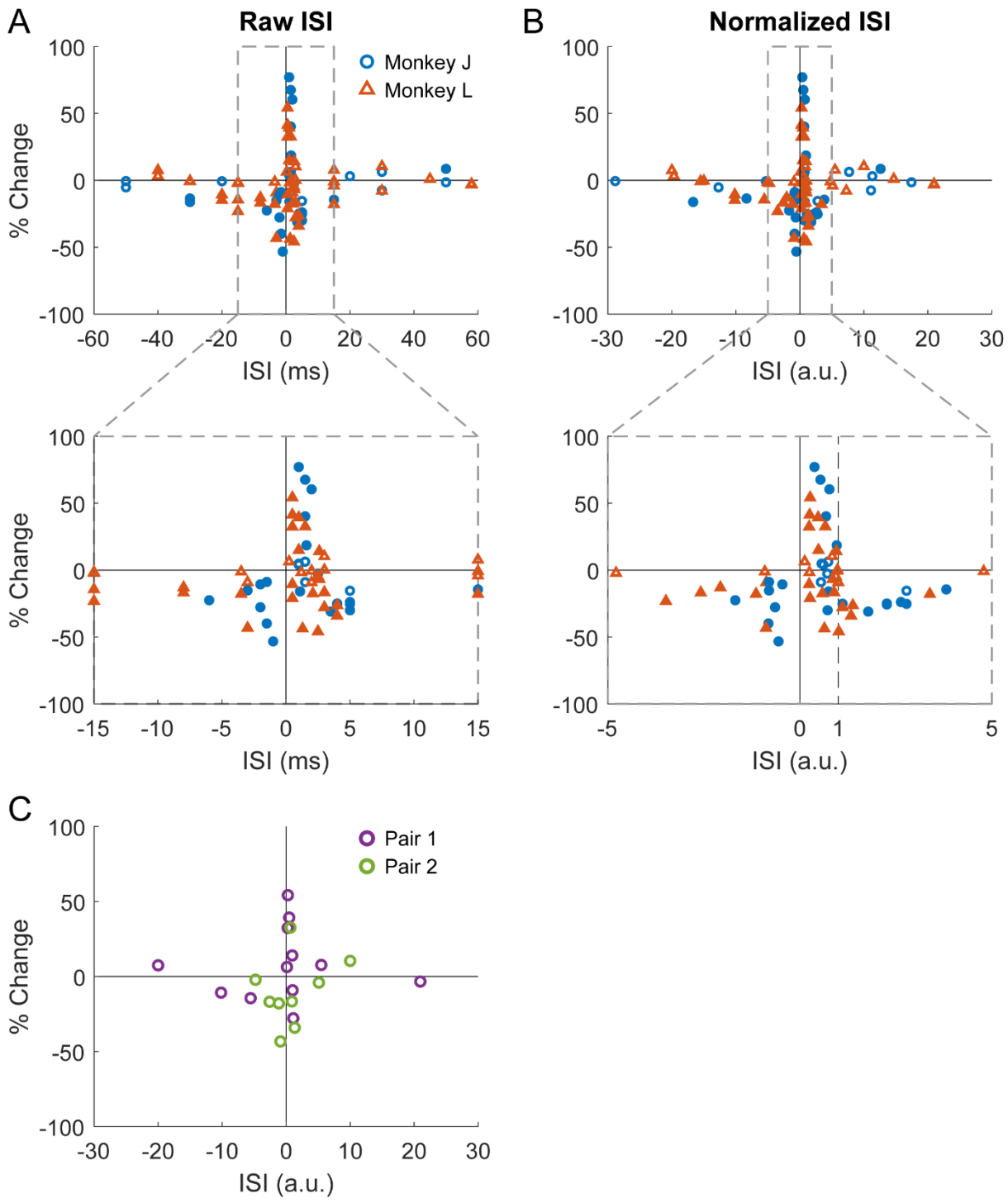

Figure 4.3 Changes in evoked spike probability with respect to ISI

Changes in evoked spike probabilities plotted against **A)** raw ISI and **B)** ISI normalized to spike latency. Filled in data points are statistically significant from 0 (Fisher's exact test, $p<0.05$). **C.** Changes in evoked spike probabilities of two pairs of presynaptic site and postsynaptic spike at different ISIs.

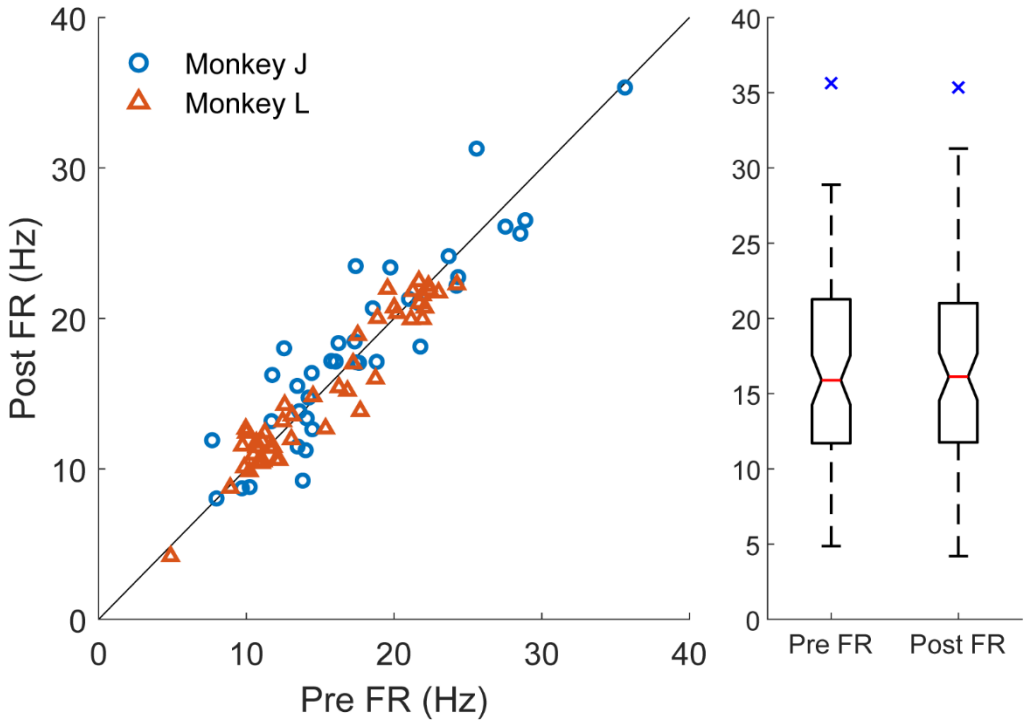

Figure 4.4 Firing rate did not affect evoked spike probabilities

The firing rate of the spikes during the Pre- and Post-test epochs (left). The diagonal line shows y=x. There was no significant difference in firing rate between the epochs as shown in the boxplot on the right (p=0.79, Wilcoxon signed-rank test). The blue x shows outliers.

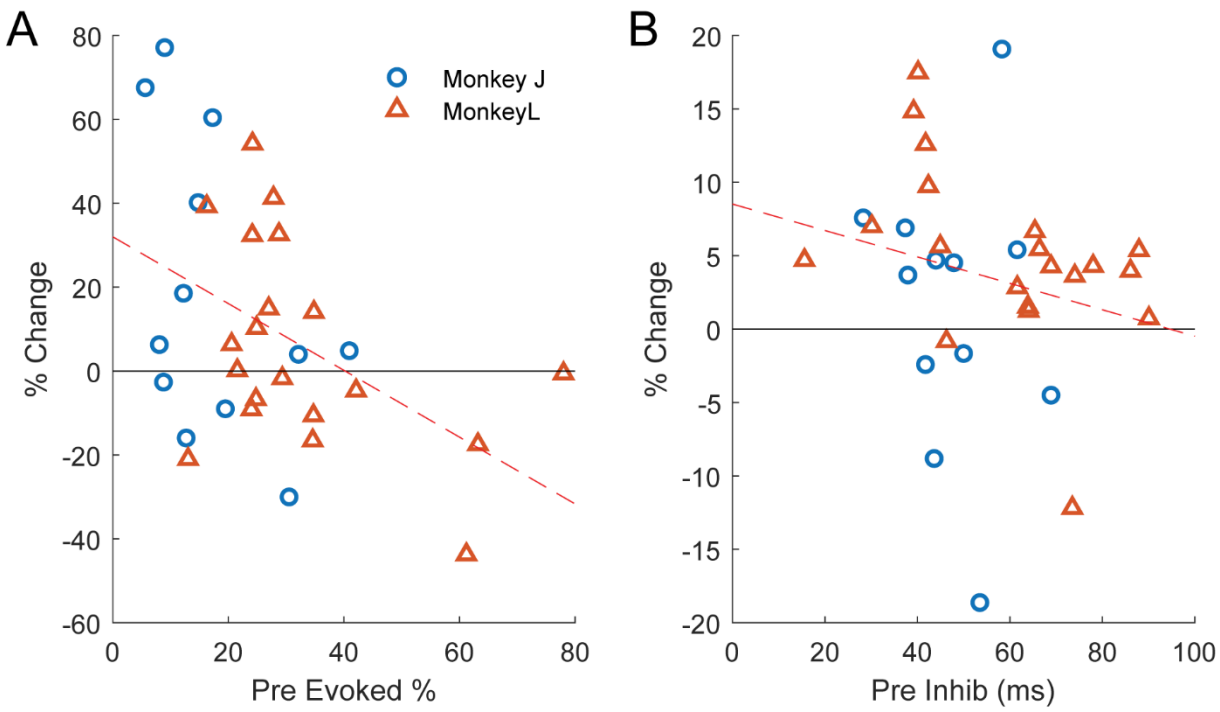

Figure 4.5 Evoked spike changes relative to initial evoked rate

A. Percent change in evoked spike probability with respect to raw evoked probability during the pre-test epoch for all sessions in which 0 < normalized ISI < 1. The dashed red line shows the linear regression (Pearson correlation, rho= -0.45, p=0.01). **B.** Percent change in inhibition duration with respect to inhibition duration during the pre-test epoch. The dashed line shows the linear regression (Pearson correlation, rho=-0.22, p=0.24).

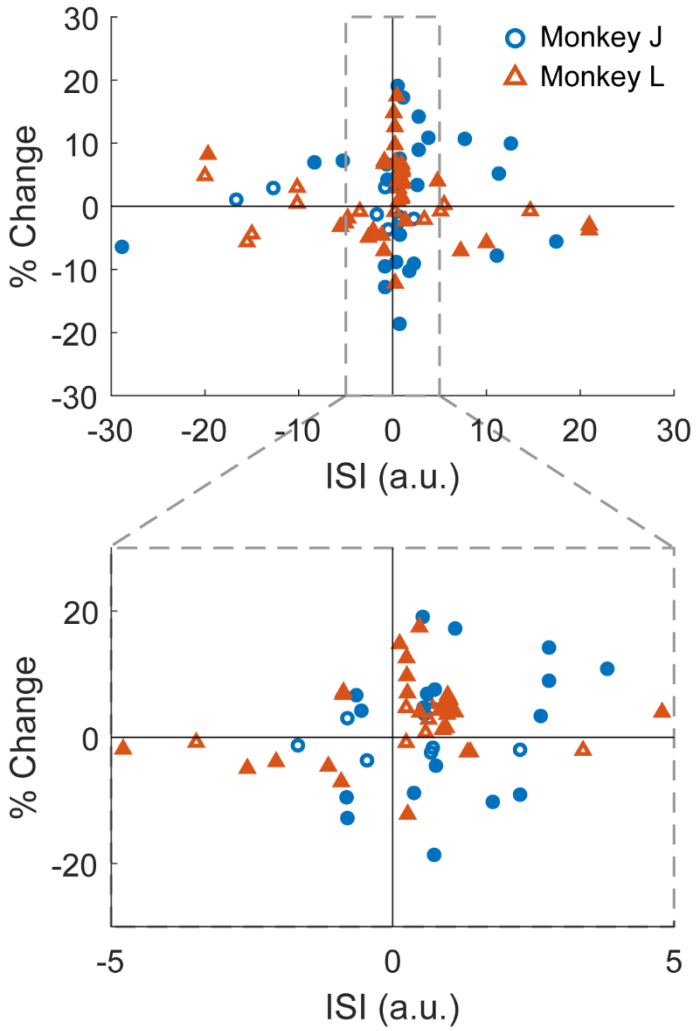

Figure 4.6 Changes in inhibition duration with respect to ISI

Raw ISI B. Normalized ISI. Filled in data points are statistically significant from 0 (Fisher's exact test, $p<0.05$).

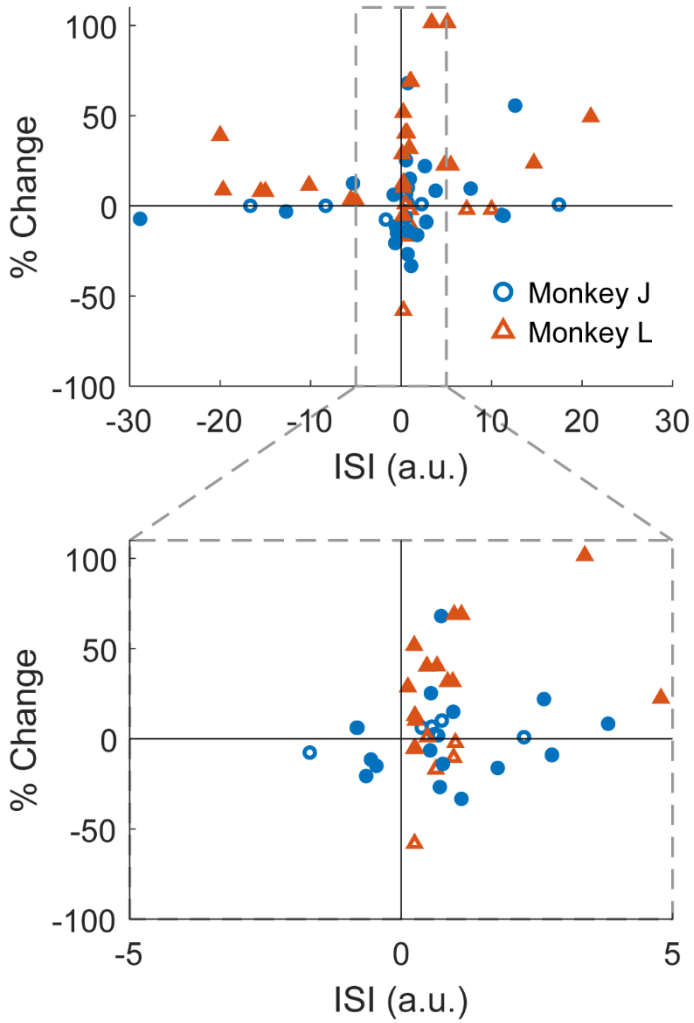

Figure 4.7 Changes in CCEP magnitude with respect to ISI

CCEP changes relative to normalized ISI. Filled in data points are statistically significant from 0 (2 sample t-test, $p<0.05$).

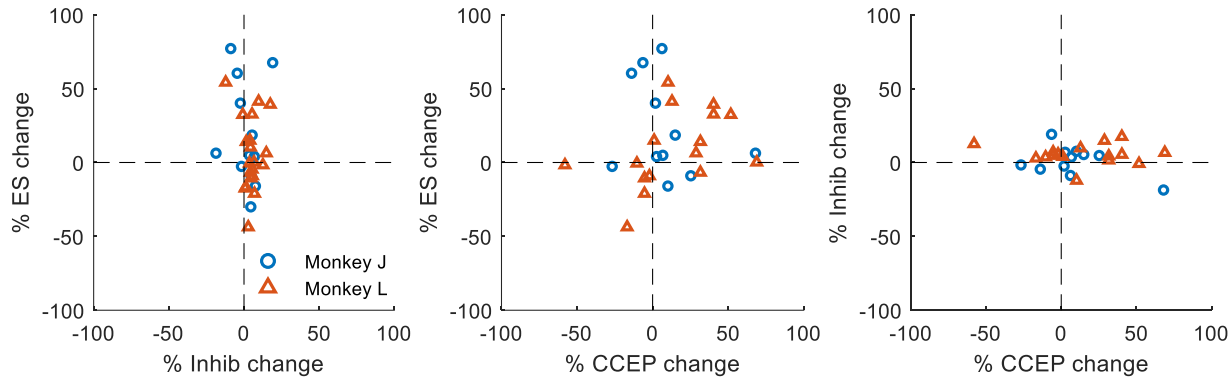

Figure 4.8 Correlation between evoked spikes, inhibition duration, and CCEP changes

There is no significant pairwise correlation between changes in evoked spike probabilities, inhibition duration, and CCEP amplitudes (Pearson correlation, rho= -0.13, p= 0.47; rho=0.11, p=0.57; rho=0.18, p=0.37).

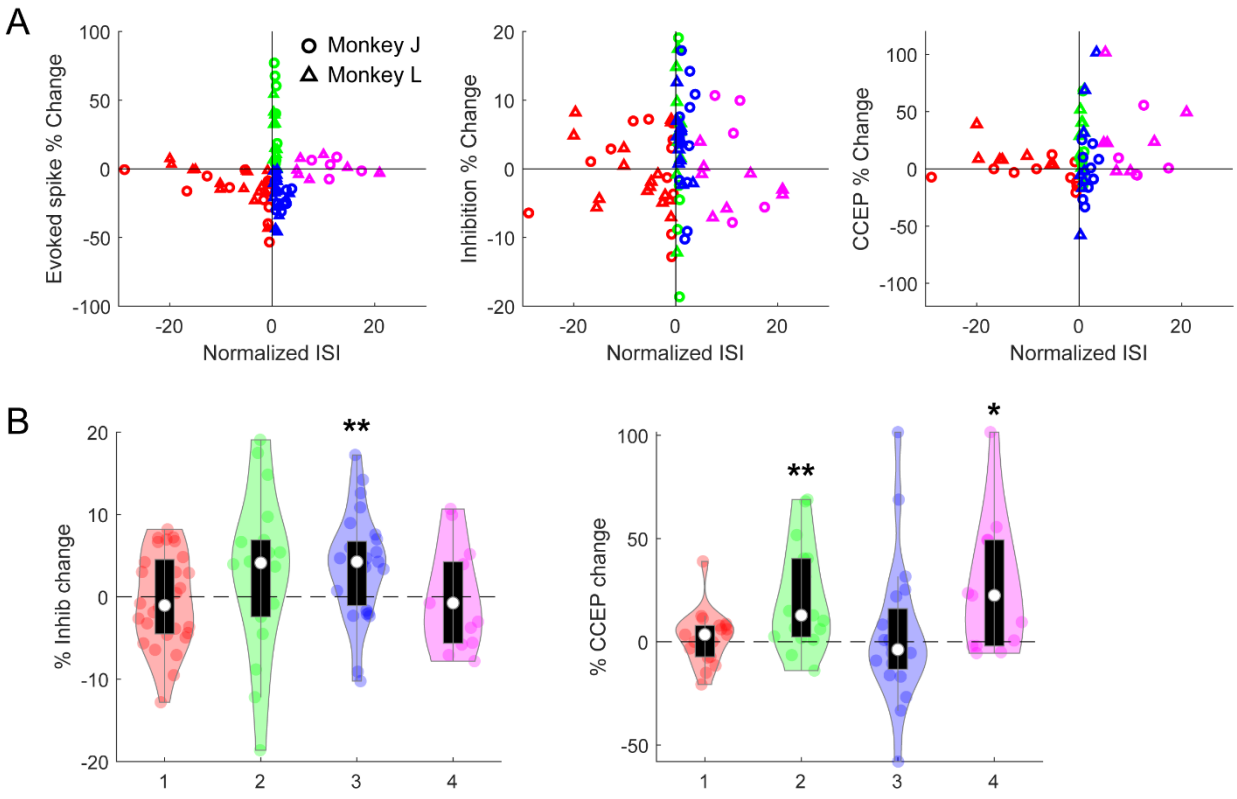

Figure 4.9 Comparisons in different ranges of ISIs

A. Four different regions of ISI: negative ISI, positive ES changes with ISI from 0 to 4, negative ES changes with ISI from 0 to 4, and ISI>4. Scatter plot of evoked spike probability change, inhibition duration change, and CCEP magnitude change shown with the 4 regions. **B.** Distributions of inhibition duration (left) and CCEP magnitude (right) changes in each region of ISI. (∗: $p<0.05$, ∗∗: $p<0.01$, Wilcoxon sign rank test) (0.004, 0.003 ,0.03 in order from left to right)

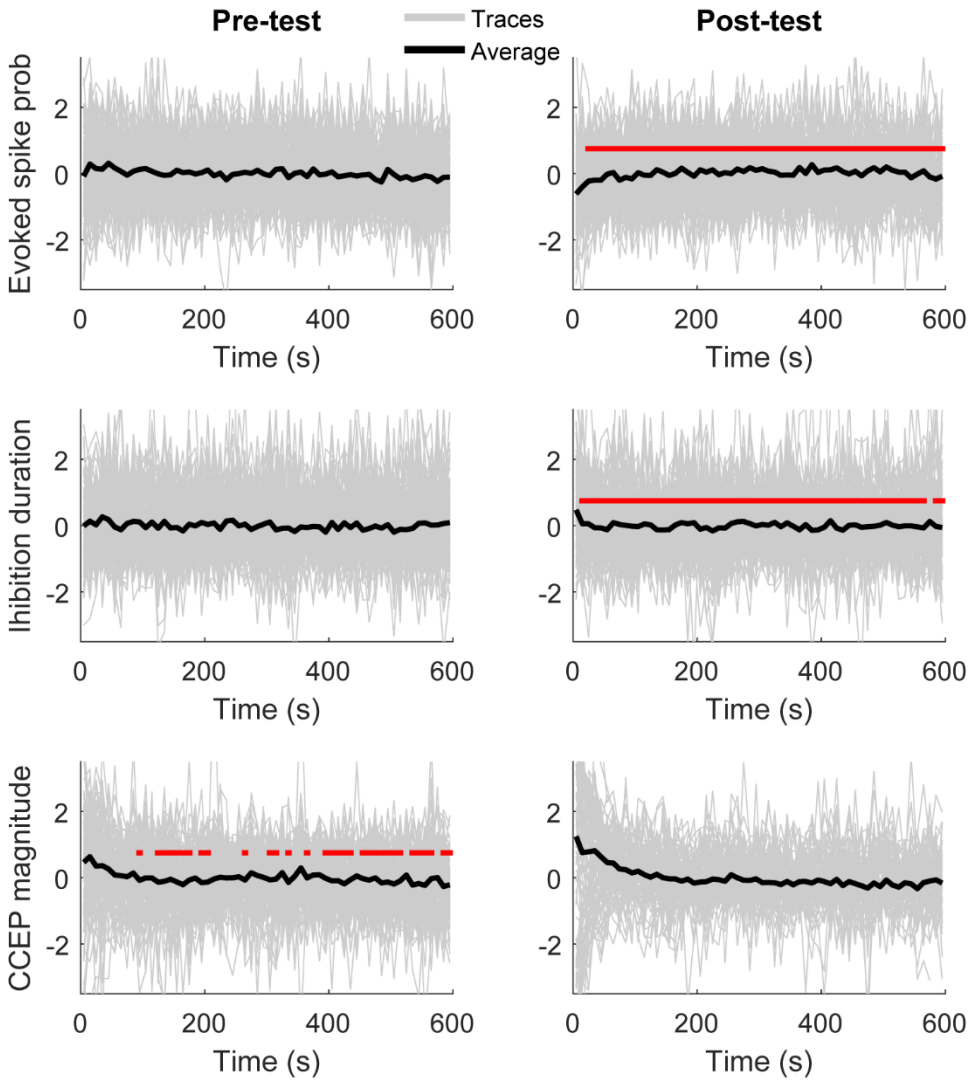

Figure 4.10 Measures over time

Average z-scored evoked spike probability (top), inhibition duration (middle), and CCEP magnitude (bottom) over time during the pre- and post-test epochs (left and right, respectively) using 10 second bins. Grey traces show individual sessions, black traces show the average, and the horizontal red bars show statistically significant difference from the first 10 seconds ($p<0.05$, Repeated measures ANOVA, Bonferroni correction post-hoc,).

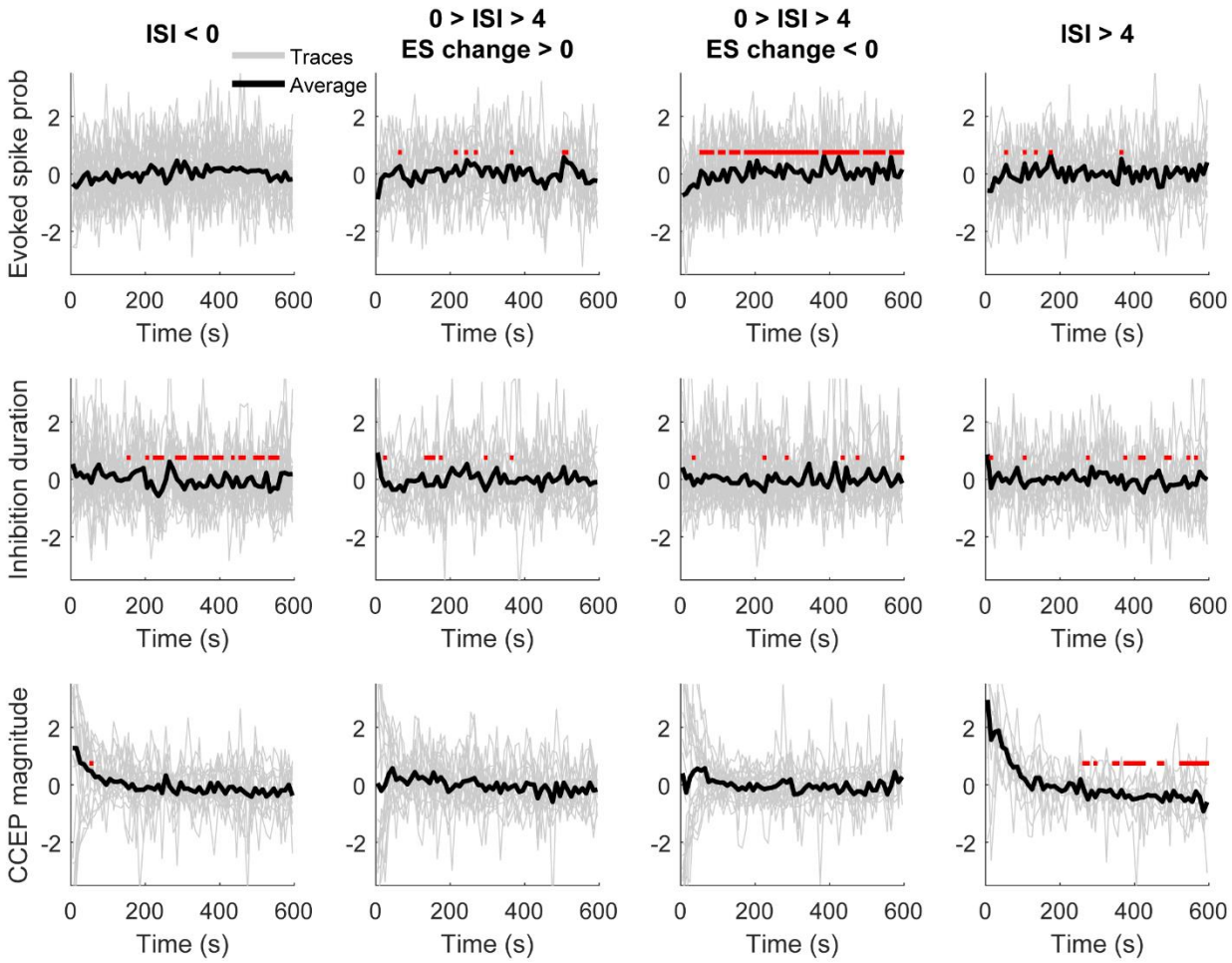

Figure 4.11 Measures over time during the post-test epoch by different regions of ISIs

Average z-scored evoked spike probability (top), inhibition duration (middle), and CCEP magnitude (bottom) over time during the post-test epochs for four different groups of normalized ISIs. Grey traces show individual sessions, black traces show the average, and the horizontal red bars show statistically significant difference from the first 10 seconds ($p<0.05$, Repeated measures ANOVA, Bonferroni correction post-hoc).

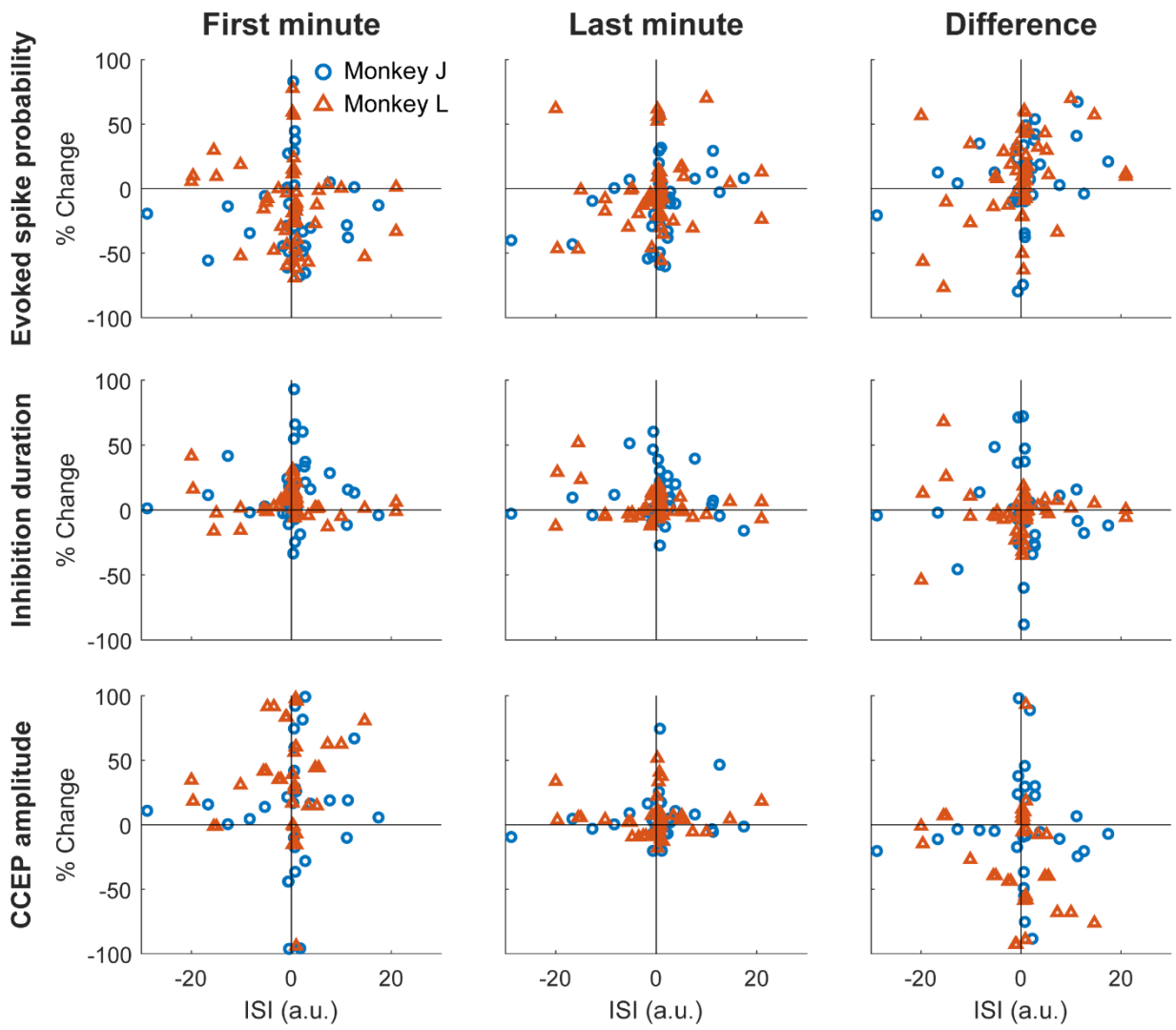

Figure 4.12 Changes in each measure during the first and last minute of the post-test epoch

Changes in evoked spike probability (top), inhibition duration (middle) and CCEP amplitude (bottom) with respect to normalized ISIs during the first (left) and last (middle) minute of the post-test epoch. The right column shows the difference between the last and first minute.

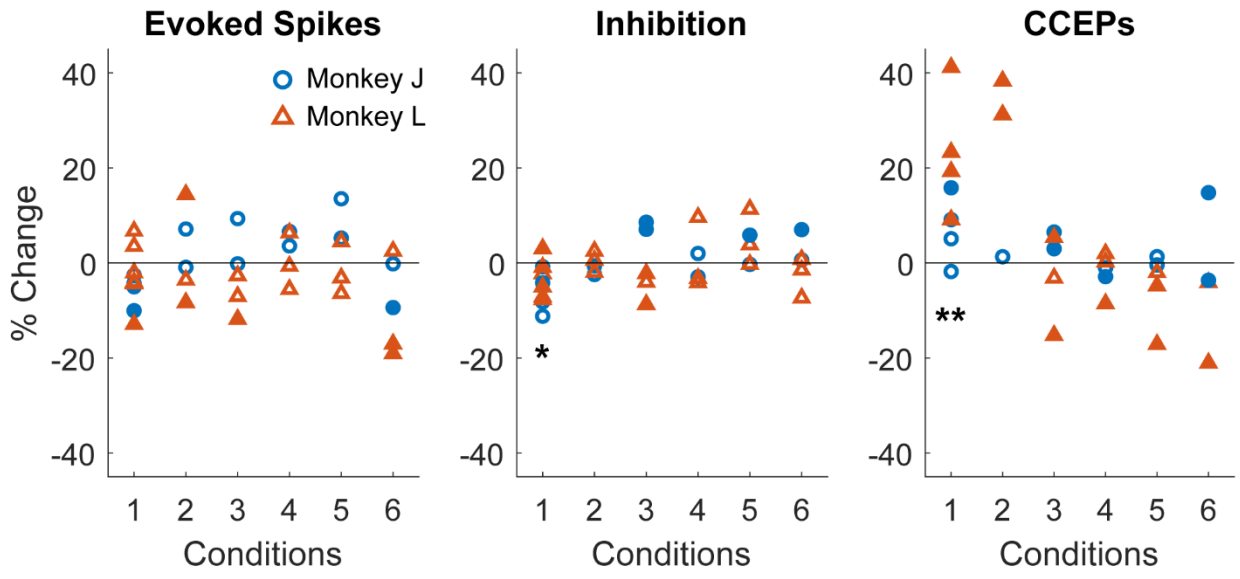

Figure 4.13 Control experiments

Percent change in evoked spike probability, inhibition duration, and CCEP magnitudes during different control experiment conditions: 1. Long delay, 2. Random stimulation, 3. Subthreshold stimulation, 4. No conditioning, 5. Pre-stimulation only, 6. Post-stimulation only. (∗: $p<0.05$, ∗∗: $p<0.01$, Wilcoxon sign rank test) ($p=0.014$ and 0.008).

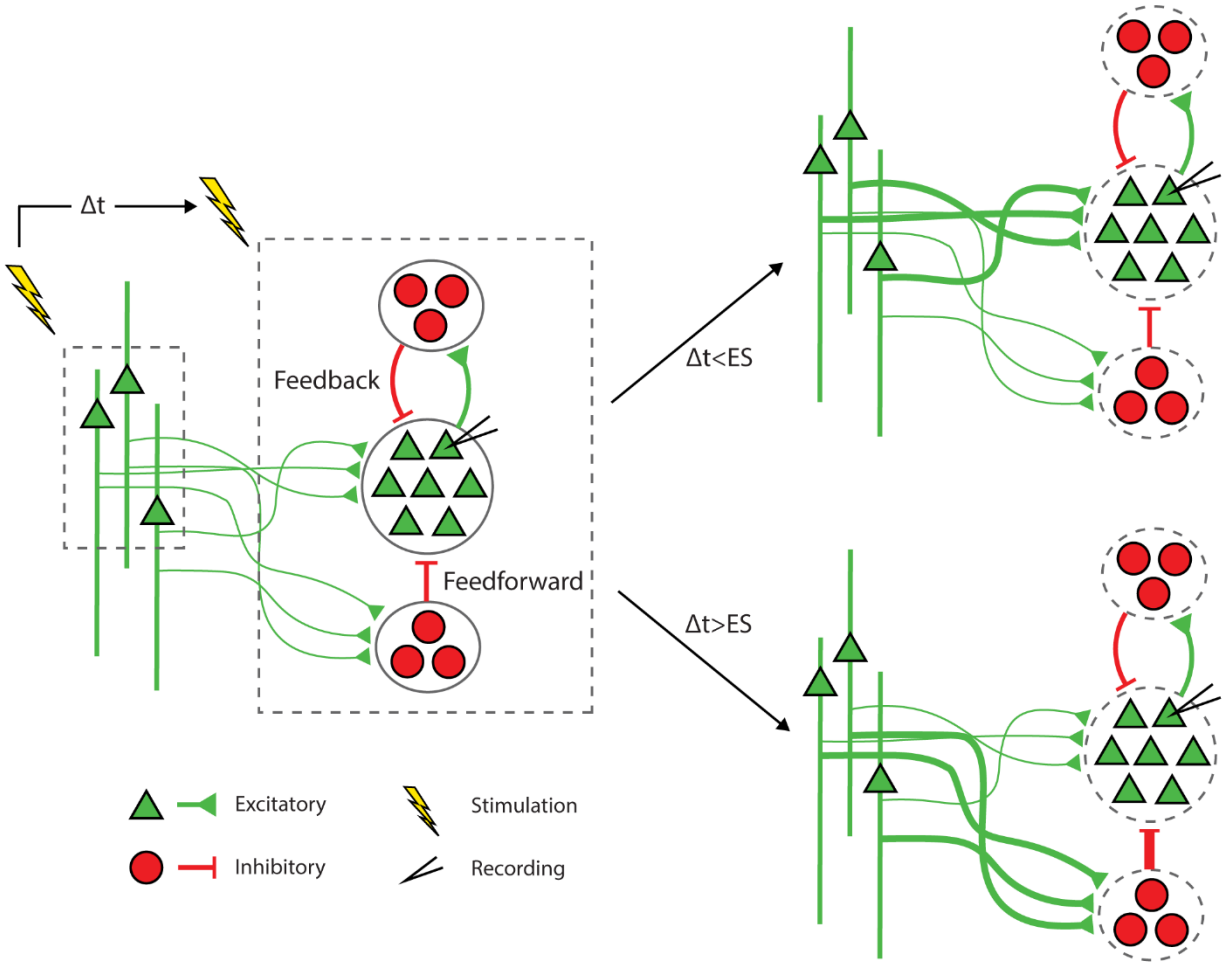

Figure 4.14 Mechanism underlying changes induced by paired stimulation *in vivo*

Stimulation at the Pre site activates excitatory horizontal fibers, activating the recorded principal neurons and the local feedforward and feedback inhibitory circuitry. Paired stimulation strengthens the projections to the principal cells if the stimulation to the Post site arrives before the evoked spike latency, whereas it strengthens the feedforward inhibitory pathway if the stimulation arrives after the evoked spike.

Chapter 5. Local field potentials and single unit dynamics in motor cortex of unconstrained macaques during different behavioral states

Abstract

Different sleep states have been shown to be vital for a variety of brain function, including learning, memory, and skill consolidation. However, our understanding of neural dynamics during sleep and the role of prominent LFP frequency bands remain incomplete. To discern changes between different behavioral states we collected multichannel LFP and spike data in primary motor cortex of unconstrained macaques for up to 24 hours using the Neurochip3. Each 8 second bin of time was classified into awake and moving (Move), awake and at rest (Rest), REM sleep (REM), or non-REM sleep (NREM) by using dimensionality reduction and clustering on the average spectral density and the acceleration of the head. LFP power showed high delta during NREM, high theta during REM, and high beta when the animal was awake. Cross-frequency phase-amplitude coupling typically showed higher coupling for deeper sleep between all pairs of frequency bands except for high delta-high gamma and theta-high gamma coupling during Move, and high theta-beta coupling during REM. Sorted single units showed decreased firing rate with deeper sleep, though with higher "bursty" patterns during NREM compared to other states. Spike-LFP synchrony showed high delta synchrony during Move, and higher coupling with all other frequency bands during NREM. These results altogether are consistent with previous findings showing reactivation of cortical circuitry activated during the day, which may be driven by the delta band LFP.

Introduction

The discovery of rapid-eye movement (REM) sleep by Aserinski and Kleitman showed the presence of active brain processes during sleep, which catalyzed studies on different sleep stages (Aserinsky & Kleitman, 1953). Findings have shown REM sleep to play a role in regulating the autonomous nervous system activity and to be linked with spatial and emotional memory consolidation (Boyce et al., 2016; Rechtschaffen, 1998; Siegel, 2005). Similarly, non-REM (NREM) sleep has been shown to be tied to skill consolidation and memory formation (Ramanathan et al., 2015; Siclari & Tononi, 2017).

Studies have furthered our understanding of different sleep stages by exploring the dynamics of local field potential (LFP) frequency band power and single-unit spiking characteristics in both the cortex and various deep brain structures during sleep. Slow waves and delta frequency band are typically present across the brain during NREM sleep, and high theta power in the hippocampus is present during REM sleep (Rechtschaffen & Kales, 1968; Silber et al., 2007). Single units show changes in firing rate as well as firing patterns during sleep, due to changes in connectivity and excitability, potentially reflecting reactivations of relevant cortical circuit patterns to solidify learning and memory (Arbune et al., 2020; Ramanathan et al., 2015; Tononi & Cirelli, 2014; Xu et al., 2019). Several other features of cortical activity, such as k-complexes and sleep spindles during NREM sleep, have also been identified to be associated with different stages of sleep (Fernandez & Lüthi, 2020; Huber et al., 2004; Ulrich, 2016).

Additional findings have shown that certain plasticity mechanisms, such as long-term potentiation/depression and synaptic tagging and capture, occur exclusively during sleep (E. Y. Kim et al., 2005; Vecsey et al., 2018). Subsequent research has applied this knowledge by enhancing slow waves prevalent during NREM sleep (Bellesi et al., 2014; Marshall et al., 2006)

or delivering stimulation locked to delta (Rembado et al., 2017) to augment learning and memory. However, despite our expanding tools and techniques to take advantage of sleep mechanisms, the neural dynamics underlying sleep remain unclear.

Various measures of local field potential (LFP) coupling and spike-LFP synchrony have been commonly used to elucidate mechanisms of neural dynamics. Cross-frequency phase-amplitude coupling of different LFP frequency bands, thought to reflect communication between brain circuitry, has been shown to be modulated by task performance, cognitive engagement, and memory formation in various brain regions (Canolty & Knight, 2010; Jensen & Colgin, 2007). Single units are strongly synchronized to specific phases of LFP frequency bands, notably to beta and gamma cycles in the motor cortex, suggesting beta to be a resting rhythm during movement execution and gamma to reflect local population activity (Buzsáki et al., 2012; Buzsáki & Wang, 2012; Engel & Fries, 2010; Murthy & Fetz, 1996a, 1996b). These two analyses have given us significant insight into neural signaling and the role of both spikes and LFPs in brain function, but there has yet to be a comprehensive analysis of cross-frequency coupling and spike-LFP synchrony for specific cortical sites during sleep and wake.

This study analyzes LFP and single unit dynamics in the macaque motor cortex during different behavioral states to better understand the mechanisms operating during different sleep stages as well as the roles of various LFP frequency bands. We first used the power spectral density of LFPs to distinguish between four major behavioral states shown to be relevant to plasticity and learning in the motor cortex: 1. awake and moving (Move), 2. awake and at rest (Rest), 3. rapid-eye movement (REM) sleep, and 4. non-REM (NREM) sleep. We tracked single-unit activity concurrently with LFP recordings and focused on 6 different frequency bands commonly observed in the cortex – delta, theta, alpha, beta, low gamma, and high gamma. Finally, we

assessed state-dependent changes in cross-frequency coupling between pairs of the frequency bands as well as spike-LFP synchrony with each frequency band.

Materials and Methods

Experimental design

Implants and surgical procedures

The experiments were conducted on two male *Macaca nemestrina* monkeys, Monkeys J and Kr. Monkey Kr is referred to as Monkey K in this section. Both animals were implanted with the Utah microelectrode array in the arm region of M1 as well as the halo implant to allow for overnight recordings of neuronal data. Monkey J additionally received electrooculography (EOG) electrodes on both orbits. Refer to "General Methods" for full details on implants and surgical procedures.

Electrophysiology

All data was collected with the head-mounted Neurochip3 (Shupe et al., 2021) while the monkeys were freely behaving in their home cage (Figure 5.1A). The Neurochip3 is a battery powered bidirectional brain-computer interface capable of saving data to an SD card, allowing for wireless recording and stimulation for up to 24 hours. 16 channels of the Utah array, or 14 channels of the array and 2 channels of the EOG, were recorded at 20 kHz sampling rate with a bandwidth of 0.1 Hz to 5 kHz (Figure 5.1B). The cortical channels were chosen each day with a preliminary recording to capture the largest single units present in the array. Most experiments recorded a different set of channels due to the spikes changing over time.

The Neurochip3 also has an onboard 3-axis accelerometer that was simultaneously recorded at 100 samples per second. Recording sessions lasted between 19 and 24 hours. The animal rooms had the lights off during the night for 12 hours between 6pm and 6am. We collected data from a total of 16 sessions from Monkey K and 10 sessions from Monkey J.

Data analysis

Classifying sleep states

All analyses were performed using custom MATLAB (Mathworks) and Python code. The power spectral density (PSD) of cortical local field potentials (LFPs) as well as the onboard accelerometer data from the Neurochip3 were used to classify different sleep states (Figure 5.1B). Data was down sampled to 1 kHz before performing Welch's PSD estimate between 0 and 50 Hz for each 8 second time-bin. We then converted the PSD into power and found the average power across all channels for each time-bin. The average power was further normalized by subtracting by the minimum value and dividing by the integral to ensure relative power at different frequencies played a larger role than the absolute power.

We then used the normalized average power as inputs to train a stacked sparse autoencoder for dimensionality reduction, similar to the architecture described in Tsinalis et al. 2016 (Tsinalis et al., 2016). The encoder was composed of 3 layers of 256, 128, and 64 units each, with batch normalization and ReLU activation function. The final hidden layer containing the reduced representation of the data had 32 nodes. The autoencoder was trained with minibatch sizes of 64 for 300 epochs. The loss was calculated with mean squared error with L1 regularization (regularization weight $\lambda = 1e^{-5}$) using the Adam optimizer (learning rate $\alpha = 1e^{-3}$, decay rate for first moment $\beta_1 = 0.9$, decay rate for second moment $\beta_2 = 0.999$, constant $\varepsilon = 1e^{-8}$). The autoencoder was implemented in Python using the PyTorch package (Paszke et al., 2019).

Accelerometer data was included by performing the root sum of squares across all three axes. We then found the variance of the values within each time bin and applied a logarithmic scale to better compress the data. Finally, the standard deviation was normalized to that of the encoded

dimension with the largest variance. The processed accelerometer data was included as an additional dimension in the lower dimensional representation (i.e. 33rd dimension).

To classify the data, we used k-means clustering with an assumption of 4 centroids. Data points of the lower dimensional representation within the 90th percentile of pairwise Euclidean distance were initially used for finding the centroids of clusters to avoid the influence of outliers. Each data point was assigned to the centroid with the shortest Euclidean distance.

After clustering, each group of records was assigned to one of four states – 1) awake and moving (Move) 2) awake and at rest (Rest), 3) rapid-eye movement (REM) sleep, 4) non-REM (NREM) sleep – by assessing the average accelerometer value and average normalized PSD for each cluster. First, the cluster with highest average acceleration was assigned to be Move, then the cluster with highest average delta power (0.5 to 4 Hz) was assigned be NREM, then the cluster with higher average beta power (15 to 30 Hz) was assigned to be Rest, and the remaining cluster was assigned to be REM.

To include a temporal aspect and smooth any outliers we performed a majority filter on the classification. For each time-bin, the majority state across 2 time-bins before to 2 time-bins after (±16 seconds) was considered to be the current state. Ties were resolved by keeping the original classification, or by random choice if the original classification was not part of the tie.

Validation of classification

Two EOG electrodes (one dorsal and one lateral) were simultaneously recorded from with the Neurochip3 in experiments with Monkey J. EOG signals were extracted by subtracting the lateral electrode signal from the dorsal electrode signal and then applying a band-pass filter between 1 and 20 Hz with a zero-phase second-order Butterworth filter. We performed in-booth

experiments with flashes of lights guiding the monkey's gaze to ensure we were properly capturing eye movements.

As the Neurochip3 is mounted to the monkey's heads, we performed overnight recordings with the Microsoft Kinect in conjunction to ensure there were no large discrepancies between the on-board accelerometer and whole-body movements (Libey & Fetz, 2017). Movements with the Kinect was calculated as the absolute difference between each frame of the infrared depth-finding camera and the previous frame. We captured frames as quickly as possible with the processing overhead, around 30 frames per second.

Further validation was performed with k-fold cross-validation with k=20. Each dataset was split into 20 random groups; classification was performed on 19 of the 20 groups, and the final group was classified using the centroids from the classification k-means. The training error was calculated as the difference in classification within the 19 groups used for training the classification, and the test error as the difference in classification within the final group used to test the classification. Cross-validation was bootstrapped 50 times for each session to minimize variability that can potentially be introduced by the random sampling.

Coherence

Refer to "Coherence measurements" in "General Methods."

Cross-frequency phase-amplitude coupling

To calculate cross-frequency phase-amplitude coupling we used mean vector length (MVL) (Canolty et al., 2006) (Figure 5.1C). The LFP was first filtered into 2 frequency bands of interest within the 6 frequency bands of interest – 1) delta (0.5-4 Hz), 2) theta (4-8 Hz), 3) alpha (8-12 Hz), 4) beta (15-30 Hz), 5) low gamma (30-70 Hz), and 5) high gamma (70-120 Hz) – using a

zero-phase second-order Butterworth filter. We then calculated the analytic signal, H, of each band using the Hilbert transform:

$$H(x(t)) = \frac{1}{\pi} P \int_{-\infty}^{+\infty} \frac{x(\tau)}{t-\tau} d\tau \qquad \text{Equation 5.1}$$

where P is Cauchy principal value. The phase of the complex valued analytic signal is the instantaneous phase at time t, and the magnitude of the analytic signal is the instantaneous amplitude. The mean vector was then calculated by:

$$MVL = \left| \frac{1}{n} \sum_{n} r \; exp \; (i\phi) \right| \qquad \text{Equation 5.2}$$

where r is the instantaneous magnitude of the higher frequency band and ϕ is the instantaneous phase of the lower frequency band. ϕ ranges from 0 to 2π radians where 0 is the peak and π the trough of oscillations. This calculation creates a vector for each sample in time with the phase and amplitude of the lower and higher frequency bands, respectively. The magnitude of the average of those vectors, or MVL, measures the strength of synchrony – zero indicates a uniform distribution in which the vectors "cancel" each other, and higher values indicate the degree of synchrony.

However, MVL is highly affected by the amplitude and does not have a normalized maximum value, which makes interpretation of individual values and comparisons of MVL measurements across different time points difficult. Thus, we additionally calculated the maximum possible MVL for each state. Instead of using the phase and amplitude that occurs at the same time sample in Equation 2, we paired the highest amplitudes with the most commonly occurring phases. Thus, the largest vectors were all in similar directions providing the maximum possible

length of the mean vector. We then normalized the MVL by dividing by the maximum possible MVL to assess differences in synchrony between behavioral states.

Spike sorting

Spikes were sorted offline using two-window discrimination. The cortical recording was bandpass filtered between 1000 and 2000 Hz with a first-order Butterworth filter. Then a negative threshold and two time-delayed windows were manually chosen to capture the trough and the peak of the spike waveform. All traces crossing the threshold and passing through the two windows was denoted as a spike.

As the fidelity of spikes may change over such a long period of recording, we additionally compared the shapes of the first 1000 detected spikes with the last 1000 detected spikes using the coefficient of determination (CoD):

$$CoD = 1 - \frac{\sum \left(s_{first}(t) - s_{last}(t)\right)^2}{\sum \left(s_{first}(t) - \overline{s_{first}}\right)^2} \qquad \text{Equation 5.3}$$

where s_{first} is a waveform of one of the first spikes, s_{last} is a waveform of one of the last spikes, and $\overline{s_{first}}$ is the average of the waveform.

We performed pairwise CoD on all first and last 1000 instances of each spike and compared them to the pairwise CoD between the first 1000 instances of the spike and the last 1000 instances of a different, randomly chosen spike. If the distribution of the CoD comparing the same spike was significantly higher than the distribution between the spike and another spike it was considered to be consistent overnight. Additionally, to ensure we were not capturing multiple neurons with a similar waveform, we manually assessed the autocorrelograms for each spike to ensure the presence of a refractory period and proper distribution of inter-spike intervals.

Phase-locking value

We calculated the phase-locking value (PLV) to assess the strength of synchronization of spike timing to phases of oscillations in specific frequency bands from LFPs recorded on the same channel (Figure 5.1D). First, the LFP was filtered into a frequency band of interest. The instantaneous phase of the lower frequency band was calculated as described above. We then calculated the PLV:

$$PLV = \frac{1}{n}\left|\sum_n exp\ (i\phi)\right| \qquad \text{Equation 5.4}$$

where ϕ is the instantaneous phase at spike times. The PLV effectively converts each phase into a unitary vector and finds the average of all the vectors. The magnitude of the resulting vector determines the synchrony of the phases. A value of zero, similar to MVL, indicates a uniform distribution, or no synchrony. A value of one indicates that all phases are equal, or perfect synchrony.

The average phase of spike timing was found using the circular mean:

$$average\ phase = arg\left(\sum_n exp\ (i\phi)\right) \qquad \text{Equation 5.5}$$

where arg is the argument of a complex number, or the angle between the positive real axis and the complex number in the complex plane.

Statistical analysis

We used Friedman's test to compare values between the four states due to the non-parametric nature of the distribution and because we were sampling the same spikes and LFPs across each state. Tukey's honest significance test was used post hoc to determine significant pairwise differences.

Results

Classifying sleep states

Although there have been various approaches automating sleep state classification by taking advantage of the sequential nature of the states as suggested by the American Academy of Sleep Medicine (AASM) classification (Craik et al., 2019; Silber et al., 2007; Supratak et al., 2017), studies have shown that including information from neighboring epochs does not necessarily improve classification (Sekkal et al., 2022; Tsinalis et al., 2016). Most deep learning methods also rely on supervised learning, but, due to the high inter-scorer variability in manual classification that these models rely on (Himanen & Hasan, 2000; Younes et al., 2016), we chose an unsupervised method instead. As a result, we used dimensionality reduction for feature extraction and subsequent clustering. Autoencoders were chosen as the method for dimensionality reduction due to its nonlinearity potentially extracting more salient features compared to linear methods. Though denoising autoencoders are often used for feature extraction to ensure the network does not learn to replicate the noise, our input data inherently contained noise due to the recording device being mounted on a freely behaving animal as well as the short time window of 8 seconds for our power spectral density calculations. As a result, we used a stacked sparse autoencoder for dimensionality reduction.

Sleep states were classified using the power spectral density of local field potentials (LFPs) of successive 8-second time-bins as the input to an autoencoder for dimensionality reduction then using k-means clustering with the lower dimensional representation as well as the accelerometer data that was concurrently collected through the Neurochip3 (Figure 5.2A, *Classifying sleep states* in *Methods and materials*). We assumed 4 clusters – awake and moving (Move), awake and at rest (Rest), REM sleep (REM) and non-REM sleep (NREM). Each cluster was assigned to

the state depending on the average accelerometer value and features in the average power spectral density (PSD).

Figure 5.2B shows an example of the classification over a 21-hour period and the corresponding spectral power. During lights-off we found consistent REM cycles in between NREM epochs occurring every 30 minutes to 2 hours, which became longer and more frequent closer to the morning, consistent with previous findings (Aserinsky & Kleitman, 1953; Hsieh et al., 2008; Kripke et al., 1968). NREM was absent when the lights were on in the animal room, but we often found brief periods of REM sleep concurrent with changes in the PSD, which we attributed to naps (Figure 5.2B, arrow) (Dijk et al., 1987; Moses et al., 1975). We also often found short periods of Rest or sometimes even Move during the night which were attributed to brief awakenings, typical in an average night of sleep.

Averaging the spectral power during each sleep state shows high delta power during NREM sleep, high theta power during REM sleep, and high beta power when the animal was awake, consistent with previous findings (Figure 5.2C) (Xu et al., 2019). Additionally, raw LFP traces during the states show high-frequency activity during Move, faster oscillatory activity during Rest in the beta range, slower oscillatory activity during REM sleep in the theta and alpha range, and clear K-complexes and sleep spindles along with low frequency activity around delta during NREM sleep (Figure 5.2D).

Confirming sleep state classification

As our classification scheme was unsupervised, we simultaneously recorded electrooculography (EOG) signals to validate the identified sleep states (Figure 5.3A). Eye movements detected with the EOG were clearly associated with identified sleep states; EOG variance was very high when the animal was awake, very low during NREM sleep, and elevated during REM sleep (Figure

5.3B). This relationship was present even during very brief windows of detected awakening during the night and naps during the day, indicating high accuracy of state classification.

The accelerometer used for classification was on the Neurochip3 which was mounted on the animals' head. To confirm the accuracy of detected movements, we additionally recorded the monkeys' movements overnight with a Microsoft Kinect. Compared to the movement values extracted with the Kinect, the accelerometer values were smaller when the animal was awake but larger when the animal was asleep (Figure 5.3C). This is likely due to body movements that are independent of the head (i.e., isolated limb movements) not being as accurately recorded in the accelerometer. On the other hand, when the animal is laying down at night most movements involve the head. However, these differences were minor, and the two signals were comparable throughout the recording duration.

Finally, we also performed k-fold cross-validation to verify that our classification method was consistent and robust. We used k=20 and carried out 50 repetitions per session and found the average test and training error to be less than 4%, or around 40 total minutes (Figure 5.3D). The similar but low test and training errors suggest the classification method had low variance (i.e. not overfit) and high consistency. As a result, the classification was deemed sufficient for the aims of this study.

Changes in LFP dynamics

The average spectral power per state for each animal is shown in Figure 5.4A. Delta power was high during NREM sleep due to the presence of slow waves. There was a beta peak during the wake states, though the specific frequency range differed between the animals: 25-30 Hz for Monkey K and 15-20 Hz for Monkey J. REM sleep showed slightly higher theta and alpha power compared to the wake states. However, the differences in power between each state were

not as large as expected, which may be due to different sites being recorded for different recording sessions resulting in a broader average. Although all sites were within the motor cortex and within a 4 mm wide square window, there may still be large differences in LFP spectral power across different days, especially during different behavioral states.

Average pairwise coherence per state for each animal is shown in Figure 5.4B. The features were very similar to those show in the power, but the differences were magnified, likely due to coherence showing synchrony between pairs of channels and amplifying active oscillatory signaling over baseline spectral density. In addition to the large delta peak during NREM, there was a much clearer difference between REM and the wake states, including a more distinct beta peak.

Cross-frequency phase-amplitude coupling

The phase of lower frequency bands has been observed to be coupled with the amplitude of higher frequency bands, thought to reflect coordination between brain networks (Canolty & Knight, 2010; Jensen & Colgin, 2007). We explored the coupling between every pair of low frequency band phase to high frequency band amplitude to determine whether there were state-dependent changes. We first plotted the average z-scored spectral power of higher frequencies at different phases of each frequency band (Figure 5.5). There was clear coupling between different phases and frequencies, the strength and specific phase of which changed depending on the state.

To quantify the degree of coupling we calculated the normalized mean vector length (nMVL). Figure 5.6 shows the distribution of nMVL for each pair of frequency bands during each state. There were large state-dependent fluctuations in nMVL distributions, most notably during NREM. There was significantly stronger coupling between delta and theta phases and low and high gamma amplitudes (delta/theta-gamma) during NREM. Interestingly, delta/theta-high

gamma coupling was also elevated during Move. In contrast, delta/theta-alpha and delta-beta couplings were significantly lower during NREM.

Other large differences include significantly higher theta-beta coupling during REM and higher alpha-high gamma coupling during Move. Additionally, beta and low gamma phase to higher frequency coupling is higher during sleep states than awake states.

To further characterize the coupling, we explored the distribution of the mean vectors to determine whether the phases aligned with the highest amplitudes were consistent. Figure 5.7 shows the distribution of mean vector phases for each pair of frequency bands during each state. There was very high consistency in phases during NREM across most pairs of frequency bands. Theta-beta coupling was very consistent during REM, further validating the high nMVL distribution. Beta and low gamma phase to higher frequency coupling was consistent in the phase of coupling, typically between π and $5\pi/4$.

Spike sorting

Spikes were manually sorted using two-window discrimination (Figure 5.8A). As spike waveform shape and magnitude can fluctuate over time due to electrode drift, we calculated the coefficient of determination (CoD) for all pairs of the first and last 1000 instances of each spike to ensure we tracked the same spike throughout the recording duration (Figure 5.8B). A higher distribution of CoD between the first and last 1000 instances of the same spike compared to the CoD between different spikes confirmed the consistency of the spike waveform. We tracked a total of 193 spikes (121 in Monkey K, 92 in Monkey J) that satisfied our conditions across all sessions.

The firing rates of spikes overnight were strongly and consistently modulated by different identified sleep states, especially during REM cycles during the night, further demonstrating the accuracy of the classification method (Figure 5.8C). Firing rates were consistently lower with deeper sleep.

Additionally, spikes were designated to be regular firing or fast firing depending on the location of the inter-spike interval distribution peak during Move (Figure 5.8D). If the peak occurred before 10 ms the spike was designated to be fast spiking (FS), otherwise it was designated to be regular spiking (RS) (84 FS spikes, 109 RS spikes). Assessing the differences in firing rates depending on state showed that both RS and FS spike rates significantly decrease with deeper sleep (Figure 5.8E).

Changes in spiking dynamics

To determine how spiking patterns changed between different sleep states we analyzed changes in the average ISI distributions of RS and FS spikes. The raw ISI distributions showed an overall decrease on most ISIs with deeper sleep, reflecting the diminished firing rate, but also a slight change in the timing of the distribution, especially for RS spikes (Figure 5.9A).

To quantify the differences, we calculated the difference in ISI distributions from Move (Figure 5.9B, top). FS spikes had a consistent decrease in shorter latency ISIs with deeper sleep, but RS spikes showed a large increase in short latency ISIs at around 5 ms (arrow). To determine if there were any changes in larger ISIs, we plotted the distributions against frequency (Figure 5.9B, bottom). Both FS and RS spikes showed a peak between 7 and 10 Hz during NREM and a peak between 20 and 25 Hz during Rest and REM.

We also assessed how spiking activity of one spike affects other spikes by plotting the peri-event time histogram (PETH) based on changes in individual spike firing rates. For each spike, we found times when the firing rate was over 3 times the standard deviation from the average and calculated the PETH for each other spike in the recording from -1 to 1 second around the increased firing rate. Figure 5.9C shows the average PETH of each channel pair for each state. There was consistently high spiking activity immediately following the increase of any spike's firing rate, as expected from the co-modulation of firing rates seen overnight. However, the peak of activity was significantly higher during Move and NREM, being almost identical between the two states, and the lowest during REM. The widths of the peaks were between 150 and 200 ms and was comparable between all states.

Spike field relationships

Spikes have been shown to be synchronized to various frequency bands, particularly in the motor cortex (Buzsáki et al., 2012; Murthy & Fetz, 1996b). We first analyzed the phase-amplitude distribution normalized by amplitude of each LFP band during spike timings (Figure 5.10). There was clear synchrony with spikes during NREM sleep with all LFP bands, though at varying phases. During NREM spikes typically occurred at the negative phase of delta, beta, and gamma activity, and at intermediate phases for theta ($\pi/2$) and alpha ($3\pi/4$). The synchrony was particularly apparent during high amplitudes, suggesting spikes are synchronized to active frequency band activity rather than epiphenomena arising from periodicity of spike firing patterns. During both awake states and REM sleep spikes were synchronized to the trough of beta and gamma frequencies, though less than during NREM sleep. Spikes during Move were also potentially synchronized to the delta band. All other combinations did not show apparent coordination between LFP band phase and spike timing.

To quantify the strength of these relationships, we calculated the phase-locking value (PLV) for each spike during each state for all LFP bands. Figure 5.11 shows the RS spikes' distribution of locked phases as well as the PLV for each frequency band during each state. Spikes were more synchronized to delta during both Move and NREM, validated by the consistency in the locked phases (around $\pi/2$ and $\pm\pi$, respectively). For every other frequency band, there was stronger synchrony during deeper sleep states, though the differences were often not statistically significant. The phases were extremely consistent for beta and higher frequency bands, but variable for lower frequency bands during states with lower PLVs.

Figure 5.12 shows the FS spikes' distribution of locked phases and the PLV for each frequency band during each state. One large difference from RS spikes was the synchronization with delta during Move, which was not significantly larger compared to Rest or REM. Otherwise, there was a much stronger relationship between increase in PLV and deeper sleep states, being statistically significant for each frequency band. In addition, the phase of synchrony to the low and high gamma bands was earlier in the phase for FS spikes compared to RS spikes.

Discussion

State classification

Although a guideline to standardize sleep staging was published after the discovery of sleep stages (Rechtschaffen & Kales, 1968), staging has remained an inconsistent and often arduous task. Criticisms of and modifications to the guideline (Himanen & Hasan, 2000; Silber et al., 2007) as well as various automated methods (Hamida & Ahmed, 2013; Penzel & Conradt, 2000; Sun et al., 2020) have been developed, but each approach differs in the set of defined states and the type and amount of data required. In addition, studies on sleep typically use electroencephalogram (EEG) LFP recordings, which are distinctly different from intracortical LFPs due to their lower spatial specificity and the complex frequency and phase filtering of bone and tissue, especially at higher frequencies (Buzsáki et al., 2012; Michel et al., 2004; Sejnowski et al., 2014). Beyond these difficulties, manual scoring is also compromised by high inter-scorer variability (Himanen & Hasan, 2000; Younes et al., 2016).

As a result, we developed our own classification methodology to distinguish between different sleep states. The process was relatively simple, utilizing basic dimensionality reduction and clustering on processed LFP PSDs and accelerometer values, but was remarkably consistent. We used several metrics to confirm the method – EOG recordings, concurrent recordings with the Kinect to track movement, k-fold cross validation, and changes in spike rates; they all indicated accurate and robust classification. One explanation may be that sleep states can vary between different regions of the brain (Mascetti, 2016; Siclari & Tononi, 2017). Our focus on a small region (4x4 mm) of the motor cortex and the high spatial specificity of intracortical LFPs may have produced more robust results compared to those based on EEG recordings from across the brain.

Our method could potentially be improved by using a dimensionality reduction method with higher complexity, such as a deep neural network (Malafeev et al., 2018), different clustering methods, such as hierarchical clustering (Gerla et al., 2019), and by including the EOG recordings or other biophysical measurements as additional dimensions of data (Khalighi et al., 2013). However, developing a flawless classification method was not within scope of the study and thus the method presented was deemed to be sufficiently accurate and of practical use.

LFP and spike dynamics during different sleep states

The average PSD of LFPs during each state displayed features similar to those reported previously (Rechtschaffen & Kales, 1968; Silber et al., 2007; Xu et al., 2019). We found high delta power during NREM sleep, as delta is elevated across the brain during all stages of NREM. Beta power was high during Move and Rest, as we were recording from the primary motor cortex, and beta oscillations are highly relevant in motor control (Engel & Fries, 2010; Khanna & Carmena, 2017). Finally, we found high theta power during REM sleep. The role of theta band in the cortex is still obscure, but theta in the hippocampus is also consistently high during REM (Boyce et al., 2016). We found similar features in the pairwise magnitude-squared coherence. As coherence shows synchrony between two signals, it effectively emphasizes coordinating activity from the baseline PSD.

We also observed decreased spiking activity with deeper sleep, similar to a previous study (Xu et al., 2019). In addition, the firing patterns of spikes changed due to sleep state – RS neurons had increased high frequency activity during NREM compared to Move, and all neurons had an increase low frequency activity during Rest, REM, and NREM compared to Move. The increase in beta frequency activity of neurons during REM and Rest can be explained by the fact that beta is seen as a “resting” rhythm in the primary motor cortex (Engel & Fries, 2010). RS neurons are

likely to be excitatory pyramidal cells and FS neurons are likely to be inhibitory interneurons (McCormick et al., 1985), which may explain the higher "bursty" firing pattern of RS neurons during NREM sleep, potentially due to reactivation of cortical circuitry activated during the day. This is further substantiated by the PETH of spikes to increases in firing rate showing similarly high coordination between spikes during Move and NREM compared to Rest or REM.

Cross-frequency coupling and spike-LFP synchrony

Cross frequency coupling shows that the higher frequency band modulates with the lower frequency band. Such synchrony reflects coordination of local networks operating on shorter time scales to distributed circuits synchronized at longer time scales; this could potentially play a role in neural computation of attention, learning, and memory (Canolty & Knight, 2010; Jensen & Colgin, 2007). Various measures have been proposed to quantify phase-amplitude coupling; compared to other proposed measures the MVL introduced by Canolty et al. (2006) has been shown to be accurate, the most sensitive to modulations in coupling strengths, and ideal for high quality signals over a long recording epochs (Canolty et al., 2006; Hülsemann et al., 2019; Onslow et al., 2011; Tort et al., 2010).

Spike-LFP synchrony provides another measure of synchrony between the single neurons and the composite synaptic activity of the local population (Buzsáki et al., 2012; Murthy & Fetz, 1996b; Okun et al., 2010). The magnitude indicates the strength of synchrony whereas the phase can provide insights into the timing of the spikes relative to the local population.

Most instances of cross-frequency phase-amplitude coupling and spike-LFP synchrony were stronger for deeper sleep states. This may be due to asynchronous activity during Move being driven by functional local circuitry (i.e. generating movement) whereas activity during resting

and sleep states are more attuned to baseline macroscopic rhythmic activity, potentially driven by homeostatic plasticity (Tononi & Cirelli, 2014).

Delta and high gamma

One noticeable deviation from deeper sleep resulting in stronger synchrony was delta phase to high gamma amplitude (delta-high gamma) coupling, which was significantly higher during Move compared to Rest or REM. Delta oscillations may arise in the thalamus or the cortex and are elevated during NREM. Delta has also been linked to various perceptual, sensorimotor, and cognitive operations, potentially suppressing activity not necessary to the task at hand (Güntekin & Başar, 2016; Harmony, 2013). In contrast, high gamma band LFP is representative of local spiking activity, often strongly correlated with action potentials, and can also reflect neuronal synchrony (Ray et al., 2008; Ray & Maunsell, 2011).

Evidence suggests the strength of delta-high gamma coupling is modulated by dopamine in both the prefrontal cortex and the cortico-basal ganglia network (Andino-Pavlovsky et al., 2017; Güntekin & Başar, 2016). Delta-high gamma coupling has also previously been shown to be present during sleep in both the hippocampus and the neocortex (Clemens et al., 2009; Takeuchi et al., 2015), but the underlying mechanisms are still unclear. Andino-Pavlovsky et al. (2017) showed high delta-high gamma coupling during slow wave sleep in the rodent prefrontal cortex, and Takeuchi et al. (2015) showed strong delta-high gamma coupling during REM and several NREM substages in the primate hippocampus (Andino-Pavlovsky et al., 2017; Takeuchi et al., 2015). However, neither study pursued the state-dependent comparisons, and their broad definition of gamma (>25 Hz) makes independent interpretation difficult. Specific comparisons of delta-high gamma coupling during different sleep states have not been reported.

Spike synchrony to delta band sheds additional light on the delta-high gamma relationship. In our study, only RS neurons showed higher delta-high gamma coupling during Move, and the phase of synchrony was consistently at the falling edge of the wave (Figure 5.11). During NREM both RS and FS spikes were synchronized to delta, but the phase of synchrony was immediately after the trough of the wave. These results suggest delta as a coordinating signal that reactivates cortical circuitry during sleep for consolidation (Gulati et al., 2017; Ramanathan et al., 2015; Xu et al., 2019); spiking activity during the day occurs before delta is the most depolarized, potentially driving delta activity, and delta during NREM has the highest depolarization right before spiking activity, which may reactivate the neural circuitry. Such coordination is also reflected in the cross-frequency coupling observed in our study.

Theta in the motor cortex and REM sleep

Theta oscillations have often been observed during REM sleep, and have also been shown to coordinate hippocampal place cell activity during active exploration (Buzsáki & Moser, 2013; Cantero et al., 2003). In the cortex, modulation of theta has been most prominently seen with theta burst stimulation (TBS) – bursts of gamma frequency stimulation delivered at theta intervals, typically with TMS over the motor region. TBS has been shown to increase the excitability of the motor system, observed through increased motor evoked potentials, potentially by mimicking the coupling of theta and gamma oscillations (Cárdenas-Morales et al., 2010; Huang et al., 2005; Suppa et al., 2016). Additional evidence shows that strengthening theta-high gamma coupling with transcranial alternating current stimulation (tACS) increases motor learning (Akkad et al., 2021). In agreement with these previous findings, our results show much higher theta-high gamma coupling during Move.

Theta has also been shown to be coupled to low gamma. A wealth of recent cross-frequency coupling literature has reported theta-low gamma coupling in both hippocampus and the neocortex, showing modulations dependent on task performance, cognitive engagement, and memory formation (Buzsáki & Wang, 2012; Canolty et al., 2006; Lisman & Jensen, 2013). Although stronger theta-low gamma coupling has also been observed during REM sleep, it was absent in human studies, potentially due to hippocampal theta oscillations in humans being slower than those in rodents (Cantero et al., 2003; Clemens et al., 2009; Jacobs, 2014). Similar to the human studies, we did not find significant theta-low gamma coupling during REM, but we also did not find significant delta-low gamma coupling.

Instead, we found very high theta-beta coupling during REM sleep. Theta-beta coupling is not a common topic of study; there is some evidence that suggests it plays a role in working memory and decision making, but the literature is sparse and focuses on the frontal lobe (Axmacher et al., 2010; M. X. Cohen et al., 2009; Liang et al., 2021). In our results, the maximum beta amplitude occurs right before the peak of theta (Figure 5.7), which leads to minimum beta occurring right after the trough of theta. If beta is a regulating, inhibitory rhythm in the motor cortex, perhaps theta is increasing the excitability of the cortex by minimizing beta, and thus inhibition. This may lead to more effective memory consolidation often seen during REM sleep, relevant to motor skill learning. However, more research is needed to confirm these conclusions.

Concluding Comments

We analyzed spike and LFP activity in the primate motor cortex during different behavioral states to better understand the role of sleep and various LFP frequency bands. We observed an increase in burst firing and high coordination between spikes during NREM, consistent with previous findings suggesting reactivations of cortical circuity during NREM. High cross-

frequency phase-amplitude coupling between delta and high gamma when the animal is awake and moving and during non-REM sleep, as well as spike-field synchrony with delta band LFP, suggest that delta may encode and subsequently drive these reactivations. Modulations in theta to low gamma phase-amplitude coupling, commonly observed in rodents, was not observed, similar to previous human studies. Instead, we observed high theta to beta coupling during REM, potentially driving motor learning by increasing the excitability of the cortex. We also observed high theta to high gamma coupling during Move, potentially reflecting coordination with hippocampal place cells.

Figures

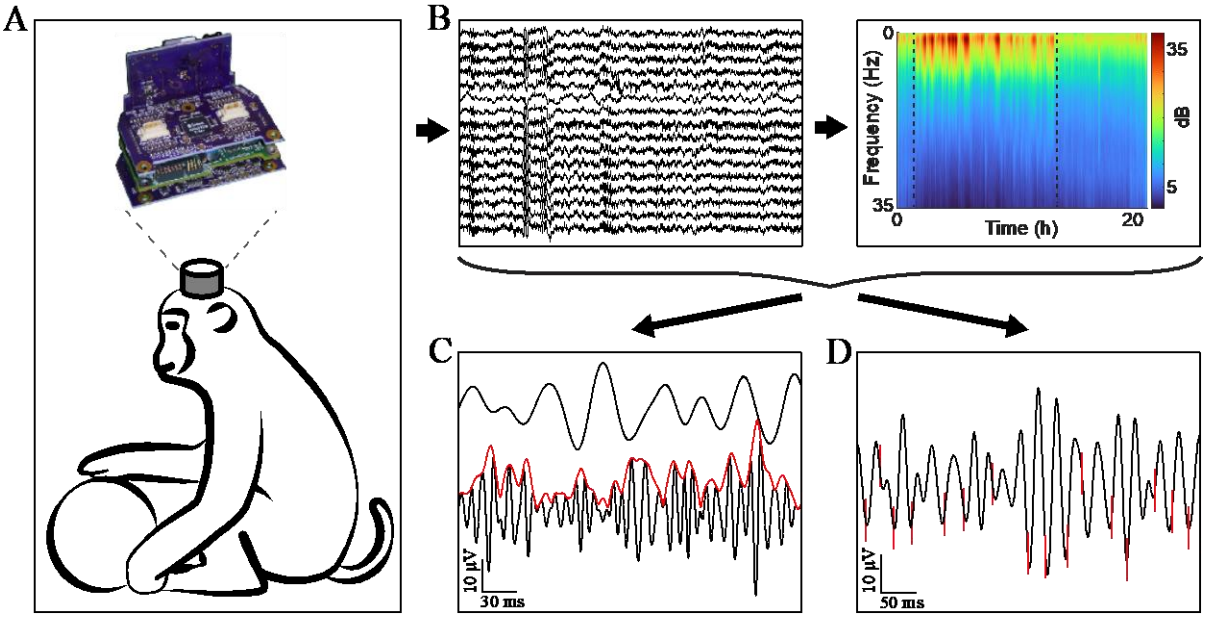

Figure 5.1 Experimental design

A. All data was gathered using the Neurochip3 on freely behaving macaques for up to 24 hours. **B.** We collected 16 channels of data at 20 kHz and obtained the spectral density of every 8-second bin to classify behavioral states. **C.** We then calculated the cross-frequency phase-amplitude coupling of every frequency band pair. The example shows the instantaneous amplitude (red) of high gamma filtered LFP (black, bottom) increasing at the trough of beta (black, top). **D.** We additionally sorted single units and found the synchrony of spikes to LFP bands. The example shows spikes (red) synchronized with the trough of beta filtered LFP.

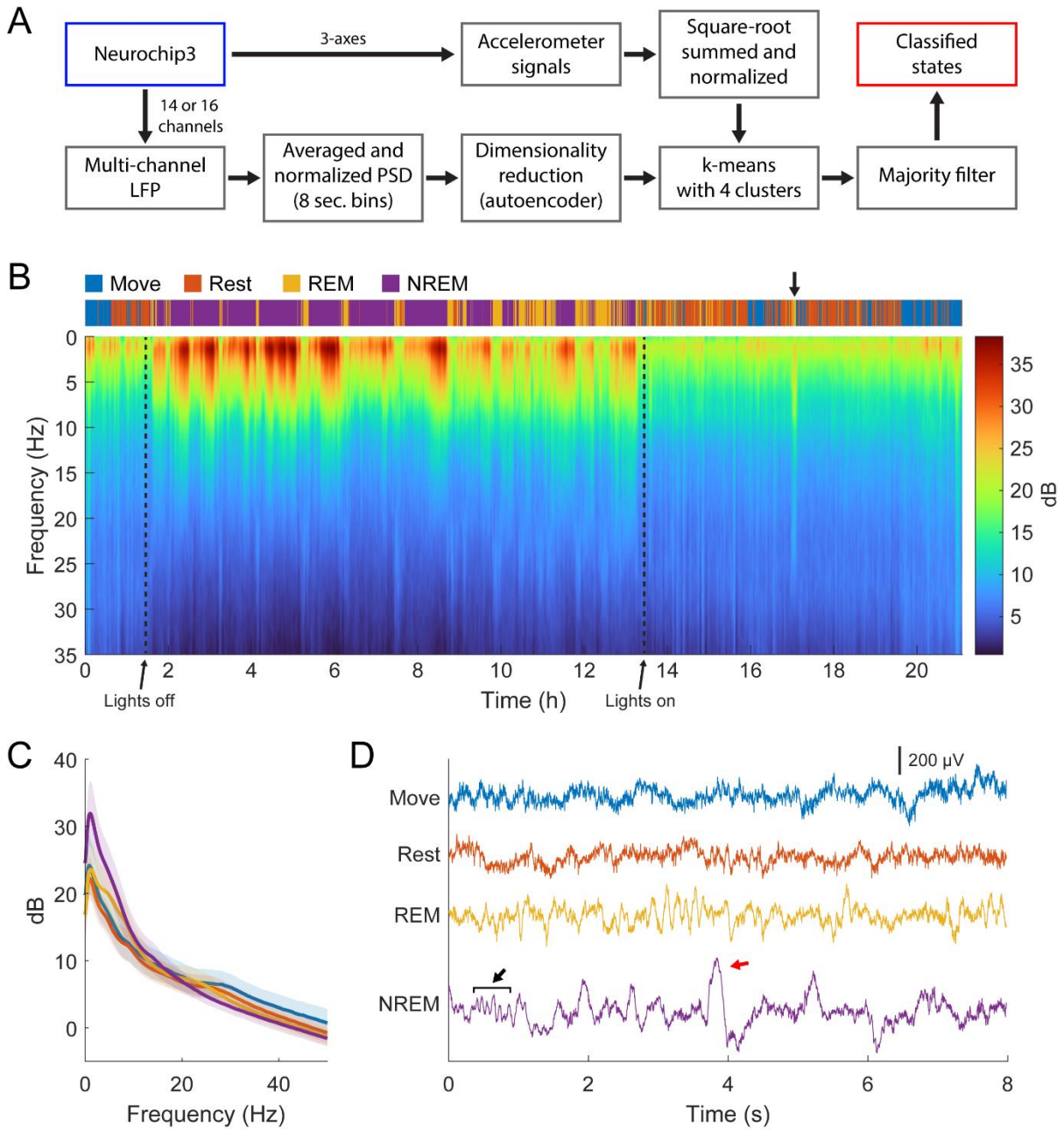

Figure 5.2 Behavioral state classification

A. Diagram of classification process. LFP and accelerometer signals are used to train an autoencoder for dimensionality reduction and subsequent k-means clustering to determine different sleep states. **B.** Example of classification and spectra over 22 hours of continuous recording. Brief periods of REM sleep were observed during the day, attributed to naps (arrow). **C.** Averaged spectra across each state for the session shown in (B). There is high delta power during NREM, theta power during REM, and beta power during Move and Rest states. **D.** Example traces of raw LFP during each state. Spindles (black arrow) and k-complexes (red arrow) were observed during NREM sleep.

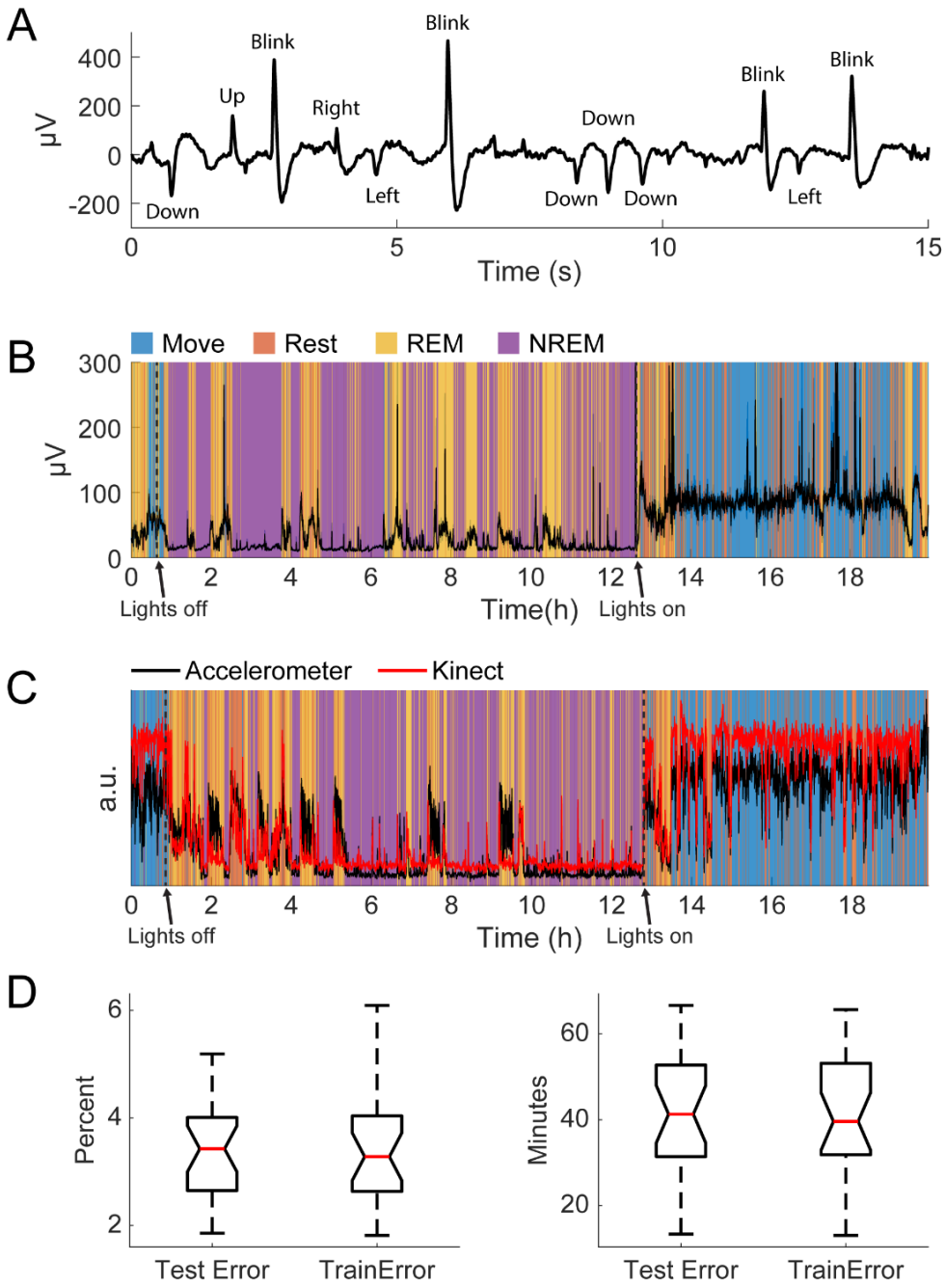

Figure 5.3 Confirmation of behavioral state classification

A. An example of filtered differential EOG signals and corresponding eye movements. **B.** Standard deviation of EOG signals overnight with respect to classified states. Note the increase in large eye movements during REM and waking. **C.** An example of the normalized variance of accelerometer data and the normalized variance of the Kinect data with respect to classified states. **D.** Test and training errors with k-fold cross-validation in percent (left) and total minutes (right).

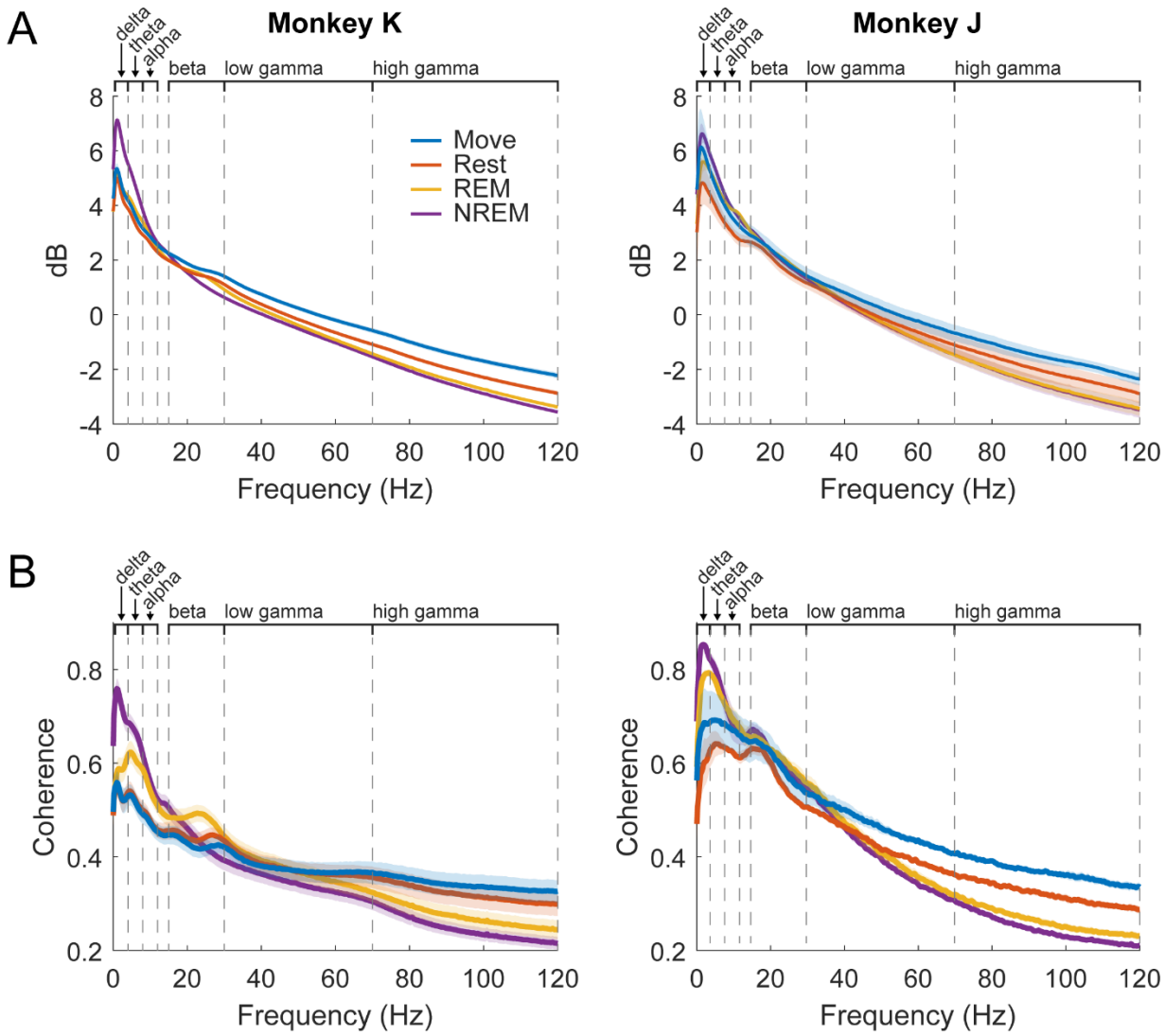

Figure 5.4 LFP dynamics during each state

A. Average spectral power in each state for each animal across all experiments. Shaded regions show standard error. **B.** Average pairwise coherence in each state for each animal across all experiments. Shaded regions show standard error.

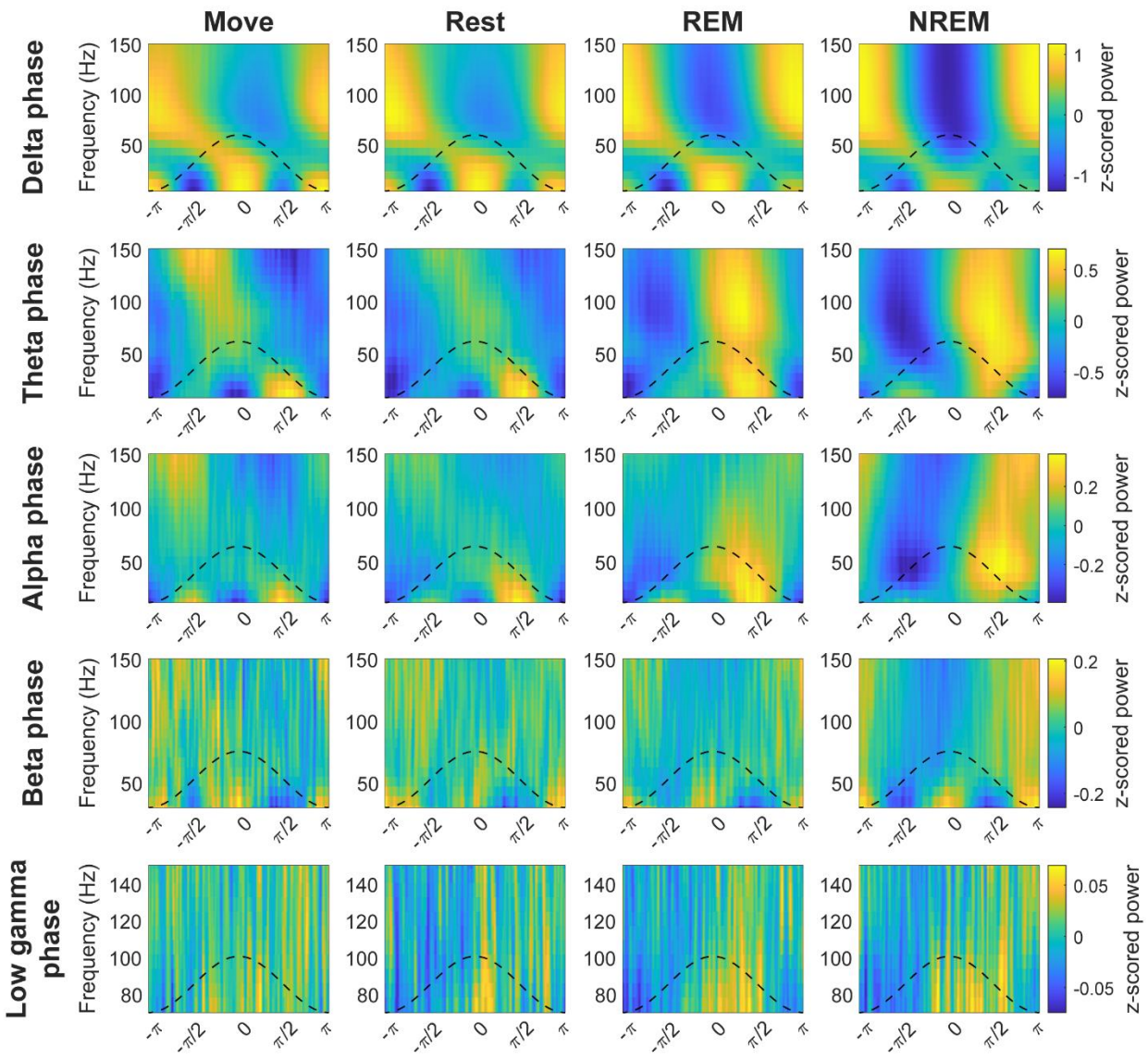

Figure 5.5 Cross-frequency phase-power distributions

Distribution of lower frequency band phase and higher frequency band power during each state. The power is z-scored for each frequency.

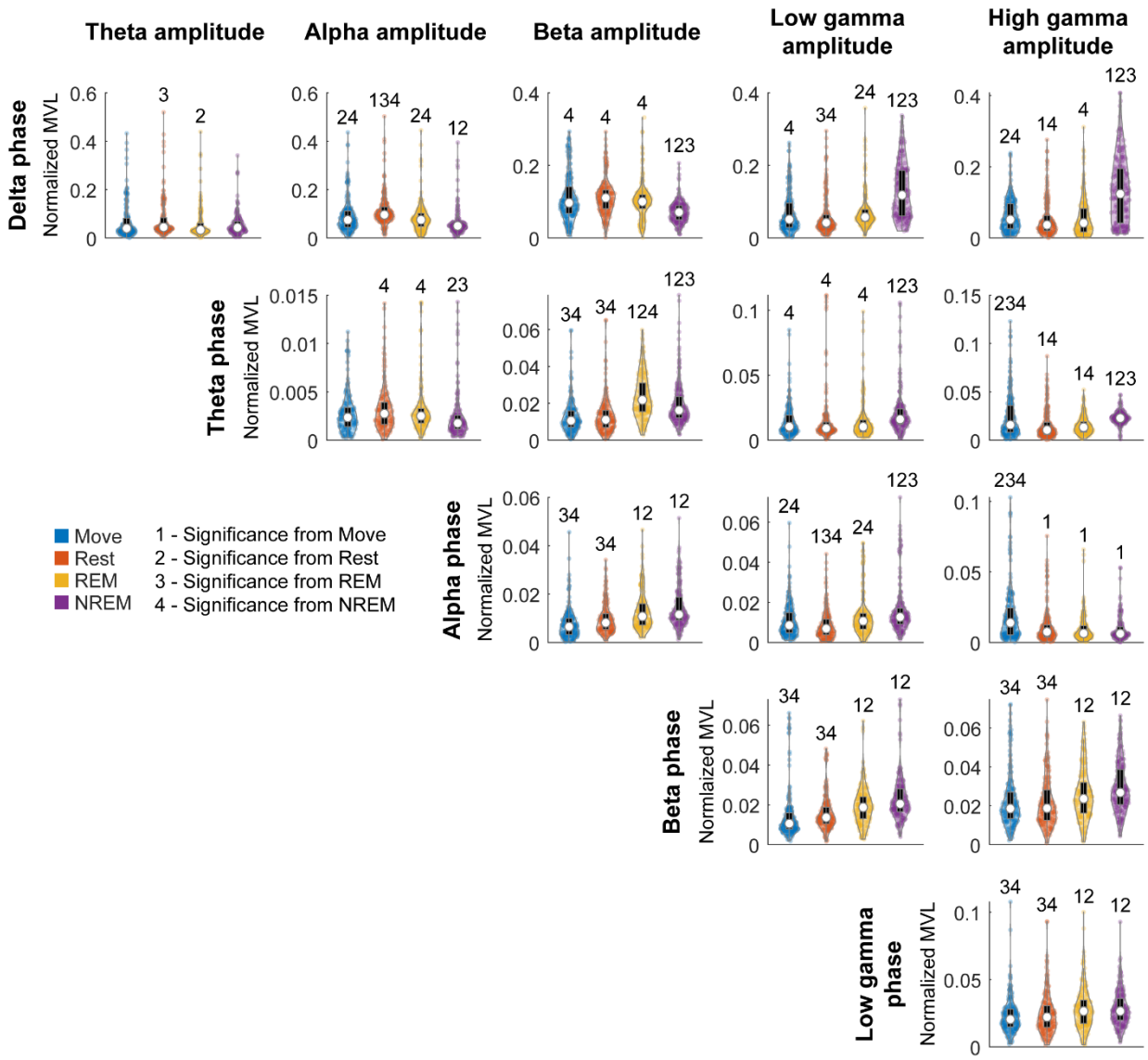

Figure 5.6 Normalized MVL distributions

Normalized MVL distributions for each lower frequency band phase and higher frequency band amplitude pair during each state. The black boxes show standard box plots with interquartile range and the white dots show median values. The numbers above each group denote significance compared to another state (Friedman's test, $p<0.05$).

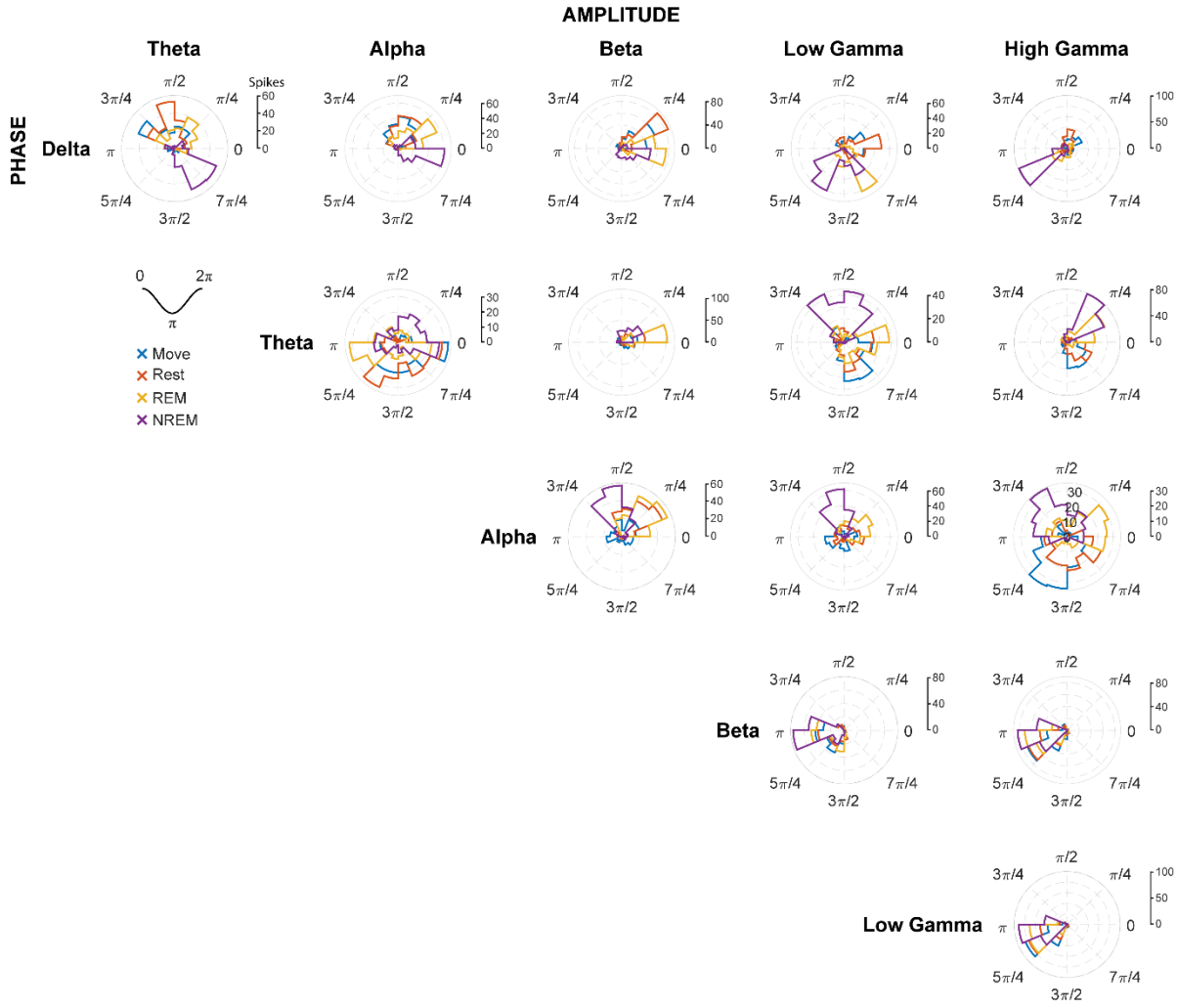

Figure 5.7 Mean vector phase distributions

The distribution of phases of mean vectors for each lower frequency band phase and higher frequency band amplitude pair during each state. The phase of the mean vector shows the phase at which the amplitude of the higher frequency band is the greatest.

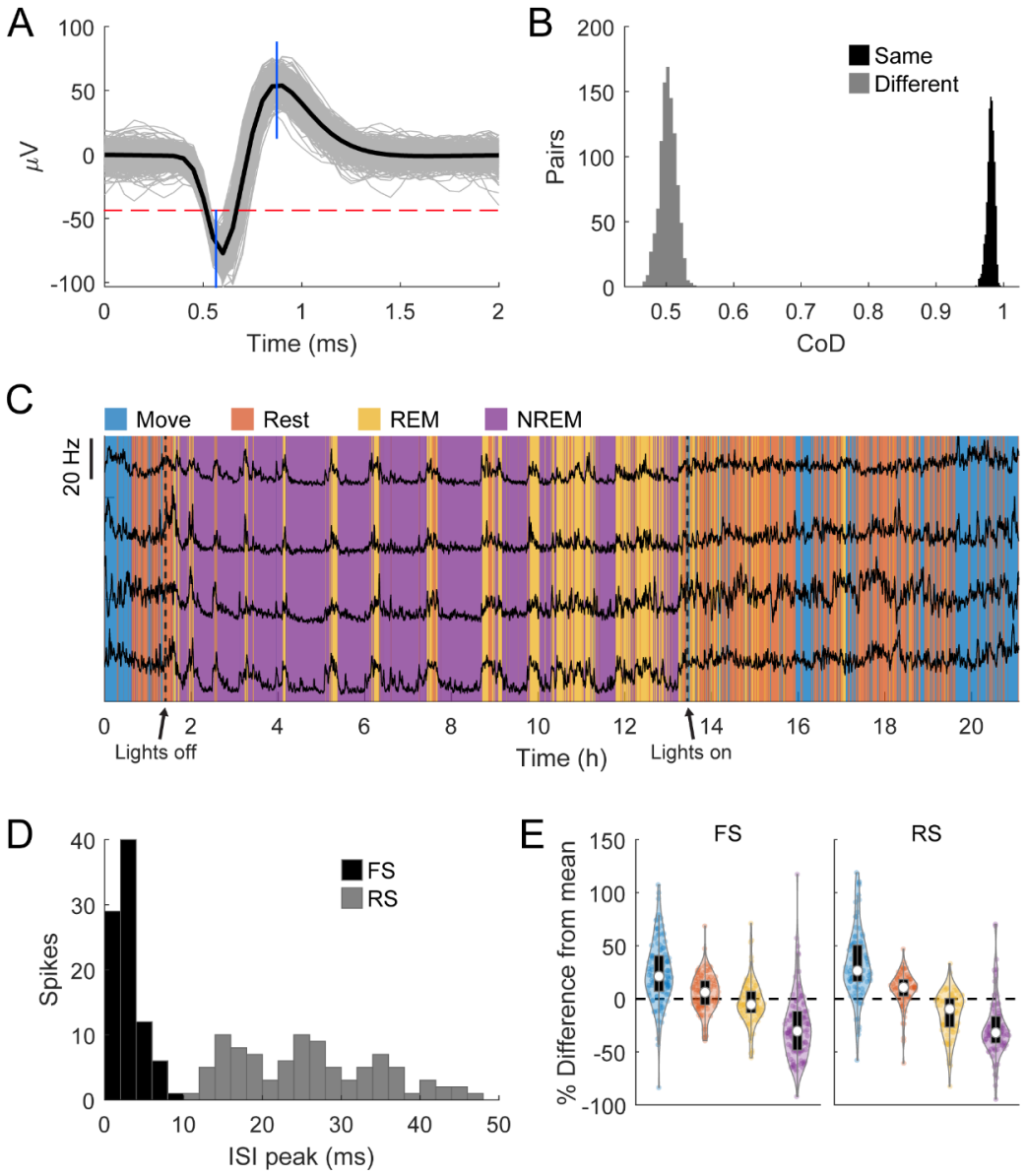

Figure 5.8 Spike sorting

A. An example of a sorted spike. The grey traces show a random sample of 1000 spikes, the black line is the average, the horizontal dashed red line shows the threshold, and the blue vertical lines show the two windows. **B.** An example of comparisons of the pairwise coefficient of determination (CoD) between the first and last 1000 instances of the same spike and the first and last 1000 instances of two different spikes. **C.** Firing rates binned every 60 seconds of four neurons overnight with classified sleep states. The changes in firing rate very closely match the changes in state. **D.** Histogram of the peak of the ISI distribution of each spike. Spikes with peaks earlier than 10 ms were denoted to be fast spiking (FS) and all others denoted to be regular spiking (RS). **E.** Percent difference of firing rate in each state from the average overall firing rate for each spike type. Each state is statistically significantly different from each other state (Friedman's test, $p<0.05$).

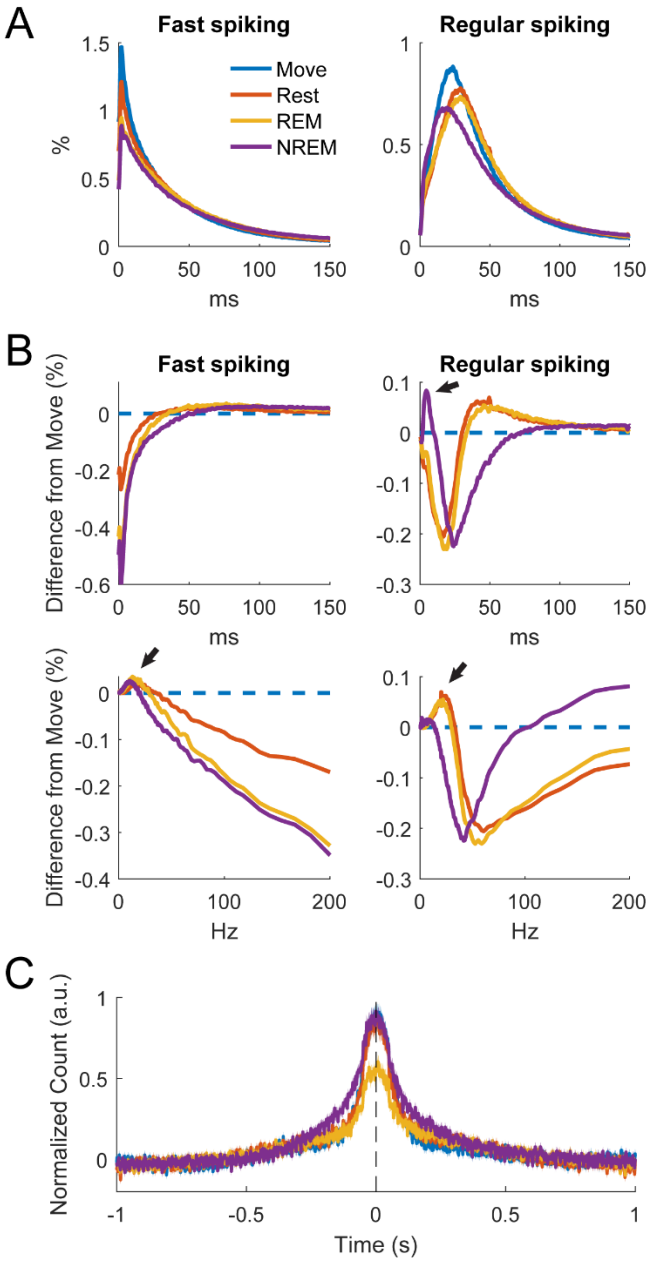

Figure 5.9 Changes in spiking patterns

A. Average ISI distributions of identified fast spiking and regular spiking neurons during each state. **B.** Difference of ISI distributions from Move plotted against time (top) and frequency (bottom). Note the peak around 5 ms during NREM for regular spiking neurons and the peaks around 7-10 Hz during NREM sleep and the peaks at around 20 and 25 Hz for REM and Rest respectively (arrows) for both neuron types. All three peaks were significantly different from 0 (Wilcoxon signed-rank test, $p<0.05$). **C.** Average normalized PETH triggered from an increase in firing rate of one spike. Each PETH trace was normalized by subtracting the mean value and then dividing by the standard deviation.

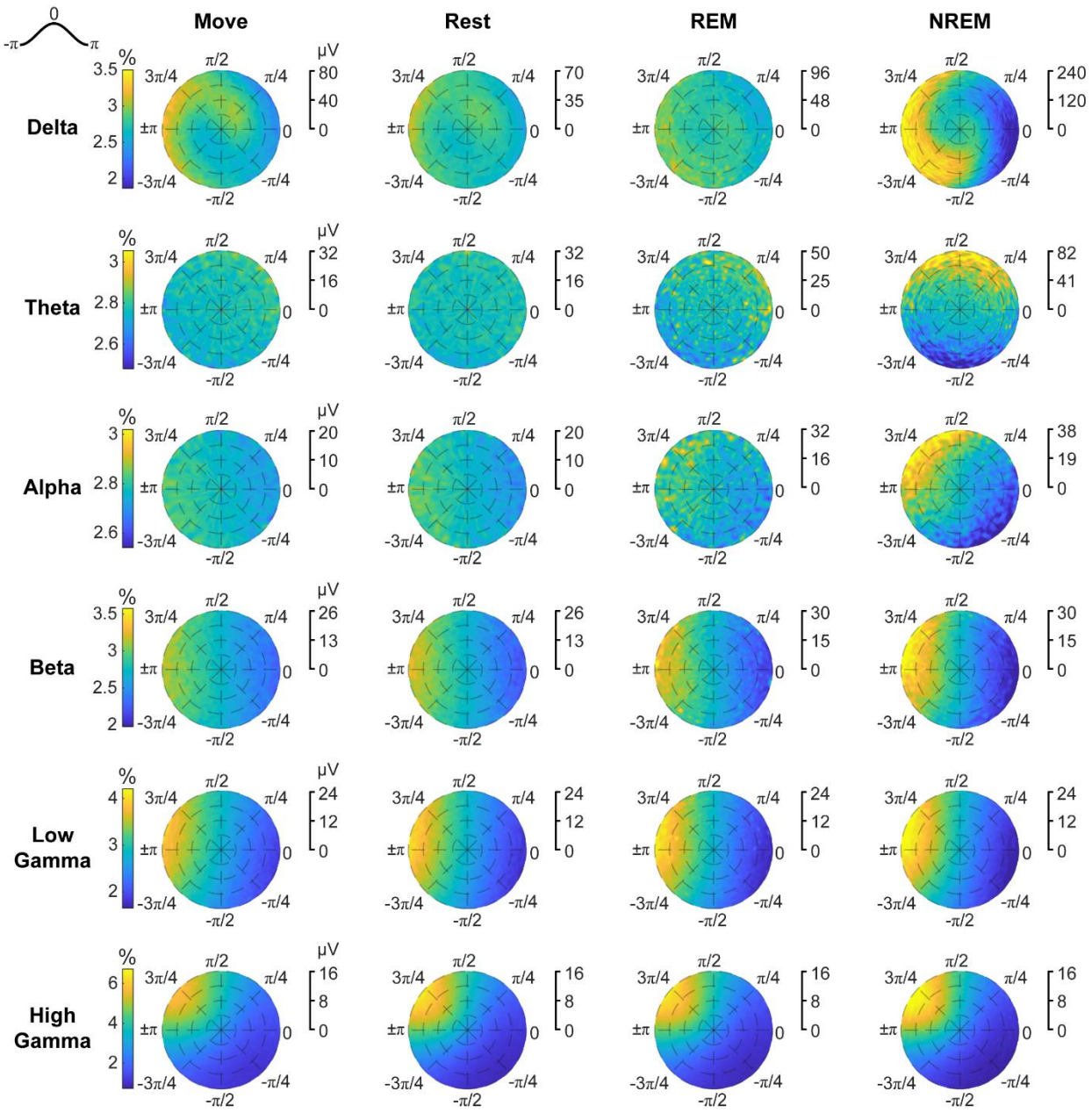

Figure 5.10 Phase distributions of LFPs at spike times

Phase distributions normalized for each amplitude during each sleep state for each LFP band.

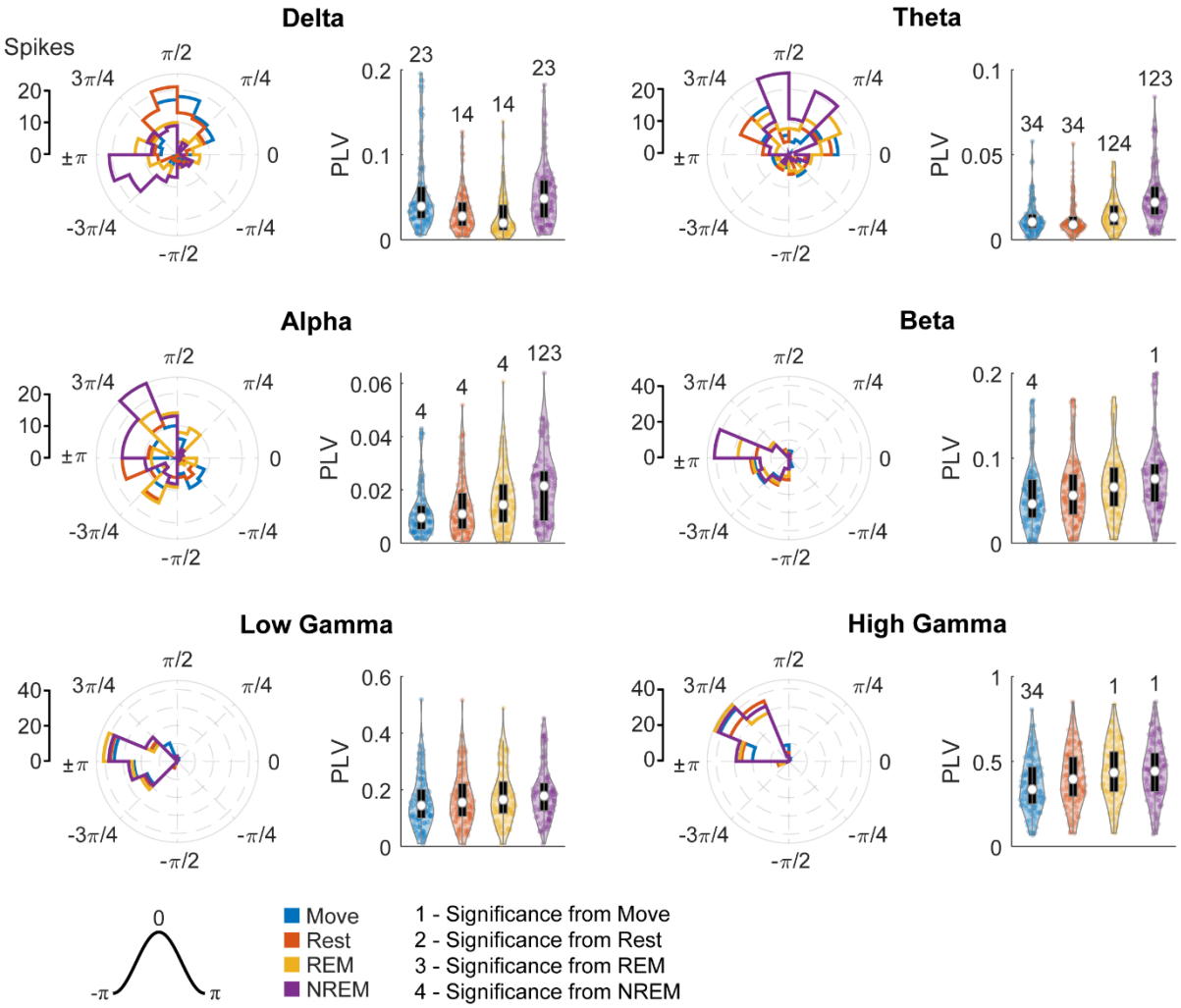

Figure 5.11 Locked phase and phase locking value distributions for regular spiking neurons

Distributions of locked phase (left) and PLVs (right) of regular spiking neurons during each sleep state for each LFP band. The numbers above each group denote significance compared to another state (Friedman's test, $p<0.05$).

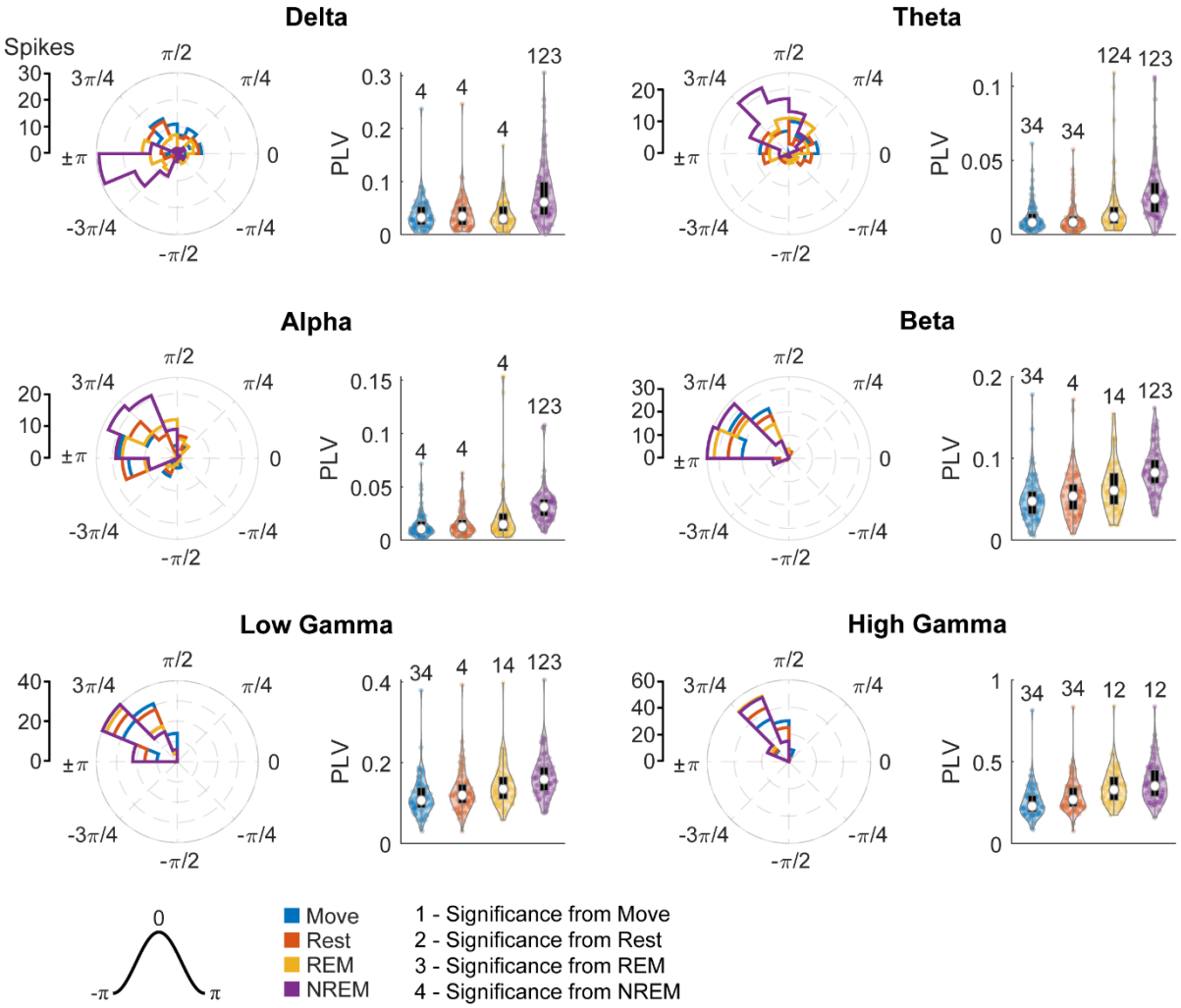

Figure 5.12 Locked phase and phase locking value distributions for fast spiking neurons

Distributions of locked phase (left) and PLVs (right) of fast spiking neurons during each sleep state for each LFP band. The numbers above each group denote significance compared to another state (Friedman's test, $p<0.05$).

Conclusions and future directions

This dissertation outlines the experiments performed to better understand mechanisms of intracortical microstimulation and its uses in stimulus-induced targeted plasticity. I explored how stimulation activates individual neurons and what we can infer from those activations in Chapter 3. The dependence of the effects of stimulation on different phases of movement were studied in Chapter 1, and the groundwork to explore the changes during different stages of sleep were established in Chapter 5. Finally, the relevance of specific stimulus timing was demonstrated in Chapters 2 and 4. These studies illustrate the significance of better understanding responses to ICMS and delivering stimulation at specific timings. Potential future experiments to further these experiments and help elucidate underlying mechanisms or improve our understanding of stimulus induced plasticity are outlined below.

i. Coincident activation of a postsynaptic site via stimulation of two presynaptic sites for induction of multi-site STDPS

Chapter 4 established a paired stimulation paradigm for STDP. These results can lead to an experiment in which stimulation is delivered to two presynaptic sites that project to the same postsynaptic site, illustrated in Figure i.1. Given two sites, Pre1 and Pre2, such that stimulating the sites generates a spike in a third site, Post, at latencies of ES1 and ES2, we can design a paired stimulation paradigm in which Pre1 then Pre2 are stimulated at a delay of ES2-ES1. This would result in the activation of Post from Pre1 and Pre2 to arrive concurrently. If the facilitation we observed in Chapter 4 was indeed due to the specific timing relative to the evoked spike latency, such coincident activation should strengthen the connections from both Pre1 and Pre2 to Post.

I was able to perform three preliminary experimental sessions. The experimental design was similar to Chapter 4 except the paired stimulation was delivered to two presynaptic sites with a delay such that the Post spike evoked by stimulation delivered to Pre1 arrived simultaneously as the Post spike evoked by stimulation delivered to Pre2. During the pre- and post-test epochs I randomly alternated between Pre1 and Pre2 for each test stimulus. One experiment resulted in strengthening of both connections, one resulted in strengthening of one connection, and the final experiment resulted in no changes. In all three experiments, the probability of evoking the Post spike during the conditioning epoch was significantly higher compared to stimulating just Pre1 or Pre2.

The variability may be due to the dependence of the synaptic changes on the initial evoked spike probability, as was demonstrated in Chapter 4. It can also be explained by the co-activation potentially strengthening projections to the inhibitory circuitry resulting in weaker potentiation. Altering the ISI such that the activations do not coincide with one another, and reassessing changes will shed light on the underlying mechanisms. Additional experiments with optogenetics will also determine how the changes may be affected by specific cell and synapse types and whether our interpretation of results from Chapter 4 was accurate.

This study can subsequently allow for strengthening of connections to a site that does not receive any stimulation, potentially enabling potentiation to difficult-to-implant locations such as the spinal cord or deeper brain structures. It may also lead to predicting changes in synaptic strength due to multi-channel stimulation, paving the way for designing complex stimulation paradigms to induce targeted changes on network level connectivity.

ii. Behavioral state dependent stimulus responses and plasticity

Chapter 5 laid the groundwork for assessing different behavioral states using spectral properties of intracortical LFP. Although the focus was on assessing changes in neural dynamics, the initial purpose was to assess the differences in efficacy of plasticity paradigms applied at various behavioral states. As mentioned in Chapter 5, there is already ample evidence that REM and NREM sleep are critical for solidification of plasticity; as mentioned in Chapter 1, stimulation delivered during active movement may be more effective than stimulation delivered at rest. However, stimulus induced STDP has not been explicitly compared between different behavioral states.

To assess changes in cortical connectivity, stimulation is typically delivered to the presynaptic site and a response measured at the postsynaptic site. To determine whether these baseline responses can change between states, we conducted preliminary experiments by delivering single-pulse stimulation every 10 seconds. We used the same method as in Chapter 5 for classifying between different behavioral states, but 2 seconds following each stimulus were blanked to prevent the stimulus response from contaminating the power spectral density. We collected 22 spike responses, 14 of which were fast spiking and 8 of which were regular spiking. The results showed that the single unit response to stimulation did not have a consistent change depending on the state, and that the subsequent inhibition increased with deeper sleep regardless of the spike type (Figure ii.1).

However, Chapter 3 showed that both the excitatory and inhibitory responses are linearly correlated with the spontaneous firing rate, and Chapter 5 showed differences in both firing rate and firing patterns of spikes between different behavioral states. Thus, we normalized the excitatory response by dividing by the firing rate and normalized the inhibitory response by

dividing by the inverse of the firing rate (i.e. multiplying by the firing rate). However, the results remained the same, with the excitatory response showing no consistent change between states and the inhibitory response increasing with deeper sleep. This suggests that the behavioral state is irrelevant to the excitatory response of neurons to stimulation, and that inhibitory neurons are much more excitable during deeper sleep that isn't fully accounted for by the decrease in excitation. These results support the previous findings of active inhibition during sleep (Brown et al., 2012; Timofeev et al., 2001), but more data and further analyses are required to confirm these conclusions and understand why excitatory responses do not change.

Once the baseline stimulus responses are fully analyzed, we can then track plasticity overnight. There are two approaches for doing so: 1) deliver stimulation only during specific behavioral states and compare their efficacies or 2) track how the effects of a plasticity paradigm delivered during the day change overnight through different behavioral states.

The first approach requires a modification of the Neurochip3 to allow for real-time assessment of behavioral state. The autoencoder and distance calculations for k-means only requires linear operations so it may be possible to add this functionality to the FPGA. The state classification for the recorded electrode set would be classified beforehand and the weights and k-means centroids uploaded to the Neurochip3 before the experimental session. I would expect plasticity to be much more readily induced during REM and NREM sleep due to their roles in learning and memory consolidation. However, the active inhibition present during sleep may prevent external stimuli from readily altering the synaptic strength.

The second approach can be implemented much easier, and simply requires continuously recording overnight after applying the stimulation paradigms of Chapter 4. For newly strengthened connections I would expect the relationship to become amplified during sleep

following the theory of reactivation of cortical circuitry. These studies will elucidate the impact of brain state on plasticity and shed light on the role of different behavioral states on cortical circuitry, possibly leading to more efficacious plasticity paradigms.

Figures

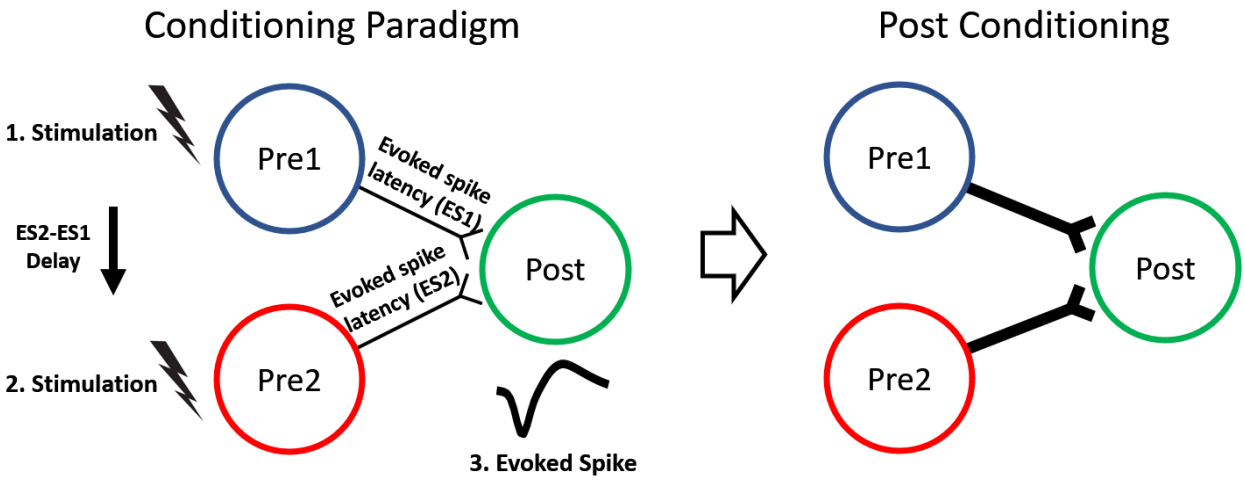

Figure i.1 Stimulating two presynaptic sites to strengthen connections to a postsynaptic site

Given two sites, Pre1 and Pre2, such that stimulating the sites generates a spike in a third site, Post, at latencies of ES1 and ES2 we can design a paired stimulation paradigm in which Pre1 then Pre2 are stimulated at a delay of ES2-ES1. This would result in the activation of Post from Pre1 and Pre2 to arrive concurrently, potentially strengthening the connections from Pre1 and Pre2 to post.

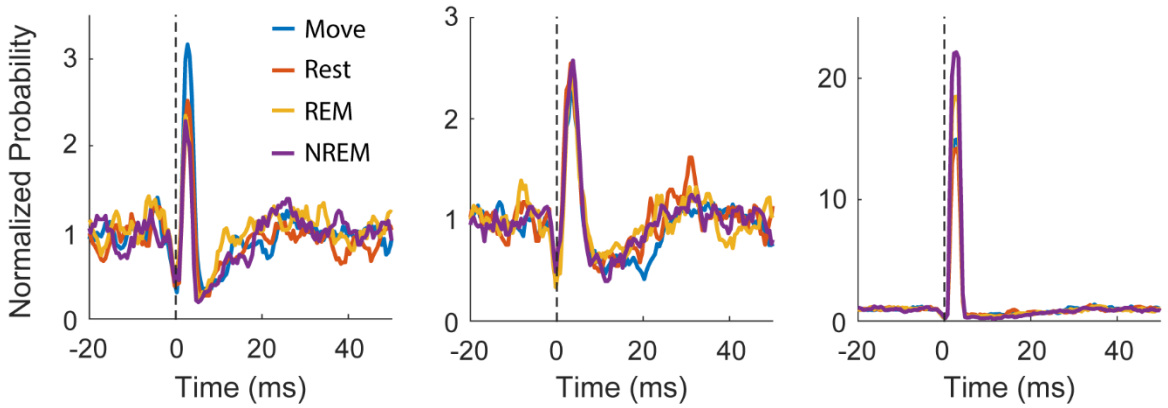

Figure ii.1 Stimulus responses during different behavioral states

Examples of responses during different behavioral states showing increases during Move (left), no changes between states (middle), and increases during NREM (right). The change in responses is inconsistent between individual spikes.

Supplementary materials

Chapter 1.

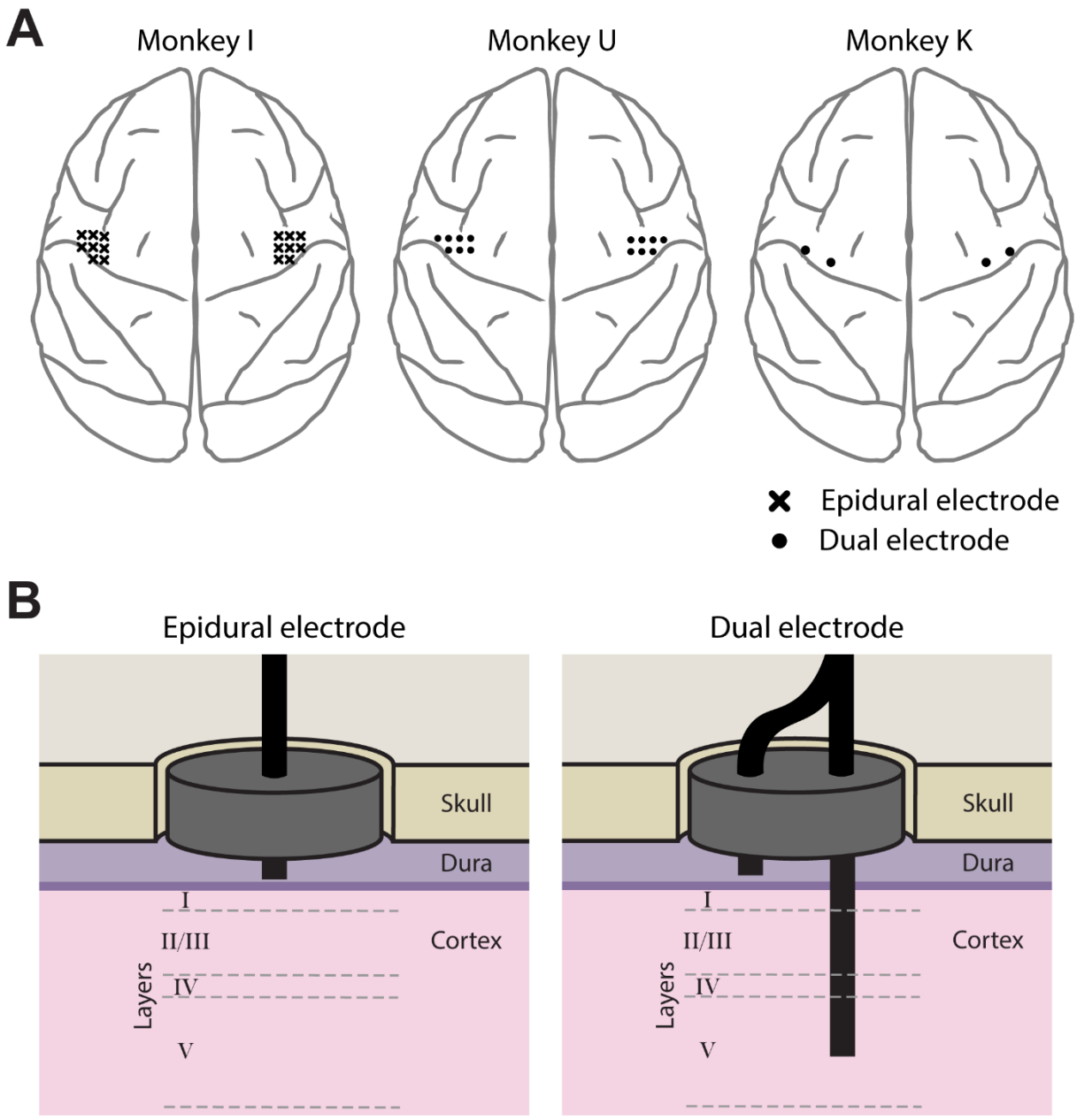

Supplementary Figure 1.1 Implant diagrams

(A) Locations of electrodes for each monkey. Electrode locations reflect positions inferred by stereotactic coordinates (3mm spaced grids) at time of implant. **(B)** Diagrams of the custom-made epidural and dual electrodes.

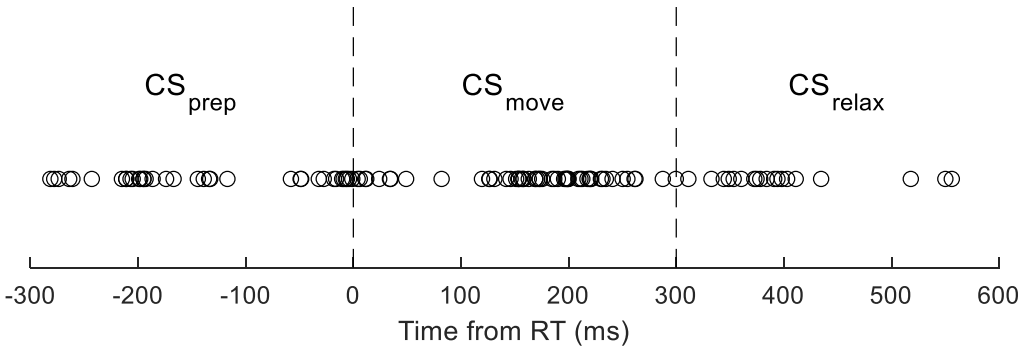

Supplementary Figure 1.2 Distribution of CS timings

Timing of CS relative to RT for each experiment. The total experiment counts are: 38 in CS_{prep}, 55 in CS_{move}, and 23 in CS_{relax}.

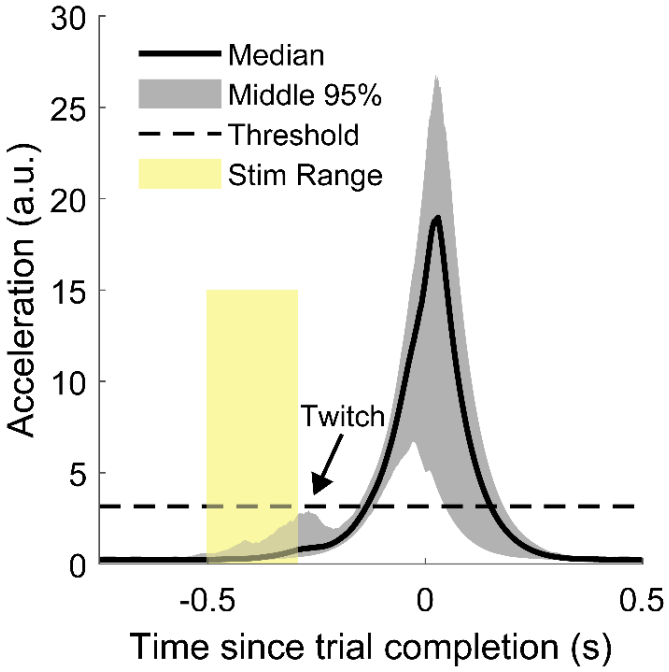

Supplementary Figure 1.3 Stimulus induced movement and calculating RT

Example of stimulus induced movement ("Twitch"), median accelerometer trace, and threshold for RT calculation. The threshold is 1/6 of the peak median acceleration as it was determined to the lowest possible threshold while not detecting the stimulus induced twitch as voluntary movement.

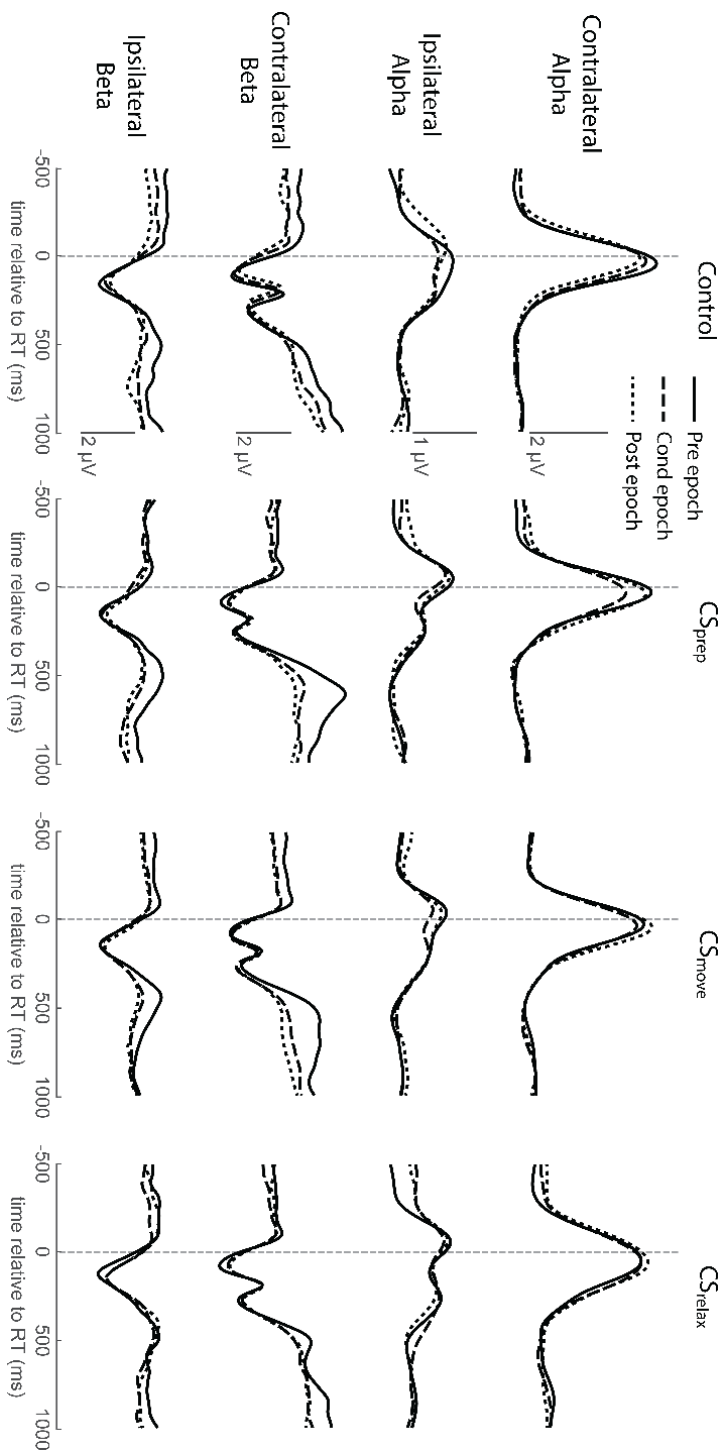

Supplementary Figure 1.4 Amplitude in Contralateral CS experiments

Instantaneous LFP band amplitude of the stimulated hemisphere for each epoch and stimulus timing during Contralateral CS experiments. Contralateral and ipsilateral refers to limb movement relative to the stimulated hemisphere.

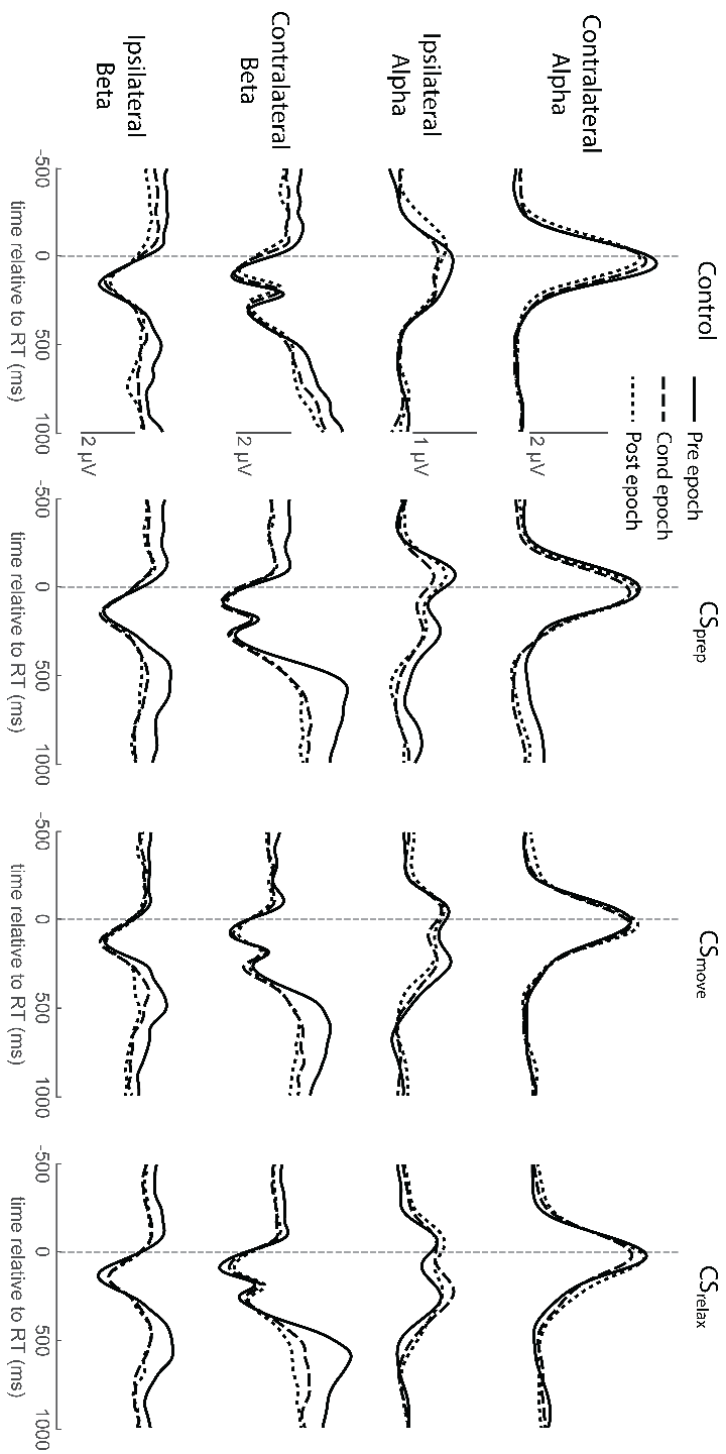

Supplementary Figure 1.5 Amplitude in Ipsilateral CS experiments

Instantaneous LFP band amplitude of the stimulated hemisphere for each epoch and stimulus timing during Ipsilateral CS experiments. Contralateral and ipsilateral refers to limb movement relative to the stimulated hemisphere.

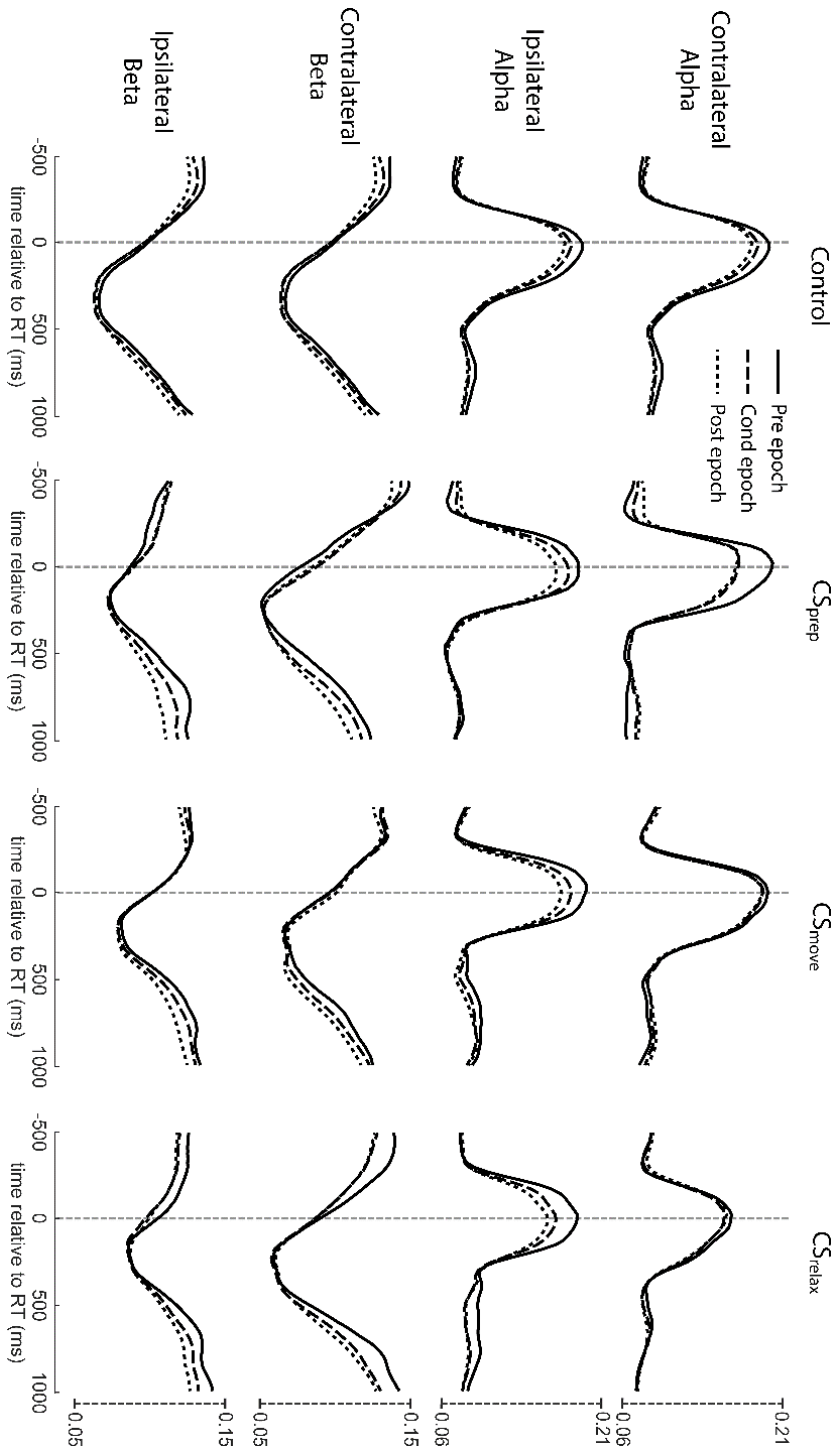

Supplementary Figure 1.6 Coherence in Contralateral CS experiments

Interhemispheric coherence for each epoch and stimulus timing during Contralateral CS experiments. Contralateral and ipsilateral refers to limb movement relative to the stimulated hemisphere.

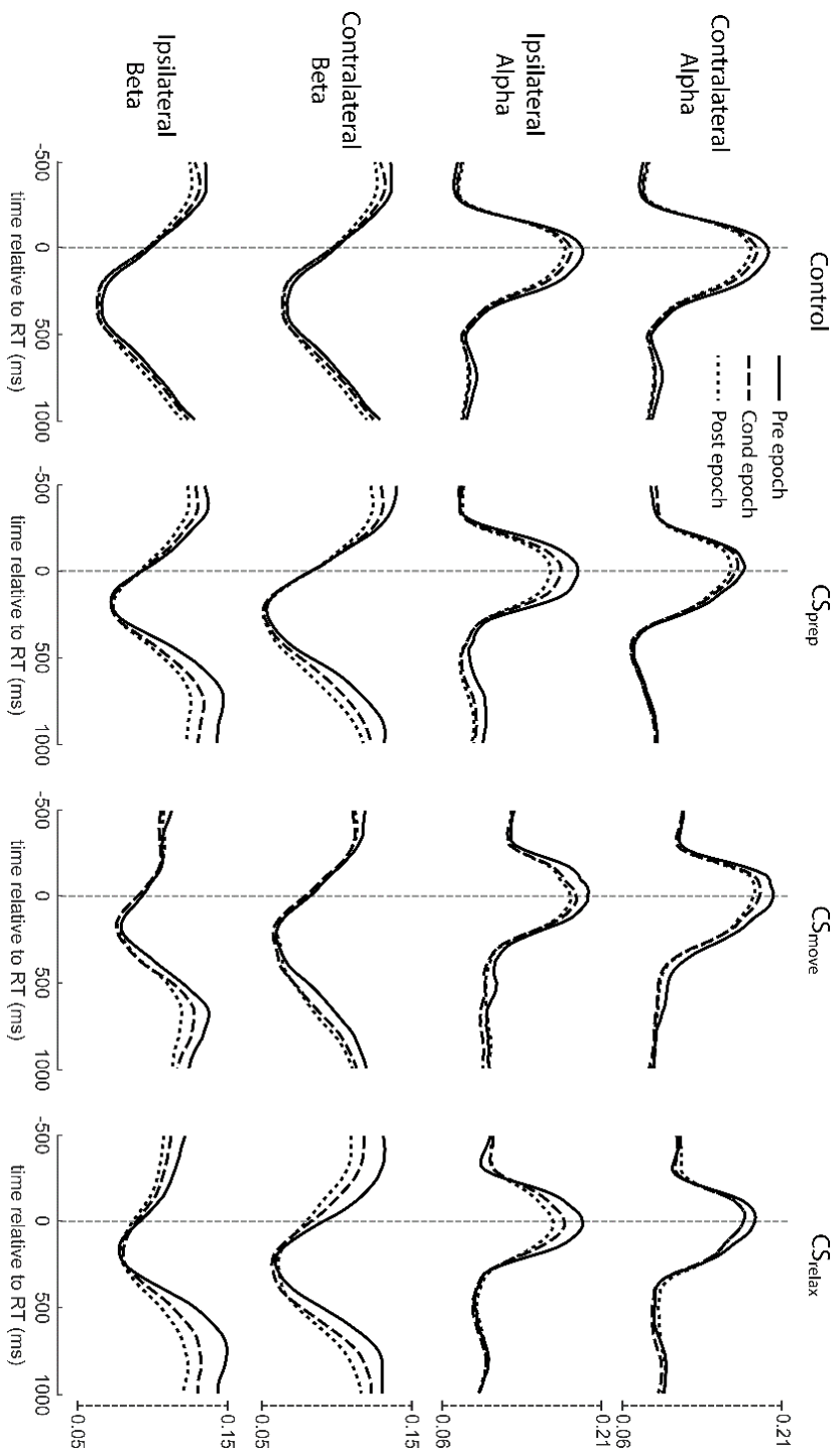

Supplementary Figure 1.7 Coherence in Ipsilateral CS experiments

Interhemispheric coherence for each epoch and stimulus timing during Ipsilateral CS experiments. Contralateral and ipsilateral refers to limb movement relative to the stimulated hemisphere.

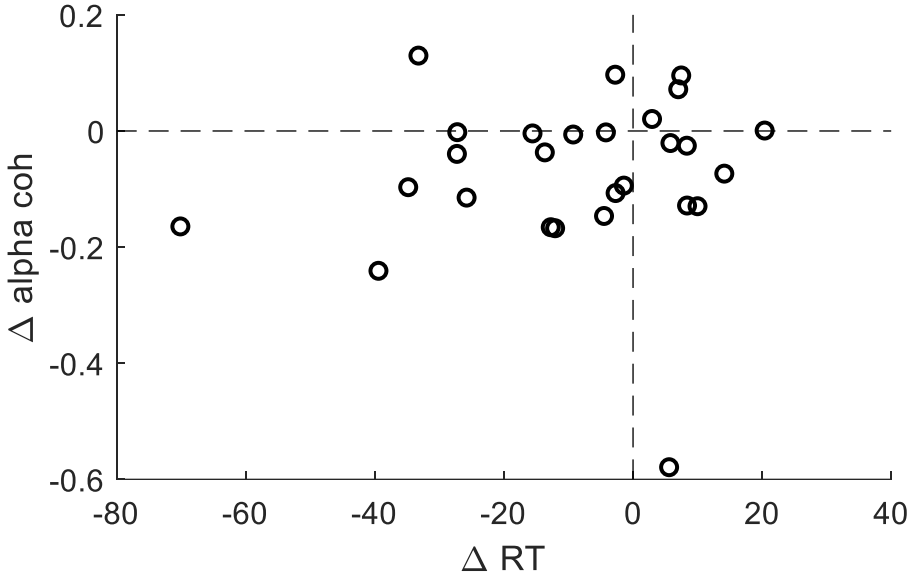

Supplementary Figure 1.8 Changes in alpha coherence compared to changes in RT

Scatter plot showing the changes in alpha coherence plotted against the changes in RT for all experiment conditions and trial types with statistically significant changes in alpha. There is no statistically significant correlation between the two measures.

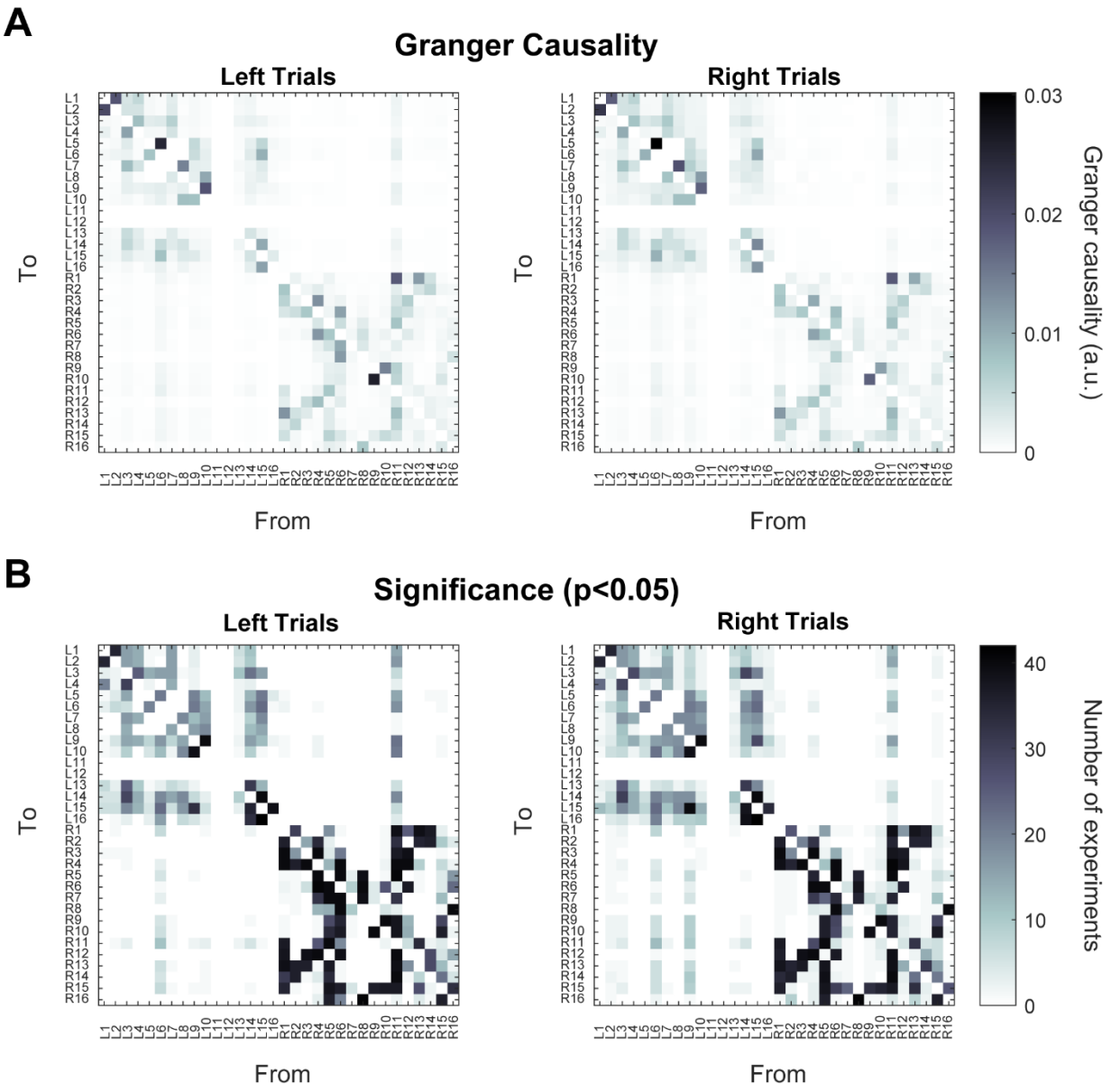

Supplementary Figure 1.9 Granger causality

Average pairwise Granger causality between all 32 channels of Monkey U during left and right trials of the Pre epoch and their significance across all conditioning experiments. 16 channels were in the left hemisphere (L channels) and 16 in the right hemisphere (R channels). Note the high causality and significance within hemispheres but sparse directionality between hemispheres.

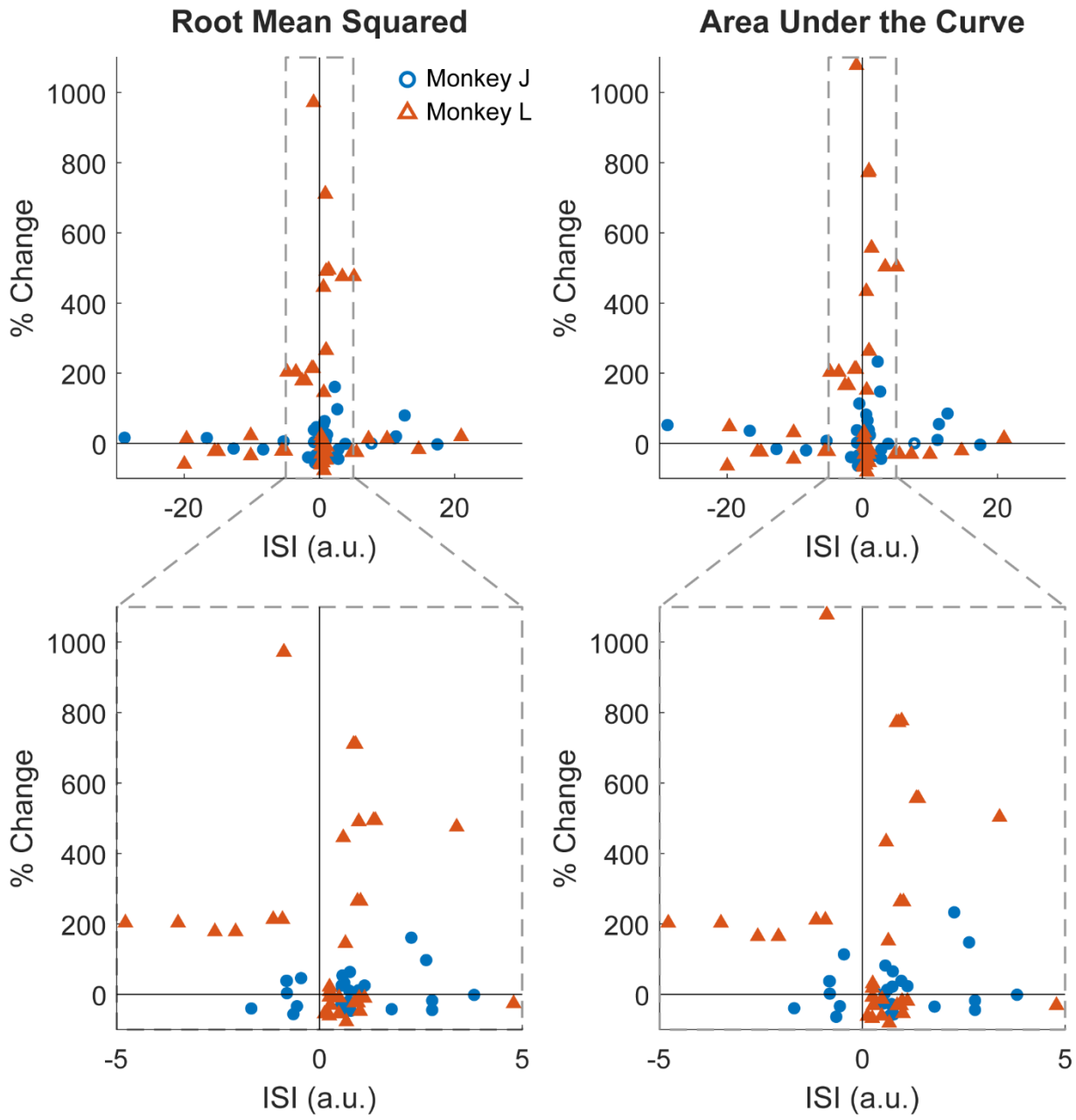

Supplementary Figure 4.1 Different CCEP measures

Changes in CCEPs before and after conditioning calculated using root-mean squared (left) or area under the curve (right) with respect to normalized ISIs.

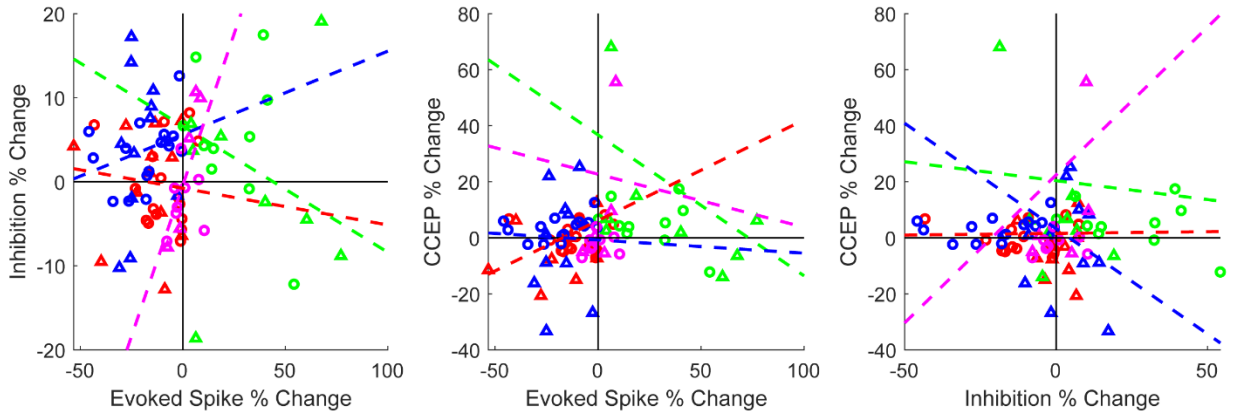

Supplementary Figure 4.2 Correlations for each region of ISI

Scatter plots and best fit lines of each ISI region for every pair of measures. There is no statistically significant correlation between any measure in any region.

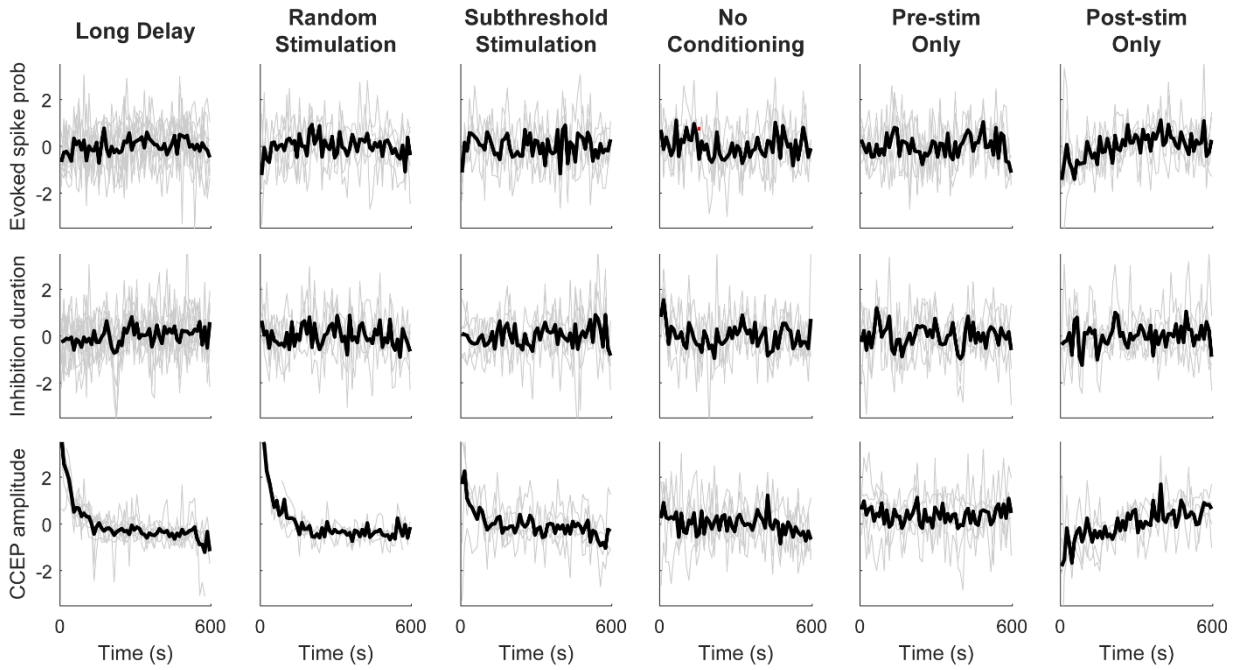

Supplementary Figure 4.3 Controls over time

Individual session traces (grey) and averages (black) of z-scored evoked spike probability (top), inhibition duration (middle), and CCEP amplitude (bottom) during the 10-minute post-test epoch for each control condition. There is no statistical significance between the first 10 seconds to the rest of the epoch in any measure (repeated measures ANOVA, $p<0.05$).

Bibliography

Abbott, L. F., & Regehr, W. G. (2004). Synaptic computation. *Nature*, *431*(October), 796–803.

Adesnik, H., & Scanziani, M. (2010). Lateral competition for cortical space by layer-specific horizontal circuits. *Nature*, *464*(7292), 1155–1160. https://doi.org/10.1038/nature08935

Akkad, H., Dupont-Hadwen, J., Frese, A., Tetkovic, I., Barrett, L., Bestmann, S., & Stagg, C. J. (2021). Increasing motor skill acquisition by driving theta-gamma coupling. *ELife*, 1–15. https://doi.org/10.7554/eLife.67355

Andino-Pavlovsky, V., Souza, A. C., Scheffer-Teixeira, R., Tort, A. B. L., Etchenique, R., & Ribeiro, S. (2017). Dopamine modulates delta-gamma phase-amplitude coupling in the prefrontal cortex of behaving rats. *Frontiers in Neural Circuits*, *11*(May). https://doi.org/10.3389/fncir.2017.00029

Arbune, A. A., Popa, I., Mindruta, I., Beniczky, S., Donos, C., Daneasa, A., Mălîia, M. D., Băjenaru, O. A., Ciurea, J., & Barborica, A. (2020). Sleep modulates effective connectivity: A study using intracranial stimulation and recording. *Clinical Neurophysiology*, *131*(2), 529–541. https://doi.org/10.1016/j.clinph.2019.09.010

Aserinsky, E., & Kleitman, N. (1953). Regularly Occurring Periods of Eye Motility, and Concomitant Phenomena, during Sleep. *Science*, *118*(3062), 273–274.

Axmacher, N., Henseler, M. M., Jensen, O., Weinreich, I., Elger, C. E., & Fell, J. (2010). Cross-frequency coupling supports multi-item working memory in the human hippocampus. *Proceedings of the National Academy of Sciences of the United States of America*, *107*(7), 3228–3233. https://doi.org/10.1073/pnas.0911531107

Baker, S. N., Kilner, J. M., Pinches, E. M., & Lemon, R. N. (1999). The role of synchrony and oscillations in the motor output. *Exp Brain Res*, 109–117.

Bardouille, T., & Bailey, L. (2019). Evidence for age-related changes in sensorimotor neuromagnetic responses during cued button pressing in a large open-access dataset. *NeuroImage*, *193*(March), 25–34. https://doi.org/10.1016/j.neuroimage.2019.02.065

Barnett, L., & Seth, A. K. (2014). The MVGC multivariate Granger causality toolbox: A new approach to Granger-causal inference. *Journal of Neuroscience Methods*, *223*, 50–68. https://doi.org/10.1016/j.jneumeth.2013.10.018

Beaulé, V., Tremblay, S., & Théoret, H. (2012). Interhemispheric control of unilateral movement. *Neural Plasticity*, *2012*(Cc). https://doi.org/10.1155/2012/627816

Bellesi, M., Riedner, B. A., Garcia-Molina, G. N., Cirelli, C., & Tononi, G. (2014). Enhancement of sleep slow waves: Underlying mechanisms and practical consequences. *Frontiers in Systems Neuroscience*, *8*(October), 1–17. https://doi.org/10.3389/fnsys.2014.00208

Berman, N. J., Douglas, R. J., Martin, K. A. C., & Whitteridge, D. (1991). Mechanisms of inhibition in cat visual cortex. *Journal of Physiology*, *440*, 697–722.

Bettler, B., Kaupmann, K., Mosbacher, J., & Gassmann, M. (2004). Molecular structure and physiological functions of GABAB receptors. *Physiological Reviews*, *84*(3), 835–867.

https://doi.org/10.1152/physrev.00036.2003

Bi, G. Q., & Poo, M. M. (1998). Synaptic modifications in cultured hippocampal neurons: dependence on spike timing, synaptic strength, and postsynaptic cell type. *The Journal of Neuroscience : The Official Journal of the Society for Neuroscience*, *18*(24), 10464–10472. https://doi.org/10.1038/25665

Blackman, A. V., Abrahamsson, T., Costa, R. P., Lalanne, T., & Sjöström, P. J. (2013). Target-cell-specific short-term plasticity in local circuits. *Frontiers in Synaptic Neuroscience*, *5*(DEC), 1–13. https://doi.org/10.3389/fnsyn.2013.00011

Boddington, L. J., & Reynolds, J. N. J. (2017). Targeting interhemispheric inhibition with neuromodulation to enhance stroke rehabilitation. *Brain Stimulation*, *10*(2), 214–222. https://doi.org/10.1016/j.brs.2017.01.006

Borchers, S., Himmelbach, M., Logothetis, N., & Karnath, H. (2012). Direct electrical stimulation of human cortex — the gold standard for mapping brain functions? *Nature Reviews Neuroscience*, *13*(January), 63–70.

Boudkkazi, S., Carlier, E., Ankri, N., Caillard, O., Giraud, P., Fronzaroli-Molinieres, L., & Debanne, D. (2007). Release-dependent bariations in synaptic latency: A putative code for short- and long-term synaptic dynamics. *Neuron*, *56*(6), 1048–1060. https://doi.org/10.1016/j.neuron.2007.10.037

Boyce, R., Glasgow, S. D., Williams, S., & Adamantidis, A. (2016). Sleep research: Causal evidence for the role of REM sleep theta rhythm in contextual memory consolidation. *Science*, *352*(6287), 812–816. https://doi.org/10.1126/science.aad5252

Boyer, A., Duffau, H., Vincent, M., Ramdani, S., Mandonnet, E., Guiraud, D., & Bonnetblanc, F. (2018). Electrophysiological Activity Evoked by Direct Electrical Stimulation of the Human Brain: Interest of the P0 Component. *Proceedings of the Annual International Conference of the IEEE Engineering in Medicine and Biology Society, EMBS*, *2018-July*, 2210–2213. https://doi.org/10.1109/EMBC.2018.8512733

Brown, R. E., Basheer, R., McKenna, J. T., Strecker, R. E., & McCarley, R. W. (2012). Control of sleep and wakefulness. *Physiological Reviews*, *92*(3), 1087–1187. https://doi.org/10.1152/physrev.00032.2011

Brunel, N., & Wang, X. J. (2003). What determines the frequency of fast network oscillations with irregular neural discharges? I. Synaptic dynamics and excitation-inhibition balance. *Journal of Neurophysiology*, *90*(1), 415–430. https://doi.org/10.1152/jn.01095.2002

Bütefisch, C. M., Khurana, V., Kopylev, L., & Cohen, L. G. (2004). Enhancing Encoding of a Motor Memory in the Primary Motor Cortex by Cortical Stimulation. *Journal of Neurophysiology*, *91*(5), 2110–2116. https://doi.org/10.1152/jn.01038.2003

Butovas, S., Hormuzdi, S. G., Monyer, H., & Schwarz, C. (2006). Effects of electrically coupled inhibitory networks on local neuronal responses to intracortical microstimulation. *Journal of Neurophysiology*, *96*(3), 1227–1236. https://doi.org/10.1152/jn.01170.2005

Butovas, S., & Schwarz, C. (2003). Spatiotemporal effects of microstimulation in rat neocortex: A parametric study using multielectrode recordings. *Journal of Neurophysiology*, *90*(5), 3024–3039. https://doi.org/10.1152/jn.00245.2003

Buzsáki, G., Anastassiou, C. A., & Koch, C. (2012). The origin of extracellular fields and currents-EEG, ECoG, LFP and spikes. *Nature Reviews Neuroscience*, *13*(6), 407–420. https://doi.org/10.1038/nrn3241

Buzsáki, G., & Draguhn, A. (2004). Neuronal oscillations in cortical networks. *Science*, *304*(5679), 1926–1929. https://doi.org/10.1126/science.1099745

Buzsáki, G., & Moser, E. I. (2013). Memory, navigation and theta rhythm in the hippocampal-entorhinal system. *Nature Neuroscience*, *16*(2), 130–138. https://doi.org/10.1038/nn.3304

Buzsáki, G., & Schomburg, E. W. (2015). What does gamma coherence tell us about inter-regional neural communication? *Nature Neuroscience*, *18*(4), 484–489. https://doi.org/10.1038/nn.3952

Buzsáki, G., & Wang, X.-J. (2012). Mechanisms of Gamma Oscillations. *Annual Review of Neuroscience*, *6*(9), 2166–2171. https://doi.org/10.1021/nl061786n.Core-Shell

Caldwell, D. J., Cronin, J. A., Wu, J., Weaver, K. E., Ko, A. L., Rao, R. P. N., & Ojemann, J. G. (2019). Direct stimulation of somatosensory cortex results in slower reaction times compared to peripheral touch in humans. *Scientific Reports*, *9*(1), 1–11. https://doi.org/10.1038/s41598-019-38619-2

Cannon, J., Mccarthy, M. M., Lee, S., Lee, J., Börgers, C., Whittington, M. A., & Kopell, N. (2014). Neurosystems: Brain rhythms and cognitive processing. *European Journal of Neuroscience*, *39*(5), 705–719. https://doi.org/10.1111/ejn.12453

Canolty, R. T., Edwards, E., Dalal, S. S., Soltani, M., Nagarajan, S. S., Kirsch, H. E., Berger, M. S., Barbare, N. M., & Knight, R. T. (2006). High gamma power is phase-locked to theta oscillations in human neocortex. *Science*, *313*(5793), 1626–1628. https://doi.org/10.1126/science.1128115

Canolty, R. T., Ganguly, K., & Carmena, J. M. (2012). Task-Dependent Changes in Cross-Level Coupling between Single Neurons and Oscillatory Activity in Multiscale Networks. *PLoS Computational Biology*, *8*(12). https://doi.org/10.1371/journal.pcbi.1002809

Canolty, R. T., & Knight, R. T. (2010). The functional role of cross-frequency coupling. *Trends in Cognitive Sciences*, *14*(11), 506–515. https://doi.org/10.1016/j.tics.2010.09.001

Cantero, J. L., Atienza, M., Stickgold, R., Kahana, M. J., Madsen, J. R., & Kocsis, B. (2003). Sleep-Dependent θ Oscillations in the Human Hippocampus and Neocortex. *Journal of Neuroscience*, *23*(34), 10897–10903. https://doi.org/10.1523/jneurosci.23-34-10897.2003

Cárdenas-Morales, L., Nowak, D. A., Kammer, T., Wolf, R. C., & Schönfeldt-Lecuona, C. (2010). Mechanisms and applications of theta-burst rTMS on the human motor cortex. *Brain Topography*, *22*(4), 294–306. https://doi.org/10.1007/s10548-009-0084-7

Cardoso, S. de O., Gribova, A., Donchin, O., Bergman, H., & Vaadia, E. (2001). Neural interactions between motor cortical hemispheres during bimanual and unimanual arm movements. *European Journal of Neuroscience*, *14*(11), 1881–1896. https://doi.org/10.1046/j.0953-816X.2001.01801.x

Chan, A. H. S., & Ng, A. W. Y. (2012). Finger response times to visual, auditory and tactile modality stimuli. *Lecture Notes in Engineering and Computer Science*, *2196*, 1449–1454.

Chen, R. (2004). Interactions between inhibitory and excitatory circuits in the human motor cortex. *Experimental Brain Research*, *154*(1), 1–10. https://doi.org/10.1007/s00221-003-1684-1

Chen, R., Yung, D., & Li, J. Y. (2003). Organization of ipsilateral excitatory and inhibitory pathways in the human motor cortex. *Journal of Neurophysiology*, *89*(3), 1256–1264. https://doi.org/10.1152/jn.00950.2002

Cheyne, D. O. (2013). MEG studies of sensorimotor rhythms: A review. *Experimental Neurology*, *245*, 27–39. https://doi.org/10.1016/j.expneurol.2012.08.030

Cincotta, M., & Ziemann, U. (2008). Neurophysiology of unimanual motor control and mirror movements. *Clinical Neurophysiology*, *119*(4), 744–762. https://doi.org/10.1016/j.clinph.2007.11.047

Citri, A., & Malenka, R. C. (2008). Synaptic plasticity: Multiple forms, functions, and mechanisms. *Neuropsychopharmacology*, *33*(1), 18–41. https://doi.org/10.1038/sj.npp.1301559

Clemens, Z., Weiss, B., Szucs, A., Eross, L., Rásonyi, G., & Halász, P. (2009). Phase coupling between rhythmic slow activity and gamma characterizes mesiotemporal rapid-eye-movement sleep in humans. *Neuroscience*, *163*(1), 388–396. https://doi.org/10.1016/j.neuroscience.2009.06.044

Cohen, M. R., & Kohn, A. (2011). Measuring and interpreting neuronal correlations. *Nature Neuroscience*, *14*(7), 811–819. https://doi.org/10.1038/nn.2842

Cohen, M. X., Elger, C. E., & Fell, J. (2009). Oscillatory activity and phase-amplitude coupling in the human medial frontal cortex during decision making. *Journal of Cognitive Neuroscience*, *21*(2), 390–402. https://doi.org/10.1162/jocn.2008.21020

Colgin, L. L. (2016). Rhythms of the hippocampal network. *Nature Reviews Neuroscience*, *17*(4), 239–249. https://doi.org/10.1038/nrn.2016.21

Connors, B. W., & Gutnick, M. J. (1990). Intrinsic firing patterns of diverse neocortical neurons. *Trends in Neurosciences*, *13*(3), 99–104.

Connors, B. W., Malenka, R. C., & Silva, L. R. (1988). Two inhibitory postsynaptic potentials, and GABAA and GABAB receptor-mediated responses in neocortex of rat and cat. *The Journal of Physiology*, *406*(1), 443–468. https://doi.org/10.1113/jphysiol.1988.sp017390

Cruikshank, S. J., Lewis, T. J., & Connors, B. W. (2007). Synaptic basis for intense thalamocortical activation of feedforward inhibitory cells in neocortex. *Nature Neuroscience*, *10*(4), 462–468. https://doi.org/10.1038/nn1861

Dadarlat, M. C., Sun, Y., & Stryker, M. P. (2019). Widespread activation of awake mouse cortex by electrical stimulation. *International IEEE/EMBS Conference on Neural Engineering, NER*, *2019-March*, 1113–1117. https://doi.org/10.1109/NER.2019.8716956

Daskalakis, Z. J., Christensen, B. K., Fitzgerald, P. B., Roshan, L., & Chen, R. (2002). The mechanisms of interhemispheric inhibition in the human motor cortex. *Journal of Physiology*. https://doi.org/10.1113/jphysiol.2002.017673

Di Lazzaro, V., Oliviero, A., Profice, P., Insola, A., Mazzone, P., Tonali, P., & Rothwell, J. C.

(1999). Direct demonstration of interhemispheric inhibition of the human motor cortex produced by transcranial magnetic stimulation. *Exp Brain Res*, *124*(4), 520–524. https://doi.org/10.1007/s002210050648

Dijk, D. J., Beersma, D. G. M., & Daan, S. (1987). EEG Power Density during Nap Sleep: Reflection of an Hourglass Measuring the Duration of Prior Wakefulness. *Journal of Biological Rhythms*, *2*(3), 207–219. https://doi.org/10.1177/074873048700200304

Dionisio, S., Mayoglou, L., Cho, S. M., Prime, D., Flanigan, P. M., Lega, B., Mosher, J., Leahy, R., Gonzalez-Martinez, J., & Nair, D. (2019). Connectivity of the human insula: A cortico-cortical evoked potential (CCEP) study. *Cortex*, *120*, 419–442. https://doi.org/10.1016/j.cortex.2019.05.019

Donchin, O., Gribova, A., Steinberg, O., Bergman, H., & Vaadia, E. (1998). Primary motor cortex is involved in bimanual coordination. *Nature*, *395*(6699), 274–278. https://doi.org/10.1038/26220

Donner, T. H., Siegel, M., Fries, P., & Engel, A. K. (2009). Buildup of Choice-Predictive Activity in Human Motor Cortex during Perceptual Decision Making. *Current Biology*, *19*(18), 1581–1585. https://doi.org/10.1016/j.cub.2009.07.066

Duque, J., Murase, N., Celnik, P., Hummel, F., Harris-Love, M., Mazzocchio, R., Olivier, E., & Cohen, L. G. (2007). Intermanual differences in movement-related interhemispheric inhibition. *Journal of Cognitive Neuroscience*. https://doi.org/10.1162/jocn.2007.19.2.204

Edwardson, M. A., Avery, D. H., & Fetz, E. E. (2015). Volitional muscle activity paired with transcranial magnetic stimulation increases corticospinal excitability. *Frontiers in Neuroscience*, *8*(DEC), 1–11. https://doi.org/10.3389/fnins.2014.00442

Enatsu, R., Kubota, Y., Kakisaka, Y., Bulacio, J., Piao, Z., O'Connor, T., Horning, K., Mosher, J., Burgess, R. C., Bingaman, W., & Nair, D. R. (2013). Reorganization of posterior language area in temporal lobe epilepsy: A cortico-cortical evoked potential study. *Epilepsy Research*, *103*(1), 73–82. https://doi.org/10.1016/j.eplepsyres.2012.07.008

Engel, A. K., & Fries, P. (2010). Beta-band oscillations-signalling the status quo? *Current Opinion in Neurobiology*, *20*(2), 156–165. https://doi.org/10.1016/j.conb.2010.02.015

Engel, A. K., Fries, P., & Singer, W. (2001). Dynamic Predictions: Oscillations and Synchrony in Top-Down Processing. *Nature Reviews Neuroscience*, *2*(October), 704–716.

Engelhard, B., Ozeri, N., Israel, Z., Bergman, H., & Vaadia, E. (2013). Inducing Gamma Oscillations and Precise Spike Synchrony by Operant Conditioning via Brain-Machine Interface. *Neuron*, *77*(2), 361–375. https://doi.org/10.1016/j.neuron.2012.11.015

English, D. F., McKenzie, S., Evans, T., Kim, K., Yoon, E., & Buzsáki, G. (2017). Pyramidal cell-interneuron circuit architecture and dynamics in hippocampal networks. *Neuron*, *96*(2), 505-520.e7. https://doi.org/10.1016/j.neuron.2017.09.033

Ermentrout, G. B., & Kopell, N. (1998). Fine structure of neural spiking and synchronization in the presence of conduction delays. *Proceedings of the National Academy of Sciences of the United States of America*, *95*(3), 1259–1264. https://doi.org/10.1073/pnas.95.3.1259

Feldman, D. E. (2012). The spike timing dependence of plasticity. *Neuron*, *75*(4), 556–571. https://doi.org/10.1016/j.neuron.2012.08.001.The

Ferbert, A., Priori, A., Rothwell, J. C., Day, B. L., Colebatch, J. G., & Marsden, C. D. (1992). Interhemispheric inhibition of the human motor cortex. *The Journal of Physiology*, *453*(1), 525–546. https://doi.org/10.1113/jphysiol.1992.sp019243

Fernandez, L. M. J., & Lüthi, A. (2020). Sleep spindles: Mechanisms and functions. *Physiological Reviews*, *100*(2), 805–868. https://doi.org/10.1152/physrev.00042.2018

Flesher, S. N., Collinger, J. L., Foldes, S. T., Weiss, J. M., Downey, J. E., Tyler-Kabara, E. C., Bensmaia, S. J., Schwartz, A. B., Boninger, M. L., & Gaunt, R. A. (2016). Intracortical microstimulation of human somatosensory cortex. *Science Translational Medicine*, *8*(361), 1–11. https://doi.org/10.1126/scitranslmed.aaf8083

Fries, P., Nikolić, D., & Singer, W. (2007). The gamma cycle. *Trends in Neurosciences*, *30*(7), 309–316. https://doi.org/10.1016/j.tins.2007.05.005

Fritsch, G., & Hitzig, E. (1870). Electric excitability of the cerebrum (Über die elektrische Erregbarkeit des Grosshirns). *Epilepsy and Behavior*, *15*(2), 123–130. https://doi.org/10.1016/j.yebeh.2009.03.001

Fry, A., Mullinger, K. J., O'Neill, G. C., Barratt, E. L., Morris, P. G., Bauer, M., Folland, J. P., & Brookes, M. J. (2016). Modulation of post-movement beta rebound by contraction force and rate of force development. *Human Brain Mapping*, *37*(7), 2493–2511. https://doi.org/10.1002/hbm.23189

Geisler, C., Brunel, N., & Wang, X. J. (2005). Contributions of intrinsic membrane dynamics to fast network oscillations with irregular neuronal discharges. *Journal of Neurophysiology*, *94*(6), 4344–4361. https://doi.org/10.1152/jn.00510.2004

Gerla, V., Kremen, V., Macas, M., Dudysova, D., Mladek, A., Sos, P., & Lhotska, L. (2019). Iterative expert-in-the-loop classification of sleep PSG recordings using a hierarchical clustering. *Journal of Neuroscience Methods*, *317*(February), 61–70. https://doi.org/10.1016/j.jneumeth.2019.01.013

Gilio, F., Rizzo, V., Siebner, H. R., & Rothwell, J. C. (2003). Effects on the right motor hand-area excitability produced by low-frequency rTMS over human contralateral homologous cortex. *Journal of Physiology*, *551*(2), 563–573. https://doi.org/10.1113/jphysiol.2003.044313

Giovannelli, F., Borgheresi, A., Balestrieri, F., Zaccara, G., Viggiano, M. P., Cincotta, M., & Ziemann, U. (2009). Modulation of interhemispheric inhibition by volitional motor activity: an ipsilateral silent period study. *The Journal of Physiology*, *587*(Pt 22), 5393–5410. https://doi.org/10.1113/jphysiol.2009.175885

Godlove, J., O'Brien, E., & Batista, A. (2014). Comparing temporal aspects of visual, tactile, and microstimulation feedback for motor control. *J Neural Eng*, *11*(4). https://doi.org/10.1088/1741-2560/11/4/046025.Comparing

Goldring, S., Jerva, M. J., Holes, T. G., O'Leary, J. L., & Shields, J. R. (1961). Direct Response of Human Cerebral Cortex. *Arch Neurol*, *4*, 22–30.

Granger, C. J. W. (1969). Investigating Causal Relations by Econometric Models and Cross-spectral Methods. *Econometrica*, *37*(3), 424–438.

Griffin, D. M., Hudson, H. M., Belhaj-Saif, A., & Cheney, P. D. (2011). Hijacking cortical motor

output with repetitive microstimulation. *Journal of Neuroscience*, *31*(37), 13088–13096. https://doi.org/10.1523/JNEUROSCI.6322-10.2011

Gulati, T., Guo, L., Ramanathan, D. S., Bodepudi, A., Ganguly, K., Service, R., Francisco, S., Affairs, V., Francisco, S., Francisco, S., Francisco, S., Affairs, V., Francisco, S., & Francisco, S. (2017). Neural reactivations during sleep determine network credit assignment. *Nature Neuroscience*, *20*(9), 1277–1284. https://doi.org/10.1038/nn.4601.Neural

Güntekin, B., & Başar, E. (2016). Review of evoked and event-related delta responses in the human brain. *International Journal of Psychophysiology*, *103*, 43–52. https://doi.org/10.1016/j.ijpsycho.2015.02.001

Gustafsson, B., & Jankowska, E. (1976). Direct and indirect activation of nerve cells by electrical pulses applied extracellularly. *The Journal of Physiology*, *258*(1), 33–61. https://doi.org/10.1113/jphysiol.1976.sp011405

Haider, B. (2006). Neocortical network activity in vivo is generated through a dynamic balance of excitation and inhibition. *Journal of Neuroscience*, *26*(17), 4535–4545. https://doi.org/10.1523/jneurosci.5297-05.2006

Hamida, S. T. Ben, & Ahmed, B. (2013). Computer based sleep staging: Challenges for the future. *2013 7th IEEE GCC Conference and Exhibition, GCC 2013*, 280–285. https://doi.org/10.1109/IEEEGCC.2013.6705790

Hanajima, R., Ugawa, Y., Machii, K., Mochizuki, H., Terao, Y., Enomoto, H., Furubayashi, T., Shiio, Y., Uesugi, H., & Kanazawa, I. (2001). Interhemispheric facilitation of the hand motor area in humans. *Journal of Physiology*. https://doi.org/10.1111/j.1469-7793.2001.0849h.x

Hao, Y., Riehle, A., & Brochier, T. G. (2016). Mapping horizontal spread of activity in monkey motor cortex using single pulse microstimulation. *Frontiers in Neural Circuits*, *10*(December), 1–16. https://doi.org/10.3389/fncir.2016.00104

Harmony, T. (2013). The functional significance of delta oscillations in cognitive processing. *Frontiers in Integrative Neuroscience*, *7*(DEC), 1–10. https://doi.org/10.3389/fnint.2013.00083

Hartmann, K., Thomson, E. E., Zea, I., Yun, R., Mullen, P., Canarick, J., Huh, A., & Nicolelis, M. A. L. (2016). Embedding a panoramic representation of infrared light in the adult rat somatosensory cortex through a sensory neuroprosthesis. *Journal of Neuroscience*, *36*(8). https://doi.org/10.1523/JNEUROSCI.3285-15.2016

Hebb, D. O. (1949). *The Organization of Behavior*. Wiley.

Heinrichs-Graham, E., Kurz, M. J., Gehringer, J. E., & Wilson, T. W. (2017). The functional role of post-movement beta oscillations in motor termination. *Brain Structure and Function*, *222*(7), 3075–3086. https://doi.org/10.1007/s00429-017-1387-1

Helmstaedter, M., Staiger, J. F., Sakmann, B., & Feldmeyer, D. (2008). Efficient recruitment of layer 2/3 interneurons by layer 4 input in single columns of rat somatosensory cortex. *Journal of Neuroscience*, *28*(33), 8273–8284. https://doi.org/10.1523/JNEUROSCI.5701-07.2008

Herrmann, C. S., Fründ, I., & Lenz, D. (2010). Human gamma-band activity: A review on cognitive and behavioral correlates and network models. *Neuroscience and Biobehavioral Reviews*, *34*(7), 981–992. https://doi.org/10.1016/j.neubiorev.2009.09.001

Himanen, S. L., & Hasan, J. (2000). Limitations of Rechtschaffen and Kales. *Sleep Medicine Reviews*, *4*(2), 149–167. https://doi.org/10.1053/smrv.1999.0086

Histed, M. H., Bonin, V., & Reid, R. C. (2009). Direct activation of sparse, distributed populations of cortical neurons by electrical microstimulation. *Neuron*, *63*(4), 508–522. https://doi.org/10.1016/j.neuron.2009.07.016

Hsieh, K. C., Robinson, E. L., & Fuller, C. A. (2008). Sleep architecture in unrestrained rhesus monkeys (Macaca mulatta) synchronized to 24-hour light-dark cycles. *Sleep*, *31*(9), 1239–1250.

Huang, Y. Z., Edwards, M. J., Rounis, E., Bhatia, K. P., & Rothwell, J. C. (2005). Theta burst stimulation of the human motor cortex. *Neuron*, *45*(2), 201–206. https://doi.org/10.1016/j.neuron.2004.12.033

Huber, R., Ghilardi, M. F., Massimini, M., & Tononi, G. (2004). Local sleep and learning. *Nature*, *430*(6995), 78–81. https://doi.org/10.1038/nature02663

Hübers, A., Orekhov, Y., & Ziemann, U. (2008). Interhemispheric motor inhibition: Its role in controlling electromyographic mirror activity. *European Journal of Neuroscience*, *28*(2), 364–371. https://doi.org/10.1111/j.1460-9568.2008.06335.x

Hülsemann, M. J., Naumann, E., & Rasch, B. (2019). Quantification of phase-amplitude coupling in neuronal oscillations:comparison of phase-locking value, mean vector length, modulation index, and generalized-linear-modeling-cross-frequency-coupling. *Frontiers in Neuroscience*, *13*(JUN), 1–15. https://doi.org/10.3389/fnins.2019.00573

Hummel, F., Andres, F., Altenmüller, E., Dichgans, J., & Gerloff, C. (2002). Inhibitory control of acquired motor programmes in the human brain. *Brain*, *125*(2), 404–420. https://doi.org/10.1093/brain/awf030

Hussin, A. T., Boychuk, J. A., Brown, A. R., Pittman, Q. J., & Campbell Teskey, G. (2015). Intracortical microstimulation (ICMS) activates motor cortex layer 5 pyramidal neurons mainly transsynaptically. *Brain Stimulation*, *8*(4), 742–750. https://doi.org/10.1016/j.brs.2015.03.003

Isaacson, J. S., & Scanziani, M. (2011). How inhibition shapes cortical activity. *Neuron*, *72*(2), 231–243. https://doi.org/10.1016/j.neuron.2011.09.027

Jackson, A., & Fetz, E. E. (2011). Interfacing with the computational brain. *IEEE Transactions on Neural Systems and Rehabilitation Engineering*. https://doi.org/10.1109/TNSRE.2011.2158586.Interfacing

Jackson, A., Mavoori, J., & Fetz, E. E. (2006). Long-term motor cortex plasticity induced by an electronic neural implant. *Nature*, *444*(7115), 56–60. https://doi.org/10.1038/nature05226

Jacobs, J. (2014). Hippocampal theta oscillations are slower in humans than in rodents: Implications for models of spatial navigation and memory. *Philosophical Transactions of the Royal Society B: Biological Sciences*, *369*(1635). https://doi.org/10.1098/rstb.2013.0304

Jensen, O., & Colgin, L. L. (2007). Cross-frequency coupling between neuronal oscillations. *Trends in Cognitive Sciences*, *11*(7), 267–269. https://doi.org/10.1016/j.tics.2007.05.003

Jensen, O., & Mazaheri, A. (2010). Shaping functional architecture by oscillatory alpha activity: Gating by inhibition. *Frontiers in Human Neuroscience*, *4*(November), 1–8. https://doi.org/10.3389/fnhum.2010.00186

Kara, P., Pezaris, J. S., Yurgenson, S., & Reid, R. C. (2002). *The spatial receptive field of thalamic inputs to single cortical simple cells revealed by the interaction of visual and electrical stimulation*. *99*(25), 1–6.

Keller, C. J., Honey, C. J., Mégevand, P., Entz, L., Ulbert, I., & Mehta, A. D. (2014). Mapping human brain networks with cortico-ortical evoked potentials. *Philosophical Transactions of the Royal Society B: Biological Sciences*, *369*(1653). https://doi.org/10.1098/rstb.2013.0528

Khalighi, S., Sousa, T., Pires, G., & Nunes, U. (2013). Automatic sleep staging: A computer assisted approach for optimal combination of features and polysomnographic channels. *Expert Systems with Applications*, *40*(17), 7046–7059. https://doi.org/10.1016/j.eswa.2013.06.023

Khanna, P., & Carmena, J. M. (2017). Beta band oscillations in motor cortex reflect neural population signals that delay movement onset. *ELife*, *6*, 1–31. https://doi.org/10.7554/eLife.24573

Kim, E. Y., Mahmoud, G. S., & Grover, L. M. (2005). REM sleep deprivation inhibits LTP in vivo in area CA1 of rat hippocampus. *Neuroscience Letters*, *388*(3), 163–167. https://doi.org/10.1016/j.neulet.2005.06.057

Kim, S. J., Manyam, S. C., Warren, D. J., & Normann, R. A. (2006). Electrophysiological mapping of cat primary auditory cortex with multielectrode arrays. *Annals of Biomedical Engineering*, *34*(2), 300–309. https://doi.org/10.1007/s10439-005-9037-9

Klimesch, W., Sauseng, P., & Hanslmayr, S. (2007). EEG alpha oscillations: The inhibition-timing hypothesis. *Brain Research Reviews*, *53*(1), 63–88. https://doi.org/10.1016/j.brainresrev.2006.06.003

Klink, P. C., Dagnino, B., Gariel-Mathis, M. A., & Roelfsema, P. R. (2017). Distinct feedforward and feedback effects of microstimulation in visual cortex reveal neural mechanisms of texture segregation. *Neuron*, *95*(1), 209-220.e3. https://doi.org/10.1016/j.neuron.2017.05.033

Kripke, D. F., Reite, M. L., Pegram, G. V., Stephens, L. M., & Lewis, O. F. (1968). Nocturnal sleep in rhesus monkeys. *Electroencephalography and Clinical Neurophysiology*, *24*(6), 581–586. https://doi.org/10.1016/0013-4694(68)90047-3

Kumar, S. S., Wülfing, J., Okujeni, S., Boedecker, J., Riedmiller, M., & Egert, U. (2016). Autonomous optimization of targeted stimulation of neuronal networks. *PLoS Computational Biology*, *12*(8), 1–22. https://doi.org/10.1371/journal.pcbi.1005054

Kuo, Y. L., Dubuc, T., Boufadel, D. F., & Fisher, B. E. (2017). Measuring ipsilateral silent period: Effects of muscle contraction levels and quantification methods. *Brain Research*, *1674*, 77–83. https://doi.org/10.1016/j.brainres.2017.08.015

Lachaux, J. P., Rodriguez, E., Martinerie, J., & Varela, F. J. (1999). Measuring phase synchrony

in brain signals. *Human Brain Mapping*, *8*(4), 194–208. https://doi.org/10.1002/(SICI)1097-0193(1999)8:4<194::AID-HBM4>3.0.CO;2-C

Lebedev, M. A., & Nicolelis, M. A. L. (2017). Brain-machine interfaces: From basic science to neuroprostheses and neurorehabilitation. *Physiological Reviews*, *97*(2), 767–837. https://doi.org/10.1152/physrev.00027.2016

Lesser, R. P., Lee, H. W., Webber, W. R. S., Prince, B., Crone, N. E., & Miglioretti, D. L. (2008). Short-term variations in response distribution to cortical stimulation. *Brain*, *131*(6), 1528–1539. https://doi.org/10.1093/brain/awn044

Leung, L. S. (1982). Nonlinear feedback model of neuronal populations in hippocampal CA1 region. *Journal of Neurophysiology*, *47*(5), 845–868. https://doi.org/10.1152/jn.1982.47.5.845

Lewis, G. N., & Perreault, E. J. (2007). Side of lesion influences interhemispheric inhibition in subjects with post-stroke hemiparesis. *Clinical Neurophysiology*. https://doi.org/10.1016/j.clinph.2007.08.027

Liang, W. K., Tseng, P., Yeh, J. R., Huang, N. E., & Juan, C. H. (2021). Frontoparietal Beta Amplitude Modulation and its Interareal Cross-frequency Coupling in Visual Working Memory. *Neuroscience*, *460*, 69–87. https://doi.org/10.1016/j.neuroscience.2021.02.013

Libey, T., & Fetz, E. E. (2017). Open-source, low cost, free-behavior monitoring, and reward system for neuroscience research in non-human primates. *Frontiers in Neuroscience*, *11*(MAY), 1–12. https://doi.org/10.3389/fnins.2017.00265

Liepert, J., Hamzei, F., & Weiller, C. (2000). Motor cortex disinhibition of the unaffected hemisphere after acute stroke. *Muscle and Nerve*, *23*(11), 1761–1763. https://doi.org/10.1002/1097-4598(200011)23:11<1761::AID-MUS14>3.0.CO;2-M

Lisman, J. E., & Jensen, O. (2013). The Theta-Gamma Neural Code. *Neuron*, *77*(6), 1002–1016. https://doi.org/10.1016/j.neuron.2013.03.007

Logothetis, N. K., Augath, M., Murayama, Y., Rauch, A., Sultan, F., Goense, J., Oeltermann, A., & Merkle, H. (2010). The effects of electrical microstimulation on cortical signal propagation. *Nature Neuroscience*, *13*(10), 1283–1291. https://doi.org/10.1038/nn.2631

Losonczy, A., Zhang, L., Shigemoto, R., Somogyi, P., & Nusser, Z. (2002). Cell type dependence and variability in the short-term plasticity of EPSCs in identified mouse hippocampal interneurones. *Journal of Physiology*, *542*(1), 193–210. https://doi.org/10.1113/jphysiol.2002.020024

Lucas, T. H., & Fetz, E. E. (2013). Myo-cortical crossed feedback reorganizes primate motor cortex output. *Journal of Neuroscience*, *33*(12), 5261–5274. https://doi.org/10.1523/JNEUROSCI.4683-12.2013

Malafeev, A., Laptev, D., Bauer, S., Omlin, X., Wierzbicka, A., Wichniak, A., Jernajczyk, W., Riener, R., Buhmann, J., & Achermann, P. (2018). Automatic human sleep stage scoring using deep neural networks. *Frontiers in Neuroscience*, *12*(NOV), 1–15. https://doi.org/10.3389/fnins.2018.00781

Markram, H., Gerstner, W., & Sjöström, P. J. (2011). A history of spike-timing-dependent plasticity. *Frontiers in Synaptic Neuroscience*, *3*(AUG), 1–24.

https://doi.org/10.3389/fnsyn.2011.00004

Markram, H., Lübke, J., Frotscher, M., & Sakmann, B. (1997). Regulation of synaptic efficacy by coincidence of postsynaptic APs and EPSPs. *Science*, *275*(5297), 213–215. https://doi.org/10.1126/science.275.5297.213

Markram, H., Wang, Y., & Tsodyks, M. (1998). Differential signaling via the same axon of neocortical pyramidal neurons. *Proceedings of the National Academy of Sciences of the United States of America*, *95*(9), 5323–5328. https://doi.org/10.1073/pnas.95.9.5323

Marshall, L., Helgadóttir, H., Mölle, M., & Born, J. (2006). Boosting slow oscillations during sleep potentiates memory. *Nature*, *444*(7119), 610–613. https://doi.org/10.1038/nature05278

Mascetti, G. G. (2016). Unihemispheric sleep and asymmetrical sleep: Behavioral, neurophysiological, and functional perspectives. *Nature and Science of Sleep*, *8*, 221–228. https://doi.org/10.2147/NSS.S71970

Matsumura, M., Chen, D., Sawaguchi, T., Kubota, K., & Fetz, E. E. (1996). Synaptic interactions between primate precentral cortex neurons revealed by spike-triggered averaging of intracellular membrane potentials in vivo. *Journal of Neuroscience*, *16*(23), 1–11.

McCormick, D. A., Connors, B. W., Lighthall, J. W., & Prince, D. A. (1985). Comparative electrophysiology of pyramidal and sparsely spiny stellate neurons of the neocortex. *Journal of Neurophysiology*, *54*(4), 782–806. https://doi.org/10.1152/jn.1985.54.4.782

McIntyre, C. C., & Grill, W. M. (2000). Selective microstimulation of central nervous system neurons. *Annals of Biomedical Engineering*, *28*(3), 219–233. https://doi.org/10.1114/1.262

McPherson, J. G., Miller, R. R., Perlmutter, S. I., & Poo, M. M. (2015). Targeted, activity-dependent spinal stimulation produces long-lasting motor recovery in chronic cervical spinal cord injury. *Proceedings of the National Academy of Sciences of the United States of America*, *112*(39), 12193–12198. https://doi.org/10.1073/pnas.1505383112

Michel, C. M., Murray, M. M., Lantz, G., Gonzalez, S., Spinelli, L., & Grave De Peralta, R. (2004). EEG source imaging. *Clinical Neurophysiology*, *115*(10), 2195–2222. https://doi.org/10.1016/j.clinph.2004.06.001

Michelson, N. J., Eles, J. R., Vazquez, A. L., Ludwig, K. A., & Kozai, T. D. Y. (2019). Calcium activation of cortical neurons by continuous electrical stimulation: Frequency dependence, temporal fidelity, and activation density. *Journal of Neuroscience Research*, *97*(5), 620–638. https://doi.org/10.1002/jnr.24370

Miller, K. D., Abbott, L. F., & Song, S. (2000). Competitive Hebbian learning through spike-timing-dependent synaptic plasticity. *Nature Neuroscience*, *3*, 919–926. http://neurosci.nature.com

Mitra, P., & Bokil, H. (2008). *Observed Brain Dynamics*. Oxford University Press.

Mitra, P., Bokil, H., Maniar, H., Loader, C., Mehta, S., Hill, D., Mitra, S., Andrews, P., Baptista, R., Gopinath, S., Nalatore, H., & Kaur, S. (2018). *chronux*. http://chronux.org/

Morishita, T., Uehara, K., & Funase, K. (2012). Changes in interhemispheric inhibition from active to resting primary motor cortex during a fine-motor manipulation task. *Journal of*

Neurophysiology, *107*(11), 3086–3094. https://doi.org/10.1152/jn.00888.2011

Moses, J. M., Hord, D. J., Lubin, A., Johnson, L. C., & Naitoh, P. (1975). Dynamics of nap sleep during a 40 hour period. *Electroencephalography and Clinical Neurophysiology*, *39*(6), 627–633. https://doi.org/10.1016/0013-4694(75)90075-9

Muller, L., Rolston, J. D., Fox, N. P., Knowlton, R., Rao, V. R., & Chang, E. F. (2018). Direct electrical stimulation of human cortex evokes high gamma activity that predicts conscious somatosensory perception. *Journal of Neural Engineering*, *15*(2). https://doi.org/10.1088/1741-2552/aa9bf9

Murase, N., Duque, J., Mazzocchio, R., & Cohen, L. G. (2004). Influence of Interhemispheric Interactions on Motor Function in Chronic Stroke. *Annals of Neurology*, *55*(3), 400–409. https://doi.org/10.1002/ana.10848

Murthy, V. N., & Fetz, E. E. (1996a). Oscillatory activity in sensorimotor cortex of awake monkeys: synchronization of local field potentials and relation to behavior. *Journal of Neurophysiology*, *76*(6), 3949–3967.

Murthy, V. N., & Fetz, E. E. (1996b). Synchronization of neurons during local field potential oscillations in sensorimotor cortex of awake monkeys. *Journal of Neurophysiology*, *76*(6), 3968–3982. http://www.ncbi.nlm.nih.gov/pubmed/8985893

Muthukumaraswamy, S. D. (2010). Functional Properties of Human Primary Motor Cortex Gamma Oscillations. *Journal Neurophysiology*, *104*, 2873–2885. https://doi.org/10.1152/jn.00607.2010.

Nishimura, Y., Perlmutter, S. I., Eaton, R. W., & Fetz, E. E. (2013). Spike-timing-dependent plasticity in primate corticospinal connections induced during free behavior. *Neuron*, *80*(5), 1301–1309. https://doi.org/10.1016/j.neuron.2013.08.028

Okun, M., Naim, A., & Lampl, I. (2010). The subthreshold relation between cortical local field potential and neuronal firing unveiled by intracellular recordings in awake rats. *Journal of Neuroscience*, *30*(12), 4440–4448. https://doi.org/10.1523/JNEUROSCI.5062-09.2010

Onslow, A. C. E., Bogacz, R., & Jones, M. W. (2011). Quantifying phase-amplitude coupling in neuronal network oscillations. *Progress in Biophysics and Molecular Biology*, *105*(1–2), 49–57. https://doi.org/10.1016/j.pbiomolbio.2010.09.007

Pascual-Leone, A., Brasil-Neto, J., Valls-Solé, J., Cohen, L. G., & Hallett, M. (1992). Simple reaction time to focal transcranial magnetic stimulation. *Brain*, *115*(1), 109–122. https://doi.org/10.1166/jnn.2012.6247

Paszke, A., Gross, S., Massa, F., Lerer, A., Bradbury, J., Chanan, G., Killeen, T., Lin, Z., Gimelshein, N., Antiga, L., Desmaison, A., Köpf, A., Yang, E., DeVito, Z., Raison, M., Tejani, A., Chilamkurthy, S., Steiner, B., Fang, L., … Chintala, S. (2019). PyTorch: An imperative style, high-performance deep learning library. *Advances in Neural Information Processing Systems*, *32*(NeurIPS).

Penzel, T., & Conradt, R. (2000). Computer based sleep recording and analysis. *Sleep Medicine Reviews*, *4*(2), 131–148. https://doi.org/10.1053/smrv.1999.0087

Perez, M. A., & Cohen, L. G. (2008). Mechanisms underlying functional changes in the primary motor cortex ipsilateral to an active hand. *Journal of Neuroscience*, *28*(22), 5631–5640.

https://doi.org/10.1523/JNEUROSCI.0093-08.2008

Perlmutter, J. S., & Mink, J. W. (2006). Deep brain stimulation. *Annual Review of Neuroscience*, *29*, 229–257. https://doi.org/10.1146/annurev.neuro.29.051605.112824

Pfurtscheller, G., Stancák, A., & Neuper, C. (1996). Post-movement beta synchronization. A correlate of an idling motor area? *Electroencephalography and Clinical Neurophysiology*, *98*(4), 281–293. https://doi.org/10.1016/0013-4694(95)00258-8

Prime, D., Woolfe, M., Rowlands, D., O'Keefe, S., & Dionisio, S. (2020). Comparing connectivity metrics in cortico-cortical evoked potentials using synthetic cortical response patterns. *Journal of Neuroscience Methods*, *334*(January), 108559. https://doi.org/10.1016/j.jneumeth.2019.108559

Proakis, J., & Manolakis, D. (2006). *Digital Signal Processing: Principles, Algorithms, and Applications*. Prentice Hall.

Ramanathan, D. S., Gulati, T., & Ganguly, K. (2015). Sleep-Dependent Reactivation of Ensembles in Motor Cortex Promotes Skill Consolidation. *PLoS Biology*, *13*(9), 1–25. https://doi.org/10.1371/journal.pbio.1002263

Ranck, J. B. (1975). Which elements are excited in electrical stimulation of mammalian central nervous system: A review. *Brain Research*, *98*(3), 417–440. https://doi.org/10.1016/0006-8993(75)90364-9

Ray, S., Crone, N. E., Niebur, E., Franaszczuk, P. J., & Hsiao, S. S. (2008). Neural correlates of high-gamma oscillations (60-200 Hz) in macaque local field potentials and their potential implications in electrocorticography. *Journal of Neuroscience*, *28*(45), 11526–11536. https://doi.org/10.1523/JNEUROSCI.2848-08.2008

Ray, S., & Maunsell, J. H. R. (2011). Different origins of gamma rhythm and high-gamma activity in macaque visual cortex. *PLoS Biology*, *9*(4). https://doi.org/10.1371/journal.pbio.1000610

Rebesco, J. M., & Miller, L. E. (2011a). Enhanced detection threshold for in vivo cortical stimulation produced by Hebbian conditioning. *Journal of Neural Engineering*, *8*(1), 016011.

Rebesco, J. M., & Miller, L. E. (2011b). Enhanced detection threshold for in vivo cortical stimulation produced by Hebbian conditioning. *Journal of Neural Engineering*, *8*(1). https://doi.org/10.1088/1741-2560/8/1/016011

Rebesco, J. M., Stevenson, I. H., Körding, K. P., Solla, S. A., & Miller, L. E. (2010). Rewiring neural interactions by micro-stimulation. *Frontiers in Systems Neuroscience*, *4*(August), 1–15. https://doi.org/10.3389/fnsys.2010.00039

Rechtschaffen, A. (1998). Current perspectives on the function of sleep. *Perspectives in Biology and Medicine*, *41*(3), 359–390. https://doi.org/10.1353/pbm.1998.0051

Rechtschaffen, A., & Kales, A. (1968). A manual of standardized terminology, techniques and scoring system for sleep stages of human subjects. *U.S. Public Health Service, U.S. Government Printing Office, Washington D.C.*

Rembado, I., Zanos, S., & Fetz, E. E. (2017). Cycle-triggered cortical stimulation during slow

wave sleep facilitates learning a BMI task: A case report in a non-human primate. *Frontiers in Behavioral Neuroscience*, *11*(April), 1–13. https://doi.org/10.3389/fnbeh.2017.00059

Richardson, A. G., & Fetz, E. E. (2017). Brain state-dependence of electrically evoked potentials monitored with head-mounted electronics. *Physiology & Behavior*, *176*(5), 139–148. https://doi.org/10.1109/TNSRE.Brain

Rilk, A. J., Soekadar, S. R., Sauseng, P., & Plewnia, C. (2011). Alpha coherence predicts accuracy during a visuomotor tracking task. *Neuropsychologia*, *49*(13), 3704–3709. https://doi.org/10.1016/j.neuropsychologia.2011.09.026

Rubin, R., Abbott, L. F., & Sompolinsky, H. (2017). Balanced excitation and inhibition are required for high-capacity, noise-robust neuronal selectivity. *Proceedings of the National Academy of Sciences of the United States of America*, *114*(44), E9366–E9375. https://doi.org/10.1073/pnas.1705841114

Rudy, B., Fishell, G., Lee, S., & Hjerling-Leffler, J. (2013). Three groups of interneurons account for nearly 100 % of Neocortical GABAergic Neurons. *Dev Neurobiol*, *71*(1), 45–61. https://doi.org/10.1002/dneu.20853.Three

Seeman, S. C., Mogen, B. J., Fetz, E. E., & Perlmutter, S. I. (2017). Paired stimulation for spike-timing-dependent plasticity in primate sensorimotor cortex. *The Journal of Neuroscience*, *37*(7), 1935–1949. https://doi.org/10.1523/JNEUROSCI.2046-16.2017

Sejnowski, T. J., Churchland, P. S., & Movshon, J. A. (2014). Putting big data to good use in neuroscience. *Nature Neuroscience*, *17*(11), 1440–1441. https://doi.org/10.1038/nn.3839

Shupe, L. E., & Fetz, E. E. (2021). An integrate-and-fire spiking neural network model simulating artificially induced cortical plasticity. *ENeuro*, *8*(2).

Shupe, L. E., Miles, F. P., Jones, G., Yun, R., Mishler, J., Rembado, I., Murphy, R. L., Perlmutter, S. I., & Fetz, E. E. (2021). Neurochip3: An autonomous multichannel bidirectional brain-computer interface for closed-loop activity-dependent stimulation. *Frontiers in Neuroscience*, *15*(August), 1–15. https://doi.org/10.3389/fnins.2021.718465

Siclari, F., & Tononi, G. (2017). Local aspects of sleep and wakefulness. *Current Opinion in Neurobiology*, *44*, 222–227. https://doi.org/10.1016/j.conb.2017.05.008

Siegel, J. M. (2005). Clues to the functions of mammalian sleep. *Nature*, *437*, 1264–1271.

Silber, M. H., Ancoli-Israel, S., Bonnet, M. H., Chokroverty, S., Grigg-Damberger, M. M., Hirshkowitz, M., Kapen, S., Keenan, S. A., Kryger, M. H., Penzel, T., Pressman, M. R., & Iber, C. (2007). The visual scoring of sleep in adults. *Journal of Clinical Sleep Medicine*, *3*(2), 121–131.

Silberberg, G., & Markram, H. (2007). Disynaptic inhibition between neocortical pyramidal cells mediated by martinotti cells. *Neuron*, *53*(5), 735–746. https://doi.org/10.1016/j.neuron.2007.02.012

Srinath, R., & Ray, S. (2014). Effect of amplitude correlations on coherence in the local field potential. *Journal of Neurophysiology*, *112*(4), 741–751. https://doi.org/10.1152/jn.00851.2013

Stoney, S. D., Thompson, W. D., & Asanuma, H. (1968). Excitation of pyramidal tract cells by

intracortical microstimulation: effective extent of stimulating current. *Journal of Neurophysiology*, *31*(5), 659–669. https://doi.org/10.1152/jn.1968.31.5.659

Strens, L. H. A., Oliviero, A., Bloem, B. R., Gerschlager, W., Rothwell, J. C., & Brown, P. (2002). The effects of subthreshold 1 Hz repetitive TMS on cortico-cortical and interhemispheric coherence. *Clinical Neurophysiology*, *113*(8), 1279–1285. https://doi.org/10.1016/S1388-2457(02)00151-7

Sun, S., Jiang, L. P., Peterson, S. M., Herron, J., Weaver, K., Ko, A., Ojemann, J., & Rao, R. P. N. (2020). Unsupervised Sleep and Wake State Identification in Long-Term Electrocorticography Recordings. *Annu Int Conf IEEE Eng Med Biol Soc.*, 629–632.

Suppa, A., Huang, Y. Z., Funke, K., Ridding, M. C., Cheeran, B., Di Lazzaro, V., Ziemann, U., & Rothwell, J. C. (2016). Ten Years of Theta Burst Stimulation in Humans: Established Knowledge, Unknowns and Prospects. *Brain Stimulation*, *9*(3), 323–335. https://doi.org/10.1016/j.brs.2016.01.006

Suppa, A., Quartarone, A., Siebner, H., Chen, R., Di Lazzaro, V., Del Giudice, P., Paulus, W., Rothwell, J. C., Ziemann, U., & Classen, J. (2017). The associative brain at work: Evidence from paired associative stimulation studies in humans. *Clinical Neurophysiology*, *128*(11), 2140–2164. https://doi.org/10.1016/j.clinph.2017.08.003

Takeuchi, S., Mima, T., Murai, R., Shimazu, H., Isomura, Y., & Tsujimoto, T. (2015). Gamma oscillations and their cross-frequency coupling in the primate hippocampus during sleep. *Sleep*, *38*(7), 1085-1091G. https://doi.org/10.5665/sleep.4818

Tanji, J., Okano, K., & Sato, K. C. (1988). Neuronal activity in cortical motor areas related to ipsilateral, contralateral, and bilateral digit movements of the monkey. *Journal of Neurophysiology*, *60*(1), 325–343. https://doi.org/10.1152/jn.1988.60.1.325

Tehovnik, E. J., Tolias, A. S., Sultan, F., Slocum, W. M., & Logothetis, N. K. (2006). Direct and indirect activation of cortical neurons by electrical microstimulation. *Journal of Neurophysiology*, *96*(2), 512–521. https://doi.org/10.1152/jn.00126.2006

Thabit, M. N., Ueki, Y., Koganemaru, S., Fawi, G., Fukuyama, H., & Mima, T. (2010). Movement-related cortical stimulation can induce human motor plasticity. *Journal of Neuroscience*, *30*(34), 11529–11536. https://doi.org/10.1523/JNEUROSCI.1829-10.2010

Thomson, A. M., & Destexhe, A. (1999). Dual intracellular recordings and computational models of slow inhibitory postsynaptic potentials in rat neocortical and hippocampal slices. *Neuroscience*, *92*(4), 1193–1215. https://doi.org/10.1016/S0306-4522(99)00021-4

Thut, G., & Pascual-Leone, A. (2010). A review of combined TMS-EEG studies to characterize lasting effects of repetitive TMS and assess their usefulness in cognitive and clinical neuroscience. *Brain Topography*, *22*(4), 219–232. https://doi.org/10.1007/s10548-009-0115-4

Timofeev, I., Grenier, F., & Steriade, M. (2001). Disfacilitation and active inhibition in the neocortex during the natural sleep-wake cycle: An intracellular study. *Proceedings of the National Academy of Sciences of the United States of America*, *98*(4), 1924–1929. https://doi.org/10.1073/pnas.98.4.1924

Tononi, G., & Cirelli, C. (2014). Sleep and the Price of Plasticity: From Synaptic and Cellular

Homeostasis to Memory Consolidation and Integration. *Neuron*, *81*(1), 12–34. https://doi.org/10.1016/j.neuron.2013.12.025

Tort, A. B. L., Komorowski, R., Eichenbaum, H., & Kopell, N. (2010). Measuring phase-amplitude coupling between neuronal oscillations of different frequencies. *Journal of Neurophysiology*, *104*(2), 1195–1210. https://doi.org/10.1152/jn.00106.2010

Traub, R. D., Whittington, M. A., Stanford, I. M., & Jefferys, J. G. R. (1996). A mechanism for generation of long-range synchronous fast oscillations in the cortex. *Nature*, *383*(6601), 621–224. https://doi.org/10.1038/383621a0

Tremblay, R., Lee, S., & Rudy, B. (2016). GABAergic interneurons in the neocortex: From cellular properties to circuits. *Neuron*, *91*(2), 260–292. https://doi.org/10.1016/j.neuron.2016.06.033.GABAergic

Tsinalis, O., Matthews, P. M., & Guo, Y. (2016). Automatic Sleep Stage Scoring Using Time-Frequency Analysis and Stacked Sparse Autoencoders. *Annals of Biomedical Engineering*, *44*(5), 1587–1597. https://doi.org/10.1007/s10439-015-1444-y

Turrigiano, G. G. (2008). The Self-Tuning Neuron: Synaptic Scaling of Excitatory Synapses. *Cell*, *135*(3), 422–435. https://doi.org/10.1016/j.cell.2008.10.008

Turrigiano, G. G. (2012). Homeostatic synaptic plasticity: Local and global mechanisms for stabilizing neuronal function. *Cold Spring Harbor Perspectives in Biology*, *4*(1), a005736. https://doi.org/10.1101/cshperspect.a005736

Ulrich, D. (2016). Sleep Spindles as Facilitators of Memory Formation and Learning. *Neural Plasticity*, *2016*. https://doi.org/10.1155/2016/1796715

Vecsey, C. G., Huang, T., & Abel, T. (2018). Sleep deprivation impairs synaptic tagging in mouse hippocampal slices. *Neurobiology of Learning and Memory*, *154*(March), 136–140. https://doi.org/10.1016/j.nlm.2018.03.016

Vincent, M., Guiraud, D., Duffau, H., Mandonnet, E., & Bonnetblanc, F. (2017). Electrophysiological brain mapping: Basics of recording evoked potentials induced by electrical stimulation and its physiological spreading in the human brain. *Clinical Neurophysiology*, *128*, 1886–1890. https://doi.org/10.1016/j.clinph.2017.07.402

Vincent, M., Rossel, O., Duffau, H., Bonnetblanc, F., & Guiraud, D. (2016). A measure of cortico-cortical potentials evoked by 10Hz direct electrical stimulation of the brain and by means of a differential recording mode of electrocorticographic signals. *Proceedings of the Annual International Conference of the IEEE Engineering in Medicine and Biology Society, EMBS*, *2016-Octob*, 4543–4546. https://doi.org/10.1109/EMBC.2016.7591738

Wang, X. J., & Buzsáki, G. (1996). Gamma oscillation by synaptic inhibition in a hippocampal interneuronal network model. *Journal of Neuroscience*, *16*(20), 6402–6413. https://doi.org/10.1523/jneurosci.16-20-06402.1996

Weihberger, O., Okujeni, S., Mikkonen, J. E., & Egert, U. (2013). Quantitative examination of stimulus-response relations in cortical networks in vitro. *Journal of Neurophysiology*, *109*(7), 1764–1774. https://doi.org/10.1152/jn.00481.2012

Werk, C. M., Klein, H. S., Nesbitt, C. E., & Chapman, C. A. (2006). Long-term depression in the sensorimotor cortex induced by repeated delivery of 10 Hz trains in vivo. *Neuroscience*,

140(1), 13–20. https://doi.org/10.1016/j.neuroscience.2006.02.004

Whittington, M. A., Traubtt, R. D., & Jefferys, B. J. G. R. (1995). Synchronized oscillations in interneuron networks glutamate receptor activation. *Nature*, *373*(February), 612–615.

Wolters, A., Sandbrink, F., Schlottmann, A., Kunesch, E., Stefan, K., Cohen, L. G., Benecke, R., & Classen, J. (2003). A temporally asymmetric Hebbian rule governing plasticity in the human motor cortex. *Journal of Neurophysiology*, *89*(5), 2339–2345. https://doi.org/10.1152/jn.00900.2002

Xu, W., de Carvalho, F., & Jackson, A. (2019). Sequential Neural Activity in Primary Motor Cortex during Sleep. *The Journal of Neuroscience*, *39*(19), 3698–3712. https://doi.org/10.1523/jneurosci.1408-18.2019

Xue, M., Atallah, B. V., & Scanziani, M. (2014). Equalizing excitation-inhibition ratios across visual cortical neurons. *Nature*, *511*(7511), 596–600. https://doi.org/10.1038/nature13321

Yamamoto, J., Suh, J., Takeuchi, D., & Tonegawa, S. (2014). Successful execution of working memory linked to synchronized high-frequency gamma oscillations. *Cell*, *157*(4), 845–857. https://doi.org/10.1016/j.cell.2014.04.009

Yazdan-Shahmorad, A., Kipke, D. R., & Lehmkuhle, M. J. (2013). High gamma power in ECoG reflects cortical electrical stimulation effects on unit activity in layers V/VI. *Journal of Neural Engineering*, *10*(6). https://doi.org/10.1088/1741-2560/10/6/066002

Yazdan-Shahmorad, A., Silversmith, D. B., Kharazia, V., & Sabes, P. N. (2018). Targeted cortical reorganization using optogenetics in non-human primates. *ELife*, *7*, 1–21. https://doi.org/10.7554/eLife.31034

Younes, M., Raneri, J., & Hanly, P. (2016). Staging sleep in polysomnograms: Analysis of inter-scorer variability. *Journal of Clinical Sleep Medicine*, *12*(6), 885–894. https://doi.org/10.5664/jcsm.5894

Yun, R., Mishler, J., Perlmutter, S. I., Rao, R. P. N., & Fetz, E. E. (2022). Responses of cortical neurons to intracortical microstimulation in awake primates. *BioRxiv*. https://doi.org/https://doi.org/10.1101/2022.03.30.486457

Zanos, S., Rembado, I., Chen, D., & Fetz, E. E. (2018). Phase-Locked Stimulation during Cortical Beta Oscillations Produces Bidirectional Synaptic Plasticity in Awake Monkeys. *Current Biology*, *28*(16), 2515-2526.e4. https://doi.org/10.1016/j.cub.2018.07.009

Zanos, S., Zanos, T. P., Marmarelis, V. Z., Ojemann, G. A., & Fetz, E. E. (2012). Relationships between spike-free local field potentials and spike timing in human temporal cortex. *Journal of Neurophysiology*, *107*(7), 1808–1821. https://doi.org/10.1152/jn.00663.2011

Zhu, J., Jiang, M., Yang, M., Hou, H., & Shu, Y. (2011). Membrane potential-dependent modulation of recurrent inhibition in rat neocortex. *PLoS Biology*, *9*(3). https://doi.org/10.1371/journal.pbio.1001032

Zucker, R. S., & Regehr, W. G. (2002). Short-term synaptic plasticity. *Annual Review of Physiology*, *64*(4), 355–405. https://doi.org/10.1146/annurev.physiol.64.092501.114547